VOLUME 76 JUNE 22, 1972 NUMBER 13

JPCHAx

THE JOURNAL OF PHYSICAL CHEMISTRY

PUBLISHED BIWEEKLY BY THE AMERICAN CHEMICAL SOCIETY

THE JOURNAL OF

PHYSICAL CHEMISTRY

AMERICAN CHEMICAL SOCIETY, *1155 Sixteenth St., N.W., Washington, D. C. 20036*

Books and Journals Division
JOHN K CRUM, *Director*
JOSEPH H. KUNEY, *Head, Business Operations Department*
RUTH REYNARD, *Assistant to the Director*

 Published biweekly by the American Chemical Society at 20th and Northampton Sts., Easton, Pa. 18042. Second-class postage paid at Washington, D. C., and at additional mailing offices.

All manuscripts should be sent to *The Journal of Physical Chemistry*, Department of Chemistry, University of Minnesota, Minneapolis, Minn. 55455.

Additions and Corrections are published once yearly in the final issue. See Volume 75, Number 26 for the proper form.

Extensive or unusual alterations in an article after it has been set in type are made at the author's expense, and it is understood that by requesting such alterations the author agrees to defray the cost thereof.

The American Chemical Society and the Editor of *The Journal of Physical Chemistry* assume no responsibility for the statements and opinions advanced by contributors.

Correspondence regarding accepted copy, proofs, and reprints should be directed to Editorial Production Office, American Chemical Society, 20th and Northampton Sts., Easton, Pa. 18042. Manager: CHARLES R. BERTSCH. Assistant Editor: EDWARD A. BORGER.

Advertising Office: Centcom, Ltd. (formerly Century Communications Corporation), 142 East Avenue, Norwalk, Conn. 06851.

Business and Subscription Information

Remittances and orders for subscriptions and for single copies, notices of changes of address and new professional connections, and claims for missing numbers should be sent to the Subscription Service Department, American Chemical Society, 1155 Sixteenth St., N.W., Washington, D. C. 20036. Allow 4 weeks for changes of address. Please include an old address label with the notification.

Claims for missing numbers will not be allowed (1) if received more than sixty days from date of issue, (2) if loss was due to failure of notice of change of address to be received before the date specified in the preceding paragraph, or (3) if the reason for the claim is "missing from files."

Subscription rates (1972): members of the American Chemical Society, $20.00 for 1 year; to nonmembers, $60.00 for 1 year. Those interested in becoming members should write to the Admissions Department, American Chemical Society, 1155 Sixteenth St., N.W., Washington, D. C. 20036. Postage to Canada and countries in the Pan-American Union, $5.00; all other countries, $6.00. Single copies for current year: $3.00. Rates for back issues from Volume 56 to date are available from the Special Issues Sales Department, 1155 Sixteenth St., N.W., Washington, D. C. 20036.

This publication and the other ACS periodical publications are now available on microfilm. For information write to: MICROFILM, Special Issues Sales Department, 1155 Sixteenth St., N.W., Washington, D. C. 20036.

Notice to Authors printed in this issue

THE JOURNAL OF

PHYSICAL CHEMISTRY

Volume 76, Number 13 June 22, 1972

JPCHAx 76(13) 1795–1918 (1972)

AUTHOR INDEX

In papers with more than one author the name of the author to whom inquiries about the paper should be addressed is marked with an asterisk in the by-line.

NOTICE TO AUTHORS

I. General Considerations

The Journal of Physical Chemistry is devoted to reporting both experimental and theoretical research dealing with fundamental aspects of physical chemistry. Space limitations necessitate giving preference to research articles dealing with previously unanswered basic questions in physical chemistry. Acceptable topics are those of general interest to physical chemists, especially work involving new concepts, techniques, and interpretations. Research that may lead to reexaminations of generally accepted views is, of course, welcome.

Authors reporting data should include an interpretation of the data and its relevance to the theories of the properties of matter. However, the discussion should be concise and to the point and excessive speculation is to be discouraged. Papers reporting redeterminations of existing data will be acceptable only if there is reasonable justification for repetition: for example, if the more recent or more accurate data lead to new questions or to a reexamination of well known theories. Manuscripts that are essentially applications of chemical data or reviews of the literature are, in general, not suitable for publication in *The Journal of Physical Chemistry*. Detailed comparisons of methods of data analysis will be considered only if the paper also contains original data, or if such comparison leads to a genesis of new ideas.

Authors should include an introductory statement outlining the scientific rationale for the research. The statement should clearly specify the questions for which answers are sought and the connection of the present work with previous work in the field. All manuscripts are subject to critical review. It is to be understood that the final decision relating to a manuscript's suitability rests solely with the editors.

Symposium papers are sometimes published as a group, but only after special arrangement with the editor.

Authors' attention is called to the "Handbook for Authors," available from the Special Issues Sales Department, American Chemical Society, 1155 Sixteenth St., N.W., Washington, D. C. 20036, in which pertinent material is to be found.

II. Types of Manuscripts

The Journal of Physical Chemistry publishes two types of manuscripts: *Articles* and *Communications*.

A. Articles should cover their subjects with thoroughness, clarity, and completeness. However, authors should also strive to make their *Articles* as concise as possible, avoiding unnecessary historical background. Abstracts to *Articles* should be brief—300 words is a maximum—and should serve to summarize the significant data and conclusions. The abstract should convey the essence of the *Article* to the reader.

B. Communications are of two types, *Letters* and *Comments*. Both types are restricted to three-quarters of a page (750 words or the equivalent) including tables, figures, and text, and both types of *Communications* are subject to critical review, but special efforts will be made to expedite publication.

Letters should report preliminary results whose immediate availability to the scientific community is deemed important, and whose topic is timely enough to justify the double publication that usually results from the publication of a *Letter*.

Comments include significant remarks on the work of others. The editors will generally permit the authors of the work being discussed to reply.

The category of *Notes* has been discontinued since the handling of such manuscripts was precisely the same as that of *Articles* save for the requirement of an Abstract, and since even a short *Article* will need an Abstract ultimately, it seems as well to ask the author to provide this. Short *Articles* will of course continue to be welcome contributions.

III. Introduction

All manuscripts submitted should contain brief introductory remarks describing the purpose of the work and giving sufficient background material to allow the reader to appreciate the state-of-knowledge at the time when the work was done. The introductory remarks in an *Article* should constitute the first section of the paper and should be labeled accordingly. In *Communications*, the introductory material should not be in such a separate section. To judge the appropriateness of the manuscript for *The Journal of Physical Chemistry*, the editors will place considerable weight on the author's intentions as stated in the Introduction.

IV. Functions of Reviewers

The editors request the scientific advice of reviewers who are active in the area of research covered by the manuscript. The reviewers act only in an advisory capacity and the final decision concerning a manuscript is the responsibility of the editors. The reviewers are asked to comment not only on the scientific content, but also on the manuscript's suitability for *The Journal of Physical Chemistry*. With respect to *Communications*, the reviewers are asked to comment specifically on the urgency of publication. Authors are encouraged to suggest, when submitting a manuscript, names of scientists who could give a disinterested and informed and helpful evaluation of the work. All reviews are anonymous and the reviewing process is most effective if reviewers do not reveal their identities to the authors. An exception arises in connection with a manuscript submitted for publication in the form of a comment on the work of another author. Under such circumstances the first author will, in general, be allowed to review the communication and to write a rebuttal, if he so chooses. The rebuttal and the original communication may be published together in the same issue of the journal. Revised manuscripts are generally sent back to the original reviewers, who are asked to comment on the revisions. If only minor revisions are involved, the editors examine the revised manuscript in light of

the recommendations of the reviewers without seeking further opinions. For the convenience of reviewers, authors are advised to indicate clearly, either in the manuscript or in a covering letter, the specific revisions that have been made.

V. Submission of Manuscripts

All manuscripts must be submitted in triplicate to expedite handling. Manuscripts must be typewritten, double-spaced copy, on $8^1/_2 \times 11$ in. paper. Legal sized paper is not acceptable. Authors should be certain that copies of the manuscript are clearly reproduced and readable. **Authors submitting figures must include the original drawings or photographs thereof, plus three xerographic copies for review purposes. These reproductions of the figures should be on $8^1/_2 \times 11$ in. paper.** Graphs must be in black ink on white or blue paper. Lettering at the sides of graphs may be penciled in and will be typeset. Figures and tables should be held to a minimum consistent with adequate presentation of information. All original data which the author deems pertinent must be submitted along with the manuscript. For example, a paper reporting a crystal structure should include structure factor tables for use by the reviewers.

Footnotes and references to the literature should be numbered consecutively within the paper; the number should also be placed in parentheses in the left margin opposite the line in which the reference first appears. A complete list of references should appear at the end of the paper. Initials of the authors referred to in the citations should be included in the complete reference at the back of the paper. Nomenclature should conform to that used in *Chemical Abstracts* and mathematical characters should be underlined for italics, Greek letters should be annotated, and subscripts and superscripts clearly marked.

Papers should not depend for their usefulness on unpublished material, and excessive reference to material in press is discouraged. References not readily available (*e.g.*, private technical reports, preprints, or articles in press) that are necessary for a complete review of the paper must be included with the manuscript for use by the reviewers.

VI. Revised Manuscripts

A manuscript sent back to an author for revision should be returned to the editor within 6 months; otherwise it will be considered withdrawn and treated as a new manuscript when and if it is returned. Revised manuscripts returned to the editor must be submitted in triplicate and all changes should be made by typewriter. **Unless the changes are very minor, all pages affected by revision must be retyped.** If revisions are so extensive that a new typescript of the manuscript is necessary, it is requested that a copy of the original manuscript be submitted along with the revised one.

VII. Supplementary Material

From time to time manuscripts involve extensive tables, graphs, spectra, mathematical material, or other "supplementary material" which, though of value to the specialized reader who needs all the data or all the detail, does not help and often hinders the effective presentation of the work being reported. The American Chemical Society has instituted a policy of including such supplementary material in the *microfilm* editions of its journals, which are available in many scholarly libraries; in addition, interested readers will be able to obtain the microfilm material directly at nominal cost. Authors are encouraged to make use of this resource, in the interests of shorter articles (which mean more rapid publication) and clearer, more readable presentation.

Supplementary material for inclusion in the microfilm edition should accompany a manuscript at the time of its original submission to an editor. It should be clipped together and attached at the end of the manuscript, along with a slip of paper clearly indicating that the material is "supplementary material for the microfilm edition." A footnote should appear in the paper indicating the nature of the supplementary material and the means by which the interested reader might be able to obtain copies of the data without use of the microfilm edition itself. The following is an example:

(3) Listings of structure factors, coordinates, and anisotropic temperature factors will appear immediately following this article in the microfilm edition of this volume of the journal. Single copies may be obtained from the Business Operations Office, Books and Journals Division, American Chemical Society, 1155 Sixteenth Street, N. W., Washington, D. C. 20036, by referring to code number JPC-00-0000. Remit check or money order for $0.00 for photocopy or $0.00 microfiche.

The amount of money to be indicated in the blanks will be filled in by the Editorial Office at Easton, Pa., after the acceptance of an article.

VIII. Proofs and Reprints

Galley proofs, original manuscript, cut copy, and reprint order form are sent by the printer directly to the author who submitted the manuscript. The attention of the authors is directed to the instructions which accompany the proof, especially the requirement that all corrections, revisions, and additions be entered on the proof and not on the manuscript. Proofs should be checked against the manuscript (in particular all tables, equations, and formulas, since this is not done by the editor) and returned as soon as possible. No paper is released for printing until the author's proof has been received. Alterations in an article after it has been set in type are made at the author's expense, and it is understood that by entering such alterations on proofs the author agrees to defray the cost thereof. The filled-out reprint form must be returned with the proof, and if a price quotation is required by the author's organization a request for it should accompany the proof. Since reprinting is generally done from the journal press forms, all orders must be filed before press time. None can be accepted later, unless a previous request has been made to hold the type. Reprint shipments are made a month or more after publication, and bills are issued by the printer subsequent to shipment. Neither the editors nor the Washington office keeps any supply of reprints. Therefore, only the authors can be expected to meet requests for single copies of papers.

A page charge is assessed to cover in part the cost of publication. Although payment is expected, it is not a condition for publication. Articles are accepted or rejected only on the basis of merit, and the editor's decision to publish the paper is made before the charge is assessed. The charge per journal page is $50.

THE JOURNAL OF
PHYSICAL CHEMISTRY

VOLUME 76, NUMBER 13 JUNE 22, 1972

The Gas-Phase Reaction of Perchloric Acid with Methane

by P. W. M. Jacobs* and J. Stevenson

Department of Chemistry, University of Western Ontario, London 72, Ontario, Canada *(Received January 14, 1972)*

Publication costs assisted by the National Research Council of Canada

The thermal decomposition of perchloric acid in the presence of methane has been investigated using a boric acid coated Pyrex reaction vessel in a flow system. The decomposition kinetics of perchloric acid are quantitatively independent of the presence of methane, showing that methane does not react directly with the acid. Chlorination of methane by chlorine produced from the perchloric acid decomposition is responsible for the principal products, methyl chloride and hydrochloric acid. Implications of these results with respect to the possible roles of ClO radicals in fuel oxidation by ammonium perchlorate and of OH radicals in perchloric acid decomposition are discussed. The small yield of carbon monoxide is attributed to hydrogen abstraction by Cl atoms from formaldehyde, which is itself formed by oxidation of methyl radicals.

Introduction

Current models for the combustion of composite solid propellants based on ammonium perchlorate (AP) presuppose that the AP dissociates into ammonia and perchloric acid and that the products from the decomposition of perchloric acid oxidize both the ammonia and the propellent fuel.[1] The oxidizing species is unknown: it may be molecular oxygen, oxygen atoms, molecular chlorine, chlorine atoms, hydroxyl radicals, or a chlorine–oxygen species (of which only ClO would seem to have the necessary stability), or some combination of these. The present program is directed toward an increased understanding of the chemical reactions occurring in the decomposition of perchloric acid and in the oxidation of simple model fuels. The reaction under investigation is that of perchloric acid with methane. A preliminary study of this reaction was undertaken by Gilbert[2] in these laboratories. His investigation was limited to systems which were very fuel rich, but he did succeed in showing that direct reaction of CH_4 and $HClO_4$ is unlikely and that oxidation of CH_4 occurs at temperatures at which perchloric acid decomposes. Since this reaction occurs at temperatures below those at which CH_4 is oxidized by molecular oxygen, the methane must be reacting with Cl_2 or some intermediate (O, OH, Cl, ClO, ClO_2) formed in the decomposition of perchloric acid.

Experimental Section

A block diagram of the apparatus is shown in Figure 1. The carrier gas flow is regulated by rotameters (A). The primary stream of carrier gas is preheated and saturated in the acid bath (B) which contains 72.4% perchloric acid and is maintained at constant temperature by means of an oil bath. The methane gas flow is measured by means of mercury manometers (D) and a calibrated flow capillary (C) and diluted by the secondary carrier gas flow before entry into the boric acid coated reaction vessel (F) which is maintained at constant temperature by an electric furnace. The two gas streams enter the reaction vessel by means of a twin jet system (J) which ensures that rapid mixing is achieved. The effluent gases are passed through sodium hydroxide solution (G) to remove acidic components before reaching the gas chromatograph sample

(1) P. W. M. Jacobs and G. S. Pearson, *Combust. Flame*, 13, 419 (1969).

(2) R. Gilbert and P. W. M. Jacobs, *ibid.*, 16, 327 (1971).

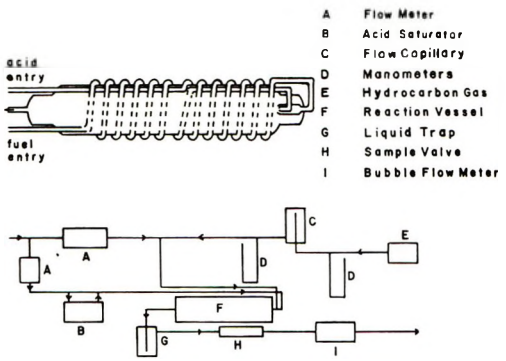

Figure 1. Block diagram of the apparatus: A, rotameter flow meters; B, oil bath containing a saturator filled with 72.4% perchloric acid; C, capillary flow meter; D, manometers; F, reaction vessel; G, trap containing NaOH solution; H, sample valve; I, bubble flow meter. The reaction vessel is shown above the block diagram on a larger scale.

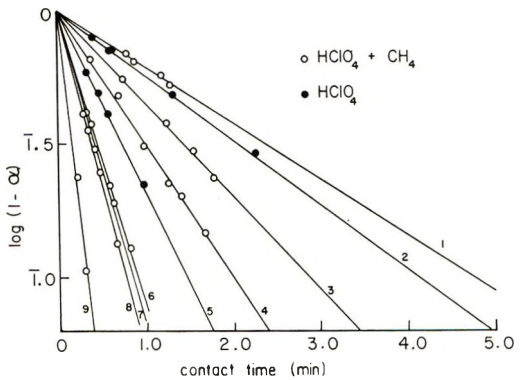

Figure 2. Plots of log $(1 - \alpha)$ where α is the fraction of $HClO_4$ decomposed in contact time t, against t. The linearity these plots confirms that the reaction is first order: 1, 568 K; 2, 579 K; 3, 594 K; 4, 615 K; 5, 633 K; 6, 647 K; 7, 651 K; 8, 659 K; 9, 684 K. Filled circles refer to $HClO_4$ alone with no methane present.

valve (H) from which samples may be drawn for qualitative and quantitative estimations by conventional gas chromatography techniques. The final overall flow rate of the gas stream is measured by a soap bubble flow meter (I).

It was hoped that a complete analysis by gas chromatography might be feasible; however, this proved impossible owing to the difficulties involved in a chromatographic analysis of mixtures of O_2, Cl_2, HCl, $HClO_4$, H_2O, CH_4, CO, and organic halides. The principal difficulty is that all tubing must be heated to 130° to prevent condensation of $HClO_4$, and that the taps in the sampling system would not stand up to hot $HClO_4$ at the total pressure (above ambient) necessary for chromatography. Some initial success was obtained by absorbing the water on barium perchlorate and the perchloric acid on barium oxide, but unfortunately irreproducible amounts of Cl_2 were also removed in these columns. With the present system in which the effluent gas is bubbled through a trap containing a standard solution of NaOH, and thence to the gas chromatograph, titrimetric analysis of the contents of the trap will give the amount of $HClO_4$ unreacted and the amount of Cl in the form of Cl_2 or HCl. Hence the total amount of $HClO_4$ passed through the reactor and the amount decomposed are obtained. Methane, carbon monoxide, and oxygen are determined by gas chromatography, the oxygen produced also being used to determine the amount of acid decomposed. Difficulties could arise if CO_2 were a product since this would react in the trap but no evidence for the formation of carbon dioxide was found (*e.g.* in dry runs in which there was no absorption of the products in NaOH).

Results

The reaction was studied at seven temperatures between 297 and 413°. At all temperatures the only chlorine-containing major product was hydrogen chloride. Where the methane–perchloric acid ratio is low, traces of chlorine were found; however, they were not sufficient to have any significant effect on the overall results. Oxygen and carbon monoxide were present as constituents of the chromatography sample, the latter appearing in very small amounts in most cases, especially at the lower temperature range. Hydrocarbon oils were present in the hydroxide trap. A qualitative study of these employing chromatography, revealed the presence of CH_3Cl, CH_2Cl_2, $CHCl_3$, and CCl_4.

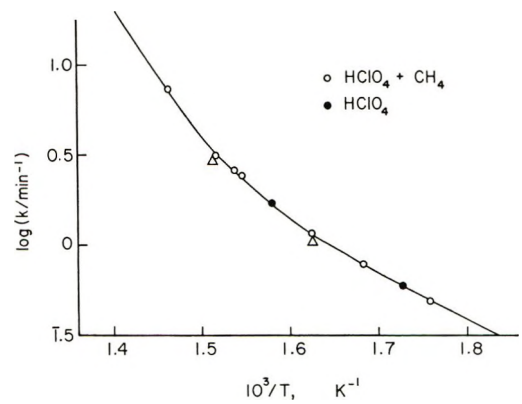

Figure 3. Arrhenius plot of the first-order rate constants for the decomposition of perchloric acid. Triangles, from oxygen analysis; circles, from titrimetric analysis; open circles, $HClO_4 + CH_4$; filled circles, $HClO_4$ with no methane. The line is a least-squares computer fit to the data assuming that k is the sum of two first-order rate constants.

The results shown in Figure 2 are based upon the amount of detectable Cl produced from the decomposition of $HClO_4$. Results based upon the amount of O_2 produced are also shown in Figure 3 and compare favorably within the experimental error. The oxygen yield is expected to be slightly low because some of the oxygen appears as carbon monoxide. The decomposition of $HClO_4$ alone was studied at 308 and 362° and

the results are also plotted in Figures 2 and 3. Both chlorine and hydrogen chloride were present in the trap solution and only oxygen in the chromatograph sample.

The Arrhenius plot, Figure 3, is in the form of a curve suggesting that the decomposition occurred by two parallel reactions. At the lower temperatures the reaction with the lower activation energy would predominate, and at the higher temperatures the reaction with the higher activation energy would predominate. The Arrhenius plot would therefore consist of a curve asymptotic to the two straight lines which correspond to these individual reactions. The Arrhenius parameters for the two reactions were found using a nonlinear least-squares computer program based on the Marquardt algorithm.[3] The reaction at higher temperature has an activation energy of 45.6 kcal mol^{-1} and a preexponential factor of 3.3×10^{13} sec^{-1}, and the reaction predominating at lower temperatures has an activation energy of 11.7 kcal mol^{-1} and a preexponential factor of 2.5×10^{2} sec^{-1}. From these results it would appear that the high-temperature decomposition is essentially a homogeneous unimolecular reaction possibly with a chain mechanism while the lower temperature reaction is influenced by a heterogeneous component. It is evident that the presence of methane is having no effect upon the decomposition of $HClO_4$, since the data for the reaction in the absence of methane fall upon the curve of the $HClO_4$–CH_4 Arrhenius plot.

The following subsidiary experiments were also undertaken with the results shown: (1) methane + oxygen: no reaction in temperature range of Figure 2 (*cf.* ref 4); (2) methane + chlorine (methane rich): CH_3Cl and HCl the only significant products; (3) methane + chlorine + oxygen: CH_3Cl and HCl the only products; (4) methyl chloride + oxygen: no reaction in relevant temperature range; (5) methyl chloride + chlorine: CCl_4, with small amounts of CH_2Cl_2 and $CHCl_3$, formed.

Discussion

The reaction of perchloric acid with methane occurs only at temperatures at which the acid will itself decompose, indicating that no direct reaction between the acid and methane takes place. Above 290° (the lowest temperature investigated) the reaction is influenced by a heterogeneous component and the work of Gilbert[2,5] has shown that a surface influence is evident in the acid decomposition. Above 370° the reaction follows a unimolecular, first-order mechanism with an activation energy of 45.6 kcal mol^{-1}. The value for the HO–ClO_3 bond energy is 48.3 kcal mol^{-1}. The discrepancy between these values cannot be explained by reference to the low-pressure limit since, although the perchloric acid pressure is only a few Torr, the total pressure is atmospheric and the high-pressure limit should be the one concerned.

The continuity of the experimental data in the presence or absence of methane and the absence of large quantities of carbon monoxide from the reaction products would indicate that the perchloric acid decomposes by a mechanism uninfluenced by methane and that methane reacts only with products from this decomposition. The mechanism of the decomposition of perchloric acid alone (in the presence of carrier gas) has been discussed fully by Gilbert and Jacobs.[5] The essential features are

$$HClO_4 = ClO + O_2 + OH \quad (1)$$

$$2ClO = Cl_2 + O_2 \quad (2)$$

$$OH + W \longrightarrow \text{removal of OH} \quad (3)$$

Now since the presence of CH_4 does not affect the rate of decomposition of $HClO_4$, it must be reacting only with one of the final products (Cl_2, O_2) or with an intermediate that is not itself important in controlling the rate of decomposition of $HClO_4$. Although methane does react with molecular oxygen at higher temperatures,[4] it was expected that the reaction of CH_4 with O_2 would be negligible at the temperatures used in this work and this was confirmed experimentally.

Clyne[6] has recently reported that the ClO radical is apparently quite unreactive and that only a very slow reaction was observed with methane at 320°. We have no evidence in favor of any reaction of CH_4 with ClO.

Oxygen atoms would be much more reactive than molecular oxygen but are unlikely to exist in any significant concentration because (a) the ClO_3 formed by initial fission of the HO–ClO_3 will decompose[7] immediately into ClO + O_2 rather than into ClO_2 + O; (b) the recombination of ClO radicals[8] by

$$ClO + ClO = Cl + ClOO \quad (4)$$

$$ClOO + Cl = Cl_2 + O_2 \quad (5)$$

$$ClOO + M = Cl + O_2 + M \quad (6)$$

does not involve O atoms; (c) the removal of OH radicals,[4] traditionally through reaction 3, but possibly through homogeneous processes,[4,9] probably does not result in a significant concentration of O atoms. The possible role of the hydroxyl radical as an oxidizing

(3) D. W. Marquardt, *J. Soc. Ind. Appl. Math.*, **11**, 431 (1963).

(4) D. E. Hoare and G. S. Milne, *Trans. Faraday Soc.*, **63**, 101 (1967).

(5) R. Gilbert and P. W. M. Jacobs, *Combust. Flame*, in press.

(6) M. A. A. Clyne, personal communication.

(7) I. P. Fisher, *Trans. Faraday Soc.*, **63**, 684 (1967).

(8) M. A. A. Clyne and J. A. Coxon, *Proc. Roy. Soc. Ser. A*, **303**, 207 (1968).

(9) W. E. Wilson and A. A. Westenberg, "Eleventh Symposium (International) on Combustion," The Combustion Institute, Pittsburgh, Pa., 1967, p 1143.

species appears much more interesting in the light of the nonreactivity of the ClO radical.

The following observations relate to the possible role of OH radicals in both the decomposition of $HClO_4$ and the reactions of methane.

(a) Baldwin, Norris, and Walker[10] have shown that when methane is added to slowly reacting mixtures of hydrogen + oxygen, consumption of methane occurs by reaction with OH radicals and only to a lesser extent by attack by H atoms. Drysdale and Lloyd[11] give the rate constant for

$$CH_4 + OH = CH_3 + H_2O \quad (7)$$

as

$$k = 2.6 \times 10^{10} \exp(-5000/RT) \text{ l. mol}^{-1} \text{ sec}^{-1} \quad (8)$$

which expression is to be preferred to an earlier estimate of $E > 8$ kcal/mol.[12] All this evidence points to the reaction of CH_4 with OH radicals being a rapid one in the temperature range of interest. However, the rate of decomposition of $HClO_4$ is unaffected by the presence of methane even when the latter is in large excess. Since CH_4 would be expected to react with OH radicals (even if this were not the only or even the main reaction by which CH_4 was consumed), this implies that OH radicals do not participate in the $HClO_4$ decomposition as suggested by Levy[13]

$$HClO_4 = HO + ClO + O_2 \quad (1)$$

$$HO + HClO_4 = H_2O + ClO_2 + O_2 \quad (9)$$

If this were so, then the apparent rate constant k_a for removal of $HClO_4$ would have to be divided by 2 to give k_1. However, the invariance of k_a with respect to the presence of methane seems to imply that (9) is unimportant and that OH radicals are removed efficiently by some other process, presumably (3); Wilson and Westenberg[9] employ a bimolecular homogeneous removal of OH.

(b) The argument presented in (a) above would be invalid if (i) OH radicals were removed by $HClO_4$ (reaction 9) at a rate such that this was unaffected by the presence of a large excess of methane; (ii) CH_4 reacts with some other species present in a concentration comparable to that of OH at a rate much faster than that of reaction 7. Condition i seems unlikely in view of the large excess of methane employed in this and earlier work.[2] Condition ii may be tested once the principal reaction by which methane is consumed has been identified.

The major products (apart from H_2O) when excess methane reacts with perchloric acid are $CH_3Cl + HCl$. These are also the only products when excess methane reacts with Cl_2 at these temperatures. The following mechanism for the methane + perchloric acid system is in harmony with the experimental data.

$$Cl_2 + M = 2Cl + M \quad (10)$$

$$CH_4 + Cl = CH_3 + HCl \quad (11)$$

$$CH_3 + Cl_2 = CH_3Cl + Cl \quad (12)$$

$$Cl + Cl + M = Cl_2 + M \quad (13)$$

Further chlorination of CH_3Cl results in the small yields of CH_2Cl_2, $CHCl_3$, and CCl_4. An increase in the chlorine/methane ratio shows an increase in the production of CCl_4 and a decrease in $CHCl_3$. The small quantities of CH_2Cl_2 and $CHCl_3$ appear unaffected. There is no evidence for the formation of chloro-C_2 compounds or of ethane in the reaction products.

To test b(ii) above we have calculated the rate constants for reactions 7 and 11, respectively, in the temperature range of interest, from (8) and the Arrhenius parameters given by Fettis and Knox.[14] These results together with comparable data for the reaction

$$CH_3Cl + Cl = CH_2Cl + HCl \quad (14)$$

appear in Table I. They show that the rate constants for hydrogen abstraction from methane by OH and Cl are of the same order of magnitude. We conclude, therefore, that (i) either OH does not react with $HClO_4$ in which case it may be reacting with CH_4, so that CH_3 radicals are produced by both (7) and (11); or (ii) that it is removed by $HClO_4$ at a rate considerably greater than that with which it would react with a large excess of methane. If OH radicals are reacting with neither $HClO_4$ nor methane, then they are being removed rapidly by some other process such as (3). Further work to elucidate the precise role of OH is envisaged.

Table I: Arrhenius Parameters and Rate Constants for Reactions 7, 11, and 14 in the Temperature Range of Interest

Reaction	$A \times 10^{10}$, l. mol^{-1} sec^{-1}	E, kcal mol^{-1}	Log (k/mol l.$^{-1}$ sec^{-1}) at t, °C: 394	329	227
			$10^3K/T$: 1.50	1.66	2.0
$CH_4 + OH$ (7)	2.9	5.00	8.78	8.60	8.23
$CH_4 + Cl$ (11)	0.6	3.83	8.52	8.39	8.10
$CH_3Cl + Cl$ (14)	1.1	3.28	8.97	8.85	8.61

It has recently been found by Clyne[6] that ClO does not affect the chlorination of methane. This is in harmony with our proposal that Cl atoms (with a possible contribution from OH radicals) are responsible

(10) R. R. Baldwin, A. C. Norris, and R. W. Walker, "Eleventh Symposium (International) on Combustion," The Combustion Institute, Pittsburgh, Pa., 1967, p 889.

(11) D. D. Drysdale and A. C. Lloyd, *Oxid. Combust. Rev.*, **4**, 157 (1970).

(12) D. E. Hoare and M. Patel, *Trans. Faraday Soc.*, **65**, 1325 (1969).

(13) J. B. Levy, *J. Phys. Chem.*, **66**, 1092 (1962).

(14) G. C. Fettis and J. H. Knox, *Progr. React. Kinet.*, **2**, 3 (1964).

for the consumption of methane in mixtures with perchloric acid.

There remains the question of the small yield of CO. Direct oxidation of CH_4 or CH_3Cl by O_2 was found not to occur under these conditions. Baldwin, Matchan, and Walker[15] have shown that, between 440 and 540°, the oxidation of methyl radicals has a negative temperature coefficient corresponding to an activation energy of −20 to −25 kcal/mol. This observation shows that oxidation of methyl radicals, proceeds, not through the bimolecular reaction

$$CH_3 + O_2 = HCHO + OH \qquad (15)$$

but through a more complicated sequence of reactions involving the methylperoxy radical CH_3O_2 and (at lower temperatures) methylperoxide CH_3OOH. Nevertheless, although the detailed path for the oxidation of methyl radicals may be rather complicated, the products are likely to be formaldehyde and OH radicals just as if reaction 15 were occurring. It seems likely that CO would be formed under these experimental conditions by successive hydrogen abstraction from HCHO by Cl atoms

$$HCHO + Cl = HCO + Cl \qquad (16)$$

$$HCO + Cl = CO + HCl \qquad (17)$$

An alternative mechanism is

$$CH_3 + ClO = CH_2O^* + HCl \qquad (18)$$

$$CH_2O^* = CO + H_2 \qquad (19)$$

for although hydrogen is not found in the products, it would be removed rapidly by the excess chlorine. There was no evidence of ethane in the products so that the alternative chain termination reaction to (13)

$$CH_3 + CH_3 = C_2H_6 \qquad (20)$$

does not occur in the presence of $Cl_2 + O_2$ where routes to formaldehyde and especially (12) are evidently preferred.

The absence of any direct reaction between perchloric acid and methane which would increase the total acid decomposition rate, would indicate that methane is a relatively poor fuel to incorporate in the ammonium perchlorate (AP) system. At higher temperatures direct oxidation of methane by molecular oxygen will occur and this may introduce some new effects. It must be noted, however, that little attention has been paid so far (*e.g.*, ref. 1) to the role of Cl in AP + fuel reactions and, substantiated by accumulating evidence on the poor reactivity of ClO, the present results may indicate that Cl rather than ClO is a major chain carrier in AP + fuel decompositions. Having said that, one should recall that the burning velocities of methane–perchloric acid flames[16,17] are approximately three times those of corresponding methane–oxygen flames and that the latter are not increased by adding H, Cl, or Cl_2. Thus the role of ClO, at least at higher temperatures, may still be an important one. Finally, it is evident that Cl is not a chain carrier in the decomposition of perchloric acid alone since the rate of decomposition of the acid is unaffected by the presence of methane which reacts rapidly with Cl.

Acknowledgments. We are grateful to the Defence Research Board of Canada for its support of this work through Contract No. DRB 715-7020300 with the Department of Supply and Services, and we thank Dr. G. S. Pearson of the British Embassy in Washington and Dr. J. A. Barnard of University College London for valuable discussions.

(15) R. R. Baldwin, M. J. Matchan, and R. W. Walker, *Combust. Flame*, **15**, 109 (1970).

(16) G. S. Pearson, *ibid.*, **11**, 89 (1967).

(17) G. S. Pearson, *Nature (London)*, **208**, 283 (1965).

Elementary Processes in the Photochlorination of 3-Methylpentane Glass at 77–97°K[1]

by Rafael Arce-Quintero and John E. Willard*

Department of Chemistry, University of Wisconsin, Madison, Wisconsin *(Received December 28, 1971)*

Publication costs assisted by the U. S. Atomic Energy Commission

The quantum yields of chlorine consumption during photolysis of chlorine with 330-nm radiation in 3-methylpentane at 300, 199, 97, 87, and 77°K are 2×10^4, 5×10^3, 270, 4.2, and 0.7, respectively. A higher Arrhenius factor below 97°K than above reflects the influence of deactivation of excited Cl_2 molecules by the cage walls, concerted reactions as opposed to chain initiation, and/or slowness of diffusion required for chain propagation. A new reaction intermediate, tentatively assumed to be a charge-transfer complex of a free radical and a chlorine molecule, is observable in the temperature range of 77–87°K by its esr signal and by its optical absorption peak at 260 nm. The quantum yield of trapped 3-methylpentyl radicals at 77°K is 0.01 while that of 3-methylpentyl chloride stable products is 0.6, indicating that many Cl_2 molecules which have absorbed a photon react to form the chloride in a concerted process rather than through a mechanism involving stabilized radicals. The decay rate of the trapped free radicals at 77°K is first order in their initial concentration and increases with initial chlorine concentration, indicating that they are removed by reaction with diffusing chlorine molecules.

Introduction

The work of this paper was initiated to learn more about the factors which control chemical reactions of solutes in glassy solids as compared to reactions of the same species in the liquid and gas. Glassy 3-methylpentane (3MP) was chosen as the matrix because it has been extensively used for studying reactions of trapped electrons, ions, and free radicals produced by ionizing radiation.[2] Photochlorination of the 3MP was chosen for investigation because the photochlorination of hydrocarbons has been extensively studied[3] in the liquid and gas phases, and because the activation energy for abstraction of hydrogen from carbon–hydrogen bonds by chlorine atoms is low enough so that the reaction might be expected to take place at a measurable rate at 77°K.

When a gaseous chlorine molecule absorbs a 330-nm photon, ground-state atoms are formed with 14 kcal mol^{-1} of kinetic energy each. In the presence of hydrocarbons at 300°K these atoms initiate chain reactions.

$$Cl_2 + h\nu(330\text{ nm}) \longrightarrow [Cl_2^*] \longrightarrow Cl^* + Cl^* \quad (1)$$

$$Cl^* + RH \longrightarrow R + HCl \quad (2)$$

$$R + Cl_2 \longrightarrow RCl + Cl \quad (3)$$

$$Cl + RH \longrightarrow R + HCl \quad (4)$$

$$R \text{ (or Cl)} + \text{an atom, radical or impurity} \longrightarrow \text{stable product, ending chain} \quad (5)$$

Chain lengths of the order of 10^4 chlorine molecules consumed per photon absorbed[3] indicate very low activation energies for the chain carrying steps. These yields are not significantly different in the liquid at 300°K indicating that geminate recombination of the Cl* atoms as a result of caging effects is not significant under these conditions.

In the present work we have investigated the yields of Cl_2 consumption, and of trapped radical, dodecane, and organic chloride production resulting from photoactivation of Cl_2 at 77°K, where the density and viscosity are much higher, and the diffusion coefficients much lower, than at 300°K. Answers to the following questions have been sought. (1) Are photoactivated Cl_2 molecules in a glassy hydrocarbon at 77°K deactivated by the solvent cage without abstracting hydrogen? (2) Can a photoactivated Cl_2 molecule react with a matrix hydrocarbon molecule to form RCl and HCl in a concerted reaction without production of a free radical as an intermediate step? (3) Are the hydrocarbon free radicals produced in pairs which undergo geminate recombination? (4) Do photochlorination chains occur in the glassy state and, if so, how fast do they grow? (5) Is photochlorination in the glassy

(1) This work has been supported in part by the U. S. Atomic Energy Commission under Contract AT(11-1)-1715, by the Economic Development Administration of the Government of Puerto Rico, and by the W. F. Vilas trust of the University of Wisconsin.

(2) For reviews and references, see: (a) J. E. Willard in "Fundamental Processes in Radiation Chemistry," P. Ausloos, Ed., Interscience, New York, N. Y., 1968, Chapter 9; (b) W. H. Hamill in "Radical Ions," E. T. Kaiser and L. Kevan, Ed., Wiley, New York, N. Y., 1968, Chapter 9.

(3) For examples and references, see: F. S. Dainton and P. B. Ayscough in "Photochemistry and Reaction Kinetics," P. G. Ashmore, F. S. Dainton, and T. M. Sugden, Ed., Cambridge University Press, New York, N.Y., 1967.

state selective with respect to primary, secondary, and tertiary C–H bonds?

A few related investigations of the photolysis of I_2 and Br_2 in organic glasses have been reported. Photobleaching of the color of I_2 in an ethyl ether–isopentane–ethyl alcohol (EPA) glass[4] was originally ascribed to dissociation of I_2 and trapping of I atoms, but it was subsequently shown[5] that this is precluded by caging effects and that the I_2 disappearance could be accounted for by photoinduced formation of HI with a low quantum yield. Unsuccessful attempts to bleach I_2 and Br_2 in 3MP glass at 77°K have been reported,[6] but a quantum yield of 2×10^{-4} molecule of Br_2 removed per photon absorbed has been demonstrated.[7] Low quantum yields for I_2 and Br_2 disappearance at 77°K are expected in view of the activation energies of 20 kcal mol^{-1} and 10–15 kcal mol^{-1} for abstraction of hydrogen from hydrocarbons by iodine and bromine atoms,[8] and also the high probability of primary recombination of halogen atoms within the parent solvent cage.[5,9]

Experimental Section[10]

Sample Preparation. Phillips Pure Grade 3-methylpentane (3MP) was passed through 55 cm of silica gel activated for 10 hr at 425°. The effluent was collected under nitrogen, degassed by the freeze–pump–thaw technique and by pumping on the liquid on a vacuum line. It was stored over a sodium mirror. The optical density of 1 cm of this 3MP at 190 nm was *ca.* 0.05, and the gas chromatographic purity was greater than 99.99%. Matheson Research Grade chlorine (99.67% minimum purity) was stored on the vacuum line in a flask closed with a Delmar greaseless stopcock. To meter aliquots the chlorine was liquefied at the temperature of Dry Ice and the vapor was allowed to fill a flask of known volume at its vapor pressure.

The reaction cells were 1 × 1 cm i.d. square quartz cells, and 3 × 2 mm i.d. Suprasil cells which allowed spectrophotometric and esr examinations to be made on the same sample.[11]

Samples for irradiation were prepared by distilling 3MP from the sodium mirror into the cell, followed by condensing chlorine from the metering volume and sealing. The sample was then melted in the dark and mixed at room temperature, following which it was frozen to the glassy state by immersing gradually in liquid nitrogen.

Irradiation Conditions. Irradiations for the purpose of determining quantum yields were made with an Osram HBO 200-W "super pressure" mercury arc and a Bausch and Lomb high-intensity monochromator with a uv-visible grating using a bandwidth at half-height of 150 Å centered at the wavelength of the 3340-Å mercury line. Samples placed at the focus of the collimating lens of the monochromator were exposed to an intensity of 1×10^{15} to 4×10^{15} photons/cm^2 sec depending on the age of the lamp. To produce radicals for the study of decay kinetics in esr cells, an AH-4 medium pressure mercury arc was used with a 2 mm thick Pyrex filter and quartz collimating lens. It gave about 5×10^{15} photons sec^{-1} over the area of the sample in the wavelength range absorbed by the Cl_2.

For photolyses at 77–87°K, samples were immersed in a liquid coolant in a flat windowed dewar (Worden Quartz Products 4503.7). With the 1 cm^2 quartz cell, the dimensions of the light beam entering the glassy sample were defined by a mask on the face of the dewar. The 3 × 2 mm cells were held in a copper cell holder with a slot which defined the beam. Temperatures of 77 and 87°K were maintained with liquid nitrogen and liquid argon, respectively, and 80 and 83°K were obtained by mixtures of the two. The temperatures were monitored with a thermocouple. Experiments at 97 and 199°K using the 1-cm^2 cells were done in a cryostat[12] which allowed the temperature to be controlled by the competition between a coolant (liquid argon or Dry Ice) and electrical heating.

Actinometry and Quantum Yield Determinations. Prior to each photolysis of a Cl_2–3MP sample for the purpose of a quantum yield determination the light intensity incident on the sample from the monochromator was determined by ferrioxalate actinometry.[13] The optical density of the actinometer was always 2 or higher throughout the illumination. Duplicate determinations with the actinometer were reproducible within ±10%. In a single comparison with a thermopile standardized with a Bureau of Standards lamp, the latter gave an intensity 20% higher than the actinometer.

The number of Cl_2 molecules removed during each photolysis was determined from Beer's law and the change in optical density of the sample at 330 nm, as measured with a Cary 14 spectrophotometer. For rigid samples (97°K and below), where diffusion was

(4) I. Norman and G. Porter, *Proc. Roy. Soc., Ser. A*, **230**, 399 (1955).

(5) S. V. Filseth and J. E. Willard, *J. Amer. Chem. Soc.*, **84**, 3806 (1962).

(6) R. G. Sowden and N. Davidson, *ibid.*, **78**, 1291 (1956).

(7) P. Mazurak, M.S. Thesis, University of Wisconsin, Madison, Wis., 1966.

(8) For examples and references, see: A. F. Trotman-Dickenson in "Advances in Free Radical Chemistry," Vol. 1, G. H. Williams, Ed., Logos Press, London, 1965.

(9) R. L. Strong and J. E. Willard, *J. Amer. Chem. Soc.*, **79**, 2098 (1957).

(10) Further details are given in the Ph.D. thesis of R. Arce-Quintero, University of Wisconsin, 1970, available from University Microfilms, Ann Arbor, Mich.

(11) These cells were made by Mr. W. J. Wheeler of the Chemistry Department Glass Shop by pulling down 12 mm Suprasil tubing over a stainless steel template 6.0 × 0.25 × 0.17 cm.

(12) T. O. Jones and J. E. Willard, *Rev. Sci. Instrum.*, **27**, 1037 (1956).

(13) (a) C. A. Parker, *Proc. Roy. Soc., Ser. A*, **220**, 104 (1953); (b) C. G. Hatchard and C. A. Parker, *ibid.*, **235**, 518 (1956).

too slow for significant mixing of the irradiated and unirradiated portions of the sample, the chlorine consumption was calculated for the volume of the solution in the light beam. For liquid samples, where mixing occurred during illumination, it was calculated on the basis of the total volume. Experimental tests confirmed these assumptions as to the mixing and nonmixing.

The quantum yield of Cl_2 consumption is given by $\Phi(Cl_2) = \Delta(Cl_2)/\Sigma I_{0(i)}(1 - 10^{\epsilon_i l \bar{c}})$ where $\Delta(Cl_2)$ is the number of molecules of chlorine consumed in a time interval of illumination t, during which the incident intensity in photons sec^{-1} was I_0 and the average of the initial and final optical densities due to Cl_2 was $\epsilon l \bar{c}$. The summation is made with respect to wavelength increments under the intensity curve of the light from the monochromator. For a typical sample containing a Cl_2 concentration of 3×10^{-3} M the calculated I_{ab} is 0.96 of its value if the extinction coefficient for all the incident light is assumed to be that at 330 nm.

Quantum yields of trapped free radicals and of stable products were all determined on samples irradiated in the esr optical cells under liquid nitrogen in the Worden dewar. Following irradiation the optical and esr spectra were determined, and a sample was taken for gas chromatographic analysis.

Analytical Procedures. Esr measurements of trapped free radicals were made with a Varian 4500 X-band spectrometer using a Varian 4531 multipurpose cavity with 100-kHz field modulation. The microwave power was 7 mW, at which power the loss in signal intensity due to saturation was less than 30%.[14] Measurements at 77°K were made with the sample in a Varian liquid nitrogen dewar. To determine the absolute number of unpaired spins, the first derivative esr signal was converted to the esr absorption curve by an electronic analog integrator, and this curve was integrated with a planimeter for comparison with a similarly integrated curve for a standard solution of the stable galvinoxyl free radical in degassed benzene. Appropriate corrections for tube size and temperature were made. The reproducibility of repeated measurements of this type is *ca.* ±10% and the precision *ca.* ±20%, the main source of error being in the double integration technique.

Gas chromatographic analysis for alkyl chloride and hydrocarbon products was made on aliquots of the melted samples, using a 10 ft long 3.8 mm i.d. column of 40–60 mesh Chromosorb-P coated with 20% by weight of GE SF-96 silicone oil. Known concentrations of 3-chloromethylpentane and 2-chloro-4-methylpentane in 3MP, used to determine the sensitivity of the flame ionization detector for alkyl chlorides, gave identical response. Boiling points of unknown effluent compounds were estimated from a curve of effluent times *vs.* boiling point for known compounds.

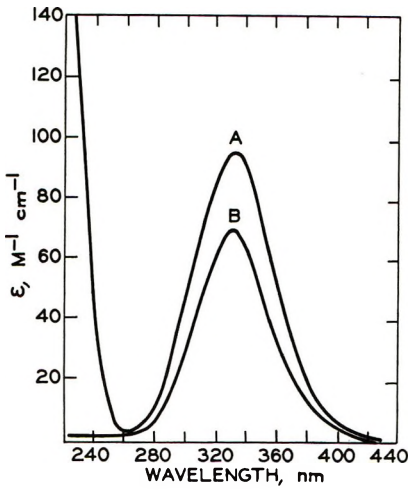

Figure 1. Absorption spectra of Cl_2: A, in the liquid at 298°K and the glass at 77°K; B, in the gas at 298°K. The values of the extinction coefficient are based on the value of 66 M^{-1} cm^{-1} at 330 nm reported[17] for the gas.

Results

Absorption Spectrum and Extinction Coefficient of Cl_2 in 3MP. The absorption spectrum of Cl_2 dissolved in liquid or glassy 3MP (Figure 1) has a near-uv maximum similar to that of Cl_2 gas but with somewhat higher extinction coefficients. In addition, it shows intense absorption in the 250–180-nm region which is absent in the gas. In a 1-cm cell the optical density of this band is off scale (OD > 2) even at Cl_2 concentrations as low as 5×10^{-4} M, for which the Cl_2 maximum at 330 nm has an OD of only 0.05. This absorption, like those of iodine and bromine in saturated hydrocarbons at wavelengths where the gases do not absorb[15] and that of Cl_2 in benzene at 290 nm[16] is presumably due to charge-transfer absorption.

To determine the extinction coefficients in liquid 3MP the amount of gaseous Cl_2 in an optical cell of known volume was first determined from its optical density. This cell was then opened through a stopcock to a second optical cell of known volume containing a known volume of 3MP. After thorough mixing of the gas (13 ml) and liquid (4 ml) phases, the amount of chlorine remaining in the gas was measured by its optical density, thus allowing the Cl_2 concentration in the 3MP to be calculated. About 85% of the Cl_2 dissolved. The data of Figure 1 are the average of four experiments which agreed within ±5%. When a solution of Cl_2 in liquid 3MP was cooled to the glassy state at 77°K, the spectrum was unchanged except for the

(14) We are indebted to Dr. Lewis Perkey of our laboratory for the power saturation measurements. The radicals produced by photolysis of Cl_2 in glassy 3MP are completely unsaturated at 3 mW and below.

(15) (a) D. R. Evans, *J. Chem. Phys.*, **23**, 1424, 1426 (1955); (b) L. E. Orgel and R. S. Mulliken, *J. Amer. Chem. Soc.*, **79**, 4839 (1957).

(16) L. J. Andrews and R. M. Keefer, *ibid.*, **73**, 462 (1951).

increase in optical density resulting from the decrease in specific volume at 77°K to 0.77 of that at 293°K.

The absolute values of the extinction coefficients of Figure 1 are based on the literature value of 66 M^{-1} cm^{-1} for gaseous Cl_2 at 330 nm.[17] The value of 95 ± 10 M^{-1} cm^{-1} for the extinction coefficient of Cl_2 at 330 nm in liquid and glassy 3MP is similar to values reported for Cl_2 in CCl_4 solution (*e.g.*, 100 M^{-1} cm^{-1} [18,19] and 94 M^{-1} cm^{-1} [20]).

Reaction Intermediate Which Absorbs at 260 nm. When glassy 3MP samples containing 10^{-4} to 10^{-3} mole fraction of Cl_2 are photolyzed at 77°K with 330-nm radiation, the chlorine absorption (A of Figure 1) decreases uniformly and can be completely bleached with continued irradiation. When a partially bleached sample is allowed to stand in the dark, a new absorption with a maximum at 260 nm (Figure 2) grows in slowly, reaching its maximum intensity only after several days. When a sample irradiated at 77°K is raised to 83°K immediately after irradiation, the 260 nm peak grows to its maximum within about 8 min. It disappears when the sample is warmed to room temperature and does not reappear when it is recooled to 77°K. During photolyses at temperatures between 80 and 87°K, the peak appears prominently in less than 5 min and grows linearly in samples identical with those which give no peak during 60-min illumination at 77°K. The rate of growth is faster at 83°K than at 80°K. Following irradiation at 80 and 83°K the peak continues to grow, but at 87°K it decays. At 83°K it grows to a plateau from which it decays to zero when transferred to 87°K. Photolysis at 260 nm following formation of the peak at 77°K bleaches the 260-nm peak.

The extinction coefficient of the 260-nm species has been estimated by photolyzing a solution of Cl_2 in 3MP glass at 77°K until *ca.* 95% of the Cl_2 absorption was bleached, allowing it to stand at 77°K for several days during which the absorption at 260 nm and a new esr spectrum (see next section) grew. Assuming that the 260-nm peak and the esr spectrum represent the same species, an extinction coefficient of 6.5×10^4 M^{-1} cm^{-1} at 260 nm and 1.5×10^4 M^{-1} cm^{-1} at 330 nm were calculated from the optical density measurements and the concentration measured by esr.

None of the expected products of photolysis (alkyl radicals, Cl atoms, HCl, and alkyl chlorides) has an absorption peak at 260 nm. The growth characteristics of the peak suggest that the species responsible must be formed by the encounter of diffusing radicals or molecules produced by the photolysis with each other or with Cl_2. To test the possibility that the absorption is due to a charge-transfer complex like RCl–Cl_2 or HCl–Cl_2, samples of 3MP containing 10^{-3} mole fraction (mf) HCl and 5×10^{-4} mf 1-chlorohexane were observed spectrophotometrically at 300°K and 77°K both with and without 4×10^{-4} mf Cl_2 present. Spectra of the Cl_2-containing samples were also recorded at 82 and 90°K. In no case did the 260-nm peak appear.

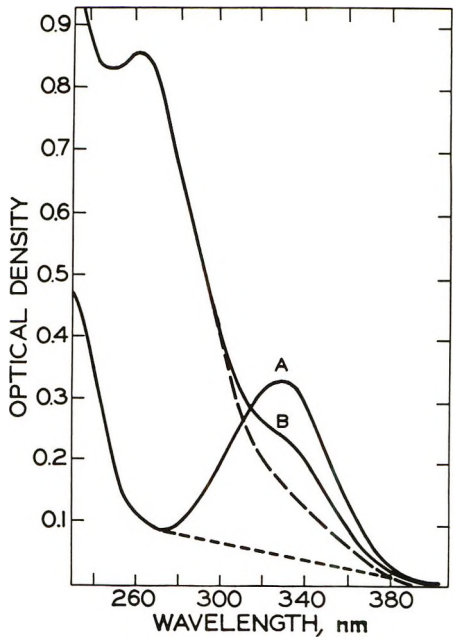

Figure 2. Growth of 260-nm absorption during photolysis of 1.7×10^{-3} mf Cl_2 in 3MP glass at 83°K: A, before photolysis; B, after 10-min photolysis. Upper dashed line is extrapolation of absorption by 260-nm species following photolysis. Lower dashed line is approximate OD of cell filled with pure 3MP.

To test the hypothesis that the 260-nm peak is due to a complex between a free radical and Cl_2, samples from which most of the Cl_2 had been removed by photolysis were observed. When such a sample which initially contained 2×10^{-3} mf Cl_2 in 3MP (initial OD at 330 nm 0.4) was raised to 82°K, the OD at 260 nm grew to 0.3 in 15 min. A similar sample containing 3.4×10^{-3} mf Cl_2 with an initial OD of 0.68 was photolyzed for a sufficient time to give a change in the OD at 330 nm of 0.45 which was approximately the same as the change induced in the first sample. Thus, after photolysis, the two samples contained about the same concentrations of free radicals and of HCl but the second sample contained about 1×10^{-3} mf Cl_2 whereas the first contained very little Cl_2. When the temperature of the second sample was raised from 77 to 82°K, the OD at 260 nm increased to 3.5 within 10 min. These and similar experiments with different chlorine concentrations and times of illumination indicate that the 260 nm absorption is not due to a complex between free radicals and HCl and suggest that it may be due to a complex between free radicals and Cl_2.

If free radicals can react with Cl_2 to form the species

(17) G. E. Gibson and N. S. Bayliss, *Phys. Rev.*, **44**, 188 (1933).

(18) M. Anbar and I. Dostrovsky, *J. Chem. Soc.*, 1106 (1954).

(19) A. Popov and J. J. Mannion, *J. Amer. Chem. Soc.*, **74**, 222 (1952).

(20) L. S. Lippin, *J. Gen. Chem., USSR*, **22**, 795 (1952).

which absorbs at 260 nm, this peak would be expected to grow in γ-irradiated samples of 3MP glass containing Cl_2. A sample of 3MP at 77°K containing 7×10^{-4} mf chlorine was exposed to a 50-sec γ dose of 4×10^{18} eV g^{-1}. After raising the temperature to 82°K, the 260-nm peak grew slowly to an OD of 0.35, as compared to a value of 2 in photolyzed samples having about the same chlorine and radical concentrations.

Rate constants at 77°K for reactions of O_2 with 3-methylpentyl radicals produced by γ irradiation of 3MP to form 3-methylpentyl peroxy radicals at 77°K and of Cl_2 with such radicals to form the species which absorbs at 260 nm are 10^{-1} M^{-1} sec^{-1} and 5.5×10^{-2} M^{-1} sec^{-1}, respectively,[10] assuming random distribution of the radicals, the O_2, and the Cl_2. In the presence of a large excess of O_2 or Cl_2 the kinetics are pseudo-first order. The rate of diffusion of the free radicals is negligible compared to that of the O_2 or Cl_2. It is not clear why the rate of radical conversion by Cl_2 is faster for the photochemically produced radicals than the γ-produced radicals, although the difference is in the direction to be expected if the γ-produced radicals are grouped in localized "spurs."

Free Radical Production. A 5-min photolysis of 9×10^{-4} mf Cl_2 in 3MP glass at 77°K in a 3-mm i.d. esr tube in the esr cavity, using the monochrometer, produced radicals giving a spectrum very similar to that of the secondary 3-methylpentyl radical[21] produced in 3MP glass by γ radiolysis or by photolysis of HI[22] (Figure 3, 1 mW). This spectrum shows a change in structure when the power is increased from 1 to 7 mW, which is not observed for radicals produced by the other methods, and is strongly saturated at 90 mW (Figure 3). The γ radiolysis of 3MP glass containing 9×10^{-4} mf Cl_2 to a dose of 2×10^{19} eV g^{-1} gave the

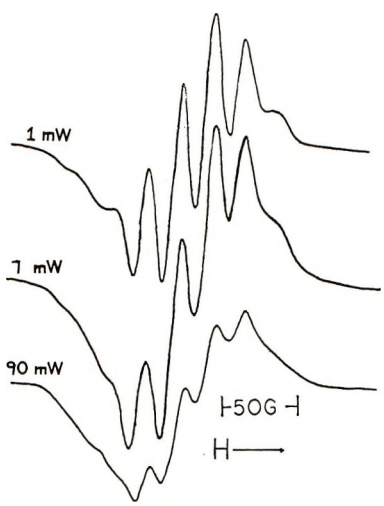

Figure 3. Esr spectra of 3MP glass containing 9.1×10^{-4} mf Cl_2, following 5-min photolyses at 330 nm and 77°K. Comparison of the three spectra illustrates the effect of increasing microwave power. The signal level settings were 200, 125, and 80, respectively for the 1-, 7-, and 90-mW spectra. The modulation amplitude was 1.4 G in each case.

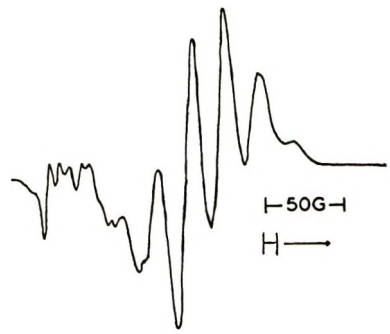

Figure 4. Esr spectrum of 3MP glass containing 9×10^{-4} mf Cl_2 following γ dose of 2×10^{19} eV g^{-1} at 77°K. Signal level, 125; modulation amplitude 1.4 G; power 7 mW.

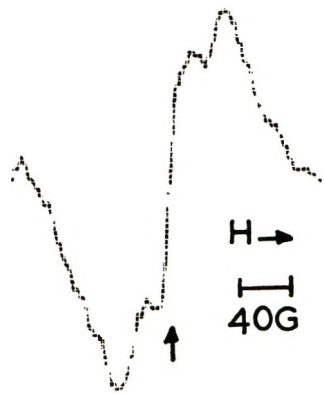

Figure 5. Esr spectrum of 3MP glass at 77°K containing 9.1×10^{-4} mf Cl_2, following photolysis for 30 min and standing for 72 hr. Signal level, 200; modulation amplitude 2.2 G; power 15 mW. The arrow indicates $g = 2.003$.

secondary 3-methylpentyl radical signal (Figure 4) with an additional low-field signal which may be attributable to Cl_2^-, which has previously been observed in cyclohexane matrices containing Na and Cl_2.[23] Photolyzed samples of Cl_2 in 3MP glass did not give any signal in the range of 3000–6000 G attributable to chlorine atoms. Such reactive atoms would not be expected to persist in the matrix, but absence of an esr signal cannot be taken as proof of their absence.[24]

When a glassy sample of Cl_2 in 3MP which had been photolyzed was allowed to stand in the dark at 77°K, its esr spectrum gradually changed from the six-line structure toward a broad singlet (Figure 5). This is similar to the structure obtained from the onset of photolysis of Cl_2 in 3MP at 83°K. The change at 77°K to the broad singlet structure occurs in parallel with the growth of the optical absorption peak at 260 nm described in the preceding section. When the sample

(21) D. Henderson and J. E. Willard, *J. Amer. Chem. Soc.*, **91**, 3014 (1969).

(22) S. Aditya and J. E. Willard, *ibid.*, **88**, 229 (1966).

(23) J. E. Bennett, B. Mile, and B. Ward, *J. Chem. Phys.*, **49**, 5556 (1968).

(24) For references, see S. Aditya and J. E. Willard, *ibid.*, **44**, 833 (1966).

which has developed the broad singlet is photolyzed with 260-nm radiation the spectrum returns to that of Figure 3a without change in the area under the absorption curve obtained by integration, while the 260-nm absorption peak disappears.

Quantum Yields. The quantum yields for consumption of Cl_2, production of free radicals, and production of alkyl chlorides during the photolysis of Cl_2 in 3MP at 77°K are 0.72 ± 0.09, 0.01, and 0.5, respectively (Table I). No $C_{12}H_{26}$ peak was found in the gas chromatographic analysis, setting an upper limit of 0.005 on its quantum yield. Yields of Cl_2 consumption at higher temperatures are given in Table II.

Table I: Quantum Yields at 77°K

I_a, photons sec^{-1} cc^{-1} $\times 10^{-16}$	Φ, $(-Cl_2)$	I_a, photons sec^{-1} cc^{-1} $\times 10^{-16}$	Φ, $(-Cl_2)$	Φ, (rad)	Φ, (RCl)
In 1-cm² Quartz Cell		In Esr Optical Cell			
0.21	0.78	5.47	0.86	0.012	
0.28	0.70	5.85	0.75	0.0094	
0.27	0.60	6.62	0.71	0.012	
0.43	0.80	7.3	0.58	0.014	
0.49	0.60	8.3	0.74	0.020	
0.82	0.65	8.8	0.57	0.009	
1.05	0.90	9.0	0.64	0.017	
1.11	0.94		0.57	0.0094	0.47
1.15	0.72		0.64	0.017	0.61
1.36	0.70	Av	0.67	0.013	0.54
1.41	0.90				
1.57	0.74				
Av	0.75				

Table II: Quantum Yields of Cl_2 Consumption as a Function of Temperature

T, °K	$[Cl_2]$, M	I_a, photons sec^{-1} cc^{-1} $\times 10^{-16}$	Φ, $(-Cl_2)$
300[a]	3.35×10^{-3}	0.0067	1.9×10^4
300	1.15×10^{-2}	0.050	1.2×10^4
199[a]	5.6×10^{-3}	0.023	5.1×10^3
97[a]	4.8×10^{-3}	0.27	270
87	1.3×10^{-2}	5.2	4.2
83	1.7×10^{-2}	6.2	2.2
80	1.3×10^{-2}	3.2	1.5
77[a]	4×10^{-3}	0.27	0.7

[a] In 1-cm² cell, others in esr optical cells.

Dependence of Rate of Cl_2 Disappearance at 77°K on Absorbed Light Intensity. A plot of log $d[Cl_2]/dt$ *vs.* log I_{ab} (Figure 6) shows that the rate of Cl_2 disappearance is proportional to the first power rather than the square root of the rate of light absorption. This indicates either that: (1) there is negligible chain reaction at 77°K; or (2) the chains are terminated by some process other than a combination of chain carriers; or (3) chain propagation is so slow at 77°K that most of the growing chains are not terminated within the time of the experiment.

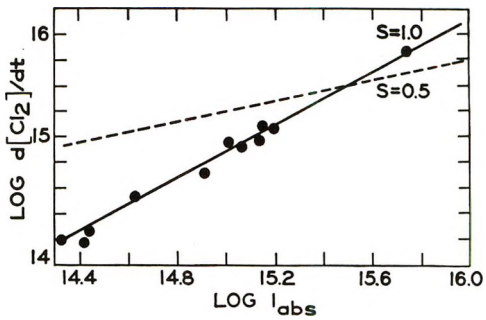

Figure 6. Dependence of rate of Cl_2 disappearance at 77°K on light intensity. The values of I_{ab} range from 0.2×10^{15} to 1.5×10^{16} photons absorbed sec^{-1} cc^{-1} in the 1-cm² cell, to 5.5×10^{15} photons sec^{-1} cc^{-1} in the esr optical cell. The slope of the solid line is 1.0 and that of the dotted line 0.5.

Identification of Alkyl Chlorides. Three gas chromatographic peaks, assignable to $C_2H_5CCl(CH_3)C_2H_5$ (bp 116°, retention time 21 min), $CH_3CHClCH(CH_3)$-C_2H_5 (retention time 23 min), and $C_2H_5CH(CH_2Cl)$-C_2H_5 (bp 126°, retention time 27 min), were observed. Presumably $CH_2ClCH_2CH(CH_3)C_2H_5$, which is expected to have the highest boiling point, was eluted under the 3-chloromethylpentane peak. At 300 and 77°K the absolute yields were secondary > primary > tertiary, with the secondary being more highly favored relative to the primary and tertiary at 77°K. Enhanced selectivity for removal of secondary hydrogen atoms from 3MP in the glassy state as compared to the gas has also been noted in previous studies.[21]

Decay of 3-Methylpentyl Radicals Formed by Cl_2 Photolysis at 77°K. The trapped 3-methylpentyl radicals formed by photolysis of Cl_2 in 3MP glass at 77°K (Table I) decay by composite first order kinetics (Figure 7); *i.e.*, the decay curves for samples with different initial concentration are superimposable after normalization for dose, indicating either that each radical is formed adjacent to another radical with which it is predestined to combine

$$Cl_2 + 2C_6H_{14} \xrightarrow{h\nu} 2C_6H_{13} + 2HCl \quad (6)$$

$$2C_6H_{13} \longrightarrow C_{12}H_{26} \quad (7)$$

or that the radicals are removed by reaction with the diffusing Cl_2 molecules which are present in large excess. In the two experiments of Figure 7 the initial Cl_2 concentration was 9.1×10^{-4} mf and the more intense photolysis decreased this only to 8.5×10^{-4} mf so the Cl_2 concentration was essentially the same during decay of both samples. In experiments with equal initial radical concentrations but different Cl_2 concentrations

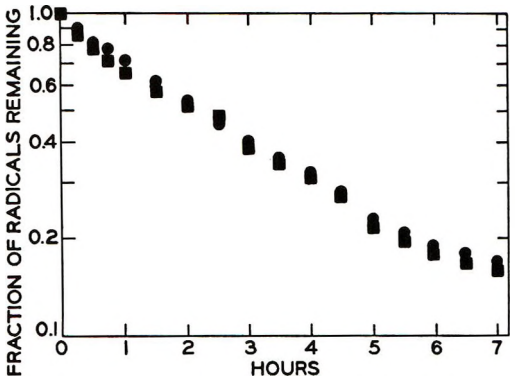

Figure 7. Decay of 3-methylpentyl radicals formed by Cl_2 photolysis at 77°K. Both samples were prepared by illumination of the sample with the AH4 lamp at the same distance, using a Pyrex filter. In one case the sample was outside the esr cavity and in the other inside, giving a factor of 2 difference in the initial radical concentrations, which have been normalized in the plot.

the decay rate was always faster at the higher Cl_2 concentration.

Discussion

Quantitative Yields and Mechanism at 77°K. The quantum yield of 0.7 for Cl_2 disappearance at 77°K (Table I) indicates that some Cl_2 molecules which are activated by 330-nm radiation in 3MP glass at this temperature are deactivated without reacting. Most of the Cl_2 molecules which react with the 3MP must do so in a concerted reaction

$$Cl_2^* + C_6H_{14} \longrightarrow C_6H_{13}Cl + HCl \qquad (8)$$

or in a two-step process involving a radical intermediate which does not last long enough for esr measurement

$$C_6H_{14} + Cl^* \longrightarrow C_6H_{13} + HCl \qquad (9)$$

$$C_6H_{13} + Cl \longrightarrow C_6H_{13}Cl \qquad (10)$$

since the yield of trapped radicals is only 0.01 while the yield of $C_6H_{13}Cl$ is 0.5.

In considering the effect of temperature on the quantum yield of Cl_2 disappearance, it is necessary to bear in mind that the yield is the sum of the yield of the concerted reaction, plus the yield of chain initiation multiplied by the chain length. From 300°K to 97°K where 3MP is "fluid" there is reason to believe that every photon absorbed produces 2 Cl atoms and every Cl atom initiates a chain. In this region the quantum yield decreases with decreasing temperature because the activation energy of the chain-carrying steps is greater than that of the chain terminating steps. The Arrhenius factor is *ca.* 1 kcal mol^{-1} for both the interval from 300 to 199°K and that from 199 to 97°K. At lower temperatures, as the viscosity[25] changes from 2.5×10^3 P at 97°K to $10^{12.5}$ P at 77°K, effects in addition to the difference between the activation energies of the chain-carrying and chain-terminating steps contribute to reduction in the quantum yield. The Arrhenius factors for the 97–87°K and 87–77°K intervals are 6 kcal mol^{-1} and 3 kcal mol^{-1}, respectively. Effects which certainly play a role are the deactivation of Cl_2^* without reaction and the onset of the concerted reaction where one Cl_2^* forms one $C_6H_{13}Cl$ and one HCl without initiating a chain reaction.

A third effect may be that chain propagation is so slow in the highly viscous media that it continues after termination of illumination and was not complete at the times the measurements at 97°K and below were made. Each time a C_6H_{13} radical is formed, completion of the next step in the chain requires that a Cl_2 molecule diffuse to the radical. The diffusion coefficient of Cl_2 in 3MP glass at 77°K is estimated[10] to be 1.4×10^{-16} cm^2 sec^{-1}. In one experiment at 97°K evidence for continuing chain propagation after illumination was observed by a decrease in optical density at 330 nm during several minutes following illumination.

Nature of the 260-nm Species. An additional factor which may affect the chain propagation rate at 77–87°K is the reaction intermediate indicated by the optical absorption at 260 nm (Figure 2) and new esr spectrum (Figure 5). Since growth of the 260-nm spectrum is coupled with a loss of resolution of the esr spectrum of the 3-methylpentyl radicals while bleaching of the 260-nm radiation regenerates the well resolved radical spectrum, and since the spectrum is not due to stable products of photolysis, our best hypothesis attributes it to a charge-transfer complex between a C_6H_{13} radical and a Cl_2 molecule. The complex forms slowly at 77°K due to the slowness of diffusion of Cl_2 to radicals. It is stable from hours to minutes in the 77–87°K range, and according to the hypothesis, converts to $C_6H_{13}Cl + Cl$ by reaction 12 above 87°K or on photolysis at 260 nm.

$$C_6H_{13} + Cl_2 \longrightarrow C_6H_{13}\cdot Cl_2 \qquad (11)$$

$$C_6H_{13}\cdot Cl_2 \longrightarrow C_6H_{13}Cl + Cl \qquad (12)$$

$$Cl + C_6H_{14} \longrightarrow C_6H_{13} + HCl \qquad (13)$$

As would be expected from this scheme, the 260-nm peak and broad esr spectrum grew back when the sample was allowed to stand in the dark after they had been removed by photolysis at 260 nm. The stability of such a complex is unexpected, but is at present the most plausible explanation for the observed phenomena.

(25) A. C. Ling and J. E. Willard, *J. Phys. Chem.*, 72, 1918 (1968).

Photocatalytic Reaction on Zinc Oxide. II. Oxidation of Carbon Monoxide with Nitrous Oxide and Oxygen

by Ken-ichi Tanaka[1] and George Blyholder*

Department of Chemistry, University of Arkansas, Fayetteville, Arkansas 72701 *(Received August 26, 1971)*

Publication costs borne completely by The Journal of Physical Chemistry

The photocatalytic and thermal catalytic oxidations of carbon monoxide with nitrous oxide and oxygen were studied on zinc oxide. The thermal catalytic reaction of carbon monoxide with nitrous oxide is first order in carbon monoxide pressure and zero order in nitrous oxide pressure. The reaction with nitrous oxide is strongly retarded by oxygen, even though the overall rate of carbon dioxide formation is not changed by the addition of oxygen. In contrast, the photocatalytic reaction of carbon monoxide with nitrous oxide obeys the kinetic expression $r = k'P_{N_2O}^{0.4}P_{CO}^{0.4}$ and is not retarded by the addition of oxygen. The photocatalytic reaction of carbon monoxide with oxygen is half-order in oxygen pressure and zero order in carbon monoxide pressure, *i.e.*, $r = k''P_{O_2}^{1/2}P_{CO}^{0}$. It is suggested that the slow steps of the thermal catalytic reactions of CO with O_2 and CO with N_2O are the reaction of weakly adsorbed carbon monoxide with the intermediate species O^- on interstitial zinc atoms or ions, while under illumination, the slow step of the reaction of CO with O_2 is the formation of O^- species and that of the reaction of CO with N_2O is the reaction between N_2O^- and CO^+ on sites produced by illumination. Carbon dioxide retards the reactions of CO with N_2O and with O_2 in the dark but only slightly retards the reactions under illumination.

Introduction

The photoeffects on the adsorption and/or desorption of oxygen[2] and the enhancement of catalytic activities for oxidation reactions[3,5] have been observed on zinc oxide and other semiconductor-type oxides. These photoeffects are qualitatively explainable by the electronic theory of catalysis. Reactions of carbon monoxide with oxygen on zinc oxide in the dark and under illumination have been studied by several investigators. However, the conductivity changes of the oxide during the reaction and the kinetics in the dark and under illumination measured by various workers have not always agreed with each other.[4-6]

We have previously found[7] that illumination changes the kinetics of the decomposition of nitrous oxide taking place on zinc oxide. The thermal catalytic decomposition of nitrous oxide on zinc oxide obeys a first-order rate equation, $r = kP_{N_2O}$, while the photocatalytic decomposition of nitrous oxide is described by completely different kinetics, $r = kP_{N_2O}/(1 + K_1P_{N_2O} + K_2P_{O_2}^{1/2})$. Both the thermal and photoreactions take place simultaneously over zinc oxide under illumination. On the basis of these results, it has been suggested that the thermal catalytic and the photocatalytic reactions proceed by different mechanisms involving different intermediates. If this rationalization is generally true, the reaction of nitrous oxide with other molecules such as carbon monoxide may be expected to proceed by different mechanisms on zinc oxide under dark and illuminated conditions.[8] To further examine this supposition and the behavior of surface intermediates, the reactions of CO with N_2O, CO with O_2, and the competitive reaction of CO with N_2O and O_2 have been studied over zinc oxide under dark and illuminated conditions. From the kinetic studies of these four reactions plus some competitive reaction experiments a better understanding of reaction mechanisms and intermediates on zinc oxide in the dark and under illumination can be obtained. The results are discussed from the point of view of the electronic theory of semiconductor catalysts.

Experimental Section

The closed circulating system, the high-pressure mercury lamp (Osram HBO 500) light source, and 2.00-g Kadox-25 zinc oxide sample are the same as those used previously,[7] except that the total volume of the apparatus is increased by the inclusion of a trap. Nitrous oxide was purified by freezing at liquid air tem-

(1) On leave from Tokyo Institute of Technology, Meguro-ku, Tokyo.

(2) Y. Fujita and T. Kwan, *Bull. Chem. Soc. Jap.*, **31**, 379 (1958); T. I. Barry and F. S. Stone, *Proc. Roy. Soc., Ser. A*, **255**, 124 (1960).

(3) I. Komuro, Y. Fujita, and T. Kwan, *Bull. Chem. Soc. Jap.*, **32**, 884 (1959); A. Berna, *J. Phys. Chem.*, **68**, 2047 (1964); T. S. Narjunan and J. G. Calvert, *ibid.*, **68**, 17 (1964); unpublished data; hydrogenation of olefins and decomposition of formic acid on zinc oxide are not promoted by illumination.

(4) H. Horiguchi, M. Setaka, K. M. Sancier, and T. Kwan, The 4th International Congress on Catalysis, Moscow, 1968.

(5) W. Doerffler and K. Hauffe, *J. Catal.*, **3**, 171 (1964); **3**, 156 (1964).

(6) F. Romero-Rossi and F. S. Stone, The 2nd International Congress on Catalysis, Paris, 1960.

(7) K. Tanaka and G. Blyholder, *Chem. Commun.*, 1133 (1970); K. Tanaka and G. Blyholder, *J. Phys. Chem.*, **75**, 1037 (1971).

(8) K. Tanaka and G. Blyholder, *Chem. Commun.*, 736 (1971).

perature and subliming at Dry Ice–methanol temperature. Oxygen and carbon monoxide from commercial cylinders were purified by passage through a liquid air trap.

The reaction of nitrous oxide with carbon monoxide, $CO + N_2O \rightarrow CO_2 + N_2$, was followed by gas chromatographic analysis of nitrogen, and the competitive reaction of carbon monoxide with nitrous oxide and oxygen was followed by the analysis of nitrogen and oxygen using a molecular sieve 5-A column. The reaction of CO with O_2 was followed by both CO_2 and O_2 analysis to verify the reaction stoichiometry. The CO_2 was analyzed by using a silica gel chromatographic column. To remove surface contamination new zinc oxide was oxidized with oxygen overnight above 400°, then evacuated to 10^{-5} Torr for several hours at the same temperature, and cooled to reaction temperature in a vacuum. This catalyst has very high initial activity for the reaction of CO with N_2O, but the activity decreases to a stable value after several runs, and a reproducible activity is obtained if the evacuation time between runs is kept constant. Kinetics of the thermal catalytic reaction were studied over the stabilized zinc oxide using 1-hr evacuations at the reaction temperatures between runs. The photocatalytic reaction was studied over oxide which was stabilized by evacuation with illumination for 10 min between runs. When other than these evacuation times were used, the evacuation time is noted with the experimental result. To avoid complications due to retardation by product CO_2, the initial rates were used to derive rate equations.

Results

1. Reactions on Fresh Zinc Oxide. The initial high catalytic activity of the zinc oxide immediately after the pretreatment described above but before stabilizing runs was found to be distinctively different from the activity after stabilization.

When nitrous oxide alone was introduced on the fresh zinc oxide at 195°, the decomposition of nitrous oxide was very slow, but addition of carbon monoxide resulted in an abrupt nitrogen evolution followed by a slow reaction as shown in Figure 1A. This behavior was reproducible on the fresh zinc oxide. To confirm that the presence of nitrous oxide is necessary for the reaction of carbon monoxide to produce the abrupt nitrogen evolution, nitrous oxide was contacted with the fresh zinc oxide and removed from the gas phase by a liquid air trap, after which carbon monoxide was added. No detectable reaction occurred until the nitrous oxide was vaporized, but then the abrupt nitrogen evolution followed by slow reaction occurred as shown in Figure 1B.

The abrupt nitrogen evolution in the initial stage of the reaction is characteristic of the reaction on fresh zinc oxide, that is, the rapid initial evolution does not appear after the second run over the same oxide when

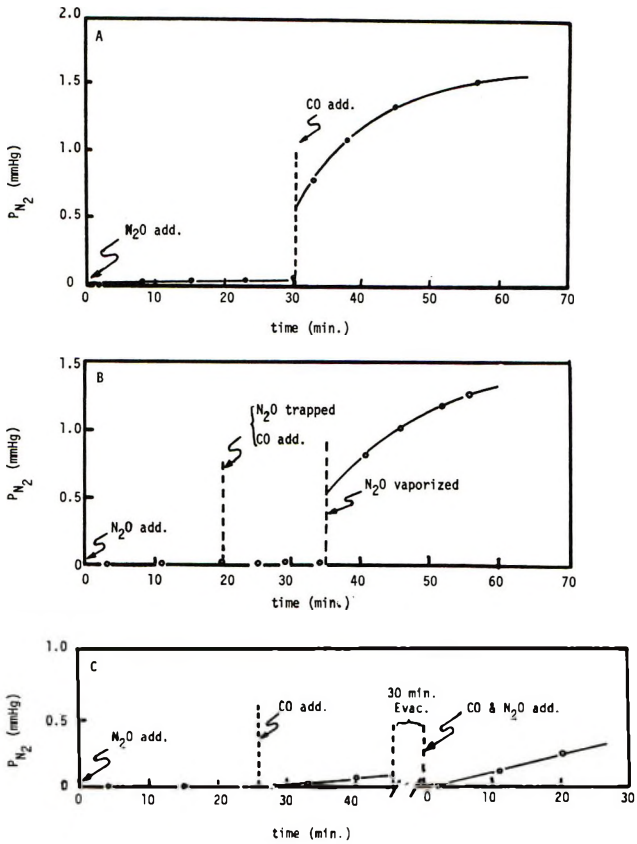

Figure 1. The dark reaction of N_2O with CO on fresh pretreated zinc oxide. (A) At 195° N_2O at 26.1 mm was introduced at time zero, and at the dotted line, CO at 16.4 mm was added. (B) At 196° N_2O at 18.8 mm was added at time zero. At the first dotted line, N_2O was trapped and CO at 19.4 mm was added. The N_2O was vaporized at the second dotted line. (C) At 186° N_2O at 16.6 mm was introduced at time zero over CO_2 poisoned zinc oxide which had been evacuated for 2 min. At the first dotted line, CO at 22.8 mm was added. After 30-min evacuation, N_2O at 22.2 mm and CO at 26.3 mm were added.

the evacuation time between runs is short. A series of runs with different evacuation times between runs of 1, 3, 16, 18, and 24 hr were made on a single catalyst sample at 202–203°. The amount of nitrogen evolved in the initial stage of the reaction increases with the evacuation time. However, the amount of the rapid evolution observed for 24-hr evacuation is less than one-fifth of that on the fresh catalyst.

It was found that the initial rapid nitrogen evolution on the fresh zinc oxide is inhibited by the adsorption of carbon dioxide. The addition of 2.1 mm of carbon dioxide for 10 min followed by 2–30 min evacuation completely inhibits the initial rapid reaction on the fresh zinc oxide, but the slow reaction is observed and its rate is greater when the evacuation time between runs is longer as shown in Figure 1C. A reproducible activity is obtained when the evacuation time between runs is kept constant.

2. Thermal Catalysis on Stabilized Zinc Oxide. Kinetics of the thermal catalytic reaction of nitrous

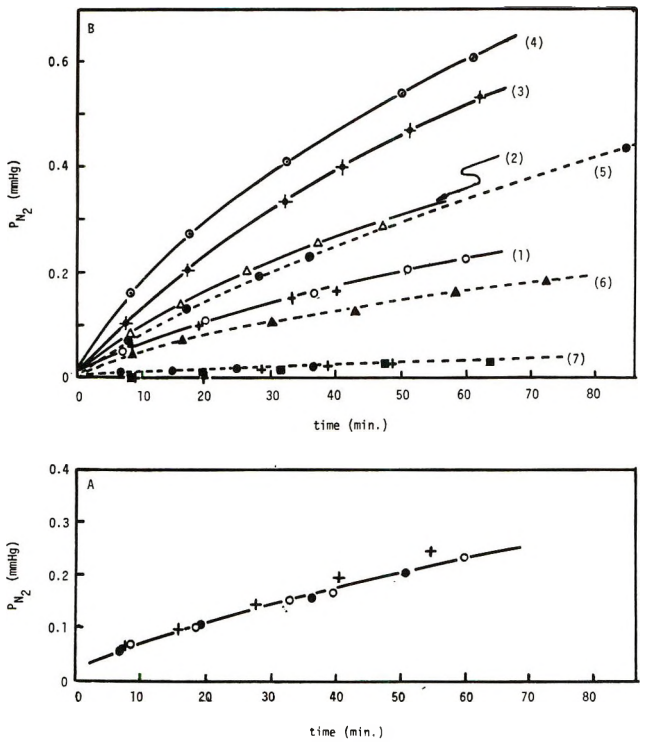

Figure 2. The reaction of CO with N_2O on stabilized zinc oxide in the dark. (A) Effect of N_2O pressures at 202°: +, P_{CO} (mm) 16.2, P_{N_2O} (mm) 69.4; ○, 16.9, 12.1; ●, 17.0, 19.6. (B) Effect of CO pressures at 203 ± 1°: (1), P_{CO} (mm) 17.0 and 16.9, P_{N_2O} (mm) 19.6 and 12.1; (2), 29.4. 25.1; (3), 35.4, 39.1; (4), 60.6, 17.3. The retardation effect of oxygen at 203° (dotted lines): (5), P_{CO} (mm) 16.0, P_{N_2O} (mm) 32.6, P_{O_2} (mm) 0; (6), 19.2, 27.7, 0.19; (7), 28.3, 16.5, and 19.1, 26.8, 34.4, and 33.1, 1.0, 2.3, and 3.3.

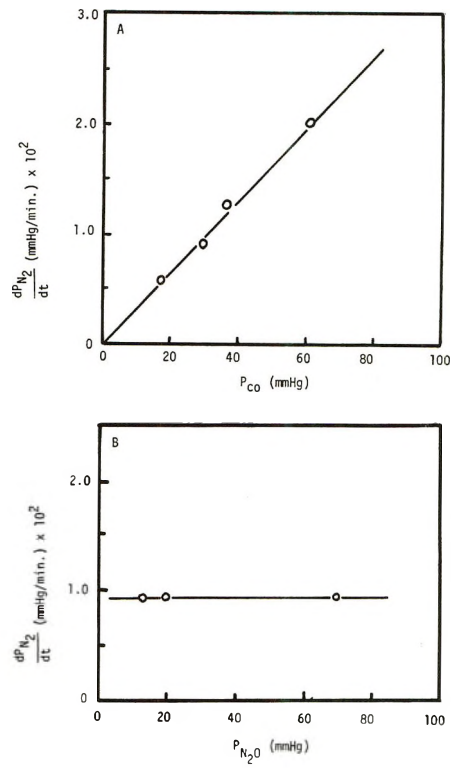

Figure 3. The pressure dependences of initial reaction rates of CO with N_2O at 203 ± 1° in the dark.

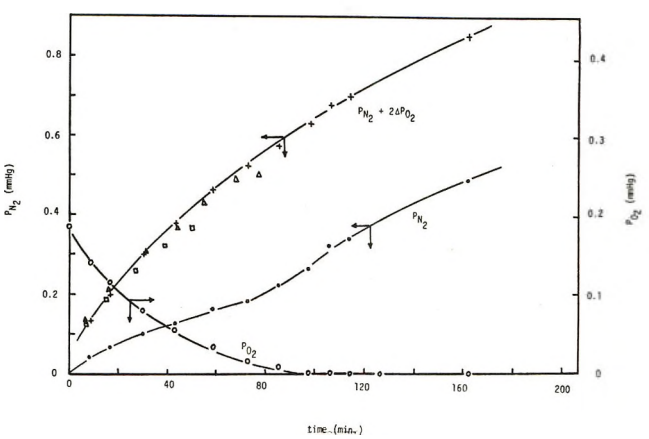

Figure 4. The competitive reaction of CO with N_2O and O_2 at 204° in the dark over the stabilized zinc oxide evacuated 16 hr. Initial pressures: P_{CO} = 19.2 mm, P_{N_2O} = 27.7 mm, P_{O_2} = 0.19 mm. ●, total reaction, $P_{N_2} + 2\Delta P_{O_2}$ where ΔP_{O_2} is the decrease in oxygen pressure. △,□, the reactions without oxygen: △, P_{CO} = 17.8 mm, P_{N_2O} = 23.1 mm, on surface evacuated 18 hr; □, P_{CO} = 16.9 mm, P_{N_2O} = 29.1 mm, on surface evacuated 16 hr.

oxide with carbon monoxide were studied over stabilized zinc oxide which was evacuated for 1 hr between runs to give a reproducible state. Figure 2A shows time courses of the reaction at 202° with initial pressures of nitrous oxide of 12.1, 19.6, and 69.4 mm and approximately constant initial pressures of carbon monoxide of 16.9, 17.0, and 16.2 mm, respectively. Nitrous oxide pressure is seen to have no influence on the time course of the reaction.

Figure 2B shows time courses of the reaction with various initial pressures of carbon monoxide, 17.0, 16.9, 29.4, 35.4, and 60.6 mm at about 203°. The pressure dependences of the reaction rate derived from the initial slopes of these time course curves are plotted in Figures 3A and B to show that the thermal catalytic reaction is zero order in nitrous oxide and first order in carbon monoxide.

The thermal catalytic reaction of nitrous oxide with carbon monoxide is markedly retarded by oxygen, *i.e.*, oxygen pressures less than 1 mm effectively retard the reaction of CO with N_2O as shown in Figure 2B with dotted lines. To get further information about the intermediate species of the oxidation reaction of carbon monoxide during catalysis, a competitive reaction of CO with N_2O and O_2 was carried out over a stabilized zinc oxide evacuated 16 hr at about 204° as shown in Figure 4. The reaction of CO with N_2O accelerates when oxygen is completely removed from the gas phase by the reaction with CO, but the overall carbon dioxide formation gives a smooth curve. The overall CO_2 production is obtained from the raw data by calculating the CO_2 pressure as the sum of the N_2 pressure plus twice the decrease in O_2 pressure as dictated by the stoichiome-

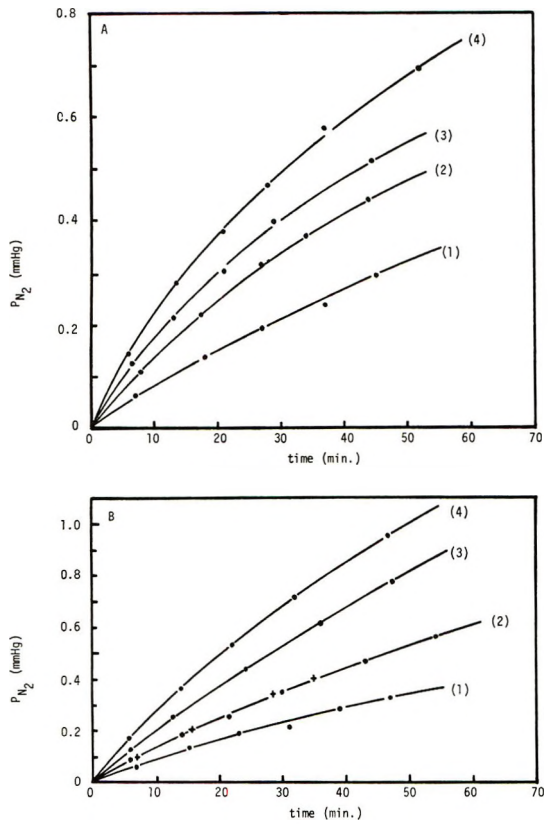

Figure 5. The reaction of CO with N_2O on the illuminated zinc oxide. A, effect of CO pressures at 203 ± 1°: (1), P_{CO} (mm) 6.2, P_{N_2O} (mm) 24.2; (2), 19.1, 25.3; (3), 50.6, 25.0; (4), 81.1, 25.0. B, Effect of N_2O pressures at 203 ± 1°: (1) P_{CO} (mm) 16.8, P_{N_2O} (mm) 7.4; (2), 17.3 and 17.5, 21.4 and 21.0; (3), 17.2, 58.1; (4), 17.4, 126.3.

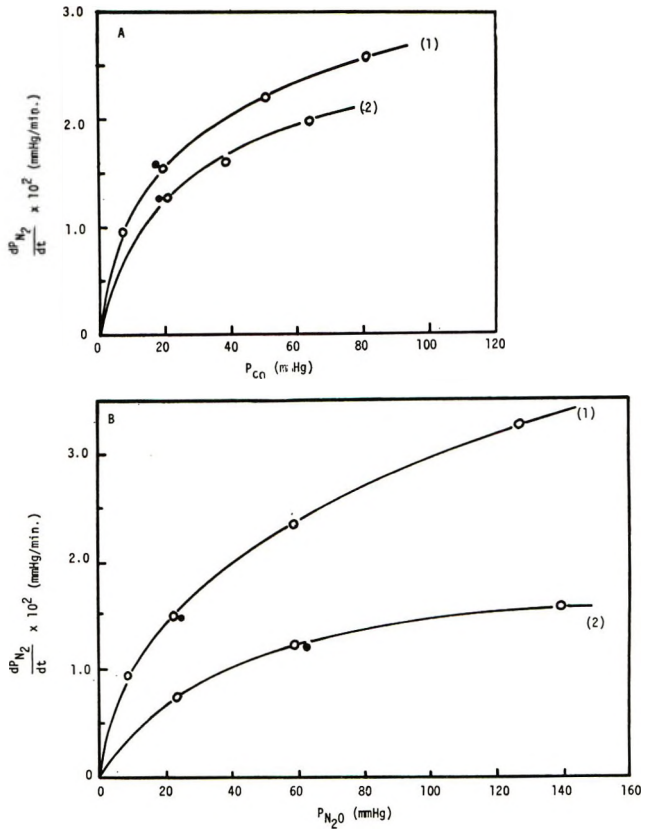

Figure 6. The pressure dependence of the reaction of CO with N_2O under illumination. A, Dependence on carbon monoxide pressures at constant N_2O pressures: (1), P_{N_2O} = 24.2–25.3 mm, 203–204°; (2), P_{N_2O} = 60.5–64.0 mm, 192–193°. Solid circles; estimated values from (B). B, Dependence on nitrous oxide pressures at constant CO pressures: (1), P_{CO} = 16.8–17.5 mm, 201–204°; (2) P_{CO} = 17.5–18.5 mm, 193°. Solid circles; estimated values from (A).

tries of the reactions, $P_{N_2} + 2\Delta P_{O_2}$. The overall reaction curve obtained in the competitive reaction is identical with the reaction curves obtained in the absence of oxygen on similar catalysts (16- and 18-hr evacuations) plotted in Figure 4 with squares and triangles.

3. Photocatalysis on Stabilized Zinc Oxide. Kinetics of the reaction of N_2O with CO were also studied over illuminated zinc oxide. The zinc oxide was evacuated for 10 min between runs with illumination at the reaction temperatures. The time course of the reaction at about 203° with various pressures of carbon monoxide from 6.2 to 81.1 mm and with approximately constant initial pressures of nitrous oxide around 25 mm are shown in Figure 5A, and the results of the reaction with various nitrous oxide pressures from 7.4 to 126.3 mm and with approximately constant pressures of carbon monoxide around 17 mm are shown in Figure 5B. Conspicuous features of the reaction under illumination are the pressure effects of carbon monoxide and nitrous oxide on the reaction rate and the retardation effect by product carbon dioxide. The pressure dependences of the reaction rate under illumination are shown in Figure 6A and B by using the initial slopes of the time course curves. These may be expressed by the equation $r' = k'P_{N_2O}^{0.4}P_{CO}^{0.4}$, which is in sharp contrast to the thermal catalytic reaction rate $r = kP_{CO}^{1.0}P_{N_2O}^{0}$.

To compare the photocatalytic reactions of CO with N_2O and O_2, the reaction of CO with O_2 was also carried out over illuminated zinc oxide. The results of the reaction at 109° with various oxygen pressures of 0.6 to 58.8 mm and approximately constant carbon monoxide pressures around 9 mm are shown in Figure 7A, and the results of the reaction at 203° with various carbon monoxide pressures from 6.0 to 73.2 mm and with approximately constant oxygen pressures around 18 mm are shown in Figure 7B. Figures 8A and B show the relations between the pressures and the reaction rate obtained from the initial slopes of the time courses. The relations indicate that the reaction rate under illumination is half-order in oxygen pressure and nearly zero order in carbon monoxide pressure above 20 mm, *i.e.*, $r = k''P_{O_2}^{1/2}P_{CO}^{0}$.

The smaller curvature of the time courses for the reaction of CO with N_2O under illumination (Figure 5) suggests a smaller retardation effect by carbon dioxide for the reaction under illumination compared to that in the dark. The effects of CO_2 and N_2O, which have

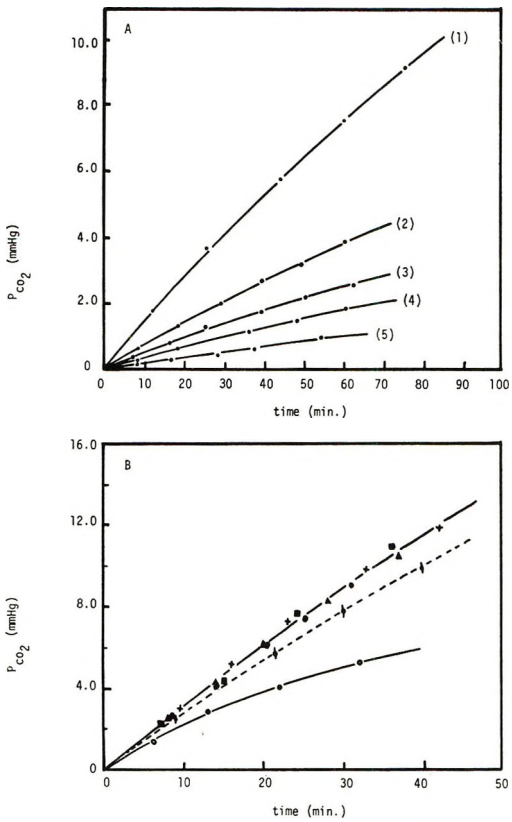

Figure 7. The reaction of CO with O_2 on illuminated zinc oxide. A, Effect on O_2 pressure at constant CO pressure at 109°: (1), P_{CO} (mm) 8.2, P_{O_2} (mm) 58.8; (2), 9.5, 14.9; (3), 8.7, 5.7; (4), 9.0, 3.0; (5), 8.8, 0.6. B, Effect of CO pressure at constant O_2 pressure and the effects of N_2O or CO_2 addition at 203°: ○, P_{O_2} = 18.1 mm, P_{CO} = 6.0 mm; ▲, P_{O_2} = 18.0 mm, P_{CO} = 21.5 mm; ●, P_{O_2} = 17.7 mm, P_{CO} = 42.5 mm; ■, P_{O_2} = 17.2 mm, P_{CO} = 73.2 mm; +, P_{O_2} = 19.8 mm, P_{CO} = 37.8 mm, P_{N_2O} = 5.4 mm; ⊕, P_{O_2} = 18.9 mm, P_{CO} = 19.4 mm, P_{CO_2} = 12.0 mm.

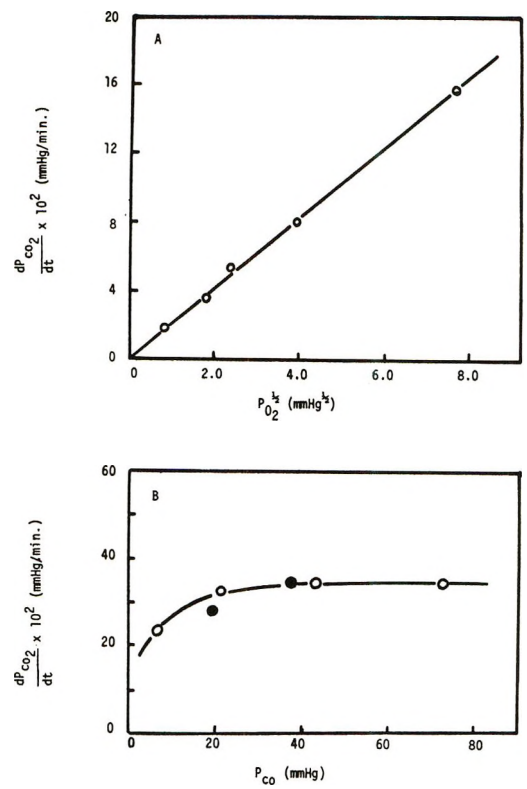

Figure 8. The pressure dependence of the reaction rate of CO with O_2 under illumination. A, Dependence on oxygen pressure at constant CO pressure at 109°. B, Dependence on carbon monoxide pressure at constant O_2 pressure at 203°: solid circles, the rates when CO_2 or N_2O are added.

similar electronic configurations, on the reaction of CO with O_2 were studied under illumination. The time course of the reaction with 12.0 mm carbon dioxide present is shown in Figure 7B with a dotted line, and the reaction rate obtained from the slope of the curve is plotted in Figure 8B with a solid circle. The result with 5.4 mm of nitrous oxide present is shown in Figure 7B with crosses. The results indicate a slight retardation by CO_2 but no retardation by N_2O on the reaction of CO with O_2 over zinc oxide under illumination.

The competitive oxidation of CO with N_2O and with O_2 was also studied over the illuminated zinc oxide. Figure 9 shows the result of the competitive reaction when only nitrous oxide pressures were changed from 22.4 (crosses) to 80.4 mm (open circles). When the nitrous oxide pressure is changed in the competitive reaction, the reaction rate between CO and N_2O is changed, but the reaction of CO with O_2 is not changed. Figure 10A shows the results of the competitive reaction when oxygen pressures are changed. The initial oxygen pressure has an obvious effect on the slope of the time courses of oxygen pressures but no effect on the reaction rate of nitrous oxide with carbon monoxide. Figure 10B shows results of the competitive reaction when carbon monoxide pressures are changed from 13.5 (open circles) to 50.4 mm (crosses). The pressure effect is readily noted on the time courses of nitrogen pressures but is negligible on the time courses of the oxygen pressures.

To get an apparent activation energy of the photocatalytic oxidation of carbon monoxide with oxygen, the reaction rates were measured at the temperatures of 214, 203, 171, 133, and 75° with approximately constant pressures of oxygen (11.1 to 11.4 mm) and of carbon monoxide (10.4 to 11.1 mm). The reaction at 203°, followed by gas chromatographic analysis of oxygen, and the reactions at the other temperatures, followed by gas chromatographic analysis of carbon dioxide, gave a linear Arrhenius plot. The apparent activation energy is approximately 5 kcal/mol.

Discussion

1. Thermal Catalytic Reactions. It is apparent from Figure 1 that two distinguishable reactions, one rapid and the other slow, occur on the fresh surface of zinc oxide and that the rapid reaction is strongly poisoned by carbon dioxide but is not poisoned by carbon monoxide. A notable difference of the rapid initial reaction from the following slow reaction is that the poisoning by CO_2

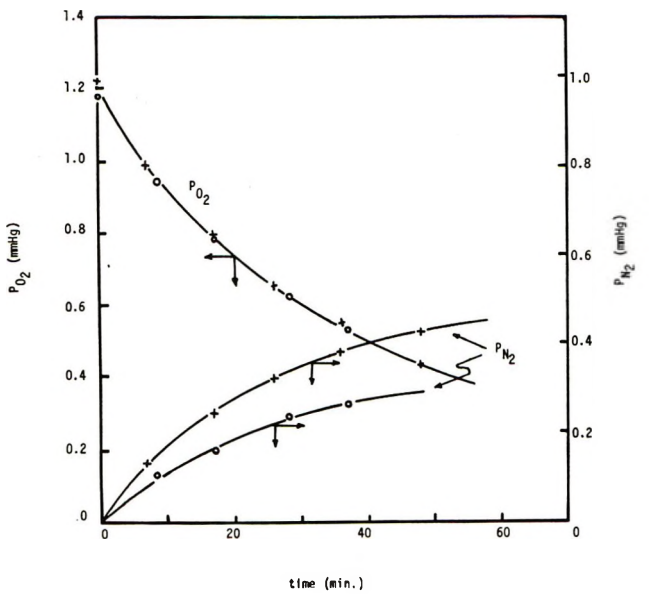

Figure 9. The competitive reaction of CO with N_2O and O_2 on the illuminated zinc oxide at 195°. N_2O pressures are changed. ●, P_{CO} = 14.6 mm, P_{O_2} = 1.2 mm, P_{N_2O} = 22.4 mm; +, P_{CO} = 13.9 mm, P_{O_2} = 1.2 mm, P_{N_2O} = 80.4 mm.

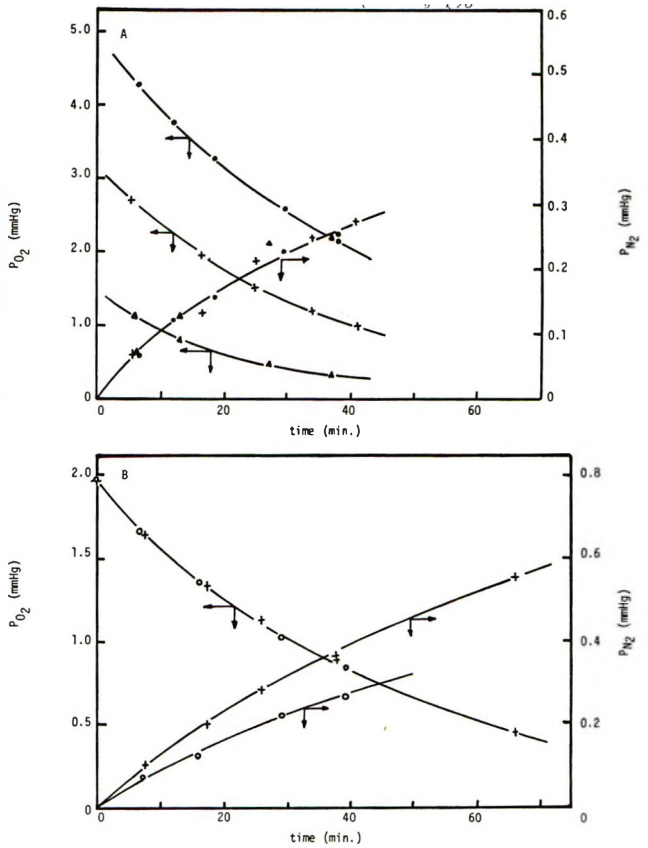

Figure 10. The competitive reaction on the illuminated zinc oxide at 190 (A) and 195° (B). A, O_2 pressures are changed: ●, P_{CO} = 20.4 mm, P_{N_2O} = 15.3 mm, P_{O_2} = 4.9 mm; +, P_{CO} = 19.9 mm, P_{N_2O} = 16.3 mm, P_{O_2} = 3.2 mm; ▲, P_{CO} = 20.5 mm, P_{N_2O} = 15.8 mm, P_{O_2} = 1.5 mm. B, CO pressures are changed: +, P_{CO} = 50.4 mm, P_{N_2O} = 33.3 mm, P_{O_2} = 1.9 mm; O, P_{CO} = 13.5 mm, P_{N_2O} = 33.9 mm, P_{O_2} = 1.9 mm.

of the rapid reaction is almost irreversible at around 200° but that for the slow reaction is reversible, that is, the active sites for the rapid reaction are blocked by the irreversible adsorption of carbon dioxide at the initial stage of the first run of the reaction. Thus, the rapid reaction observed at the initial stage of the first run can be ruled out of the discussion of catalysis in this paper.

A reversible retardation by carbon dioxide was also found in the reaction of CO with O_2 on zinc oxide.[9] The reversible retardation effects of carbon dioxide are well explained by the characteristics of carbon dioxide adsorbed on zinc oxide. Amigues and Teichner[10] found that the adsorption of carbon dioxide on a virgin zinc oxide is accompanied by neither acceptance nor donation of electrons, but that the adsorption of carbon dioxide on a surface with presorbed oxygen at 261° caused the reversible replacement of adsorbed oxygen and electrons release to the conduction band. Temperature-programmed desorption of oxygen from zinc oxides gives two peaks with maxima at 180–190 and 280–290° for the adsorption of oxygen at room temperature, but adsorption about 200° gives only the high temperature peak.[13] The fact that O^- does not desorb up to about 280° agrees with the result that the conductivity of evacuated zinc oxide decreases in oxygen and is not returned to the original value by a subsequent evacuation below 261°, but is above 300°.[10] Kwan, *et al.*,[4] observed O^- species by esr spectroscopy when nitrous oxide was added at room temperature over zinc oxide degassed for 1 hr at 500°. In view of all of the above work we suggest that the reversible retardation by CO_2 observed in the reaction of CO with N_2O is caused by the replacement of O^- species with CO_2.

It has been established that the adsorption of oxygen on zinc oxide gives two adsorbed species O_2^- and O^- depending on the condition,[11–13] and the main species of adsorbed oxygen on degassed zinc oxide at low temperatures is O_2^- which changes to O^- above 160° with some activation energy.[4] Temperature-programmed desorption[13] suggests that O^- formed on zinc oxide does not change rapidly to O_2^- even at about 200°. Consequently, it is not clear whether O_2^- or O^- is the more likely reaction intermediate in the oxidation of carbon monoxide over zinc oxide catalyst. Since N_2O gives O^- and O_2 gives O_2^- and/or O^-, the results of the competitive reaction runs in Figure 4 that O_2 retards the CO +

(9) K. Otsuka, K. Tanaka, and K. Tamaru, *J. Chem. Soc. Jap.*, **88**, 830 (1967).

(10) P. Amigues and S. J. Teichner, *Discuss. Faraday Soc.*, **No. 41**, 362 (1966).

(11) J. H. Lunsford and J. P. Jayne, *J. Chem. Phys.*, **44**, 1487 (1966).

(12) M. Codell, J. Weisberg, H. Gisser, and R. D. Iyengar, *J. Amer. Chem. Soc.*, **91**, 7762 (1969); A. Tench and T. Lawson, *Chem. Phys. Lett.*, **8**, 177 (1971).

(13) K. Tanaka and G. Blyholder, *Chem. Commun.*, 1343 (1971).

N_2O reaction while the total CO_2 production in the CO reactions with N_2O and O_2 remains unchanged indicates a common intermediate which must then be O^-. This together with the kinetics being first order in CO and zero order in N_2O suggests that the active sites for the slow thermal reaction are covered with O^- species which are supplied competitively from N_2O and O_2 during the reaction, and the rate-determining step is the reaction between O^- and either gas phase CO or weakly adsorbed CO.

Sancier[14] observed two different changes of esr signals when CO was added to zinc oxide with presorbed oxygen at room temperature and assumed that two types of reaction proceed on the surface, one being a rapid reaction with O^- and the other a slow reaction with O_2^-. Hauffe, *et al.*,[5] proposed O_2^- as an intermediate for the reaction of CO with O_2 at 160°, while Teichner, *et al.*,[10] explained their kinetics by assuming uncharged oxygen, O, as an intermediate of the reaction at 261°. The present experiments at around 200° clearly indicate that O^- is the most important intermediate in the reactions of CO with O_2 and N_2O. The observed kinetics and results are explicable by the following scheme.

$$Zn_i \rightleftharpoons Zn_i^+ + (e) \quad (1)$$

$$Zn_i^+ \rightleftharpoons Zn_i^{2+} + (e) \quad (2)$$

$$N_2O \text{ or } O_2 + (e) + Zn_i \text{ or } Zn_i^+ \longrightarrow O^-(Zn_i \text{ or } Zn_i^+) \quad (3)$$

$$CO + O^-(Zn_i \text{ or } Zn_i^+) \not\longrightarrow CO_2(Zn_i \text{ or } Zn_i^+) + (e) \text{ (slow step)} \quad (4)$$

where Zn_i, Zn_i^+, and Zn_i^{2+} indicate interstitial zinc atoms and ions and (e) is an electron in the conduction band, eq 1 and 2 represent the thermal equilibrium ionization of donors, and eq 4 is the rate-determining step of the slow reaction over the stabilized surface. The reversible poisoning by carbon dioxide of the slow reaction is not caused by an electron capture process but by the blocking of the active sites as suggested by Teichner, *et al.*,[10] in the competitive adsorption of CO_2 and O_2. The retardation by oxygen of the reaction of CO with N_2O and the results of the competitive reaction of CO with N_2O and O_2 indicate that the sites are occupied preferentially by oxygen from gas phase O_2 rather than from the decomposition of N_2O. As will be discussed below, this model for the thermal catalytic reaction can explain the differences of the thermal catalytic from the photocatalytic reaction over zinc oxide.

2. Photocatalytic Reactions. Under dark conditions both the reactions of CO with N_2O and O_2 are first order in CO pressure on the stabilized zinc oxide, but under illumination these two reactions each have different kinetics. The pressure dependence of the reaction rate of CO with N_2O shown in Figure 6 is described by the equation $r = k'P_{CO}^{0.4}P_{N_2O}^{0.4}$. The reaction of CO with O_2 on the illuminated zinc oxide is half-order in oxygen pressure and approximately zero order in carbon monoxide pressure above 20 mm CO pressure, $r = k''\cdot P_{CO}^0 P_{O_2}^{1/2}$, while at pressures lower than 20 mm the pressure dependence of carbon monoxide appears as shown in Figure 8B.

The different orders with respect to carbon monoxide pressure in the two photooxidations could in general be ascribed to either (1) that the CO surface intermediate contributes to the slow step of each reaction in a different manner, or (2) that the surface characteristics are different during each reaction so that there are different concentrations of the CO intermediate. That (2) is not the case is shown in Figure 10B by the orders with respect to CO being different for the reactions with N_2O and O_2 since both reactions are taking place competitively where the surface conditions must be identical. The facts that N_2O and O_2 have no mutual retardation, which is in marked contrast to the dark reactions, and that the orders with respect to CO for the competitive photooxidations with N_2O and O_2 are different indicate that the photooxidations of CO with N_2O and O_2 have different slow steps and that the contributions of the CO surface intermediates to the slow steps are different in each reaction.

Concerning the reaction of CO with O_2, Hauffe, *et al.*,[5] reported more complex results than our observations. At about 200° the photoeffects they noted were less marked than our observations and above 250° they no longer observed photoeffects; furthermore, above 200° their rate was only dependent on oxygen pressure both in the dark and under illumination but at temperatures lower than 200° the rate was promoted by illumination and the reaction became CO pressure dependent. These results disagree with our results. It is difficult to pinpoint reasons for these differences, but it may be noted that besides differences in pretreatment their catalyst was in the form of small pellets with glass spheres while our catalyst is a fine powder.

For the reaction of CO with N_2O, the rates in the dark and under illumination are comparable, but the pressure dependences are markedly different. This suggests that the thermal catalytic reaction may not take place over the illuminated zinc oxide. This inference is supported by the retardation effect of carbon dioxide, which strongly retards the thermal but only slightly effects the photocatalytic reaction of CO with O_2. These phenomena may be explained by assuming the active sites for the thermal catalytic reactions are Zn_i or Zn_i^+ which are ionized into a higher oxidation state by illumination to lose their catalytic activity. The photocatalytic oxidation may then take place on the sites produced by illumination, *i.e.*, the sites with electrons or electron and hole pairs. A reasonable reaction scheme is described as

(14) K. M. Sancier, *J. Catal.*, 9, 331 (1967).

$$N_2O + e \rightleftharpoons N_2O^- \quad (5)$$

$$CO + h \rightleftharpoons CO^+ \quad (6)$$

$$N_2O^- + CO^+ \not\rightarrow CO_2 \text{ (slow step)} \quad (7)$$

$$O_2 \rightleftharpoons 2O \quad (8)$$

$$O + e \not\rightarrow O^- \text{ (slow step)} \quad (9)$$

$$O^- + CO^+ \longrightarrow CO_2 \quad (10)$$

where e and h are electrons and holes produced by illumination. Equation 5 represents the adsorption of N_2O in the form of N_2O^-, which is an unstable ion in the gas or liquid phase, but the presence of surface N_2O^- has been inferred over illuminated zinc oxide during the decomposition of N_2O.[7] The results obtained here also support the presence of an N_2O^- species during the reaction of CO with N_2O over the illuminated zinc oxide. The facts that the reactions of CO with N_2O and with O_2 proceed independently and that the reaction rate of CO with N_2O is much slower than with O_2 indicates the decomposition of N_2O^- to O^- and N_2 is relatively slow under the reaction conditions. Equation 6 represents the photoadsorption of CO as has been observed by Terenin, *et al.*,[15] in which holes produced by the illumination are trapped by adsorbed CO. Since this type of carbon monoxide adsorption is not expected in the dark at around 200°, the difference of the orders with respect to CO pressures under dark and illuminated conditions is reasonably explained. The slow step of the reaction of CO with N_2O is presumed to be the reaction between N_2O^- and CO^+.

To explain the kinetics of the reaction of CO with O_2, a preliminary dissociation of oxygen as described by eq 8, followed by an electron transfer process, eq 9, is assumed. The photocatalytic oxidation of CO with O_2 having no mutual retardation with N_2O and being approximately zero order in CO suggests that the slow step of the reaction of CO with O_2 is an adsorption process of oxygen to give O^- as described by eq 9, and that the reaction between O^- and CO^+ is very rapid.

It may be noted that the active sites for the thermal catalysis are effectively blocked by strong adsorbents such as oxygen or carbon dioxide, but that the active sites for the photocatalysis are not so sensitive to poisoning. Such differences are presumably caused by the characters of the active sites, that is, the thermal catalysis proceeds on interstitial zinc while the photocatalysis proceeds on lattice zinc and/or oxide with electrons and holes produced by the illumination.

Acknowledgment. This investigation was supported in part by Research Grant No. APOO818 from the Air Pollution Control Office, Environmental Protection Agency.

(15) A. Terenin and Yu. Solonitzin, *Discuss. Faraday Soc.*, **No. 28**, 28 (1959).

Pulse Radiolysis Studies on Br^- in Aqueous Solution: the Mechanism of Br_2^- Formation[1]

by D. Behar

Radiation Research Laboratories and Center for Special Studies, Mellon Institute of Science, Carnegie-Mellon University, Pittsburgh, Pennsylvania 15213 *(Received December 28, 1971)*

Publication costs assisted by Carnegie Mellon University and the U. S. Atomic Energy Commission

The reaction of hydroxyl radicals with Br^- has been investigated in the pH regions 9–11.5. The maximum absorption of Br_2^- was followed spectrophotometrically at 365 nm as a function of $[Br^-]$ and $[OH^-]$. The intermediate species, $BrOH^-$, is suggested as a precursor in the oxidation mechanism of Br^-.

Introduction

Previous studies on the oxidation of halides and pseudohalides (*e.g.*, SCN^-, SH^-) by OH radicals using pulse radiolysis techniques[2-7] have shown the production of X_2^- radical complexes. These complexes absorb strongly in the 340–475-nm region and, therefore, are conveniently used in competitive systems as references for determining rate constants of OH radicals with different solutes.[8-10]

The oxidation mechanism usually adopted assumes an electron transfer reaction from the halide ion to the OH radical

$$OH + X^- \longrightarrow OH^- + X \qquad (1)$$

followed by

$$X + X^- \rightleftarrows X_2^- \qquad (2)$$

It is well known that the formation of X_2^- is pH dependent. The higher the electronegativity of the halogen atom the lower the pH needed to suppress the X_2^- formation. In the case of chloride at millimolar concentrations, pH 3 is sufficient to suppress Cl_2^- formation,[2] while in the case of the bromide, pH ~11 is the critical limit.[3,4] For SCN^- the critical pH is even higher (pH ~14[11]). Several explanations have been suggested for this pH dependence. For Cl^- the following reaction was introduced

$$OH + Cl^- + H_3O^+ \longrightarrow Cl + 2H_2O \qquad (3)$$

For Br^-, Cercek, *et al.*,[3] suggested that O^- does not react with Br^-, and the pH dependence is a result of the OH dissociation into O^-. Later Matheson, *et al.*,[4] suggested the formation of $BrOH^-$ which is in equilibrium with Br^- and OH, and also with Br and OH^- to account for that pH dependence.

Linnenbom and Cheek[12] studied the effect of pH on the evolution of hydrogen from irradiated bromide solutions and found that the protection efficiency of the bromide on the molecular hydrogen yield decreases on increasing the pH. They suggested the reverse of reaction 1 to account for that pH dependence.

In a recent publication by Behar, Bevan, and Scholes[13] the oxidation mechanism of SCN^- by OH radicals has been investigated, and the absorption spectra of the precursors of $(SCN)_2^-$ were observed. It was concluded there that the reaction of OH with SCN^- leads to the formation of $SCNOH^-$ as an intermediate, and reaction 4 may take place in the mechanism of $(SCN)_2^-$ formation

$$XOH^- + X^- \longrightarrow X_2^- + OH^- \qquad (4)$$

Preliminary studies of aqueous alkaline iodide solutions[14] also indicate the formation of IOH^-. Zehavi and Rabani[10,15] studied the competition between ethanol and Br^- for OH and found dependence of the relative rate constants on the absolute concentration of Br^-. This dependence could not be explained by reactions 1 and 2. They interpreted their results also

(1) Supported in part by the U. S. Atomic Energy Commission.

(2) M. Anbar and J. K. Thomas, *J. Phys. Chem.*, **68**, 3829 (1964).

(3) B. Cercek, M. Ebert, C. W. Gilbert, and A. J. Swallow, "Pulse Radiolysis," Academic Press, New York, N. Y., 1965, p 83.

(4) M. S. Matheson, W. A. Mulac, J. L. Weeks, and J. Rabani, *J. Phys. Chem.*, **70**, 2092 (1966).

(5) J. K. Thomas, *Trans. Faraday Soc.*, **61**, 702 (1965).

(6) J. H. Baxendale, P. L. T. Bevan, and D. A. Stott, *ibid.*, **64**, 2389 (1968).

(7) W. Karmann, G. Meissner, and A. Henglein, *Z. Naturforsch. B*, **22**, 273 (1967).

(8) G. E. Adams, J. W. Boag, J. Currant, and B. D. Michael, "Pulse Radiolysis," Academic Press, New York, N. Y., 1965, p 131.

(9) N. Getoff, F. Schworer, V. M. Marcovic, K. Sehested, and S. O. Nielson, *J. Phys. Chem.*, **75**, 749 (1971).

(10) D. Zehavi and J. Rabani, *ibid.*, **75**, 1738 (1971).

(11) D. Behar, P. L. T. Bevan, and G. Scholes, submitted to *J. Phys. Chem.*

(12) V. J. Linnenbom and C. H. Cheek, IUPAC Meeting, Moscow, 1965.

(13) D. Behar, P. L. T. Bevan, and G. Scholes, *Chem. Commun.*, **22**, 1486 (1971).

(14) G. Scholes, private communication.

(15) D. Zehavi and J. Rabani, *J. Phys. Chem.*, **76**, 312 (1972).

by assuming the formation of $BrOH^-$ which reacted with Br^- according to (4). Symons and coworkers have recently identified $ClOH^-$, $BrOH^-$, and IOH^- in irradiated frozen aqueous solutions of the alkali metal halides[16] by esr spectroscopy.

In view of the above-mentioned findings we chose the bromide as a representative halide to investigate its reaction with the hydroxyl radicals. The hydroxyl radicals produced in the pulse reacted with Br^- near the pH region where formation of Br_2^- is suppressed by OH^-, and from the dependence of the absorption of Br_2^- on Br^- and OH^- concentrations we have attempted to elucidate the mechanism of oxidation of the bromide ion by hydroxyl radicals.

Experimental Section

KBr, Na_2HPO_4, Na_3PO_4, and KOH used were all Baker Analyzed reagents. Solutions were prepared with triply distilled water. All solutions were bubbled with Baker nitrous oxide for at least 1 hr. The nitrous oxide served to convert e_{aq}^- into OH. No precaution was taken to eliminate traces of oxygen in the N_2O.

In most experiments the concentration of Br^- was kept constant, and the pH was varied by adding solid Na_2HPO_4, Na_3PO_4, or KOH. The solutions were driven through the irradiation cell where each solution received a single pulse. Every measurement was repeated at least four times, and the average optical density was taken.

Samples were irradiated in a fused silica cell 2 cm long with the light passing twice through the cell. The optical arrangement is identical with that described by Patterson and Bansal.[17] Pulses of 2.8-MeV electrons of 0.5-μsec duration from a Van de Graaff generator were used. The current deposited in the irradiated solution was collected on an electrode mounted in the output of the cell, and the relative charge input was monitored by a current integrator circuit. Absorbed doses were in the range 100–200 rads. All absorption signals were normalized to a common dose. The deviations in the normalized absorptions were less than 5%.

Results and Discussion

Alkaline Br^- solutions were saturated with nitrous oxide ($\sim 2 \times 10^{-2}$ M in N_2O) in order to convert the solvated electrons into hydroxyl radicals

$$e_{aq}^- + N_2O \longrightarrow N_2 + O^- \qquad (5)$$

$$OH + OH^- \rightleftarrows O^- + H_2O \quad (pK = 11.8^{18}) \qquad (6)$$

The reactions of both OH and O^- radicals with the bromide anion yield the Br_2^- complex radical which has a maximum absorption at 360–365 nm.[3,4,19] This absorption reaches a maximum value and then decays in a second-order process. At low doses the second-order decay of Br_2^- can be neglected at relatively short times after the pulse, and the maximum absorption can be detected easily. In most of our experiments the decay of the Br_2^- was negligible. Figure 1 is a typical oscillogram where maximum absorption of Br_2^- is attained.

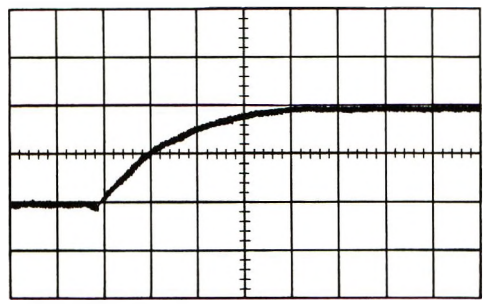

Figure 1. Absorption of Br_2^- at 365 nm in pulse radiolysis of N_2O-saturated solution containing 1.1×10^{-4} M Br^- at pH 10.0. Time scale 5 μsec per division, absorption 2.5% per division.

In the study of the SCN^- and I^- systems by Baxendale, Bevan, and Stott[6] the maximum absorption of $(SCN)_2^-$ and I_2^- was shown to be pH independent in the pH region 2–7, and reactions 1 and 2 were suggested to account for the dependence of the maximum absorption on the halide concentration. In our experiments we choose the Br^- and OH^- concentrations in such a region where the maximum absorption of Br_2^- is pH dependent. In general the absorption due to Br_2^- qualitatively decreases with increased pH when $[Br^-]$ is kept constant. Figure 2 demonstrates the dependence of the maximum optical density D on the concentration of OH^- at various Br^- concentrations. The dependence of D_0/D on $[OH^-]$ is given below (see eq II). D_0 in the ordinate of Figure 2 is the maximum optical density obtained when full conversion of the OH radicals into Br_2^- occurs. $D_0 = [OH]_0 \times \epsilon_{Br_2^-} \times l$ where $[OH]_0$ is the total concentration of OH radicals produced from the pulse, $\epsilon_{Br_2^-}$ is the extinction coefficient of Br_2^- at 365 nm, and l the light path (4 cm).

As shown in Figure 2 at constant Br^- concentration the reciprocal value of the maximum optical density D is linear with OH^- concentration. When increasing Br^- concentration, the slopes of the lines decrease. The following mechanism is consistent with these results

$$OH + Br^- \rightleftarrows BrOH^- \qquad (7)$$

$$BrOH^- + Br^- \rightleftarrows Br_2^- + OH^- \qquad (8)$$

Assuming that equilibria 7 and 8 are established when the optical density of Br_2^- reaches its maximum value

(16) (a) R. C. Catton and M. C. R. Symons, *J. Chem. Soc. A*, 446 (1969); (b) I. Marov and M. C. R. Symons, *ibid.*, 201 (1971).

(17) L. K. Patterson and K. M. Bansal, submitted to *J. Phys. Chem.*

(18) J. L. Weeks and J. Rabani, *ibid.*, **70**, 2100 (1966).

(19) L. I. Grossweiner and M. S. Matheson, *ibid.*, **61**, 1089 (1957).

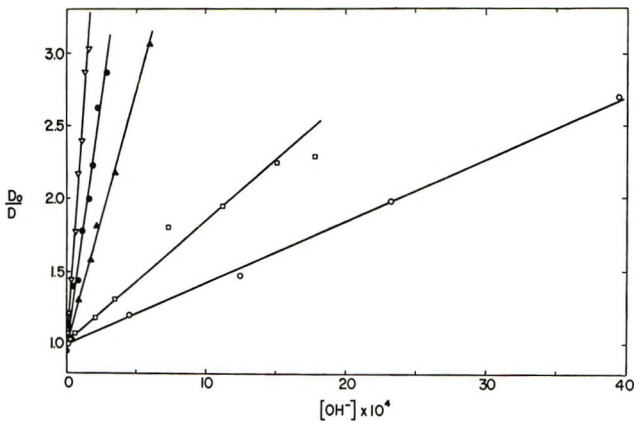

Figure 2. The dependence of D_0/D as defined in the text on $[OH^-]$ for various bromide solutions: ▽, 1.0×10^{-4}; ●, 1.47×10^{-4}; ▲, 2.0×10^{-4}; □, 5.1×10^{-4}; ○, 7.7×10^{-4} M.

D, then the radicals OH, $BrOH^-$, and Br_2^- coexist and

$$\frac{D_0}{D} = \frac{[Br_2^-] + [BrOH^-] + [OH]}{[Br_2^-]} \qquad (I)$$

Equation I holds only if $BrOH^-$ has negligible absorption at 365 nm. Absorption spectra measured in the region 320–420 nm at different times after the pulse, during the growth of the Br_2^- absorption were identical. If $BrOH^-$ has a different absorption spectrum than that of Br_2^- with a significant extinction coefficient in that region, the spectrum measured in the very early stage of formation should differ from that after the Br_2^- formation is completed. Since no significant differences were observed one can conclude that $BrOH^-$ either does not absorb at 365 nm or has exactly the same spectrum as Br_2^-. The latter case which seems less probable would result in a smaller K_7 and K_8 than those measured.

Substituting $[BrOH^-]/[Br_2^-]$ and $[OH]/[Br_2^-]$ from the definition of K_7 and K_8 ($K_7 = [BrOH^-]/[OH][Br^-]$ and $K_8 = [Br_2^-][OH^-]/[BrOH][Br^-]$) one gets

$$\frac{D_0}{D} = 1 + \frac{[OH^-](1 + K_7[Br^-])}{K_7K_8[Br^-]^2} \qquad (II)$$

On plotting D_0/D *vs.* $[OH^-]$ at constant $[Br^-]$ one should get a straight line. The plots in Figure 2 for different bromide solutions demonstrate the dependence given in eq II. The slopes θ of these lines are given by

$$\theta = \frac{1 + K_7[Br^-]}{K_7K_8[Br^-]^2} \qquad (III)$$

and

$$\theta \times [Br^-] = \frac{1}{K_7K_8[Br^-]} + \frac{1}{K_8} \qquad (IV)$$

In Table I values of θ for different values of $[Br^-]$ are present. To avoid overcrowding only a few representative results have been plotted in Figure 2.

Table I: Dependence of θ^a on $[Br^-]$ at the pH Region 9–11.5

$[Br^-] \times 10^4$, M	θ, M^{-1}
0.92	11,750
1.01	13,500
1.11	9,250
1.11	10,370
1.25	8,250
1.47	6,530
1.68	6,030
1.83	4,450
2.00	3,500
2.50	2,830
3.35	2,100
5.10	930
5.71	390
7.70	390
8.60	473
11.3	297

[a] θ's are the slopes of the lines such as in Figure 2.

On plotting $\theta \times [Br^-]$ *vs.* $1/[Br^-]$ according to eq IV one should get a linear dependence. This plot is given in Figure 3. The line in Figure 3 is that resulting from a least-mean-square calculation giving intercept 0.271 and slope 9.47×10^{-5}. Points at small $1/[Br^-]$ values, which may approach the intercept value, could not be taken since then relatively high pH's are needed to have incomplete conversion of OH into Br_2^- radicals but at high pH's the system behaves differently. Instead of a linear dependence of D_0/D on $[OH^-]$, a dependence on $[OH^-]^2$ was found. No simple mechanism could be suggested for this behavior in the very alkaline region.

From eq IV and the parameters of the line in Figure 2 one obtains $K_7 = (2.86 \pm 1.4) \times 10^3$ M^{-1} and $K_8 = 3.7 \pm 1.5$.

Another approach has been examined to verify the suggested mechanism. Buffered solutions at the same pH were pulse irradiated at different Br^- concentrations and the optical density ratio D_0/D was plotted as a function of $[Br^-]$ (Figure 4). Equation II was used to calculate D_0/D for different $[Br^-]$ taking K_7 and K_8 as free parameters and adjusting them to obtain the best fit with the experimental D_0/D values. Figure 4 demonstrates the agreement between the experimental results and the calculated curve when taking $K_7 = 2300$ M^{-1} and $K_8 = 4.35$. These numbers are in a good agreement with the values determined previously using the linear plot of eq IV (Figure 3).

In the course of these studies Zehavi and Rabani[15] studied competition reactions between Br^- and alcohols for OH radicals where they determined k_7 and k_{-7}. One can obtain $K_7 = 320$ M^{-1} from their measurements.

At this stage it seems appropriate to consider the nature of reaction 8. Although in first view this reac-

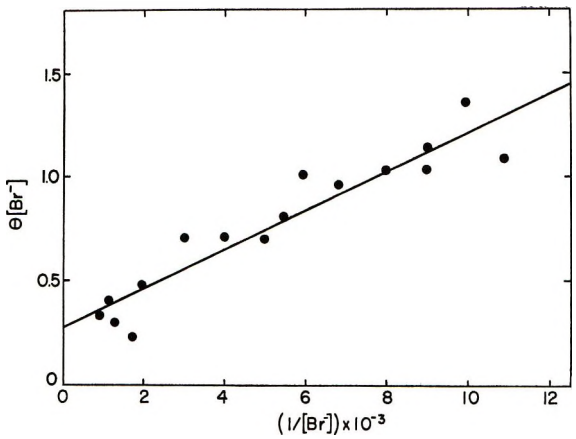

Figure 3. $\theta \times [Br^-]$ as a function of $1/[Br^-]$. θ are the slopes of the lines of D_0/D *vs.* $[OH^-]$ at constant $[Br^-]$ such as in Figure 2. For complete data see Table I. The straight line has the least-mean-square parameters calculated from the experimental points.

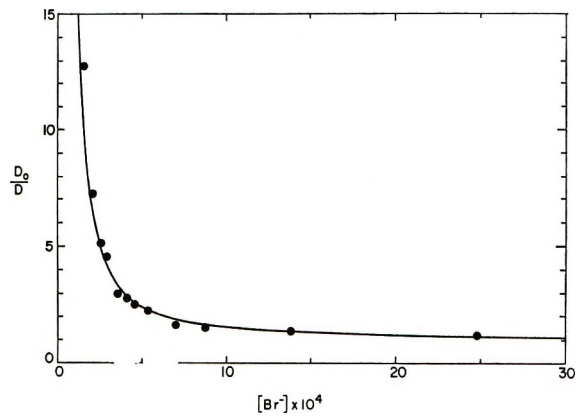

Figure 4. A calculated curve of D_0/D as a function $[Br^-]$ according to eq II taking $K_7 = 2300\ M^{-1}$, $K_8 = 4.35$ at $[OH^-] = 1.65 \times 10^{-3}\ M$. The dots are the experimental points measured in the pulse radiolysis of Br^- solutions at the same OH^- concentration; $[OH^-] = 1.65 \times 10^{-3}\ M$. The optical densities D were normalized to a common dose.

tion might seem peculiar, if one considers the OH^- as a pseudohalide, then one finds in the literature[20-22] several examples of analogous exchange reactions, namely

$$XY^- + X^- \rightleftarrows X_2^- + Y^- \qquad (9)$$

where X and Y stand for Cl, Br, I, and SCN. In this view reaction 8 can be accepted.

Although the proposed mechanism is in agreement with the experimental results, it is not the only one that can fit those results. It can, however, be shown that the earlier mechanism suggested by Linnenbom and Cheek[12] with the reaction sequence 10 and 11 is not sufficient to account for all our findings

$$Br^- + OH \rightleftarrows Br + OH^- \qquad (10)$$

$$Br + Br^- \rightleftarrows Br_2^- \qquad (11)$$

If this mechanism is adopted, the expression for D_0/D where OH, Br, and Br_2^- coexist is

$$D_0/D = 1 + \frac{1}{K_{11}[Br^-]} + \frac{[OH^-]}{K_{10}K_{11}[Br^-]^2} \qquad (V)$$

In this case at constant $[Br^-]$, also a linear dependence of D_0/D on $[OH^-]$ should be observed, which is in accordance with our results. (The term $1/K_{11}[Br^-]$ is negligible at $[Br^-] > 10^{-4}\ M$ taking $K_{11} = 2.1 \times 10^5$ as measured in acid solution.[3] K_{11} should not be affected by the pH.) But on plotting $\theta \times [Br^-]$ (θ are the slopes of the lines in Figure 2) *vs.* $1/[Br^-]$ one should get a straight line with zero intercept. ($\theta \times [Br^-] = 1/K_{10}K_{11}[Br^-]$ is obtained from (V).) Our results, although having large deviations, clearly show a finite intercept different from zero.

A different mechanism which accounts for all our results can be suggested. If one assumes the reaction sequence 7, 12, and 11

$$BrOH^- \rightleftarrows Br + OH^- \qquad (12)$$

then

$$\frac{D_0}{D} = 1 + \frac{1}{K_{11}[Br^-]} + \frac{[OH^-](1 + K_7[Br^-])}{K_7K_{11}K_{12}[Br^-]^2} \qquad (VI)$$

For $[Br^-] > 10^{-4}\ M$, $1/K_{11}[Br^-]$ is negligible and (VI), which has the same form as (II), will show the same dependence of D_0/D on $[OH^-]$ and $[Br^-]$ as (II) does. If that mechanism involving reactions 7, 11, and 12 is correct, then from Figure 2, K_7 will be the same as determined before, but K_8 has to be replaced by $K_{11} \times K_{12}$. Taking $2.1 \times 10^5\ M^{-1}$ for K_{11}[3] one arrives at 2×10^{-5} for K_{12}. This value for K_{12} suggests that reaction 12 might be important in near-neutral and acid solution, but less important in alkaline solutions. This mechanism might, therefore, be dominant in near-neutral and acid regions but not in alkaline solutions where equilibrium 12 is shifted to the left.

(20) M. Schoneshofer and A. Henglein, *Ber. Bunsenges. Phys. Chem.*, **73**, 289 (1969).

(21) M. Schoneshofer and A. Henglein, *ibid.*, **74**, 393 (1970).

(22) M. Schoneshofer, *Int. J. Radiat. Phys. Chem.*, **1**, 505 (1969).

An Electron Spin Resonance Study of X-Irradiated Heptanal Oxime Trapped in a Urea Inclusion Crystal. Evidence of a Bimolecular Reaction Product[1a]

by G. Bruce Birrell,[1b] Zofia Ciecierska-Tworek,[1c] and O. Hayes Griffith*

Institute of Molecular Biology and Department of Chemistry, University of Oregon, Eugene, Oregon 97403
(Received October 4, 1971)

Publication costs assisted by The National Science Foundation

Free radicals trapped in X-irradiated heptanal oxime–urea inclusion crystals were investigated using electron spin resonance techniques. In addition to an iminoxy radical, R—CH=NO·, two secondary radicals were observed. Spectral simulations and a table of coupling constants and g values are presented. Esr spectra and selective deuteration suggest that the secondary radicals are of the type R–N–R′ and RR′NO .

I. Introduction

In recent years a large number of studies have dealt with radical formation in oxime molecules. Most often in solution[2-6] and in single crystals[7,8] the stable free radical has been the iminoxy radical, R–CH=NO·, formed by abstraction of the –OH hydrogen atom. Recent solution studies of oximes have shown that under the proper conditions nitroxide free radicals, RHNO·, can also be produced.[9,10] After X-irradiation at low temperatures R–CH=NO· . . . ·ON=CH–R radical pairs have been identified in single crystals of several glyoxime derivatives[7,11] and the sodium and potassium salts of oximinopropionic acid.[12] Several of the studies of the iminoxy radical have noted the presence of secondary nitrogen-containing radicals in addition to the principal radical;[5,6,12,13] however, the nature of these secondary radicals remains unclear. We report here a study of the iminoxy radical and secondary radicals from heptanal oxime, $CH_3(CH_2)_5CH{=}NOH$, trapped in a urea inclusion crystal.

Inclusion compounds are crystalline substances in which one of the components fits into cavities formed by the other.[14] Crystallographic data have been reported on the crystals formed between urea and acids, alcohols, ethers and several n-hydrocarbons.[15,16] By comparing X-ray powder diffraction patterns, it has been concluded that all of these systems have similar hexagonal crystal structures. Furthermore, a detailed crystal structure analysis of the n-hexadecane–urea compound has been completed.[17] The hexadecane molecules are in an extended zigzag conformation with their long axes parallel to the crystalline needle axis and are enclosed in tubular cavities formed by spirals of hydrogen-bonded urea molecules. Employing crystal structure and chemical composition data on hydrocarbon–urea complexes, Smith has concluded that the ends of successive hydrocarbon molecules in a given cavity are in normal van der Waals contact.[17] In addition to the crystallographic work, dielectric absorption,[18] nuclear magnetic resonance,[19] and electron spin resonance[20,21] investigations of several urea inclusion compounds have been reported. Results from all of these studies support the conclusion that the guest molecules fit only loosely in the tubular cavities of the host and undergo a large degree of molecular motion. Urea is a convenient host for the otherwise transient species

(1) (a) This work was supported by the National Science Foundation under Grant No. GP-16341; (b) NIH Postdoctoral Fellow (Fellowship No. 5 FO3 CA 42789-02 from the National Cancer Institute); (c) Fulbright-Hays Exchange Scholar.

(2) R. O. C. Norman and B. C. Gilbert, *J. Phys. Chem.*, 71, 14 (1967).

(3) J. R. Thomas, *J. Amer. Chem. Soc.*, 86, 1446 (1964).

(4) B. C. Gilbert and R. O. C. Norman, *J. Chem. Soc. B*, 123 (1968).

(5) B. C. Gilbert and R. O. C. Norman, *ibid.*, 86 (1966).

(6) M. Betoux, H. Lemaire, and A. Rassat, *Bull. Soc. Chim. Fr.*, 1985 (1964).

(7) Y. Kurita, *J. Chem. Phys.*, 41, 3926 (1964).

(8) I. Miyagawa and W. Gordy, *ibid.*, 30, 1590 (1959); M. C. R. Symons, *J. Chem. Soc.*, 1189 (1963).

(9) D. J. Edge and R. O. C. Norman, *J. Chem. Soc. B*, 182 (1969).

(10) J. Q. Adams, *J. Amer. Chem. Soc.*, 89, 6022 (1967).

(11) Y. Kurita and M. Kashiwagi, *J. Chem. Phys.*, 44, 1727 (1966).

(12) H. Hayashi, K. Itoh, and S. Nagakura, *Bull. Chem. Soc. Jap.*, 40, 284 (1967).

(13) P. Smith and W. M. Fox, *Can. J. Chem.*, 47, 2227 (1969).

(14) J. F. Brown, Jr., *Sci. Amer.*, 207, 82 (1962).

(15) A. E. Smith, *J. Chem. Phys.*, 18, 150 (1950).

(16) W. Schlenk, Jr., *Ann.*, 565, 204 (1949).

(17) A. E. Smith, *Acta Crystallogr.*, 5, 224 (1952).

(18) R. J. Meakins, *Trans. Faraday Soc.*, 51, 953 (1955).

(19) D. F. R. Gibson and C. A. McDowell, *Mol. Phys.*, 4, 125 (1961).

(20) O. H. Griffith, *J. Chem. Phys.*, 41, 1093 (1964).

(21) O. H. Griffith, *ibid.*, 42, 2644 (1965); G. B. Birrell, A. A. Lai, and O. H. Griffith, *ibid.*, 54, 1630 (1971).

because at room temperature the trapped molecules are magnetically equivalent at all crystalline orientations.[20,21] The lifetimes of radicals derived from guest molecules by X-irradiation normally range from several minutes to several days at room temperature. Furthermore, background is minimal since urea does not form significant concentrations of free radicals under the conditions employed.[20,21]

II. Experimental Section

Single crystals of the heptanal oxime–urea inclusion compound were prepared by dissolving heptanal oxime (Eastman Organic Chemicals) in a saturated solution of urea in methanol until inclusion crystals began to precipitate from solution. The precipitate was then dissolved by adding excess methanol; large hexagonal inclusion crystals were obtained by slow evaporation of the methanol. Urea inclusion crystals of the deuterated heptanal oxime, $CH_3(CH_2)_5CD{=}NOH$, were prepared in the same manner using 98 atom % deuterium-enriched heptanal oxime from Merck Sharp and Dohme. The z axis was defined to lie along the needle axis of the hexagonal crystals, and the xy plane was perpendicular to the needle axis. The crystals were X-irradiated for 2 hr at 77°K using a GE XRD-5 tungsten target X-ray tube operated at 40 kV and 20 mA. Esr spectra were recorded at room temperature on a Varian E-3 esr spectrometer. Spectral simulations were performed with a Varian 620/i computer. The simulation program uses a first-order Hamiltonian (secular terms only) to generate first a stick spectrum and then a simulation of actual line shapes.[22] Gaussian line shapes and experimental line widths were specified as input parameters and best fits were determined by visual inspection.

III. Results and Discussion

A. The Iminoxy Radical. Esr spectra recorded at room temperature immediately after X-irradiation of heptanal oxime–urea at 77°K indicated the presence of one short-lived radical in relatively large concentration; spectral lines belonging to lower concentrations of secondary radicals were also evident. The first derivative esr spectrum and corresponding spectral simulation of this short-lived radical are shown in Figures 1a and b, respectively. The spectra of Figure 1 were recorded with the magnetic field parallel to the crystalline z axis (needle axis) of the hexagonal inclusion crystal. The esr spectra are anisotropic except in the crystalline xy plane. This behavior is characteristic of urea inclusion compounds and results from rapid motion of the long-chain guest molecules in the tubular cavities formed by the urea matrix. The net effect is to reduce the number of principal crystalline axes from three to two (*i.e.*, perpendicular and parallel to the z axis, respectively). The six-line

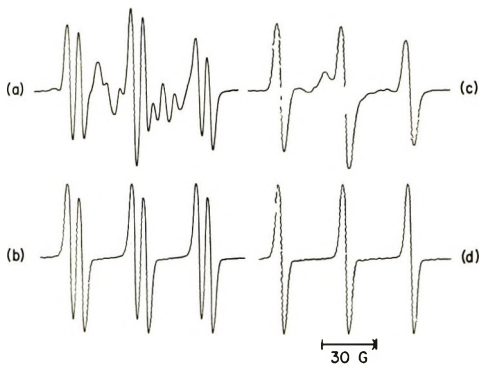

Figure 1. Experimental (a) and computer-simulated (b) esr spectra of the iminoxy radical produced by X-irradiation of heptanal oxime–urea inclusion crystals. (c) and (d) are the corresponding spectra from heptanal oxime-1-*d*–urea inclusion crystals. Experimental spectra were recorded with the magnetic field parallel to the crystalline z axis. The simulations were performed on a Varian 620/i computer using the data of Table I.

spectrum of Figure 1a arises from one large, slightly anisotropic nitrogen coupling constant and one small isotropic proton coupling constant. Each of these lines is further split by two small proton coupling constants (a^H = 2.0 G) when the magnetic field is perpendicular to the crystalline z axis. Figure 1c is the experimental spectrum from X-irradiated $CH_3(CH_2)_5CD{=}NOH$, recorded at the same crystalline orientation as Figure 1a; Figure 1d is the computer simulation of Figure 1c. From a comparison of Figures 1a and c it is clear that the 6-G proton coupling constant is due to the hydrogen replaced by deuterium in heptanal oxime-1-*d*; the deuterium hyperfine splittings are, as expected, too small to be detected and were not used in the simulation (Figure 1d). The unambiguous identification of the hydrogen responsible for the 6-G splitting and the large nitrogen coupling constant indicate that the short-lived radical from X-irradiated heptanal oxime is the iminoxy radical

$$CH_3(CH_2)_4{-}CH_2{-}\overset{\displaystyle H}{\overset{|}{C}}{=}NO\cdot$$

Coupling constants and g values for the above radical obtained at the principal orientations are indicated in Table I.

An estimate of the isotropic component, a_0^N, of the anisotropic nitrogen coupling constant can be obtained using the relation[20]

$$a_0^N = (1/3)(2a_{xy}^N + a_z^N) \quad (1)$$

where a_{xy}^N and a_z^N are the values of the nitrogen coupling constant measured with the magnetic field in the crystalline xy plane and parallel to the z axis, respectively. Using eq 1 and the data of Table I (and

(22) L. J. Libertini and O. H. Griffith, *J. Chem. Phys.*, **53**, 1359 (1970).

Table I: Hyperfine Coupling Constants and g Values for the Iminoxy Radical from Heptanal Oxime and Heptanal Oxime-1-d[a,b]

Heptanal oxime	(1) $a_z^N = 36.0 \pm 0.2$ G	(1) $a_{xy}^N = 29.3 \pm 0.2$ G
	(1) $a_z^H = 6.0 \pm 0.2$ G	(1) $a_{xy}^H = 6.0 \pm 0.2$ G
		(2) $a_{xy}^H = 2.0 \pm 0.1$ G
	$g_z = 2.0038 \pm 0.0002$	$g_{xy} = 2.0062 \pm 0.0002$
Heptanal oxime-1-d	(1) $a_z^N = 36.0 \pm 0.2$ G	(1) $a_{xy}^N = 29.3 \pm 0.2$ G

[a] z and xy indicate the direction of the magnetic field with respect to the crystalline axes. [b] The numbers in parentheses are the total number of species with a given coupling constant.

assuming a_{xy}^N and a_z^N are of the same sign), a_0^N = 31.5 G. The large isotropic nitrogen splitting is in good agreement with values reported for iminoxy radicals produced in other oximes.[2-6]

Spectra were recorded at numerous orientations of the inclusion crystals. Rotations of the magnetic field in the xy plane produced no observable changes in the esr spectra. This spectral isotropy results from rapid molecular motion of guest molecules in the tubular cavities of the crystal, and it has been observed in all urea inclusion crystals studied thus far.[20,21] At no orientation of the magnetic field was there evidence for magnetically distinguishable sites of the free radicals. This was experimentally verified for all free radicals discussed in these pages and is a result of rapid molecular motion. The spectra are, of course, anisotropic with respect to rotation about an arbitrary axis. The anisotropy is due to the variation of the nitrogen coupling constant a^N (the proton coupling constants are isotropic). The variation in a^N can be analyzed by the standard methods used previously by Libertini and Griffith in a study of nitroxide free radicals.[22] The appropriate equations are

$$a^N = a_z^N \cos^2\theta + a_{xy}^N \sin^2\theta \quad (2)$$

or

$$a^N = [(a_z^N)^2 \cos^2\theta + (a_{xy}^N)^2 \sin^2\theta]^{1/2} \quad (3)$$

where θ is the angle between the magnetic field and the crystalline z axis. Equation 3 is a better approximation than eq 2, but both equations are widely used in interpreting anisotropic esr data.[23] Both equations, using the values of a_z^N and a_{xy}^N given in Table I, provided an excellent fit to the experimental anisotropy curve. The largest deviation between the experimental and calculated values was ±0.2 G for eq 2 or eq 3.

B. The Secondary Radicals. The two radicals responsible for the complex spectrum which remained after the spectral lines due to the iminoxy radical had disappeared were individually isolated by (a) subjecting a crystal to uv light from a 110-W PEK mercury lamp for up to 18 hr (with no indication of radical formation due to the uv light) and (b) heating a crystal to 50° for 5 days. The first derivative esr spectrum of the uv-stable radical (that isolated by treatment a) from heptanal oxime recorded with the magnetic field in the crystalline xy plane and its spectral simulation are shown in Figures 2a and b, respectively. Figures 2c and d are the corresponding spectrum and computer simulation for the heat stable radical (isolated by treatment b) from heptanal oxime. The spectra of the uv-stable radical result from one anisotropic nitrogen coupling constant and two large, nearly isotropic proton coupling constants. The esr spectra of the heat stable radical arise from one anisotropic nitrogen coupling constant and two isotropic proton hyperfine splittings, one >30 G and the second 6.0 G.

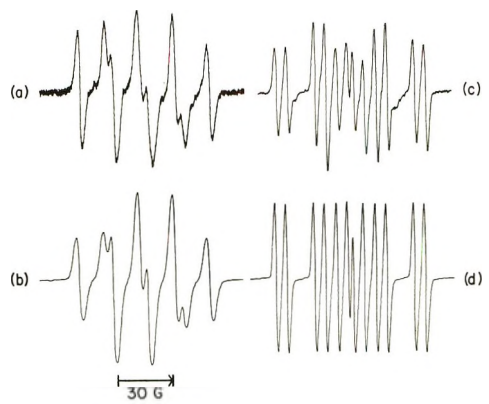

Figure 2. Experimental (a) and computer-simulated (b) esr spectra of the uv-stable radical obtained from heptanal oxime–urea inclusion crystals. (c) and (d) are the corresponding spectra of the heat-stable radical from the same compound. Spectra were recorded with the magnetic field perpendicular to the crystalline z axis. Spectral simulations were performed using the data of Table II.

Esr spectra of the uv-stable radical from $CH_3(CH_2)_5$-CD=NOH are not well resolved at most crystalline orientations; however, with the magnetic field 45° to the crystalline z axis, a well-resolved spectrum was obtained (Figure 3a). The spectral simulation (Figure 3b) was calculated using one nitrogen coupling constant of 14.8 G (consistent with the value obtained from nondeuterated heptanal oxime at this orientation) and two deuterium hyperfine splittings of 2.5 G; splittings of this magnitude would be expected if two hydrogen atoms with 17-G coupling constants were both re-

(23) P. C. Jost and O. H. Griffith in "Methods in Pharmacology," Vol. 2, C. Chignell, Ed., Appleton-Century-Crofts, New York, N. Y., 1972; P. Jost, L. J. Libertini, V. C. Hebert, and O. H. Griffith, *J. Mol. Biol.*, 59, 77 (1971).

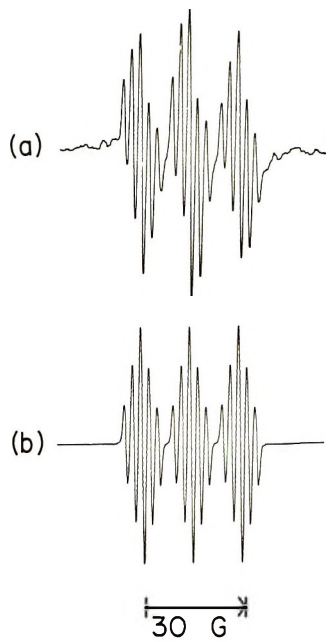

Figure 3. Experimental (a) and computer-simulated (b) esr spectra of the uv-stable radical from heptanal oxime-1-*d*-urea inclusion crystals, recorded with the magnetic field direction 45° from the crystalline *z* axis. Coupling constants used in the simulation were a^N = 14.8 G (one nitrogen) and a^D = 2.5 G (two deuterium nuclei).

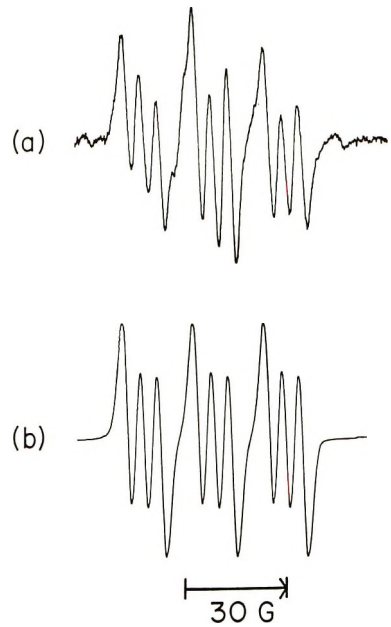

Figure 4. Experimental (a) and computer-simulated (b) esr spectra of the heat-stable radical from heptanal oxime-1-*d*-urea inclusion crystals, recorded with the magnetic field perpendicular to the crystalline *z* axis. Coupling constants used in the simulation were a^N = 21.0 G (one nitrogen) and a^D = 5.0 G (one deuterium).

placed with deuterium. Deuterium splittings used in the computer simulation (Figure 3b) were those measured directly from the experimental spectrum.

Spectra of the heat stable radical from $CH_3(CH_2)_5$-CD=NOH are well resolved except with H$||z$ and result from one anisotropic nitrogen coupling constant and one isotropic deuterium splitting of 5 G. Apparently the hydrogen atoms responsible for the proton hyperfine splittings in the heat stable radical from $CH_3(CH_2)_5CH$=NOH are both replaced by deuterium when the radical is formed from $CH_3(CH_2)_5CD$=NOH, the 33-G proton coupling constant becoming a deuterium splitting of 5 G and the 6-G proton splitting becoming a deuterium whose splittings are too small to be observed. The experimental and calculated spectra of the heat stable radical from $CH_3(CH_2)_5$-CD=NOH recorded with the magnetic field in the crystalline *xy* plane are shown in Figures 4a and b, respectively. The simulation was obtained using the nitrogen coupling constant and the 5-G deuterium splitting (the second deuterium splitting was negligible). Coupling constants and *g* values for the two secondary radicals from heptanal oxime and heptanal oxime-1-*d* are indicated in Table II.

In addition to these data, spectra were also recorded at 10° intervals between the *z* axis and the *xy* plane. For both radicals eq 3 provides a good representation of the anisotropy of nitrogen coupling constants. Maximum deviations between the experimental and calculated points occur midway between θ = 0° and θ = 90° and are 1.2 and 0.5 G for the uv-stable radical and the heat-stable radical, respectively. The agreement using the more approximate relation, eq 2, was less satisfactory, and the maximum error in this case was 2.5 G for both the uv-stable and heat-stable radicals. At no orientation of the crystal did the nitrogen coupling constants fall outside the range given by the principal values (a_{xy}^N and a_z^N) of Tables I and II. The relative signs of a_{xy}^N and a_z^N were not determined in these single crystal experiments.

Spectra were also recorded from both X-irradiated $CH_3(CH_2)_5CH$=NOD and $CH_3(CH_2)_5CD$=NOD (made by growing the inclusion crystals from deuterated urea and deuterated methanol); esr spectra of each of the secondary radicals from $CH_3(CH_2)_5CH$=NOD and $CH_3(CH_2)_5CD$=NOD were identical with the corresponding spectra from $CH_3(CH_2)_5CH$=NOH and $CH_3(CH_2)_5CD$=NOH, respectively. Thus, the -NOH proton does not give rise to observable hyperfine splittings in the esr spectra.

The presence of two deuterium hyperfine splittings in the esr spectra from both secondary radicals implies that both radicals are bimolecular reaction products formed where adjacent heptanal oxime molecules are oriented in the tubular cavities head-to-head.[24]

(24) Although it is possible that urea molecules participate in the radical formation with the trapped radicals, interactions of this type would be expected to reduce greatly the molecular motion of the oxime molecules in the urea cavities, and this is not observed. The results from the experiments with deuterated urea also support the contention that the urea is not directly involved in radical formation.

Table II: Hyperfine Coupling Constants and g Values for the Secondary Radicals from Heptanal Oxime and Heptanal Oxime-1-d[a]

Heptanal oxime (uv-stable radical)	(1) a_z^N = 7.1 ± 0.5 G (1) a_z^H = 17.2 ± 0.3 G (1) a_z^H = 17.2 ± 0.3 G g_z = 2.0058 ± 0.0002	(1) a_{xy}^N = 19.0 ± 0.3 G (1) a_{xy}^H = 19.0 ± 0.3 G (1) a_{xy}^H = 14.5 ± 0.3 G g_{xy} = 2.0058 ± 0.0002
Heptanal oxime-1-d[b] (uv-stable radical)	(1) a_z^N = 6.0 ± 1.5 G	(1) a_{xy}^N = 19.0 ± 0.3 G
Heptanal oxime (heat-stable radical)	(1) a_z^N = ~4 G[c] (1) a_z^H = 31.3 ± 0.3 G (1) a_z^H = 6.0 ± 0.2 G g_z = 2.0062 ± 0.0002	(1) a_{xy}^N = 21.0 ± 0.3 G (1) a_{xy}^H = 33.0 ± 0.3 G (1) a_{xy}^H = 6.0 ± 0.2 G g_{xy} = 2.0039 ± 0.0002
Heptanal oxime-1-d (heat-stable radical)	a_z^N = unresolved a_z^D = unresolved	(1) a_{xy}^N = 21.0 ± 0.3 G (1) a_{xy}^D = 5.0 ± 0.2 G

[a] z and xy indicate the direction of the magnetic field with respect to the crystalline axes. The numbers in parentheses are the total number of species with a given coupling constant. [b] Esr spectra from the uv-stable radical from heptanal oxime-1-d were poorly resolved at all orientations except where the magnetic field direction was 45° to the crystalline z axis; at the 45° orientation (2) $a_{45°}^D$ = 2.5 ± 0.1 G. [c] Unresolved at the z orientation but estimated from an extrapolation of a plot of the angular dependence of a^N.

Interactions of this type are not unusual in cavities of inclusion compounds.[25] Monomers such as vinyl chloride, acrylonitrile, and 1,3-butadiene have been polymerized while trapped in urea;[26] similarly, polymers have been formed from a variety of monomers in the somewhat larger channels of thiourea inclusion compounds.[27]

The fact that only two proton splittings are observed for each radical makes it necessary to postulate either unsaturation at the carbon atoms attached to these hydrogens or ring formation in the urea cavity. Values of a_0^N, calculated for the uv-stable radical and the heat-stable radical from heptanal oxime using the experimental data of Table II and eq 1, are each approximately 15 G, similar to splittings observed in numerous studies of nitroxide free radicals[28,29] and also to values recently reported for several dialkylamino[30,31] (R–N̈–R) and alkylalkoxyamino[13,32] (R–N̈–O–R′) radicals. Experimental g value data can also be related to the isotropic g value, g_0, to a good approximation using the relation[20]

$$g_0 = (1/3)(2g_{xy} + g_z) \quad (4)$$

For the uv-stable radical (using eq 4 and the data of Table II), g_0 = 2.0058, close to values reported for various nitroxides;[9,33] for the heat-stable radical, g_0 = 2.0047, reminiscent of the 2.0043–2.0046 values observed in dialkylamino radicals.[30,31] The large proton coupling constant (>30 G) observed in the heat-stable radical from heptanal oxime is also consistent with the magnitude of β-proton coupling constants from dialkylamino radicals and is substantially larger than proton hyperfine splittings previously reported for nitroxides.[28,29] The experimental evidence available for the secondary radicals from heptanal oxime thus suggests that the heat-stable radical is of the dialkylamino (or alkylalkoxyamino) type and the uv-stable radical is a nitroxide.

Although it is not possible from the experimental data to make an unambiguous identification of the two secondary radicals from heptanal oxime, two possible radicals are indicated below.

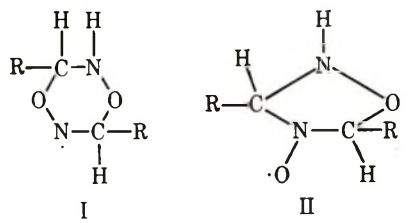

I II

Models of these types would account for both the >30 and 6-G proton coupling constants of the heat-stable radical (structure I) and the two nearly equivalent proton coupling constants of the uv-stable radical (structure II). The proton coupling constants of the uv-stable radical, somewhat larger than would be expected from a straight chain nitroxide,[28,29] are also consistent with a slightly strained five-membered ring.[28] *However, these structures are only suggestions since other radicals of the type R–N̈–R and RR′N–O· can be drawn which could account for the experimental data.*

(25) E. E. Wedum and O. H. Griffith, *Trans. Faraday Soc.*, **63**, 819 (1967).

(26) D. M. White, *J. Amer. Chem. Soc.*, **82**, 5678 (1960).

(27) J. F. Brown, Jr., and D. M. White, *ibid.*, **82**, 5671 (1960).

(28) G. Chapelet-Letourneux, H. Lemaire, and A. Rassat, *Bull. Soc. Chim. Fr.*, 3283 (1965).

(29) J. Q. Adams, S. W. Nicksic, and J. R. Thomas, *J. Chem. Phys.*, **45**, 654 (1966).

(30) W. C. Danen and T. T. Kensler, *Tetrahedron Lett.*, 2247 (1971); W. C. Danen and T. T. Kensler, *J. Amer. Chem. Soc.*, **92**, 5235 (1970).

(31) D. W. Pratt, J. J. Dillon, R. V. Lloyd, and D. E. Wood, *J. Phys. Chem.*, **75**, 3486 (1971).

(32) W. C. Danen and C. T. West, *J. Amer. Chem. Soc.*, **93**, 5582 (1971); Z. Ciecierska-Tworek, G. B. Birrell, and O. H. Griffith, *J. Chem. Phys.*, **56**, 1001 (1972).

(33) T. S. Kawamura, S. Matsunami, and T. Yonezawa, *Bull. Chem. Soc. Jap.*, **40**, 1111 (1967).

The essential point is that the two protons contributing to the esr spectra were originally α protons of adjacent oxime molecules. Thus, both the heat-stable and uv-stable radicals are bimolecular reaction products formed between two oxime molecules. The reacting oximes are undoubtedly oriented in head-to-head fashion in the urea lattice. The geometrical restraints imposed by the tubular cavities of urea inclusion crystals facilitate reactions that would not be easily observed in studies of the pure oximes.

Acknowledgments. We are grateful to Professors John F. W. Keana and Charles E. Klopfenstein for useful discussions.

Electron Spin Resonance Evidence for the C–F Bond Rupture by Dissociative Electron Attachment

by Kazumi Toriyama and Machio Iwasaki*

Government Industrial Research Institute, Nagoya, Hirate, Kita, Nagoya, Japan *(Received May 5, 1971)*

Publication costs assisted by the Government Industrial Research Institute

To examine the possibility of the C–F bond rupture by dissociative electron attachment to fluorine, esr study has been carried out using irradiated glasses of 2-methyltetrahydrofuran containing small amounts of fluorinated compounds such as CFH_2CONH_2, CHF_2COOEt, CF_3CONH_2, CF_3COOEt, CF_3COOH, c-C_6F_{12}, and $CF_2ClCONH_2$. Among these, the first three compounds gave clear evidence that radicals are formed from the rupture of the C–F bond by electron attachment followed by the dissociative process. The results obtained from a series of compounds indicate that the partially fluorinated compounds are favorable to the dissociative electron attachment and that the electron-withdrawing tendency of the functional group is another important factor for the dissociative process. Our results may suggest that the dissociative electron attachment plays an important role in the formation of radicals in some irradiated fluorine-containing compounds, although the cross section is not so large as compared with that in chlorine-containing compounds.

Dissociative electron attachment to organic halides [$RX + e^- \rightarrow \cdot R + X^-$] in irradiated organic glasses has been thoroughly studied by esr and optical measurements.[1] It has been pointed out that the dissociative process occurs when the electron affinity of X exceeds the bond dissociation energy of R–X.[1,2] Since the C–F bond strength exceeds the electron affinity of the fluorine atom, it is believed that the electron attachment to some fluorinated compounds is nondissociative.[1,3–6] In this connection, the mechanism of the C–F bond rupture in the γ radiolysis of fluorocarbons and hydrocarbon–fluorocarbon mixtures has been the subject of many recent studies.[3–9]

On the other hand, we have found in our previous work[10] that $\dot{C}H_2CONH_2$ is produced in a crystal of monofluoroacetamide irradiated at 77°K and that upon warming $\dot{C}H_2CONH_2$ abstracts an hydrogen atom from the neighboring molecule forming $\dot{C}HFCONH_2$. This means that the primary radical in partially fluorinated compounds is the one formed by the selective breakage of the C–F bond and that the secondary radical is produced by the selective abstraction of the hydrogen atom. It was also found that the radical pair between $\dot{C}H_2CONH_2$ and $\dot{C}HFCONH_2$ is formed at 77°K as a minor product. Although a mechanism involving hot fluorine atoms liberated from the direct breakage of the C–F bond was assumed in our previous paper,[10] we became aware of the importance of ionic processes shortly after submitting our manuscript.[11]

(1) W. H. Hamill, "Radical Ions," E. T. Kaiser and L. Kevan, Ed., Interscience, New York, N. Y., p 321.

(2) D. W. Skelly, R. G. Hayes, and W. H. Hamill, *J. Chem. Phys.*, **43**, 2795 (1965).

(3) L. A. Rajbenbach, *J. Amer. Chem. Soc.*, **88**, 4275 (1966).

(4) N. H. Sagert and A. S. Blair, *Can. J. Chem.*, **46**, 3284 (1968).

(5) L. A. Rajbenbach, *J. Phys. Chem.*, **73**, 356 (1969).

(6) N. H. Sagert, J. A. Reid, and R. W. Robinson, *Can. J. Chem.*, **47**, 2655 (1969).

(7) N. H. Sagert, *ibid.*, **46**, 95 (1968).

(8) N. H. Sagert and J. A. Reid, *ibid.*, **48**, 2429 (1970).

(9) M. B. Fallgatter and R. J. Hanrahan, *J. Phys. Chem.*, **74**, 2806 (1970).

(10) M. Iwasaki and K. Toriyama, *J. Chem. Phys.*, **46**, 4693 (1967).

(11) M. Iwasaki and K. Toriyama, Tenth Symposium on Radiation Chemistry, Hiroshima, Japan, Oct 1967.

We therefore examined the possibility that radicals are formed from the rupture of the C–F bond by the dissociative electron attachment in irradiated 2-methyltetrahydrofuran (MTHF) glasses of monofluoroacetamide and its related compounds. We have then found evidence for the dissociative electron attachment to such fluorinated compounds as monofluoroacetamide, ethyl difluoroacetate, and trifluoroacetamide in MTHF glasses. No such evidence has been obtained for other fluorinated compounds such as trifluoroacetic acid, ethyl trifluoroacetate, and perfluorocyclohexane.

Experimental Section

MTHF used was purified by passing through a column of silica gels. CH_2FCONH_2, CF_3CONH_2, CHF_2COOEt, CF_3COOEt, CF_3COOH, and $CClF_2CONH_2$, which were used as solutes in this experiment, were obtained from Pierce Chemical Co. Perfluorocyclohexane was supplied from the fluorine chemistry laboratory of our Institute. Esr samples were prepared in a vacuum line by distilling MTHF into the Spectrosil tube containing each of these fluorinated compounds in an amount of 1–2 mol %. Irradiations were made by ^{60}Co γ rays to a dose of 5×10^4 rads at 77°K in the dark. Esr spectra were measured at 77°K by a JEOLCO 3BS-X spectrometer operated at X band.

Results and Discussion

Figure 1a shows the esr spectrum of the trapped electron in the MTHF glass containing no additives. When 2 mol % of CHF_2COOEt is added, the single line due to the trapped electron is replaced by a pair of doublets as shown in Figure 1b. The central seven lines are mainly from the MTHF radical. The pair of doublets can be interpreted by the hyperfine line shape as due to anisotropic α-fluorine coupling. As previously reported[12,13] the large anisotropy of the α-fluorine coupling is known to give the wing peaks corresponding to the large value of $A_{||}$, which ranges from 180 to 200 G.[14] It has also been demonstrated that the wing peaks further split into the hyperfine lines due to the small couplings with other nuclei. It is evident that the wing peak separation of about 200 G in Figure 1b arises from the coupling with one α-fluorine nucleus. The small splitting, 22 G, of each wing peak indicates the existence of the α-proton coupling. The hyperfine lines corresponding to the $A_\perp$ component of the α-fluorine coupling tensor are superposed on the central lines due to the MTHF radical, resulting in considerable changes in the intensity ratio of the seven-line spectrum of the MTHF radical. Thus the radical responsible for this spectrum can be assigned to $\dot{C}HFCOOEt$ produced by the C–F bond rupture. Since this radical is formed in the MTHF glass, we conclude that the C–F bond scission occurs by dissociative electron attachment

$$CHF_2COOEt + e^- \longrightarrow \cdot CHFCOOEt + F^- \quad (1)$$

A similar experiment was also carried out using CH_2FCONH_2 as a solute. In this case, the radical expected from dissociative electron attachment is $\dot{C}H_2CONH_2$ having no α fluorine, so that the superposition of the spectrum due to the MTHF radical makes it difficult to obtain clear evidence for the formation of this radical. However, the signal due to the trapped electron was greatly reduced by adding 2 mol % of CH_2FCONH_2, and the spectrum obtained after photobleaching of the remaining trapped electron was found to be a superposition of the signals due to $\dot{C}H_2CONH_2$ and MTHF radical. This was confirmed by comparing the spectrum with that obtained from the MTHF glass containing $CH_2ClCONH_2$ which is expected to give $\dot{C}H_2CONH_2$. The spectra were reasonably similar except that the addition of 1–2 mol % of $CH_2ClCONH_2$ resulted in the complete disappearance of the signal of the trapped electron. This may mean that the cross section for electron attachment is smaller in CH_2FCONH_2 than in $CH_2ClCONH_2$.

To compare the cross section for dissociative electron attachment to fluorine with that for chlorine, a similar experiment was also carried out using $CClF_2CONH_2$. In this case the only radical formed was $\dot{C}F_2CONH_2$,

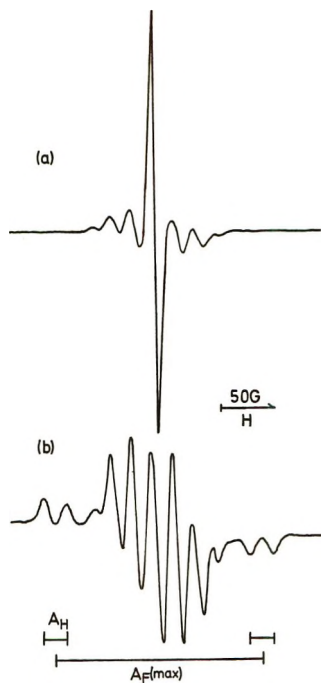

Figure 1. Esr spectra of (a) MTHF glass and (b) CHF_2COOEt (2 mol %) in MTHF glass, γ-irradiated at 77°K to a dose of about 5×10^4 rads. Spectrum b was measured with a gain five times higher than spectrum a.

(12) M. Iwasaki, K. Toriyama, and B. Eda, *J. Chem. Phys.*, **42**, 63 (1965).
(13) M. Iwasaki, *ibid.*, **45**, 990 (1966).
(14) M. Iwasaki, *Fluorine Chem. Rev.*, **5**, 1 (1971).

and no evidence for $\dot{C}ClFCONH_2$ was obtained. This means that the cross section for dissociative electron attachment to fluorine is very much smaller than that to chlorine.

On the other hand, no spectral evidence was obtained for the formation of $\dot{C}F_2COOEt$ in MTHF glass containing CF_3COOEt. This is in marked contrast to the case of $CF_2HCOOEt$ and may result from the lower C–F bond strengths of the partially fluorinated compounds compared to those of the trifluoro compounds.[15] It was, however, found that in a series of trifluoro compounds, CF_3COOH, CF_3COOEt, and CF_3CONH_2, having different functional groups, only the last compound having the least electron-withdrawing group gave the radical $\dot{C}F_2CONH_2$ formed from C–F bond rupture. This suggests that the electron-withdrawing tendency of the functional group is another important factor for the dissociative process.

Since the γ radiolysis of cyclohexane–perfluorocyclohexane mixture has been the subject of many recent studies in view of the mechanism of the C–F bond rupture,[4-9] a similar experiment was also carried out using perfluorocyclohexane. However, no spectral evidence was obtained for the formation of $c\text{-}C_6F_{11}\cdot$ in the MTHF glass containing $c\text{-}C_6F_{12}$, although its formation is reported in pure $c\text{-}C_6F_{12}$ irradiated at 77°K.[16]

In our previous work[10] on an irradiated single crystal of CH_2FCONH_2, we have assumed the direct breakage of the C–F bond by ionizing radiation producing the $\dot{C}H_2CONH_2$ and a hot fluorine atom which reacts with the surrounding molecules to form the radical pair. However, the results obtained in the present study suggest that the ionic process plays an important role in the formation of the isolated $\dot{C}H_2CONH_2$ radical as well as the radical pair as described in our paper on the pairwise trapping of radicals in normal hydrocarbons.[17]

Acknowledgment. The authors wish to thank Dr. Z. Kuri of Nagoya University for his suggestion of the possibility of the ionic process in irradiated CH_2FCONH_2. They also wish to thank Mr. H. Muto of our laboratory for his cooperation in the experiments carried out for the MTHF glasses containing $c\text{-}C_6F_{12}$ and CF_3COOH. They are grateful to Dr. S. Nagase and Mr. H. Baba of our Institute for providing the sample of $c\text{-}C_6F_{12}$.

(15) L. Pauling, "The Nature of the Chemical Bond," Cornell University Press, Ithaca, N. Y., 1960, p 314.

(16) C. Chachaty, A. Forchioni, and M. Shiotani, *Can. J. Chem.*, **48**, 435 (1970).

(17) M. Iwasaki, T. Ichikawa, and T. Ohmori, *J. Chem. Phys.*, **50**, 1991 (1969).

Infrared and Raman Spectra of Group I Nitrate Aggregates in Carbon Dioxide Matrices and Glassy Thin Films

by Gary Pollard, Norman Smyrl, and J. Paul Devlin*

Department of Chemistry, Oklahoma State University, Stillwater, Oklahoma 74074 *(Received January 10, 1972)*

Publication costs assisted by the National Science Foundation

Aggregates of the group I nitrates in CO_2 matrices have been prepared by reducing the matrix gas-to-sample ratio to well below the value required for complete monomer isolation. The infrared and Raman spectra of the resulting $LiNO_3$ aggregates, through comparison with published melt spectra, clearly indicate a glassy rather than crystalline structure. It has further been discovered that deposition of the nitrate vapors at −180°, in the absence of any matrix gas, permits the formation of pure glass thin films and presents the possibility of preparation of bulk quantities of the group I nitrate glasses.

Introduction

It has recently been shown that the alkali metal nitrates and $TlNO_3$ can be volatilized smoothly with very little decomposition at temperatures near their respective melting points.[1-4] Consequently, it was possible to characterize spectroscopically the monomers (MNO_3), and, in some cases, the dimers $(MNO_3)_2$, of a number of the group I nitrates[4] using the familiar methods of matrix isolation of high temperature

(1) A. Büchler and J. L. Stauffer, *J. Phys. Chem.*, **70**, 4092 (1966).

(2) C. J. Hardy and B. O. Field, *J. Chem. Soc.*, 5130 (1963).

(3) J. P. Nalta, N. W. Schubring, and R. A. Dork, from "Thin Film Dielectrics Symposium," The Electrochemical Society, New York, N. Y., 1969, p 236.

species.[5-7] For such studies it is well known that reduction of the matrix to sample ratio below some limiting value will result in the formation of aggregates of the isolated species as evidenced by their characteristic spectra. Thus, Pimental, *et al.*,[8] observed the formation of $(H_2O)_n$ polymers as well as the water monomer and dimer as the H_2O concentration in an N_2 matrix was varied over an appropriate range.

It was, therefore, predictable that the use of high MNO_3 to matrix gas ratios in the cocondensation of MNO_3 vapors with an inert gas would result in the formation of $(MNO_3)_n$ aggregates. It has recently been reported that the vibrational spectra of such aggregates are very similar to the spectra of the corresponding melts.[9] It is also known that the spectra for the internal modes of bulk glasses, such as $Ca(NO_3)_2$–KNO_3,[10] are insensitive to transition to the liquid state as assumed by Angell, *et al.*[11] Thus there is evidence that the aggregates that form in the nitrate rich matrices are glassy in structure.

In this paper the infrared and Raman spectra for $LiNO_3$, KNO_3, and $TlNO_3$ isolated and aggregated in a CO_2 matrix will be presented and compared with published spectra for the corresponding melts. Further, the spectra of pure nitrate thin films, vapor deposited and sampled at $-180°$, will be presented as evidence that such films are also glasses. A preparation of the pure alkali metal nitrate glasses by thermal quenching of tiny liquid droplets has been reported,[11] but previous attempts to prepare samples suitable for quantitative studies have, in general, been unsuccessful.

Experimental Section

The infrared and Raman (5145-Å excitation) sampling techniques and instrumentation have been described for the study of the matrix-isolated monomers and dimers of MNO_3.[4] In the present study all deposits were prepared at a substrate temperature of $\sim -180°$ and only CO_2 was used as a matrix gas. The nitrates were vaporized from a Pyrex glass Knudsen cell which made precise measurement of the vaporization temperature impossible, but also eliminated leakage problems encountered with the stainless steel cells used in the earlier study. Suitable vaporization temperatures were established by trial and error, the choice for $LiNO_3$ and $TlNO_3$ being the highest temperature at which nitrate decomposition is insignificant ($\sim$350 and $\sim$250°, respectively). Nitrate decomposition was easily monitored using the intense N_2O_4 bands near 1750 and 1260 cm^{-1}, as NO_2 diffuses and associates in CO_2 at $-180°$.

An attempt will be made in a few cases to determine the temperature, on warming, at which significant spectroscopic changes occur (*i.e.*, the glass crystallization temperature). These temperatures are presently being carefully established using a Displex[12] closed cycle helium refrigeration system and will be reported in a later paper.

Results and Discussion

Though a limited amount of data consistent with the following discussion has been obtained for other systems (*i.e.*, $NaNO_3$ and $RbNO_3$), the results for $LiNO_3$, KNO_3, and $TlNO_3$ will be emphasized. Of these, the $LiNO_3$ data are the most informative, primarily because the nitrate ion's internal vibrational spectrum is considerably more sensitive to the sample phase of the MNO_3 when the cation is lithium. Thus, the infrared and Raman spectra of molten $LiNO_3$ are sufficiently different from those of crystalline $LiNO_3$ that there is no problem in identifying the matrix aggregate spectra with the former rather than the latter. Regardless of the system, however, discussion will be based primarily on the ν_1 symmetric stretching mode ($\sim$1050 cm^{-1}) and the ν_3 doubly degenerate asymmetric stretching mode ($\sim$1350 cm^{-1}) of the undistorted (D_{3h} symmetry) nitrate ion. Except for $TlNO_3$, the ν_4 mode is so weakly infrared active that it has not been observed. The ν_2 out-of-plane bending mode is observed in all cases but is useful to the present development only in the $LiNO_3$ case.

$LiNO_3$. The $LiNO_3$ infrared absorption in the ν_1 and ν_2 region is presented in Figure 1 as a function of the CO_2 concentration for the low-temperature deposits along with the molten salt ν_1 and ν_2 infrared bands as well as an indication of the solid state ν_1 and ν_2 values. In Figure 2, the ν_1 Raman curves are indicated for the pure low-temperature deposit, the liquid and the crystalline $LiNO_3$. Though the ν_1 band has been observed by Raman scattering for both the isolated monomer and the aggregates of other nitrates in matrices,[4] this has not proved possible with $LiNO_3$ apparently because of interference from the fluorescence of a small amount of NO_2 in the matrix.

The nitrate ν_1 mode is infrared inactive in the D_{3h} anion, but the sharp features at 1017 and 1030 cm^{-1} in Figure 1a result from activation of this mode through the strong cation distortion of the anion in the monomer and dimer, $(MnO_3)_2$.[4] A lower CO_2 ratio is reflected in

(4) D. Smith, D. W. James, and J. P. Devlin, *J. Chem. Phys.*, **54**, 4437 (1971).

(5) G. C. Pimentel, D. A. Dows, and E. J. Whittle, *ibid.*, **22**, 1943 (1954).

(6) W. Weltner and J. R. Warn, *ibid.*, **37**, 292 (1962).

(7) M. J. Linevsky, *ibid.*, **34**, 587 (1961).

(8) M. Van Thiel, E. D. Becker, and G. C. Pimental, *ibid.*, **27**, 486 (1957).

(9) D. Smith and J. P. Devlin, Paper I-1, Twenty-sixth Symposium on Molecular Structure and Spectroscopy, Ohio State University, June 1971.

(10) D. W. James and J. P. Devlin, unpublished work.

(11) C. A. Angell, J. Wong, and W. F. Edgell, *J. Chem. Phys.*, **51**, 4519 (1969).

(12) A trade name for the closed-cycle helium refrigeration unit marketed by Air Products and Chemicals, Inc., Allentown, Pa.

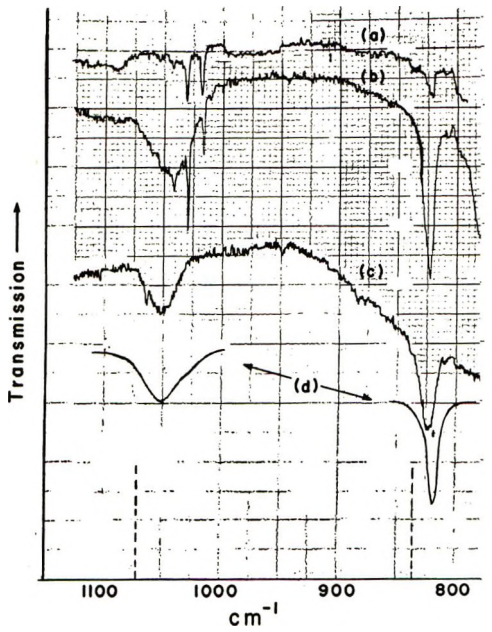

Figure 1. The infrared spectra for $LiNO_3$ (ν_1 and ν_2 modes) in different environments: (a) matrix isolated in CO_2; (b) isolated–aggregated mixture in CO_2; (c) pure film deposited at $-180°$; and (d) the molten salt at 275°. The vertical dashed lines represent the solid state $LiNO_3$ ν_1 and ν_2 transverse frequencies (25°).

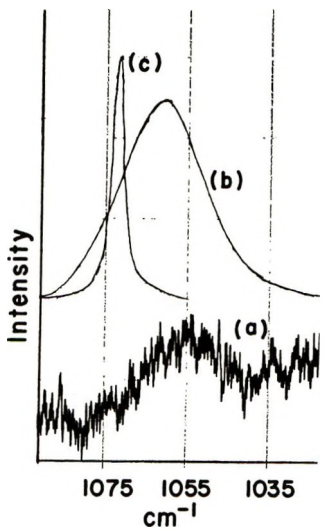

Figure 2. Raman bands for the ν_1 mode of $LiNO_3$: (a) pure film deposited at $-180°$; (b) molten salt; and (c) crystal at 25°

Figure 1b by the broad underlying feature peaked near 1045 cm^{-1} as well as new sharp bands (1043 and 1054 cm^{-1}) possibly attributable to an isolated trimer. The precise position of the broad feature (1052 cm^{-1}) is more obvious for the pure deposit (Figure 1c). By comparison, the liquid atr ν_1 peak is at 1053 cm^{-1},[13] while the crystalline ν_1 value (infrared inactive) is 18 cm^{-1} higher.[14]

The different Raman ν_1 band frequencies compare similarly as is apparent from Figure 2. Thus the

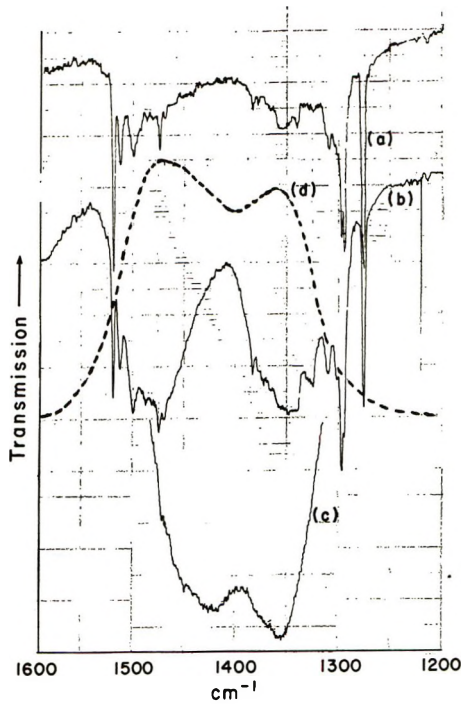

Figure 3. Infrared bands for the ν_3 mode of $LiNO_3$: (a) matrix isolated in CO_2; (b) isolated–aggregated mixture in CO_2; (c) pure film deposited at $-180°$. Curve d is the Raman band complex for the molten salt.

ν_1 data strongly suggest that $LiNO_3$ associates to a glassy state at $-180°$ with a structure similar to the $LiNO_3$ melt. The ν_2 infrared curves support this view as the matrix aggregate and pure deposit frequencies are both 823 cm^{-1}, a value comparable to the liquid values of 819 (atr) and 824 cm^{-1} (Raman),[13,15] but well below the crystalline values of 836 (TO) and 846 (LO).[16]

The foregoing interpretation is affirmed by the $LiNO_3$ ν_3 infrared curves of Figure 3. Though the sharp isolated-species bands (Figure 3a) interfere somewhat in Figure 3b the aggregates clearly produce two well-defined absorption maxima at ~1350 and 1475 cm^{-1}. These maxima agree to within 5 cm^{-1} with the maxima in the Raman liquid curve (Figure 3d). In the total absence of CO_2 the deposit has a somewhat different infrared ν_3 transmission band complex (Figure 3c). The latter fact is no doubt a result of the strong wavelength dependence of the dielectric constant (reflectivity) of $LiNO_3$ in the region of the extremely intense ν_3 absorption. This wavelength dependence is reduced in significance for the glass imbedded in a matrix for which the refractive index

(13) J. P. Devlin, P. C. Li, and G. Pollard, *J. Chem. Phys.*, **52**, 2267 (1970).

(14) R. E. Miller, R. R. Getty, K. L. Trevil, and G. E. Leroi, *ibid.*, **51**, 1385 (1969).

(15) M. H. Brooker, A. S. Quist, and G. E. Boyd, *Chem. Phys. Lett.*, **9**, 242 (1971).

(16) J. P. Devlin and R. P. J. Cooney, *ibid.*, **52**, 5495 (1970).

is >1.0, but is a dominant factor in the pure glass thin film "transmission" spectrum. It would have been more surprising had the ν_3 band not appeared differently in the two cases.

Before leaving the $LiNO_3$ study, two additional features in the ν_1 band region are worthy of comment. It has previously been pointed out that the Raman ν_1 peak for molten $LiNO_3$ (1062 cm^{-1}) is nearly 10 cm^{-1} above the infrared band maximum (1053 cm^{-1}).[13] A similar but somewhat smaller difference has been found for the glass Raman (1057 cm^{-1}) and infrared (1052 cm^{-1}) peak values. Secondly, attention is called to the rather dramatic fashion in which the isolated monomer, dimer, trimer, etc., sharp ν_1 features "march" up the low-frequency side of the glass aggregate band (Figure 1b). We believe that these two features combined suggest a model of the glass (and, therefore, of the melt) that resembles, in some respects, a view recently suggested by Irish and Brooker.[17] These authors have suggested that the nitrate ion in the $LiNO_3$ melt may assume two or more quite different environments (sites). Our data can be similarly interpreted if one recalls that the ν_1 infrared intensity is determined by the extent of anion distortion. Thus, relatively few nitrate ions, inhabiting sites in the glass resembling those in the monomer and dimer, and, therefore, having a relatively large ν_1 extinction coefficient, could produce the ν_1 infrared wing that cuts off very near the monomer frequency (~1015 cm^{-1}) (see Figure 1b). A significantly greater number of nitrate ions, in more symmetric[18] but nevertheless distorting sites and thus, with a lower extinction coefficient, could then produce the infrared maximum near 1050 cm^{-1}. The remaining and by far the greatest fraction of nitrate ions, occupying sites nearly as symmetric as in the trigonal crystal and with a vanishingly small ν_1 extinction coefficient, dominate the ν_1 Raman scattering (~1060-cm^{-1} peak) but contribute only weakly to the infrared band (*i.e.*, the scattering cross section is less sensitive to anion distortion than is the extinction coefficient so that the Raman band is more representative of the number of ions in a particular environment). The Raman ν_1 band has a weak low frequency shoulder as required by this view. A continuous distribution of nitrate ions as a function of site symmetry, ranging from the one limit represented by the monomer (MNO_3) and the other limit represented by the crystal, is the essence of this view of the glass.

The foregoing deviates from an earlier suggestion that the melt infrared–Raman ν_1 peak differences are a result of the dynamical coupling of nitrate ions in the melt[13] but does not rule out the possibility that the ν_3 splitting is produced by some such coupling.[19] In contrast to the case for ν_1, the infrared intensity in the ν_3 region would arise largely from the high percentage of anions at the more symmetric sites.

KNO_3. As mentioned above, it is not possible to present a strong independent argument that KNO_3 forms glassy aggregates in a nitrate rich CO_2 matrix because of the relatively small shifts in the nitrate ion internal mode frequencies that accompany the various changes in phase. For example, a ν_1 difference of 15 cm^{-1} (1035 *vs.* 1050) between the KNO_3 monomers and crystal can be contrasted with the 54-cm^{-1} difference (1017 *vs.* 1071) for $LiNO_3$. Nevertheless, with the $LiNO_3$ results as a guide an interpretation of the corresponding KNO_3 data (Figure 4) in terms of a glass structure is natural.

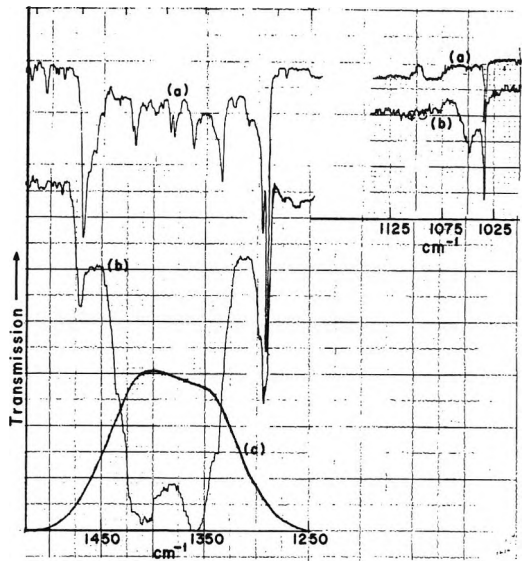

Figure 4. Infrared bands for the ν_1 and ν_3 modes of KNO_3: (a) isolated in CO_2; (b) isolated–aggregated mixture in CO_2. Curve c is the Raman band for molten KNO_3 at 360°.

In the ν_3 region the sharp side bands (1295 and 1470 cm^{-1} in Figure 4b) clearly correspond to the previously reported monomer frequencies,[4] while the aggregate band maxima (1360 and 1410 cm^{-1}) fit nicely within the broad melt Raman band (Figure 4c). Also, the sharp ν_1 feature (1035 cm^{-1} in Figure 4b) is that of the monomer, while the broader feature at 1048 cm^{-1} is near the 1045 cm^{-1} melt atr value and is thus assigned to the glass. In Figure 5 the matrix-isolated monomer Raman band is evident at 1036 cm^{-1} (Figure 5a) while the aggregate Raman band peak value (1048 cm^{-1}) agrees with the infrared value within experimental error.

Perhaps more noteworthy is the similarity in half bandwidths for the ν_1 melt (Figure 5b) and glass aggregate (Figure 5a) bands, both being ~12 cm^{-1}. The infrared and Raman ν_1 bands of KNO_3 each have less than half the width of the corresponding $LiNO_3$

(17) This view is referred to in ref 15 and is presented in more detail in an article to be published by M. H. Brooker, G. Chang, A. R. Davis, and D. E. Irish.

(18) Symmetry is given a qualitative attribute in this discussion that it lacks in a rigorous sense.

(19) J. P. Devlin, D. W. James, and R. Frech, *J. Chem. Phys.*, **53**, 4394 (1970).

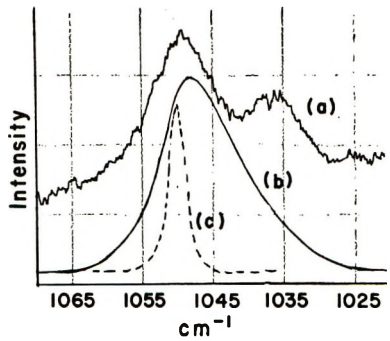

Figure 5. Raman ν_1 bands for KNO_3: (a) isolated–aggregated mixture in CO_2; (b) molten salt at 360°; and (c) crystal at 25°. Curve a was obtained at 3-cm^{-1} spectral slit width and a count rate of 500/sec.

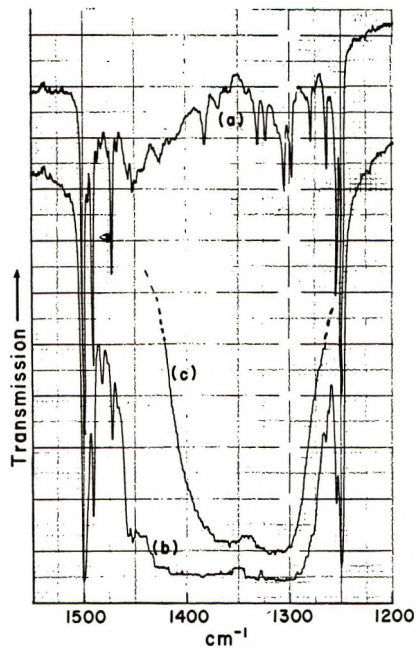

Figure 6. Infrared bands for the ν_3 mode of $TlNO_3$: (a) isolated in CO_2; (b) isolated–aggregated mixture in CO_2; and (c) pure film deposited at −180°.

features (~27 cm^{-1} in Figures 1 and 2). This is strong support of the view that the liquid ν_1 bandwidth and shape is determined by the distribution of nitrate ions over sites varying from monomer-like to crystal-like, since, as stressed above, this range is compressed for KNO_3 relative to $LiNO_3$. Further, $NaNO_3$ is known to have an intermediate range (1023–1069 cm^{-1}) and the $NaNO_3$ glass and liquid ν_1 bandwidths are ~17 cm^{-1}.

$TlNO_3$. The infrared and Raman spectra for $TlNO_3$ appear in Figures 6–8. The ν_3 region is describable in the terms used for $LiNO_3$ and KNO_3 for the three cases of isolated monomer, $TlNO_3$-rich CO_2 matrix and low temperature pure film deposit (Figure 6). Sharp monomer features near 1250 and 1500 cm^{-1} are still obvious in Figure 6b, but an intense broad

Figure 7. Infrared bands for the ν_1 mode of $TlNO_3$: (a) isolated in CO_2; (b) isolated–aggregated mixture in CO_2; (c) pure film deposited at −180°; and (d) crystal at 25°.

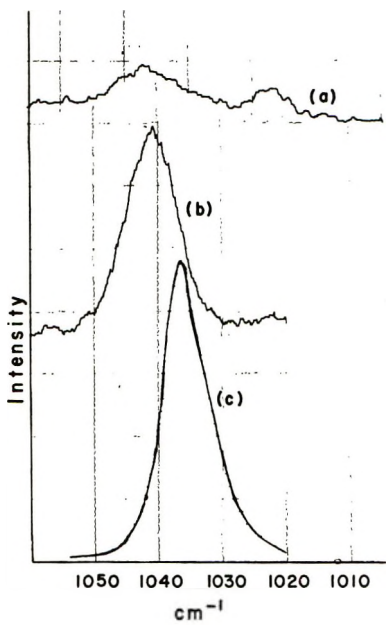

Figure 8. Raman ν_1 bands for $TlNO_3$: (a) isolated–aggregated mixture in CO_2; (b) pure film deposited at −180°; and (c) molten salt at 225°. Curve a was obtained at 3-cm^{-1} spectral slit width and a count rate of 500/sec.

doublet developed as the $TlNO_3$ concentration in the matrix was increased. The maxima for this doublet

(1310 and 1390 cm^{-1}) are each less than 10 cm^{-1} from published melt Raman values,[20] supporting the notion that $TlNO_3$ also forms glassy aggregates when deposited at −180°. The ν_3 infrared band is markedly different for the pure deposit (Figure 6c) with the influence of the dielectric constant variation with wavelength the probable cause (as discussed for $LiNO_3$).

The influence of aggregate formation on the infrared ν_1 band of matrix-isolated $TlNO_3$ is shown in Figure 7, but it should be noted that the aggregate band near 1040 cm^{-1} is close to the solid-state Raman value (1041 cm^{-1} for $TlNO_3$ III) as well as the melt Raman frequency (1036 cm^{-1}).[20] Nevertheless, the reduction of the ν_1 half bandwidth upon annealing (from 11 to 4 cm^{-1}), is suggestive of a glass–crystal phase transition. Further, the Raman melt ν_1 half bandwidth has been reported as 8 cm^{-1} at 230°,[20] while Figure 8 shows that the aggregate and thin film Raman bands have comparable widths (~10 cm^{-1}). Figure 8a also shows, once again, the ability to observe the monomer ν_1 mode (1022 cm^{-1}) in the Raman spectra of matrix isolated group I nitrates, as well as the relative influence of nitrate ion site symmetry on the ν_1 infrared and Raman intensities (*i.e.*, the badly distorted monomer nitrate infrared band dominates Figure 7b whereas the nitrates in the glassy aggregates, being more numerous, dominate the Raman curve (Figure 8a). It may be significant that the $TlNO_3$ glass ν_1 band is higher in frequency than for the melt (Figure 8) whereas the reverse is apparently the case for $LiNO_3$ (Figure 2) and there is no detectable difference in the band positions for the two phases of KNO_3 (Figure 5).

Acknowledgment. This research was supported by National Science Foundation Grant GP-24256.

(20) D. W. James and J. P. Devlin, *Aust. J. Chem.*, **24**, 743 (1971).

Raman Spectra and Structure of Molten Cadmium Chloride, Molten Cadmium Bromide, and Their Molten Mixtures with Alkali Metal Halides

by J. H. R. Clarke,* P. J. Hartley, and Y. Kuroda

Chemistry Department, The University of Southampton, Southampton SO9 5NH, England *(Received December 29, 1971)*

Publication costs borne completely by The Journal of Physical Chemistry

The distribution of symmetric Cd–Cl stretching frequencies in molten $CdCl_2$ and molten mixtures of $CdCl_2$ with LiCl, KCl, and CsCl has been studied by means of laser-Raman spectroscopy. Detailed comparisons are made with spectra of related crystalline compounds. Limited studies were made for molten $CdBr_2$ and molten mixtures of $CdBr_2$ with KBr. Spectra of the pure molten cadmium halides are explained in terms of a fluctuating local structure based on octahedral coordination of Cd^{2+}. Addition of alkali metal halides in each case results in the eventual replacement of octahedral by tetrahedral Cd^{2+} coordination sites. Specific influences of different alkali metal cations are discussed in the light of current theories. Bandwidth measurements indicate that $CdCl_4^{2-}$ has kinetic identity in molten alkali metal chloride solutions.

Introduction

Few molten salt systems have aroused such controversy regarding their structure as the cadmium halides and their binary mixtures with alkali metal halides. Complex ions such as $CdCl_3^-$, $CdCl_4^{2-}$, and $CdCl_6^{4-}$ have all been separately proposed[1-4] as being formed in the mixtures. On the basis of calorimetric studies, Bredig has argued strongly in favor of the stability of tetrahedral $CdCl_4^{2-}$ and has concluded[2] that in such binary systems this species should be expected to predominate even to the exclusion of all other complexes. A number of Raman spectral investigations have been reported[1,4,5] for pure molten cadmium chloride and the system $CdCl_2$–KCl, but the data and interpretation have often been of questionable reliability and it is not surprising that conflicting conclusions were obtained. As pointed out recently,[5] the under-

(1) W. Bues, *Z. Anorg. Allg. Chem.*, 279 (1955).

(2) M. A. Bredig in "Molten Salts," G. Mamantov, Ed., Marcel Dekker, New York, N. Y., 1969.

(3) H. Bloom, *Pure Appl. Chem.*, **7**, 398 (1963).

(4) M. Tanaka, K. Balasubramanyam, and J. O'M. Bockris, *Electrochim. Acta*, **8**, 261 (1963).

(5) V. A. Maroni and E. J. Hathaway, *ibid.*, **15**, 1837 (1970).

lying problem has been that there is not sufficient detail in the Raman spectra to permit a reliable structural analysis by applying the usual group theoretical selection rules.

In this investigation special attention has been afforded to the frequency distribution and intensity of symmetric Cd–Cl stretching modes in the Raman spectra. Extensive comparisons have been made with the spectra of crystalline cadmium chloro complexes of known structure, and studies of molten binary mixtures have been extended to the general system CdX_2–AX (A = Li, K, Cs). In this way a clearer understanding has been achieved of the nature of the liquid structures and the specific influence of alkali metal cations. Additional studies were made for molten cadmium bromide and its mixtures with potassium bromide. The kinetic stability of cadmium chloro complexes also is discussed in the light of the temperature dependence of Raman bandwidths.

Experimental Section

A sectional diagram of the furnace and Raman cell is shown in Figure 1. The furnace is supported by a stainless steel tripod, the feet of which are located in a brass cooling plate on the spectrometer. The laser beam enters through the furnace base plate, and the light scattered at right angles is observed through ports in the walls of the furnace. The heating element consists of nichrome wire wound on a pyrophyllite former. Power dissipation in the upper portion of the furnace is regulated by a rheostat to reduce temperature differences. To eliminate temperature gradients over the length of the sample a stainless-steel block is incorporated in the lower half of the furnace. Design is such that no thermal radiation from the furnace enters the aperture of the spectrometer. Spectra have been obtained with good signal-to-noise ratios at temperatures up to 1000°. A control thermocouple passes through the furnace wall, the pyrophyllite former, and the steel liner to make contact with the Raman cell. The temperature of a sample is constant to ±4°.

The sample tubes are similar to those described previously.[6] The important features of the design are that samples can be prepared and/or purified *in situ* immediately prior to an experiment and that only small samples (0.5 ml) are required. The cell is closed at the top by means of a ground-glass cone arrangement which may be connected either to a dry nitrogen supply or a vacuum line. The same connections are available at the side arm of the cell. Mixing of the samples was achieved prior to filtration by bubbling dry nitrogen up through the sintered disk.

Anhydrous cadmium chloride was prepared from the hydrated "Analar" grade reagent by treatment with refluxing thionyl chloride.[7] Anhydrous cadmium bromide was prepared from the hydrated salt by heating to 600° while flushing continuously with dry hydrogen bromide. Alkali metal halides were dried *in vacuo* at 360° for 24 hr. All the solid compounds of cadmium chloride with alkali metal chlorides were prepared by cooling melts of the required composition. The compound NH_4CdCl_3 was prepared as described in the literature.[8]

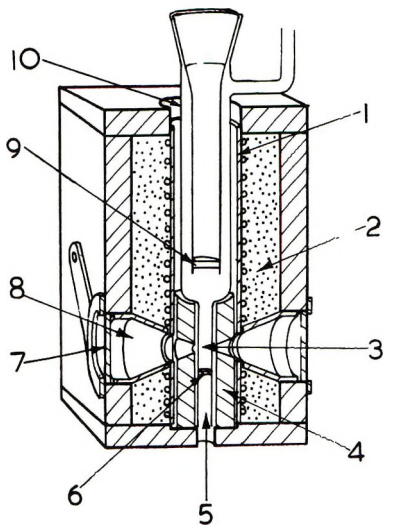

Figure 1. Sectional diagram of the sample furnace: 1, pyrophyllite former; 2, Fyberfax insulation; 3, thermocouple position; 4, steel liner; 5, entrance for laser beam; 6, optical flat; 7, Pyrex windows; 8, pyrophyllite cone; 9, sintered disk; 10, Raman cell.

All melts were clear and stable. Spectra were obtained using a Spex 1401 double monochromator with instrumental resolution chosen between 0.5 and 2.0 cm^{-1}. The 514.5-nm line of an argon ion laser (Spectra-Physics Model 140) was used to excite spectra of the chloride melts. For the bromide mixtures (red to yellow colors), the 647.1-nm line of an argon–krypton ion laser (Coherent Radiation Model 52MG) was employed.

Results and Discussion

The Raman spectrum of liquid $CdCl_2$–2CsCl is shown in Figure 2. This spectrum is typical in general form of all spectra obtained in this study.

Two particular regions of Raman scattering can be distinguished, associated with Cd–Cl stretching modes (200–270 cm^{-1}) and Cl–Cd–Cl deformation modes (70–120 cm^{-1}). The latter mentioned modes appear as depolarized bands in the Raman spectrum. However, since they are comparatively ill-defined we shall discuss them no further. Raman bands in the region 200–270 cm^{-1} are all highly polarized (ρ values of 0.05–0.10) indicating that the stretching vibrations are symmetric in character. Although we also expect

(6) J. H. R. Clarke, C. Solomons, and K. Balasubramanyam, *Rev. Sci. Instrum.*, **38**, 655 (1967).

(7) D. M. Adams, J. Chatt, J. M. Davidson, and J. Gerratt, *J. Chem. Soc.*, 2189 (1963).

(8) H. Brasseur and L. Pauling, *J. Amer. Chem. Soc.*, **60**, 2886 (1938).

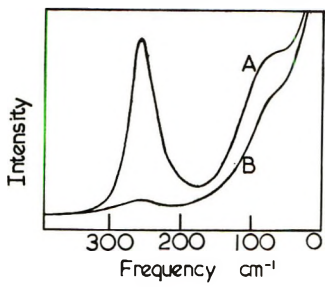

Figure 2. Raman spectrum of molten $CdCl_2$–2CsCl at 520° showing (A) polarized and (B) depolarized components. Spectral noise was so low as not to be reproducible.

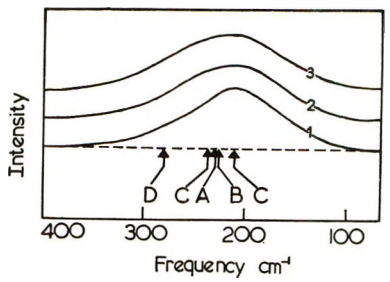

Figure 3. Raman spectrum of molten $CdCl_2$ in the Cd–Cl stretching region corrected to a horizontal base line: (1) 600°, (2) 800°, (3) 900°. The vertical arrows indicate the CdCl stretching frequencies at 580°, for the crystalline compounds (A) $CdCl_2$, (B) K_4CdCl_6, and (C) NH_4CdCl_3. (D) indicates the symmetric stretch frequency reported[17] for molecular $CdCl_2$ dissolved in TBP at 25°.

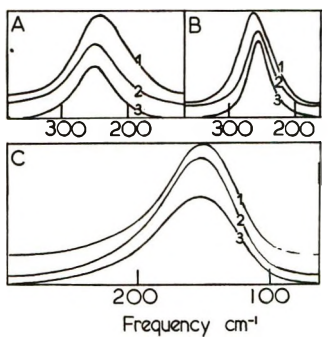

Figure 4. Raman spectra of selected melts in the Cd–Cl stretching region corrected to a horizontal base line: A1, $CdCl_2$–LiCl at 640°; A2, $CdCl_2$–2LiCl at 700°; A3, $CdCl_2$–5LiCl at 700°; B1, $CdCl_2$–CsCl at 580°; B2, $CdCl_2$–2CsCl at 600°; B3, $CdCl_2$–5CsCl at 588°; C, $CdBr_2$, (1) at 585°, (2) at 730° (3) at 810°.

some asymmetric stretching modes to appear[9] in the spectrum (as depolarized bands), these could never be distinguished, presumably because they are very weak and/or very broad.

The assumption in the following discussion is that the frequency distribution of intensity in the Cd–Cl stretching bands can be used as a fingerprint of the instantaneous distribution of Cd^{2+} coordination sites. The question as to whether or not any of these sites can be identified as a kinetically stable species will be considered separately. The advantage of studying symmetric stretching modes is that generally the vibration frequency shows a direct correlation with the coordination number and the extent of charge neutralization on the metal ion. This approach can be criticized[10] as not recognizing implicitly the coupling between vibrational modes in a dense medium, *i.e.*, the "collective" nature of vibrations. However, at present there is no adequate general treatment relating the phonon distribution in molten salts to structural properties. Also, it is generally true that symmetric vibrations are the least sensitive to coupling effects so that vibration frequencies can be related to a good approximation to *local* structural properties. It will be seen that this conclusion finds confirmation in, for instance, the invariance of band frequency with composition for moderately dilute solutions of cadmium chloride in different molten alkali metal chlorides.

Profiles of the Cd–Cl and Cd–Br stretching bands for the pure liquid cadmium halides and for various mixtures with alkali metal halides are collected together in Figures 3 and 4.

Spectra of Crystalline Compounds. Before considering the spectra of the molten samples it is useful to discuss spectra characteristic of crystalline cadmium chloro complexes of known structure. These data are summarized in Table I.

Firstly, we consider the spectrum of crystalline $CdCl_2$ which has the well-known layer structure,[11] containing octahedrally coordinated Cd^{2+} and in which *all* the chlorides are triply coordinated. For the polycrystalline sample, only one band is observed in the region of the Cd–Cl stretching vibrations—at 235 cm^{-1} (25°)—and this feature is assigned to the symmetric "breathing" mode of six Cl^- ions around each Cd^{2+} (A_{1g} symmetry for the factor group D_{3d}[5]).[12] This vibration frequency is very similar in magnitude to that of the terminal Cd–Cl (symmetric) stretching vibration at 229 cm^{-1} in K_4CdCl_6 which contains discrete $CdCl_6^{4-}$ units.[11] This surprising result is explained by assuming that the influence of the sharing of chloride ions in $CdCl_2$ and the neutralization of the positive charge on Cd^{2+} in $CdCl_6^-$ are approximately equivalent.

There are a number of crystalline compounds of general formulas $ACdCl_3$ and A_2CdCl_4, and the structures are all based on octahedral coordination of Cd^{2+}. In $CsCdCl_3$[13] and NMe_4CdCl_3[14] there are

(9) J. H. R. Clarke and R. E. Hester, *J. Chem. Phys.*, **50**, 3106 (1969).

(10) C. A. Angell, J. Wong, and W. F. Edgell, *ibid.*, **51**, 4519 (1969).

(11) A. F. Wells, "Structural Inorganic Chemistry," Oxford University Press, London, 1962.

(12) D. J. Lockwood and J. H. Christie, *Chem. Phys. Lett.*, **9**, 559 (1971).

(13) S. Siegel and E. Gerbert, *Acta Crystallogr.*, **17**, 790 (1964).

(14) D. M. Adams and D. C. Newton, *J. Chem. Soc. A*, 3499 (1971).

Table I: Raman Spectral Data for Compounds Containing $CdCl_6$ Octahedra[a]

Crystalline compound	Structure (references as in text)	(Symmetric) Cd–Cl —stretching frequencies, cm^{-1}— At 25°	At 580° (extrapolated)	Coordination of chloride ions
$CdCl_2$	Layer structure[b]	235	229	Triply shared
K_4CdCl_6	$CdCl_6^{4-}$ units[b]	229	222	Terminal
$CsCdCl_3$	Perovskite structure[c]	250	244	Doubly shared
Cs_2CdCl_4	K_2NiF_4 structure[c]	251	244	Terminal
		231	225	Doubly shared
NH_4CdCl_3	Two linked chains[d] of $CdCl_6$ octahedra	244 (244)[e]	238	Terminal
		219 (222)[e]	213	Doubly shared
		Not observed[e]		Triply shared
NMe_4CdCl_3	Single chains of $CdCl_6$ octahedra[e]	251[e]	...	Doubly shared

[a] Except as indicated all frequency values are from this work. [b] Reference 11. [c] Reference 13. [d] Reference 8. [e] Reference 14.

chains of $(CdCl_3^-)_\infty$ units, and all the chlorides are doubly coordinated. For each of these compounds a single symmetric Cd–Cl stretching vibration is observed, at 251 cm^{-1} for NMe_4CdCl_3[14] and 250 cm^{-1} for $CsCdCl_3$. By comparison with $CdCl_2$ these frequencies are remarkably high and may reflect weak interaction forces between cations and the $(CdCl_3^-)_\infty$ chains.[14] Crystalline NH_4CdCl_3 has a more complicated structure[8] derived from the $CdCl_2$ layer structure. It contains both doubly and triply coordinated Cl^- as well as terminal Cd–Cl bonds. The overall structure is that of two linked chains of $CdCl_6$ octahedra sharing edges. The Raman spectrum was determined at 25°, and there are two intense bands assigned to Cd–Cl stretching vibrations (244 and 219 cm^{-1}). On the basis of recent single crystal studies[14] these bands are assigned, respectively, to (symmetric) stretching modes involving mainly terminal and doubly coordinated chlorides. We note that the decrease of the characteristic stretching frequency involving terminal Cd–Cl bonds in passing from NH_4CdCl_3 (244 cm^{-1}) to K_4CdCl_6 (229 cm^{-1}) appears to reflect an increasing degree of charge neutralization on the cadmium ion. We can define a range from 219 to about 250 cm^{-1} at 25° over which frequencies associated with multiply coordinated chlorides can occur. It is not possible to be more specific since the forms of the normal modes are unknown and probably are very complicated (*e.g.*, the unit cell of NH_4CdCl_3 contains four formula units). In addition we have not taken account of the influence of the cations in the crystal lattices.

The peak frequencies discussed above decrease monotonically with increasing temperature up to the melting or decomposition points of the crystalline compounds. These decreases are associated with corresponding increases in the lattice dimensions. It is possible from these trends to estimate the frequencies that would be characteristic of the various (crystalline) structures at 580°, which is just above the melting point of cadmium chloride. These values are listed in Table I and are indicated in Figure 3. It is evident that they correspond to the central part of the Cd–Cl stretching band in molten cadmium chloride. It is worth noting that band half-widths for the crystals are very temperature sensitive. At 510°, the 230-cm^{-1} band of $CdCl_2$ has a full width at half-height of 32 cm^{-1} which is 28% of the value for the liquid state band.

Molten Cadmium Chloride. The broad Raman scattering, peaked at 215 cm^{-1} (Figure 3), was assigned by Bues[1] to remnants of the layer lattice in the melt. However, if we are to accept an explanation in terms of a polymeric structure, it must be recognized to be very different from that existing in, for instance, molten zinc chloride. Whereas the latter shows all the expected macroscopic properties of a polymeric melt[15] (*e.g.*, high viscosity and low conductivity), the macroscopic properties of molten cadmium chloride are similar in value to those observed for simple ionic melts.[15]

The spectra in Figure 3 show that the Cd–Cl stretching band of molten cadmium chloride has a complex shape which changes with temperature. It is our conclusion that a number of different coordination sites of Cd^{2+} are represented in the band contour. Band contour analysis was not considered to be a useful procedure for molten cadmium chloride. There are no sharp peaks with which to fix component frequencies and the results obtained are artificial. However, a brief description will be given of a melt structure which is consistent with our observations and which recognizes the dynamic aspect of liquid structure. The model is based on essentially octahedral coordination[2] sites for Cd^{2+}. It is clear from comparison with the solid state that chloride ions readily coordinate with two or three adjacent cadmium ions so that it is not surprising to find a large intensity of scattering in the

(15) G. J. Janz, "Molten Salts Handbook," Academic Press, New York, N. Y., 1967.

region 213–244 cm^{-1}. Substantial intensity for the melt at 580° occurs at frequencies somewhat lower than this range. However, the volume increase upon fusion may result in a further decrease of the characteristic frequencies of octahedrally coordinated Cd^{2+}.

Owing to liquid disorder we do not expect Cd^{2+} necessarily to be found in symmetric environments so that there will be a range of Cd–Cl bond distances. Also, chloride ions will not necessarily be shared equally with surrounding Cd^{2+} ions as they are in the solid. Hence the effective coordination number will vary from one Cd^{2+} to another as will the extent of charge neutralization. Consequently we expect a range of Cd–Cl vibration frequencies. High vibration frequencies in the spectra are associated with terminal Cd–Cl bonds involving Cd^{2+} with low net coordination numbers and low charge neutralization. The limiting distortion from octahedral coordination might be written, formally, as $Cd\text{–}Cl^+$. However it is not implied that $Cd\text{–}Cl^+$ or indeed any of these local coordination sites is a distinct species. The distribution of bonding interactions of a particular cadmium ion with surrounding chlorides may change quite rapidly, according to the structural relaxation time of the liquid, although this time will be long compared with the time for a vibration. The shift of intensity to higher frequencies with increasing temperature indicates that lower net coordination numbers are formed at the expense of bridging interactions.

Molten Cadmium Bromide. The temperature effects observed for spectra of molten cadmium bromide were similar to those of the chloride (Figure 4). However, the high-frequency wing of the Cd–Br stretching band is more pronounced than in the case of the chloride, indicating that lower net coordination numbers are more stable. This may be explained by assuming that coordination with the more polarizable bromide ion leads to more effective charge neutralization on Cd^{2+}. Indeed, this was found to be the case for cadmium bromide dissolved in molten sodium–potassium nitrate.[16]

Molten $CdCl_2$–ACl and $CdBr_2$–ABr Mixtures. The effect of adding alkali metal chloride to molten cadmium chloride is eventually to replace the broad complex Raman band in each case with a comparatively well-defined band at 255 ± 5 cm^{-1} (Figure 4). Following the remarks made in the preceding discussion it might at first seem possible to attribute this feature to octahedrally coordinated Cd^{2+}. However, detailed considerations do not support this explanation. For instance, at melt temperatures (>600°) the predicted range of Cd–Cl stretching frequencies characteristic of octahedral coordination (213–244 cm^{-1}) is significantly lower than the limiting peak frequencies for the molten $CdCl_2$–ACl mixtures (Figure 5).

Comparisons with studies of cadmium chloro complexes in molten sodium–potassium nitrate[16] and in other solvents[17] suggest that the 255-cm^{-1} band is

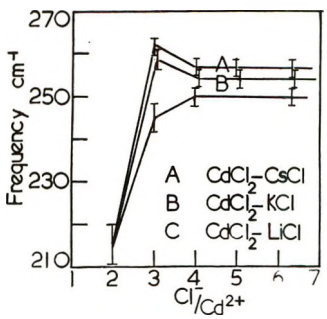

Figure 5. The dependence of the Cd–Cl stretching frequency on the ratio $Cl\text{–}Cd^{2+}$ for a series of molten mixtures. The accuracy of each frequency measurement is indicated by the vertical error bars.

characteristic of either $CdCl_3^-$ or $CdCl_4^{2-}$. In an attempt to resolve this situation, integrated intensities of the 255-cm^{-1} band were measured as a function of R (the chloride-to-cadmium ratio) for a series of $CdCl_2$–CsCl mixtures. Each contained 8 mol % of dissolved cesium sulfate and the 981-cm^{-1} band (ν_1 of SO_4^{2-}) was used as an internal intensity standard.[16] The intensity per mole of Cd^{2+} increased to a maximum limiting value at $R = 4$ indicating that the band is due to $CdCl_4^{2-}$ and that no further chloride ions become coordinated. Similar results were obtained for $CdBr_2$–KBr mixtures. It is interesting that using sodium–potassium nitrate as a solvent,[16] Raman spectral studies indicate that while $CdBr_4^{2-}$ is again readily formed, the highest stable chloro complex in this case is $CdCl_3^-$.

Further insight regarding the changes in coordination accompanying the addition of alkali metal chloride is obtained from the trends in peak frequency and band shape with changing melt composition (Figure 5). When either CsCl or KCl is added to molten $CdCl_2$, the bandwidth decreases very rapidly and becomes symmetric, and the peak frequency increases to a maximum value at $R = 3$. When R is increased from 3 to 4, this band decreases in intensity and is replaced by a new band of similar shape with a peak frequency ~5 cm^{-1} lower. At $R = 3.5$ the peak frequency is intermediate in value, and the band is a simple superposition of those observed for $R = 3$ and $R = 4$. When R is increased above 4, there is no further change in either peak frequency or half-width, and this is confirmatory evidence that the final coordination is $CdCl_4^{2-}$ (probably tetrahedral). However, the maximum in peak frequency observed at $R = 3$ is entirely unexpected if we merely assume a simple equilibrium between octahedral and tetrahedral coordination sites. The indication is that a different coordination site exists over a narrow composition change

(16) J. H. R. Clarke, P. J. Hartley, and Y. Kuroda, *Inorg. Chem.*, 11, 29 (1972).

(17) J. E. Davies and D. A. Long, *J. Chem. Soc. A*, 2054 (1968).

at $R \approx 3$. The higher Cd-Cl stretching frequency is associated with less neutralization of the charge on Cd^{2+} than in $CdCl_4^{2-}$. The structural unit involved may be $CdCl_3^-$ or else $CdCl_4^{2-}$ with two chlorides shared with neighboring cadmium ions.

The rapid changes in the distribution of Cd–Cl stretching vibrations caused by the addition of cesium or potassium chloride do not occur on the addition of lithium chloride. In this case, at $R = 3$ the band is asymmetric to lower frequencies. The residual scattering in the 220-cm^{-1} region is ascribed to retention of octahedral coordination sites. The peak frequency does not achieve a constant value of 250 cm^{-1} until $R = 4$. At this point the band is symmetric, as would be expected for a structure based on a single coordination geometry of Cd^{2+}. The band shows no further change in characteristics as R is further increased (Figures 4 and 5), and it is assigned, as before, to $CdCl_4^{2-}$. This conclusion is at variance with the interpretation of calorimetric measurements[18] on molten systems of the type $CdCl_2$–ACl (A = Cs^+ or Li^+). The enthalpy interaction parameter, λ^M, shows a minimum value at 33 mol % $CdCl_2$ for the system $CdCl_2$–CsCl indicating stabilization of $CdCl_4^{2-}$. A similar effect was not observed for the system $CdCl_2$–LiCl which was taken to indicate that $CdCl_4^{2-}$ was not formed in this system. However, a shallow minimum may have been obscured by the errors inherent[19] in these measurements. Also the interpretation of calorimetric results is less convincing for mixtures with LiCl, in which entropy effects probably are important.[20]

The average stretching frequency associated with tetrahedral coordination sites decreases regularly along the series $Cs^+ > K^+ > Na^+ > Li^+$. This trend can be understood as due to a corresponding increase in the polarizing power of the surrounding alkali metal cations and a consequent reduction in the Cd–Cl force constant. This "shell" of cations will not generally be symmetrically disposed about $CdCl_4^{2-}$ and fluctuations of the associated electric field will be greater for the lighter more polarizing cations. This accounts in general terms for the increase in bandwidth along the series $Cs^+ < K^+ < Na^+ < Li^+$.

If our interpretation is correct, then the reluctance of cadmium to take up tetrahedral coordination on the addition of lithium chloride is some confirmation of the theories put forward by Lumsden[20] and by Bredig[2] that in molten mixtures of the type MCl_2–ACl octahedral coordination sites are stabilized when A = Li, whereas tetrahedral coordination is more readily formed when A = K or Cs. This effect has been reported[21] extensively for the coordination of Ni^{2+} in chloride media. However, it should be emphasized that there is no evidence that cadmium can be induced to take up octahedral coordination for relatively dilute solutions in molten lithium chloride, as has been shown[21] to occur for Ni^{2+}. The liquidus curve for the system $CdCl_2$–LiCl is rather flat over the whole composition range[22] giving the appearance that there is solid solution formation in the system. It has been suggested[23] that such mixing of the two octahedral structures in the solid state would imply stabilization of octahedral coordination in the liquid state. However, not only is extensive solid solution formation in this system unlikely[24] on the basis of the widely different ionic radii of Cd^{2+} and Li^+ (respectively, 0.97 and 0.60 Å), but also our spectral measurements of solidified melt samples indicate that, in reality, there *is* compound formation in this system. It is seen from Table II that over a wide composition range the spectra can be explained in terms of the formation of a single compound, Li_2CdCl_4, at 25°. (The presence of lithium chloride is not evident since it has no first-order Raman spectrum.) The spectrum of Li_2CdCl_4 is similar to that of $CsCdCl_3$, and the two compounds may have similar structures (based on infinite chains of $CdCl_3^-$ units). At high temperatures the predicted frequency range of octahedrally coordinated Cd^{2+} in the lithium salt, as before, is considerably lower than the limiting peak frequency observed for the liquid mixtures. It is difficult to avoid the conclusion that the liquid state band arises from $CdCl_4^{2-}$

Table II: Raman Spectra of Solidified Melt Samples in the System $CdCl_2$–LiCl[a]

Mol % $CdCl_2$	Raman peaks (cm^{-1}) at 25°				
100	...	235 (10)	...	132 (8)	...
85	...	235 (10)	...	132 (8)	...
50	249 (4, sh)	236 (10)	149 (3, sh)	132 (8)	98 (3)
66.6	249 (10)	...	150 (6)	...	97 (6)
20	251 (10)	...	153 (6)	...	98 (5)
$CsCdCl_3$	250 (10)	...	131 (4)	117 (4)	70 (2)

[a] sh = shoulder. Relative intensities for each spectrum are given in parentheses.

In conclusion, it appears that octahedral coordination of Cd^{2+} is a property of the crystalline state and only those molten mixtures very rich in cadmium. It

(18) G. N. Papatheodorou and O. J. Kleppa, *Inorg. Chem.*, **10**, 872 (1971).

(19) G. N. Papatheodorou and O. J. Kleppa, *J. Inorg. Nucl. Chem.*, **32**, 889 (1970).

(20) J. Lumsden, "Thermodynamics of Molten Salt Mixtures," Academic Press, New York, N. Y., 1966.

(21) G. P. Smith, J. Brynestad, C. R. Boston, and W. E. Smith, in "Molten Salts," G. Mamantov, Ed., Marcel Dekker, New York, N. Y., 1969.

(22) (a) A. Ferrari and A. Baroni, *Atti Acad. Naz. Lincei, Cl. Sci. Fis., Mat. Natur., Rend.*, 7, 1040 (1929); (b) E. P. Dergunov, *Dokl. Akad. Nauk SSSR*, 64, 517 (1949).

(23) M. A. Bredig, private communication.

(24) R. C. Evans, "An Introduction to Crystal Chemistry," Cambridge University Press, New York, N. Y., 1964.

is interesting to compare these results with the exact opposite trend observed[9] for the coordination of In^{3+} in $InCl_3$–ACl mixtures (A = Cs, K, or Li). In this case the presence of Li^+ favors decomposition of $InCl_6^{3-}$ to $InCl_4^-$ but the less polarizing Cs^+, for instance, stabilizes the octahedral complex.

Changes in the shape and frequency of the Cd–Br stretching band on the addition of KBr to $CdBr_2$ show very similar trends to those observed for the $CdCl_2$–KCl system. The limiting frequency, 161 cm^{-1}, is close to that assigned previously to $CdBr_4^{2-}$ in molten sodium–potassium nitrate.[16] The transition from octahedral to tetrahedral coordination is not smooth, however, since a maximum peak frequency (165 cm^{-1}) occurs at $R = 3$. Once again this indicates the intermediate formation either of $CdBr_3^-$, or $(CdBr_3^-)_2$, with tetrahedral coordination of Cd^{2+}.

Bandwidth Measurements. Concern has been expressed as to the kinetic stability of complexes such as $CdCl_4^{2-}$ in molten salts.[10] In pure chloride media there is indeed the possibility of facile chemical exchange reactions with surrounding chloride ions. Any such exchange reaction should contribute to the Raman bandwidth for the $CdCl_4^{2-}$ stretching vibration. However, most of the broadening of this band can be attributed to the effects of dynamic disorder. This is evident from the fact that the full width at half-height (half-width) for $CdCl_4^{2-}$ in molten $CdCl_2$–CsCl, for example, is little different in value (43 cm^{-1}) from that observed[16] for $CdCl_3^-$ in molten sodium–potassium nitrate (40 cm^{-1}). Both chloride and bromide complexes of cadmium have very high thermodynamic stability in the latter solvent,[16] so there is no doubt that they are also kinetically stable.

We can investigate any chemical exchange contribution from the temperature dependence of bandwidths since the diffusion coefficient of Cl^- in $CdCl_2$–CsCl mixtures increases[25] by about 50% over the temperature range 500 to 700°. An estimate of the half-width contribution (W) from diffusion-controlled ligand exchange can be obtained at various temperatures by substituting[26] the apparent activation energies[25] for diffusion (ΔE) in the expression $W = h/kT \exp(\Delta E/RT)$. The predicted temperature dependence of W is shown in Figure 6 along with the observed changes in half-width for $CdCl_4^{2-}$ in $CdCl_2$–4CsCl. It is seen that the variation in half-width for $CdCl_4^{2-}$ does not approach the behavior expected for a diffusion-limited lifetime. In fact the variation is little greater than that observed for the symmetric stretch vibration of SO_4^{2-} (the half-width of $\nu_1(SO_4^{2-})$ in the $(Li,Na,K)_2SO_4$ eutectic at 540° is 29 cm^{-1}). Since the instrumental resolution was limited to 0.5 cm^{-1}, the precise kinetic stability of $CdCl_4^{2-}$ could not be determined. However, the measurements suggest that the lifetime of $CdCl_4^{2-}$ is longer than the relaxation times associated with diffusional motions.

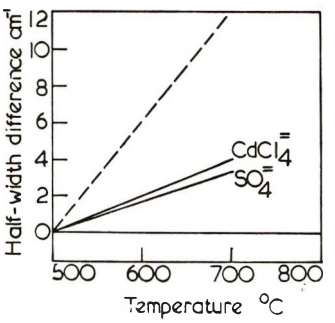

Figure 6. The temperature dependence of the full width at half-height for symmetric stretching bands of $CdCl_4^{2-}$ and SO_4^{2-}. The calculated temperature dependence, assuming diffusion-limited ligand exchange, is shown as a dashed line.

Acknowledgment. The authors express thanks to the U. K. Central Electricity Generating Board and the North Atlantic Treaty Organization for financial support. Also we are grateful to Dr. M. A. Bredig for his many helpful comments concerning the manuscript of this article.

(25) J. Koster, Thesis, University of Amsterdam (1971).

(26) H. Bloom and J. O'M. Bockris in "Fused Salts," B. R. Sundheim, Ed., McGraw-Hill, New York, N. Y., 1964.

Structural Evolution of Chromia

by P. Ratnasamy and A. J. Léonard*

Laboratoire de Physico-Chimie Minérale, Institut des Sciences de la Terre, 42, de Croylaan, 3030, Heverlee-Louvain, Belgium
(Received November 8, 1971)

Publication costs assisted by Musée Royal de l'Afrique Centrale, M. E. N. C. (Belgium)

The evolution of the structure of α-Cr_2O_3 from chromium hydroxide has been followed using X-ray diffraction, radial electron density distribution, differential thermal analysis, and ir spectroscopic techniques. The material obtained by drying in air at 25° contains crystalline $Cr(OH)_3$. At and above drying temperature of 60°, the gel passes through many amorphous phases, crystallization of the corundum phase occurring at 390°. Both radial distribution and ir spectroscopy reveal that there are regions in all the amorphous phases wherein the "short-range structure" is similar to that in $HCrO_2$. The crystallite size, lattice strain, and crystalline fraction of the various crystalline phases have also been analyzed and are reported.

Introduction

Chromia gel, either alone or supported on alumina or silica, is used to catalyze a wide variety of reactions.[1-3] Some fairly detailed information is now available on the adsorption and catalytic properties of this material. The same cannot be said, however, about the structural features. This is especially true of the amorphous precursors to α-Cr_2O_3. When $Cr(H_2O)_6^{3+}$ ions are neutralized, the hydrogel obtained is usually amorphous or poorly crystalline, though a crystalline material has been reported.[4] When the resulting material is heated in air, the amorphous material is converted into microcrystalline α-Cr_2O_3 around 400°. Though the structure of α-Cr_2O_3 is well known,[5] the evolution of its structure from the starting material is not known in detail. This is due to the inadequecy of the conventional X-ray diffraction techniques for the study of amorphous solids. In the present report, X-ray scattering techniques[6] yielding information on the radial distribution of electron density have been utilized to elucidate the short-range structure. It may be mentioned that this technique is especially suited for the study of amorphous material. Additional information is also being provided from the X-ray diffraction, DTA, and ir spectra of the gels. From all these data, a coherent picture of the structural evolution of chromia is provided.

Experimental Section

Materials. Sample A was prepared[7] by the addition of 0.1 *M* chromium nitrate to 0.25 *M* ammonia until a pH of 10.5 was reached. The gel obtained was allowed to settle. It was separated by centrifugation and then washed twice with distilled water, three times with acetone, slurried with diethyl ether, and again separated by centrifugation. It was dried for 24 hr at room temperature in air. Samples B, C, D, E, F, and G were obtained from sample A by heating in an air oven for 24 hr at 60, 110, 240, 400, 500, and 900°, respectively.

Apparatus. The X-ray diffractograms were obtained using a Philips diffractometer (Cu Kα radiation). The X-ray scattering technique used in the radial electron distribution has already been described in detail.[6] The ir spectra were taken with a Beckman IR 12 double beam grating spectrophotometer. The setting of the instrument was: slit 2× standard slit; gain 5.0%; period 2 sec; scanning speed 80 cm^{-1}/sec, the spectral slit width was 0.8 mm at 2800 cm^{-1} and the spectral resolution was of the order of 2 cm^{-1}. Films of the gel in KBr (1% by wt) were prepared by pressing the mixture at 500 kg/cm^2. The ir spectrum was scanned in the region 400–4000 cm^{-1}. For the DTA measurements a Netzsch Model 406 apparatus was used. α-Al_2O_3 was used as the standard for the DTA measurements. A linear heating rate of 12°/min was used.

Results

X-Ray Diffraction. The powder diffractograms of samples A to G are shown in Figure 1. The $\sin^2\theta$ values and the corresponding *hkl* indices of the planes for samples E, F, and G were calculated from the spectra of Figure 1 and are given in Table I.

Samples B, C, and D are completely amorphous to X-rays as may be seen from Figure 1. Sample A was indexed using an orthorhombic system of lattice. Samples E, F, and G belong to the hexagonal system

(1) R. L. Burwell, Jr., G. L. Haller, K. C. Taylor, and J. F. Read, *Advan. Catal.*, **20**, 1 (1969).

(2) H. S. Taylor and L. M. Yeddanapalli, *Bull. Soc. Chim. Belg.*, **47**, 162 (1938).

(3) P. Ratnasamy, V. Krishnasamy, and L. M. Yeddanapalli, *Indian J. Chem.*, **9**, 131 (1971).

(4) W. O. Milligan, *J. Phys. Colloid Chem.*, **55**, 497 (1951).

(5) (a) L. Pauling and S. B. Hendricks, *J. Amer. Chem. Soc.*, **47**, 781 (1925); (b) R. E. Newnham and Y. M. de Haan, *Z. Kristallogr.*, **117**, 235 (1962).

(6) P. Ratnasamy and A. J. Léonard, *Catal. Rev.*, **6** (2), 293 (1972).

(7) F. S. Baker, J. D. Carruthers, R. E. Day, K. S. W. Sing, and L. J. Stryker, paper presented at the Faraday Society discussions, Brunel University, 1971.

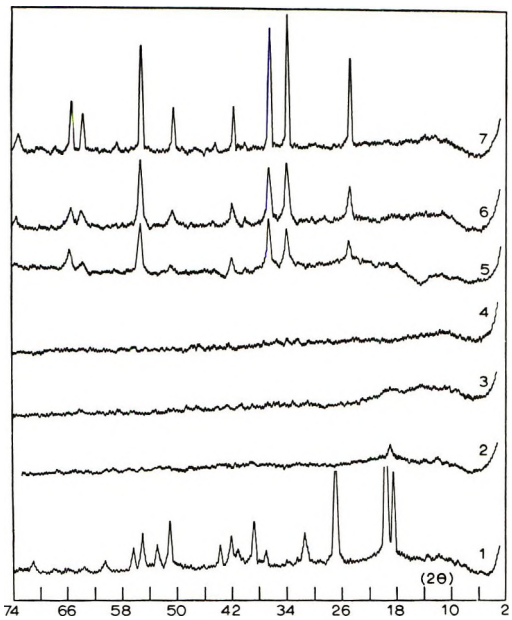

Figure 1. X-ray diffractograms of samples A–G. The numbers 1 through 7 refer to samples A to G; Cu Kα radiation.

Table I: X-Ray Diffraction Results for Samples E, F, and G

hkl	$\sin^2\theta_{calcd}$	E $\sin^2\theta_{obsd}$	F $\sin^2\theta_{obsd}$	G $\sin^2\theta_{obsd}$
102	0.0452	0.0458 (55)[a]	0.0458 (52)	0.0457 (68)
104	0.0839	0.0845 (76)	0.0845 (92)	0.0840 (100)
110	0.0970	0.0981 (96)	0.0981 (88)	0.0979 (92)
006	0.1161			0.1165 (7)
113	0.1259	0.1267 (36)	0.1273 (38)	0.1261 (34)
201	0.1330			0.1367 (33)
204	0.1808	0.1833 (11)	0.1826 (25)	0.1813 (34)
116	0.2129	0.2153 (100)	0.2146 (100)	0.2132 (78)
108	0.2385			0.2358 (12)
109	0.2933	0.2934 (34)		
214	0.2776		0.2792 (18)	0.2777 (28)
300	0.2907		0.2903 (30)	0.2903 (37)
119	0.3579		0.3580 (10)	0.3555 (17)

[a] The values in parentheses refer to relative intensity values.

of axes and space group D_{3d}^6. The observed $\sin^2\theta$ values are seen (Table I) to agree well with those calculated. A Fortran IV program utilizing a numerical solution for the multiple regression analysis was used for calculating the unit cell parameters. These values are given in Table II. The standard deviations as well as the von Neumann ratios[8] are also given therein.

Hall[9] has derived a general relationship between the broadening of the lines in the X-ray diagram and the major factors causing it, namely crystallite size D and lattice strain, η

$$B \cos\theta = \frac{\kappa\lambda}{D} + \eta \sin\theta$$

In the equation, B is the integral breadth of the line at a diffraction angle θ, λ is the wavelength of the radiation (1.5418 Å in our case), and κ is a shape factor (taken as unity). The crystallite size and the lattice strain were estimated from the plot of $B \cos\theta$ against $\sin\theta$ for seven lines in the case of sample A. The corresponding numbers for samples E, F, and G are 2, 6, and 8, respectively. The values are given in Table III. The value for sample E is less accurate than those of others. The lattice strain values have been normalized to that of sample G. Thus, there is 4% more lattice strain in sample F compared to sample G. The corresponding value for sample E is 20%. The crystalline fractions in samples E, F, and G were estimated from the variation in the total integrated intensity values of the 104, 116, and 110 lines. The values have been normalized with respect to that of sample G.

Table II: Unit Cell Parameters for Samples E, F, and G

Sample	Space group	*a*, Å	*c*, Å	von Neumann ratio
E	D_{3d}^6	4.912 ± 0.003	13.555 ± 0.002	2.223
F	D_{3d}^6	4.947 ± 0.003	13.583 ± 0.002	2.29
G	D_{3d}^6	4.942 ± 0.002	13.644 ± 0.002	1.70

Table III: Crystallite Size, Lattice Strain, and Crystalline Fraction from X-Ray Line Broadening

Sample	Crystallite size, Å	Lattice strain[a]	Fraction crystalline[a]
A	590 ± 30		
E	159 ± 50	1.20	0.35
F	233 ± 35	1.04	0.47
G	505 ± 20	1.0	1.0

[a] In arbitrary relative units.

Sample A was obtained by drying in air, at room temperature, the gel got by precipitation. A similar crystalline material has also been reported by Milligan.[4] The X-ray pattern was found to be[4] similar to that of alumina bayerite with about 4% linear expansion of the lattice spacings. Bayerite also belongs to the orthorhombic system[10] with unit cell parameters of 4.713, 8.674, and 5.061 Å, respectively. The structural features of our sample A fitted very well that of chromium trihydroxide, $Cr(OH)_3$, listed in ASTM files.[11]

(8) D. K. Faddev and V. N. Faddeva, "Computational Methods in Linear Algebra," W. H. Freeman, San Francisco, Calif., 1963.

(9) W. K. Hall, *Proc. Phys. Soc.*, **A62**, 741 (1949).

(10) B. C. Lippens, "Structure and Texture of Aluminas," Thesis, University of Delft, 1961.

(11) A.S.T.M. File No. 16-817.

There is, however, an appreciable amount of amorphous matter in the sample as indicated by the high value of the background intensity.

Samples E, F, and G are identified as containing increasing fractions of α-Cr_2O_3 in view of the good agreement of the calculated and observed $\sin^2\theta$ values. The unit cell parameters of α-Cr_2O_3 are[12] a = 4.954 Å and c = 13.584 Å which agree well with those in Table II. Samples E and F, however, differ from sample G with regard to crystallite size, lattice strain, and amount of crystalline matter as may be seen in Table III.

Radial Electron Distribution (RED). The method of calculating the RED patterns and their significance have already been published.[6] The RED patterns of the amorphous samples B, C, and D, as well as sample E, are illustrated in Figure 2. Table IV identifies the various peaks in the pattern with interatomic distances in different plausible structures.

Table IV: Radial Electron Distribution in Samples B–E

Interatomic distance	Length[d] of the bands, Å — Samples B	C	D	E	Calcd values
Cr–O in CrO_4	1.58	1.62	1.58	1.59	1.60[a]
Cr–O_1 in $HCrO_2$, Cr_2O_3	1.96	1.98		1.95	1.97[b,c]
O–O in $HCrO_2$		2.50	2.55	2.54	2.55[b]
Cr_1–Cr_2 in α-Cr_2O_3	2.64	2.69		2.66	2.65[c]
Cr_1–Cr_3 in α-Cr_2O_3	2.88	2.86		2.90	2.89[c]
Cr–Cr in $HCrO_2$	2.98	2.98	3.0		2.98[b]
Cr_1–Cr_4 in α-Cr_2O_3	3.42			3.44	3.43[c]
Cr–O in $HCrO_2$	3.51	3.50	3.45		3.49[b]
Cr_1–Cr_5, Cr_6 in α-Cr_2O_3	3.64	3.62		3.64	3.65[c]

[a] A. F. Wells, "Structural Inorganic Chemistry," 3rd ed, Oxford University Press, Amen House, London, E.C.4, 1962, p 443. [b] R. M. Douglass, *Acta Crystallogr.*, **10**, 423 (1957). [c] R. E. Newnham and Y. M. de Haan, *Z. Kristallogr.*, **117**, 235 (1962). [d] The values are accurate to about ±0.03 Å.

The results may be summarized as follows: both samples B and C contain regions wherein the structural features are similar to those in CrO_4^{2-}, $HCrO_2$, and α-Cr_2O_3. It must be emphasized that these are only local characteristics and do not extend to more than, say, 7 Å, since no lines at all are seen in the X-ray diagram (Figure 1). In sample D, distances that correspond to those in $HCrO_2 \cdot CrO_4^{2-}$ groups are probably present only on the surface accounting for the vector at 1.58 Å. Sample E contains, of course, an appreciable fraction of α-Cr_2O_3 as evident from the X-ray diffractograms, but Table IV reveals that the amorphous part contains short-range structures which are similar to that in $HCrO_2$. Again the vector at 1.59 Å probably originates from surface regions containing the chromate ion.

Differential Thermal Analysis. The differential thermogram of sample A is shown in Figure 3. The temperature range covered was from 25 to 1000°. As may be seen, there are three endothermic peaks at 140, 155, and 250° and an exothermic peak at 390°. Similar phenomena had been observed by Bhattacharya, *et al.*[13] The peaks at 140 and 155° are attributed to loss of two forms of loosely bound water, the precise difference between them not being clear. We attribute the peak at 250° to the loss of water by condensation of hydroxyl groups. The presence of hydroxyl groups in the sample is also supported by ir (Figure 4) and RED data. The exothermic peak at 390° has been attributed[13] to the onset of crystallization of α-Cr_2O_3. This is further confirmed in our study by the fact that the crystalline X-ray pattern of α-Cr_2O_3 is observed only at 400° or above (Figure 1).

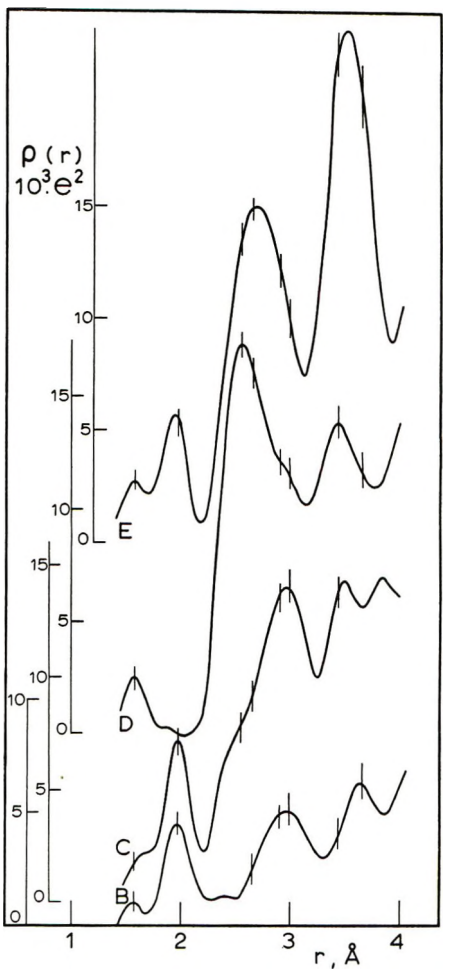

Figure 2. The radial electron distribution in samples A–G. The vertical lines correspond to the interatomic vectors in Table IV.

Ir Spectroscopy. The ir spectra of samples A–G in KBr disks (1% by wt) are shown in Figures 4 and 5. The frequencies of the various bands together with

(12) R. W. G. Wyckoff, "Crystal Structures," Vol. 2, Interscience, New York, N. Y., 1964, p 6.

(13) S. K. Bhattacharya, V. S. Ramachandran, and J. C. Ghosh, *Advan. Catal.*, **9**, 114 (1957).

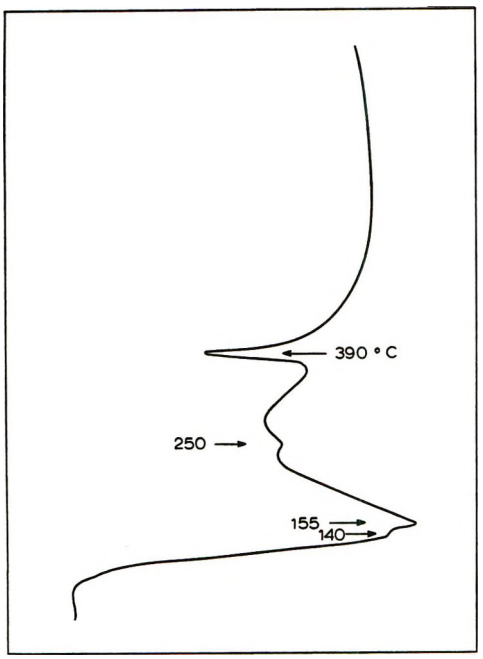

Figure 3. The differential thermal analysis curve of sample A.

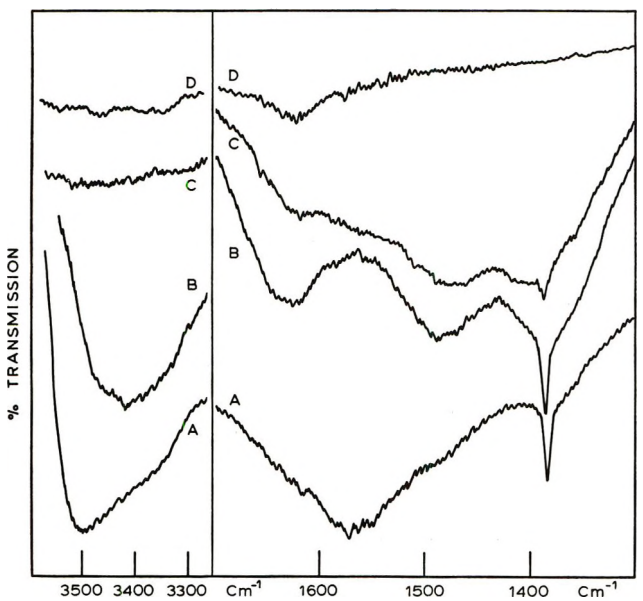

Figure 4. Ir spectra of samples A–D in the region 1300–1700 and 3300–3600 cm^{-1} (KBr pellets).

their relative intensities are given in Table V. Samples E, F, and G did not have any significant absorption band in the region 1300–4000 cm^{-1}. Thus, their spectra are omitted in Figure 4. None of the samples exhibits any absorption in the range 1700–3300 cm^{-1}. A weak band at 1095 cm^{-1} is observed for sample A and two are observed (at 1010 and 1045 cm^{-1}) for sample G. These are not shown in the figure but are indicated in Table V. There were no absorption bands for the other samples in the region 1000–1300 cm^{-1}.

Zecchina, *et al.*,[14] have recently carried out an extensive ir investigation of the adsorption of H_2O, CO, O_2, and CO_2 on chromia activated at 400° under vacuum or O_2 or CO atmospheres. Marshall, *et al.*,[15] have published ir spectra of single crystals of α-Cr_2O_3. Burwell, *et al.*,[1] report a very broad band at 525 cm^{-1} in amorphous chromia which is split into two bands at 618 and 550 cm^{-1} when the sample is converted into crystalline α-Cr_2O_3.

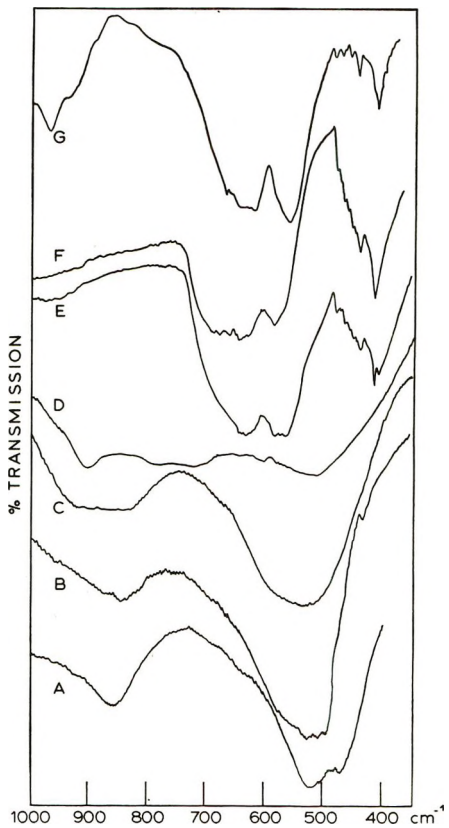

Figure 5. Ir spectra of samples A–G in the region 400–1000 cm^{-1} (KBr pellets).

In accord with Zecchina, *et al.*, we assign the bands at 3510 (sample A) and 3420 cm^{-1} (sample B) to the stretching of surface hydroxyls originating from a dissociative chemisorption of water and to the OH stretching of nondissociated water molecules. The bands at 1572 (sample A) and 1625 (samples B and C) are assigned to the bending modes of nondissociated water molecules. However, the persistence of this band even at 240° (sample D) is quite surprising. From DTA experiments it is known that all the loosely bound water is expelled below 200°; only surface hydroxyl groups are present at 240°. The band at 1625 cm^{-1} in sample D cannot be assigned to the bending mode of a hydroxyl group because the corresponding stretching mode in the region 3300–3800 cm^{-1} is absent. Now RED studies reveal the presence of regions in sample D which possess the same "short-

(14) A. Zecchina, S. Coluccia, E. Guglielminotti, and G. Ghiotti, *J. Phys. Chem.*, 75, 2774 (1971).

(15) R. Marshall, S. S. Mitra, P. J. Gielisse, J. N. Plende, and L. C. Mansur, *J. Chem. Phys.*, 43, 2893 (1965).

Table V: Ir Spectrum of Samples A–G (cm^{-1})

Samples[a]						
A	B	C	D	E	F	G
470 (s)	495–530 (vs)	535 (vs)	575 (vs)	420 (s)	420 (s)	412 (s)
525 (vs)	845 (s)	825–925 (s)	955 (s)	443 (ms)	445 (ms)	443 (ms)
855 (s)	1385 (vs)	1385 (w)	1625 (w)	575 (vs)	575 (vs)	560 (s)
1095 (w)	1488 (s)	1475 (w)		635 (vs)	650 (vs)	625–650 (vs)
1382 (s)	1625 (s)	1625 (w)		975 (w)		880 (w)
1572 (s)	3420 (s)					940 (w)
3510 (s)						970 (s)
						1010 (w)
						1045 (vw)

[a] Legend: vs, very strong; s, strong; ms, medium strong; w, weak; vw, very weak.

range order" as in $HCrO_2$ (see above). Crystalline $HCrO_2$ exhibits[16] a very broad band in the region 1600–2000 cm^{-1} due to O–H stretching vibration in OHO groups. The oxygen–oxygen distance across the hydrogen bond is about 2.45 Å. The band at 1625 cm^{-1} in our sample D is therefore assigned to the presence of similar groups in our sample also. Douglas[16] observed a fairly strong band at 1100–1200 cm^{-1} which he attributed to chromium–oxygen vibration. The band at 955 cm^{-1} (sample D) is also assigned to the same cause. The presence of these two bands lends additional support to the presence of "$HCrO_2$-like" regions in sample D.

We consider next the bands in the region 1300–1500 cm^{-1} (Table V). These have been assigned by Zecchina, *et al.*,[14] to strongly adsorbed CO_2 molecules. The absence of a band at 2360 cm^{-1} indicates the absence of linear, weakly adsorbed CO_2. CO_2 is most probably adsorbed as a carbonatelike surface species.

The weak band at 1095 cm^{-1} (sample A) is assigned to a Cr=O stretching vibration arising from the dissociative chemisorption of oxygen. The frequency is higher than that of Zecchina, *et al.* (1024 cm^{-1}). It is probably due to the greater coordinatively unsaturated nature of the Cr ions in our sample. In compounds of vanadium[17–19] the M=O stretching frequency is known to increase with decreasing coordination number of vanadium. That the band is due to adsorbed oxygen is also supported by its absence at higher temperatures.

For samples A, B, C, and D absorptions in the region 450–900 cm^{-1} are due to groups of the type in CrO_4^{x-} type[20] where $x = 2$, 3, or 4. It is known that in amorphous chromia Cr^{3+} ions undergo surface oxidation to higher oxidation states.[21] These bands arise from Cr–O–Cr vibrations.

For sample G (whose X-ray diffraction pattern is identical with that of α-Cr_2O_3), the absorption bands at 880, 970, 1010, and 1045 cm^{-1} are assigned to the combination lattice modes of $2E_2'$, $E_2' + E_3'$, $E_1' + A_2'$, and $E_2' + A_2'$, respectively. The theoretical values calculated by Marshall, *et al.*,[15] for α-Cr_2O_3 are 876, 971, 1010, and 1041 cm^{-1}, respectively. Zecchina, *et al.*,[14] have assigned the band at 940 cm^{-1} to the mode $(E_1' + E_3')$. The infrared-active fundamental modes for α-Cr_2O_3 occur[15] at 410, 440, 550, and 618 cm^{-1}. They belong to the modes E_1, E_2, E_3, and E_4 (as well as A_2), respectively. These are in good agreement with the observed values for samples E, F, and G. The absence of the combination modes in samples E and F may be due to the fact that these samples are not sufficiently crystalline to exhibit sufficiently intense combination modes. In fact, the relative crystalline fraction in samples E and F are (Table III) only 35 and 47%, respectively.

Discussion

The main features of all our results may be summarized as follows: sample A consists of crystalline $Cr(OH)_3$ (Figure 1). There is an appreciable number of water molecules, probably confined to the surface region (Figure 5 and Table V). Samples B, C, and D (60–250°) are completely amorphous (Figure 1). All the bound water is eliminated below 200° (Figure 3 and Table V). An appreciable fraction of the hydroxyl groups is removed at 250° (Figure 3). Both RED (Figure 2 and Table IV) and ir data (Figure 5 and Table V) lead to the conclusion that there are regions in all the three samples B, C, and D, wherein the "short-range structure" is similar to that in $HCrO_2$. Samples B and C contain, in addition, Cr–Cr and Cr–O vectors characteristic of α-Cr_2O_3. The absence of the α-Cr_2O_3 features in sample D is discussed later. However, these features extend only to a few ångströms (5 to 7 Å), and no definite long-range order is present. Sample E (400°) contains crystalline α-Cr_2O_3 as

(16) R. M. Douglas, *Acta Crystallogr.*, **10**, 423 (1957).

(17) J. Selbin, L. H. Holmes, Jr., and S. P. McGlynn, *J. Inorg. Nucl. Chem.*, 25, 1358 (1963).

(18) K. Ueno and A. E. Martell, *J. Phys. Chem.*, **60**, 934 (1956).

(19) I. R. Beattie and T. R. Gilson, *J. Chem. Soc.*, 2322 (1969).

(20) C. N. R. Rao, "Chemical Applications of Infrared Spectroscopy," Academic Press, New York, N. Y., 1963, p 340.

(21) W. Weller and S. E. Voltz, *J. Amer. Chem. Soc.*, **76**, 4695 (1954).

evidenced by the X-ray pattern. DTA data confirm the evolution of a crystalline phase around 400° (Figure 3). Samples F and G contain varying amounts of crystalline α-Cr_2O_3, the latter being practically pure crystalline α-Cr_2O_3.

Since the evolution of the structure of the final material involves $HCrO_2$ as intermediate, its salient features will be briefly pointed out.[16] The structure of $HCrO_2$ consists of oxygen ions, at the vertices of deformed octahedra, around Cr^{3+} ions. Each octahedron shares edges with surrounding coplanar octahedra to form continuous $(CrO_2)^{n-}$ sheets in which the anions are close-packed. A proton lies in twofold coordination between each pair of superposed oxygen ions. The hydrogen bonds thus formed satisfy the excess negative charge of the sheets and serve to hold them together. In α-Cr_2O_3, the O^{2-} ions are arranged in approximately one-third and two-thirds of the distance between the oxygen layers. Each Cr^{3+} ion is surrounded by six O^{2-} ions at the corners of a slightly distorted octahedron. Three of the oxygens are a few per cent nearer the Cr^{3+} than the other three. Each O^{2-}, in turn, is surrounded by four Cr^{3+} ions at the corners of a slightly distorted tetrahedron.

Thus, in our samples B to G, the structure evolves through an amorphous phase wherein regions of sheet-structure (consisting of distorted octahedra and tetrahedra) are clearly discernible. In addition, the beginnings of the corundum structure are also evident, though these are confined to regions too small to give rise to sharp lines in the X-ray pattern. At 400°, these sheets grow into hexagonally close-packed three-dimensional structures of O^{2-} ions wherein two-thirds of the octahedral holes are filled with Cr^{3+} ions. The main new feature of the present results is the light it throws on the "structure" of the amorphous material that is the immediate precursor of crystalline α-Cr_2O_3.

The absence of α-Cr_2O_3 features in sample D, though puzzling at first sight, is actually in order, since, in the evolution of the sheet structure towards the hcp structure the primary controlling factor is known to be the greater delocalization of the cations.[22] This delocalization of the Cr^{3+} ions will affect the three-dimensional α-Cr_2O_3 regions more than those wherein the two-dimensional $HCrO_2$ structure exists.

Acknowledgment. It is a pleasure to thank Professor J. J. Fripiat for his constant encouragement and support. We are also grateful to Mr. J. C. Meeus and Mr. C. Defossé for their competent technical assistance. The work was financially supported by I.R.S.I.A. We are grateful to the referees for pointing out some erroneous conclusions in the original manuscript of the paper.

(22) G. W. Brindley, *Progr. Ceram. Sci.*, **3**, 1 (1963).

Magnetic Circular Dichroism of Molecules in Dense Media. I. Theory

by D. J. Shieh,[1a] S. H. Lin,[1b] and H. Eyring*[1a]

Department of Chemistry, University of Utah, Salt Lake City, Utah, and Department of Chemistry, Arizona State University, Tempe, Arizona *(Received August 30, 1971)*

Publication costs assisted by the National Institutes of Health

The magnetic circular dichroism (MCD) of molecules dissolved in dense media has been investigated for the case in which the Franck–Condon principle applies and for the case in which the electronic transition is symmetry-forbidden but vibronic-allowed. In the adiabatic approximation and the approximation that the effect of the static magnetic field on the energy and wave function of nuclear motion is negligible, we have shown that the band shape of MCD is mainly determined by nuclear motion, while the electronic portion of the system is responsible for the strength of MCD. MCD and absorption coefficient are compared. It is found that for nondegenerate systems, for a particular electronic transition in which the Franck–Condon principle applies, the band shapes of MCD and absorption spectra are identical. The moment relations of MCD are also discussed. As an application, we study the MCD for the n → π^*, $\pi \rightarrow \pi^*$, and n → σ^* transitions of the formaldehyde molecule.

I. Introduction

In this paper, we are concerned with the discussion of the role of electronic and nuclear motion of molecules in the magnetic circular dichroism (MCD) of molecules dissolved in dense media. For this purpose, the adiabatic approximation is employed, and it is assumed that the effect of the static magnetic field on the vibrational wave function and energy of molecules and the nonadiabatic effect (the breakdown of the adiabatic approximation) are negligible. As with Moffit and Moscowitz[2] and Lin and Bersohn,[3] we are of the opinion that the damping effect is not important in the discussion of the band shape of circular dichroism.[4] It will be shown that each MCD band for an electronic transition of the molecule consists of series of lines corresponding to various vibrational transitions associated with the electronic transition under consideration. The strength of each line is mainly determined by the Franck–Condon factor. In this investigation, we study both the case in which the Franck–Condon principle applies and the case of the symmetry-forbidden but vibronic-allowed transitions. In the derivation of MCD, for simplicity the higher order effects which are not important in most cases are neglected but can easily be included.[5-7]

II. MCD in the Franck–Condon Approximation

A. Degenerate Systems. For the case in which the Franck–Condon principle applies, in the adiabatic approximation we have[4b,6-8]

$$P_{\pm}(\alpha v \rightarrow \beta v') = |\langle\psi_\alpha|X \pm iY|\psi_\beta\rangle|^2|\langle\theta_{\alpha v}|\theta_{\beta v'}\rangle|^2 = P_{\pm}(\alpha \rightarrow \beta)|\langle\theta_{\alpha v}|\theta_{\beta v'}\rangle|^2 \quad (1)$$

Using eq 1, the MCD can be expressed as

$$\Delta k(\mathrm{A} \rightarrow \mathrm{B}) = \frac{a\omega}{2c} N \sum_{\alpha}^{A} \sum_{\beta}^{B} \Delta P(\alpha \rightarrow \beta) P_\alpha^{(e)} f_{\alpha\beta}(\omega) \quad (2)$$

where $f_{\alpha\beta}(\omega)$ represents the band shape function defined by

$$f_{\alpha\beta}(\omega) = \sum_v \sum_{v'} P_v^{(v)} |\langle\theta_{\alpha v}|\theta_{\beta v'}\rangle|^2 \delta(\omega - \omega_{\beta v', \alpha v}) \quad (3)$$

As can be seen from eq 3, the MCD band consists of a series of lines that merge into a single broad band; the strength of each line is determined by the Franck–Condon factor, $|\langle\theta_{\alpha v}|\theta_{\beta v'}\rangle|^2$. It can easily be shown that $\int_0^\infty d\omega f_{\alpha\beta}(\omega) = 1$. If $\vec{\mu}$ represents the magnetic moment, $\mu = \sum_i (e/2mc)[(\vec{r}_i \times \vec{P}_i) + 2\vec{S}_i]$, and He, the static magnetic field, then the electronic part of the Boltzmann factor $P_\alpha^{(e)}$ can be simplified as[6,7,9]

$$P_\alpha^{(e)} = \frac{1}{g_A}[1 + \theta He(\hat{\mu}_z)_{\alpha\alpha}]$$

to the first order of approximation with respect to He. g_A represents the degeneracy of the electronic state A and $\theta = 1/kT$. In the presence of the magnetic field

(1) (a) University of Utah; (b) John Simon Guggenheim Fellow, Arizona State University.

(2) W. Moffit and A. Moscowitz, *J. Chem. Phys.*, **30**, 648 (1959).

(3) S. H. Lin and R. Bersohn, *ibid.*, **44**, 3768 (1966).

(4) (a) S. H. Lin, *ibid.*, **54**, 1177 (1971); (b) S. H. Lin, *ibid.*, **55**, 3546 (1971).

(5) E. U. Condon, W. Altar, and H. Eyring, *ibid.*, **5**, 753 (1937); also, E. U. Condon, *Rev. Mod. Phys.*, **9**, 432 (1937).

(6) A. D. Buckingham and P. J. Stephens, *Ann. Rev. Phys. Chem.*, **17**, 399 (1966).

(7) P. J. Stephens, *J. Chem. Phys.*, **52**, 3489 (1970). It should be noted that a factor of $\omega/2c$ should be included in Stephens' expression for MCD.

(8) D. J. Caldwell and H. Eyring, "The Theory of Optical Activity," Wiley-Interscience, New York, N. Y., 1971, p 69.

(9) R. Serber, *Phys. Rev.*, **41**, 489 (1932).

He, the band shape function $f_{\alpha\beta}(\omega)$ will also be affected. Writing $\omega_{B_{v'},A_v}^{\circ} - \Delta\omega_{\beta\alpha}He$ for $\omega_{\beta v',\alpha v}$ with $\Delta\omega_{\beta\alpha} = [(\mu_z)_{\alpha\alpha} - (\hat{\mu}_z)_{\beta\beta}]/\hbar$, and noticing that the effect of the magnetic field on the nuclear wave function is ignored, we can simplify $f_{\alpha\beta}(\omega)$ as

$$f_{\alpha\beta}(\omega) = f_{AB}^{\circ}(\omega) - f_{AB}'(\omega)\Delta\omega_{\beta\alpha}He \quad (4)$$

by Taylor's expansion. Here $f_{AB}^{\circ}(\omega)$ and $f_{AB}'(\omega)$ are defined by

$$f_{AB}^{\circ}(\omega) = \sum_{v'}\sum_{v} P_v^{(v)}|\langle\theta_{Av}|\theta_{Bv'}\rangle|^2\delta(\omega - \omega_{B_{v'},A_v}^{\circ}) \quad (5)$$

and

$$f_{AB}'(\omega) = \sum_{v'}\sum_{v} P_v^{(v)}|\langle\theta_{Av}|\theta_{Bv'}\rangle|^2\delta'(\omega - \omega_{B_{v'},A_v}^{\circ}) \quad (6)$$

where $\delta'(x)$ represents the derivative of the delta function and $P_v^{(v)}$, the Boltzmann factor of nuclear motion. Considering the effect of the magnetic field *He* on $P_{\pm}(\alpha \rightarrow \beta)$, by straightforward expansion we obtain[6,7,9]

$$P_{\pm}(\alpha \rightarrow \beta) = P_{\pm}(\alpha \rightarrow \beta)^{\circ} + HeP_{\pm}(\alpha \rightarrow \beta)' \quad (7)$$

where

$$P_{\pm}(\alpha \rightarrow \beta)^{\circ} = |\langle\psi_{\alpha}^{\circ}|X \pm iY|\psi_{\beta}^{\circ}\rangle|^2 = |(R^{\pm})_{\alpha\beta}|^2 \quad (8)$$

and

$$P_{\pm}(\alpha\rightarrow\beta)' = 2Re\left[\sum_{\gamma}' \frac{(\hat{\mu}_z)_{\beta\gamma}}{\hbar\omega_{GB}^{\circ}}(R^{\pm})_{\alpha\beta}(R^{\mp})_{\gamma\alpha} + \sum_{\gamma}' \frac{(\hat{\mu}_z)_{\gamma\alpha}}{\hbar\omega_{GA}^{\circ}}(R^{\pm})_{\alpha\beta}(R^{\mp})_{\beta\gamma}\right] \quad (9)$$

Substituting eq 4 and 7 into eq 2 yields[6,7,9]

$$\Delta k(A \rightarrow B) = -\frac{2a\omega N}{3c}He\left[\frac{1}{\hbar}A(A \rightarrow B)f_{AB}'(\omega) + \{B(A \rightarrow B) + \theta C(A \rightarrow B)\}f_{AB}^{\circ}(\omega)\right] \quad (10)$$

$A(A \rightarrow B)$, $B(A \rightarrow B)$, and $C(A \rightarrow B)$ are given in the papers by Buckingham and Stephens[6] and Stephens,[7] and will not be produced here. From eq 10, we can see that

$$\left[\frac{1}{\omega}\Delta k(A \rightarrow B)\right] = \int_0^{\infty}\frac{d\omega}{\omega}\Delta k(A \rightarrow B) = -\frac{2aN}{3c}He[B(A \rightarrow B) + \theta C(A \rightarrow B)] \quad (11)$$

since $\int_0^{\infty} d\omega f'(\omega) = 0$. Thus we have shown that the nuclear part of the molecule is mainly involved in the band shape, and the electronic part of the molecule determines the strength of MCD.

If the molecules are randomly oriented, we have to carry out the averaging process of $\Delta k(A \rightarrow B)$ over molecular orientations. In this case the relations $A(A \rightarrow B)$, $B(A \rightarrow B)$, and $C(A \rightarrow B)$ can be written[5]

$$A(A \rightarrow B) = \frac{1}{2g_A}\sum_{\alpha}^{A}\sum_{\beta}^{B}[(\vec{\mu}_m)_{\beta\beta} - (\vec{\mu}_m)_{\alpha\alpha}]\cdot I_m(\vec{r}_{\alpha\beta} \times \vec{r}_{\beta\alpha}) \quad (12)$$

$$B(A \rightarrow B) = \frac{1}{g_A}\sum_{\alpha}^{A}\sum_{\beta}^{B} I_m\left[\sum_{\gamma}'\frac{(\vec{\mu}_m)_{\beta\gamma}\cdot(\vec{r}_{\alpha\beta} \times \vec{r}_{\gamma\alpha})}{\hbar\omega_{GB}^{\circ}} + \sum_{\gamma}'\frac{(\vec{\mu}_m)_{\gamma\alpha}\cdot(\vec{r}_{\alpha\beta} \times \vec{r}_{\beta\gamma})}{\hbar\omega_{GA}^{\circ}}\right] \quad (13)$$

and

$$C(A \rightarrow B) = \frac{1}{2g_A}\sum_{\alpha}^{A}\sum_{\beta}^{B}(\vec{\mu}_m)_{\alpha\alpha}\cdot I_m(\vec{r}_{\alpha\beta} \times \vec{r}_{\beta\alpha}) \quad (14)$$

where $(\vec{\mu}_m)_{\beta\gamma}$ and $\vec{r}_{\alpha\beta}$ denote the matrix elements of electronic magnetic and electric moments in the molecular coordinate, respectively.

The evaluation of the band shape function $f_{\alpha\beta}^{\circ}(\omega)$ of the molecules dissolved in dense media has been extensively investigated in connection with absorption spectra,[10] emission spectra,[11] natural CD,[4] ORD,[3] nonradiative decay,[12,13] resonance energy transfer,[14] etc., and will not be discussed here.

B. MCD of Nondegenerate Systems. In this case, $(\hat{\mu}_z)_{\alpha\alpha}$ and $(\hat{\mu}_z)_{\beta\beta}$ are zero and the expression for MCD becomes

$$\Delta k(A \rightarrow B) = -\frac{2a\omega N}{3c}HeB(A \rightarrow B)f_{AB}^{\circ}(\omega) \quad (15)$$

Let us compare MCD with the absorption coefficient. The expression for the absorption coefficient in this case can be written as[10]

$$\epsilon(A \rightarrow B) = \frac{4a\omega N}{3c}|\vec{r}_{AB}|^2 f_{AB}^{\circ}(\omega) \quad (16)$$

Comparing eq 15 with eq 16, we can see that the band shapes of MCD and absorption spectra for a particular electronic transition are identical, and while the strength of the absorption coefficient for an electronic transition is determined by the matrix element of dipole transition moment $|\vec{r}_{AB}|^2$, the strength of MCD for the electronic transition is determined by $B(A \rightarrow B)$. Furthermore, we have

$$\left[\frac{1}{\omega}\Delta k(A \rightarrow B)\right] = -\frac{2aN}{3c}HeB(A \rightarrow B); \quad \left[\frac{1}{\omega}\epsilon(A \rightarrow B)\right] = \frac{4aN}{3c}|\vec{r}_{AB}|^2 \quad (17)$$

(10) S. H. Lin, *Theor. Chim. Acta*, **10**, 301 (1968); C. O. Hill and S. H. Lin, *Trans. Faraday Soc.*, **67**, 2833 (1971).

(11) L. Colangelo, S. H. Lin, and H. Eyring, *Proc. Nat. Acad. Sci. U. S.*, **68**, 2135 (1971).

(12) S. H. Lin, *J. Chem. Phys.*, **44**, 3759 (1966); *ibid.*, **53**, 3766 (1970); S. H. Lin and R. Bersohn, *ibid.*, **48**, 2732 (1968).

(13) K. F. Freed, *ibid.*, **52**, 1345 (1970); R. Englman and J. Jortner, *Mol. Phys.*, **18**, 145 (1970).

(14) S. H. Lin, *ibid.*, **21**, 853 (1971).

It should be noted that although the band shapes of MCD and absorption spectra may change with temperature, the areas under the curves of $(1/\omega)\Delta k(A \rightarrow B)$ *vs.* ω and $1/\omega\epsilon(A \rightarrow B)$ *vs.* ω for a particular electronic transition are temperature independent. From eq 15, 16, and 17, we obtain

$$\frac{\left[\frac{1}{\omega}\Delta k(A \rightarrow B)\right]}{\left[\frac{1}{\omega}\epsilon(A \rightarrow B)\right]} = -\frac{HeB(A \rightarrow B)}{2|\vec{r}_{AB}|^2} = \frac{\Delta k(A \rightarrow B)}{\epsilon(A \rightarrow B)} \quad (18)$$

Next we shall consider the moment relations in MCD. For this purpose we introduce the integral representation for the delta function[12] into $f_{AB}^{\circ}(\omega)$ to obtain[11]

$$\Delta k(A \rightarrow B) = -\frac{2a\omega N}{3c} HeB(A \rightarrow B) \times \frac{1}{2\pi}\int_{-\infty}^{\infty} \exp(-i\omega t) G_{AB}(t) dt \quad (19)$$

where

$$G_{AB}(t) = \sum_v \sum_{v'} P_v^{(v)} |\langle\theta_{Av}|\theta_{Bv'}\rangle|^2 \times \exp(it\omega_{Bv',Av}^{\circ}) = -\left[\frac{2aN}{3c} HeB(A \rightarrow B)\right]^{-1} \times \int_{-\infty}^{\infty} \frac{d\omega}{\omega} \Delta k(A \rightarrow B) \exp(i\omega t) \quad (20)$$

A similar expression for $\epsilon(A \rightarrow B)$ can be given. Equation 20 indicates that $G_{AB}(t)$ can be determined from the Fourier transformation of $1/\omega\Delta k(A \rightarrow B)$ which is experimentally measurable, and from $G_{AB}(t)$, one can determine the Franck–Condon factors (*cf.* eq 20), *vice versa*. Expanding $G_{AB}(t)$ and $\exp(i\omega t)$ in power series of t, and comparing the coefficients of t^n, yields

$$\int_{-\infty}^{\infty} d\omega \omega^{n-1} \Delta k(A \rightarrow B) = -\frac{2aN}{3c} HeB(A \rightarrow B) G_{AB}^{(n)}(0) i^{-n} = [\omega^{n-1}\Delta k(A \rightarrow B)] = -\frac{2aN}{3c} HeB(A \rightarrow B) \sum_v \sum_{v'} \omega_{Bv'^{n}Av}^{\circ} P_v^{(v)} |\langle\theta_{Av}|\theta_{Bv'}\rangle|^2 \quad (21)$$

which are the so-called moment relations. From eq 21 one can determine $G_{AB}^{(n)}(0)$ and from $G_{AB}^{(n)}(0)$, $G_{AB}(t)$ can be obtained in principle by using the relation $G_{AB}(t) = \sum_{n=0}^{\infty} \frac{t^n}{n!} G_{AB}^{(n)}(0)$. The determination of $G_{AB}(t)$ and hence $f_{AB}^{\circ}(\omega)$ is very important, because these quantities are transferable to other phenomena like absorption,[10] emission,[11] CD,[4] nonradiative decay,[12,13] energy transfer,[14] etc. The theoretical calculation of the right-hand side of the moment relations given by eq 21 has been investigated[11] for the harmonic oscillator model, *i.e.*, both intramolecular vibration and libration are regarded as harmonic. The moment relations of MCD for degenerate systems can be discussed similarly and will not be produced here.

III. MCD for Symmetry-Forbidden but Vibronic-Allowed Transitions

Here for simplicity we shall assume both upper and lower electronic states are nondegenerate. In this case, we can expand the electronic transition moment $\vec{r}_{AB} = \langle\psi_A|e\sum_i \vec{r}_i|\psi_B\rangle$ in terms of normal coordinates, Q_i

$$\vec{r}_{AB} = \vec{r}_{AB}^{\circ} + \sum_i \left(\frac{\partial \vec{r}_{AB}}{\partial Q_i}\right)_0 Q_i + \ldots \quad (22)$$

The coefficients $(\partial\vec{r}_{AB}/\partial Q_i)_0$, etc., are related to the matrix elements of the vibronic coupling and have been given by Weigang.[15] In most cases, the upper electronic state is more easily perturbed by the vibronic interaction than the lower electronic state. By going through the derivation similar to that given in the previous sections, we obtain the expression for MCD for symmetry-forbidden but vibronic-allowed transitions as eq 15 with $B(A \rightarrow B)$ and $f_{AB}^{\circ}(\omega)$ defined by

$$B(A \rightarrow B) = D_i I_m\left[\left(\frac{\partial \vec{r}_{AB}}{\partial Q_i}\right)_0 \times \left(\sum_G{}' \frac{\vec{r}_{BA} x(\vec{\mu}_m)_{BG}}{\hbar\omega_{GB}^{\circ}} + \sum_G{}' \frac{\vec{r}_{BG} x(\vec{\mu}_m)_{GA}}{\hbar\omega_{GA}^{\circ}}\right)\right] \quad (23)$$

and

$$f_{AB}^{\circ}(\omega) = \frac{1}{D_i} \sum_v \sum_{v'} P_v^{(v)} \times \langle\theta_{Av}|Q_i|\theta_{Bv'}\rangle\langle\theta_{Bv'}|\theta_{Av}\rangle\delta(\omega - \omega_{Bv',Av}^{\circ}) \quad (24)$$

where $D_i = \sum_v P_v^{(v)} \langle\theta_{Av}|Q_i|\theta_{Av}\rangle$. Here the relation $\vec{r}_{AB}^{\circ} = 0$ for symmetry-forbidden transitions has been used, the assumption that only one normal mode is responsible for the vibronic interaction has been made, and only the dominating term in MCD is retained. From eq 23 and 17, we can see that because of D_i, we may expect the MCD for symmetry-forbidden transitions to be weak as D_i equals zero in the harmonic oscillator approximation. The case in which electronic states are degenerate can be discussed similarly.

Let us compare the MCD with the absorption coefficient in this case. The absorption coefficient for symmetry-forbidden but vibronic-allowed transitions is given by

$$\epsilon(A \rightarrow B) = \frac{4a\omega}{3c} N \left|\left(\frac{\partial \vec{r}_{AB}}{\partial Q_i}\right)_0\right|^2 \sum_v \sum_{v'} P_v^{(v)} \times |\langle\theta_{Av}|Q_i|\theta_{Bv'}\rangle|^2 \delta(\omega - \omega_{Bv',Av}^{\circ}) \quad (25)$$

(15) O. E. Weigang, Jr., *J. Chem. Phys.*, **43**, 3609 (1965).

From eq 25, we obtain

$$\left[\frac{1}{\omega}\epsilon(\mathrm{A} \rightarrow \mathrm{B})\right] = \frac{4aN}{3c}\left|\left(\frac{\partial \vec{r}_{\mathrm{AB}}}{\partial Q_i}\right)_0\right|^2 \sum_v P_v^{(v)}\langle\theta_{\mathrm{A}v}|Q_i^2|\theta_{\mathrm{A}v}\rangle \quad (26)$$

If the normal mode of Q_i is harmonic, eq 26 reduces to

$$\left[\frac{1}{\omega}\epsilon(\mathrm{A} \rightarrow \mathrm{B})\right] = \frac{4aN}{3c}\left|\left(\frac{\partial \vec{r}_{\mathrm{AB}}}{\partial Q_i}\right)_0\right|^2 \frac{\hbar}{2\omega_i}\coth\frac{\theta}{2}\hbar\omega_i \quad (27)$$

which should be compared with eq 17. It should be noted that eq 27 corresponds to the equation adopted by Pople and Sidman[16] for calculating the intensity of the symmetry-forbidden electronic absorption band of formaldehyde.

IV. Application

To illustrate an application of the derivation given in the previous sections, we discuss the MCD for the $n \rightarrow \pi^*$, $n \rightarrow \sigma^*$, and $\pi \rightarrow \pi^*$ transitions of the formaldehyde molecule. For these electronic transitions both initial and final states are nondegenerate, and hence $A(\mathrm{A} \rightarrow \mathrm{B})$ and $C(\mathrm{A} \rightarrow \mathrm{B})$ vanish. Thus to compare the magnitude of the MCD for these transitions, we have to consider only $B(\mathrm{A} \rightarrow \mathrm{B})$. $B(\mathrm{A} \rightarrow \mathrm{B})$ in this case can be used to represent the strength of MCD. It is apparent from the derivation given in the previous sections that the origin for calculating the matrix elements of electric and magnetic moments should be at the center of mass of the molecule under consideration. The existence of the summations in $B(\mathrm{A} \rightarrow \mathrm{B})$ makes the calculation of MCD very complicated. It would seem desirable to treat MCD by using the variation-perturbation approach,[17,18] which is currently in progress. In this section, we shall attempt only the order-of-magnitude estimation of the MCD for the $n \rightarrow \sigma^*$ and $\pi \rightarrow \pi^*$ transitions. For this purpose, the simple MO's[19] are employed and the summations in eq 13 are truncated by limiting to the use of the electronic states, $(n\pi^*)$, $(n\sigma^*)$, $(\pi\pi^*)$, $(\sigma\pi^*)$, and $(\pi\sigma^*)$. Detailed SCF LCAO MO's of formaldehyde are available,[20] however. The matrix elements of electric and magnetic moments, which have been obtained by neglecting the two-centered integrals, are given in Tables I and II.

A. The $^1A_1 \rightarrow {}^1A_2$ Transition. It is well known that the $^1A_1 \rightarrow {}^1A_2$ $(n \rightarrow \pi^*)$ transition is symmetry-forbidden, and the forbiddenness is removed by including the effect of vibronic interactions.[16] Because of this symmetry-forbiddenness, the intensity of the electronic absorption band for the $^1A_1 \rightarrow {}^1A_2$ transition is weak compared with that for the allowed transition. Using the character table for the formaldehyde molecule (C_{2v}), one can obtain the electronic states ψ_G in $\langle\psi_G|e\sum_i \vec{r}_i|\psi_A\rangle$ and $\langle\psi_B|\vec{\mu}_m|\psi_G\rangle$, which are allowed on symmetry

Table I: Matrix Elements of Transition Moment $\langle\varphi_i|e\sum_i \vec{r}_i|\varphi_f\rangle$

φ_i	φ_f	$\langle\varphi_i\|e\sum_i \vec{r}_i\|\varphi_f\rangle$
$\varphi(^1A_1)$	$\varphi(^1A_2)_{n\pi^*}$	$0.0326\ \hat{\imath}\ ea_0$[a]
$\varphi(^1A_1)$	$\varphi(^1B_1)_{n\sigma^*}$	$-0.220\ \hat{\imath}\ ea_0$
$\varphi(^1A_1)$	$\varphi(^1A_1)_{\pi\pi^*}$	$0.679\ \hat{k}\ eR$[b]
$\varphi(^1A_1)$	$\varphi(^1B_2)_{\sigma\pi^*}$	$0.189\ \hat{j}\ ea_0$
$\varphi(^1A_1)$	$\varphi(^1B_2)_{\pi\sigma^*}$	$0.184\ \hat{j}\ ea_0$
$\varphi(^1A_2)_{n\pi^*}$	$\varphi(^1B_1)_{n\sigma^*}$	$0.434\ \hat{j}\ ea_0$
$\varphi(^1A_2)_{n\pi^*}$	$\varphi(^1A_1)_{\pi\pi^*}$	$0.0308\ \hat{\imath}\ ea_0$
$\varphi(^1A_2)_{n\pi^*}$	$\varphi(^1B_2)_{\sigma\pi^*}$	$-0.0209\ \hat{\imath}\ ea_0$
$\varphi(^1A_1)_{\pi\pi^*}$	$\varphi(^1B_1)_{n\sigma^*}$	0
$\varphi(^1A_1)_{\pi\pi^*}$	$\varphi(^1B_2)_{\sigma\pi^*}$	$-0.361\ \hat{j}\ ea_0$
$\varphi(^1A_1)_{\pi\pi^*}$	$\varphi(^1B_2)_{\pi\sigma^*}$	$0.434\ \hat{j}\ ea_0$
$\varphi(^1B_1)_{n\sigma^*}$	$\varphi(^1B_2)_{\sigma\pi^*}$	0
$\varphi(^1B_1)_{n\sigma^*}$	$\varphi(^1B_2)_{\pi\sigma^*}$	$0.0308\ \hat{\imath}\ ea_0$
$\varphi(^1B_2)_{\pi\sigma^*}$	$\varphi(^1B_2)_{\sigma\pi^*}$	0

[a] The small contribution from the $(\sigma\pi^*)$ state which gives rise to the polarization in the y direction has been omitted. [b] R represents the C–O bond length, $R = 1.26$ Å.

Table II: Matrix Elements of Magnetic Moment $\langle\varphi_i|\vec{\mu}_m|\varphi_f\rangle$

φ_i	φ_f	$\langle\varphi_i\|\vec{\mu}_m\|\varphi_f\rangle$
$\varphi(^1A_1)$	$\varphi(^1A_2)_{n\pi^*}$	$-0.848\ \hat{k}\ \frac{e\hbar}{2imc}$
$\varphi(^1A_1)$	$\varphi(^1B_1)_{n\sigma^*}$	$0.778\ \hat{j}\ \frac{e\hbar}{2imc}$
$\varphi(^1A_1)$	$\varphi(^1A_1)_{\pi\pi^*}$	0
$\varphi(^1A_1)$	$\varphi(^1B_2)_{\pi\sigma^*}$	$\hat{\imath}\left(-1.174 + 0.133\frac{R}{a_0}\right)\frac{e\hbar}{2imc}$
$\varphi(^1A_1)$	$\varphi(^1B_2)_{\sigma\pi^*}$	$i\left(1.68 - 0.134\frac{R}{a_0}\right)\frac{e\hbar}{2imc}$
$\varphi(^1A_2)_{n\pi^*}$	$\varphi(^1A_1)_{\pi\pi^*}$	$0.800\ \hat{k}\ \frac{e\hbar}{2imc}$
$\varphi(^1A_2)_{n\pi^*}$	$\varphi(^1B_1)_{n\sigma^*}$	$\hat{\imath}\left(-0.190 + 0.125\frac{R}{a_0}\right)\frac{e\hbar}{2imc}$
$\varphi(^1A_2)_{n\pi^*}$	$\varphi(^1B_2)_{\sigma\pi^*}$	$-0.740\ \hat{j}\ \frac{e\hbar}{2imc}$
$\varphi(^1A_1)_{\pi\pi^*}$	$\varphi(^1B_1)_{n\sigma^*}$	0
$\varphi(^1A_1)_{\pi\pi^*}$	$\varphi(^1B_2)_{\sigma\pi^*}$	$\hat{\imath}\left(-0.298 + 0.0652\frac{R}{a_0}\right)\frac{e\hbar}{2imc}$
$\varphi(^1A_1)_{\pi\pi^*}$	$\varphi(^1B_2)_{\pi\sigma^*}$	$\hat{\imath}\left(-0.190 + 0.125\frac{R}{a_0}\right)\frac{e\hbar}{2imc}$
$\varphi(^1B_1)_{n\sigma^*}$	$\varphi(^1B_2)_{\sigma\pi^*}$	0
$\varphi(^1B_1)_{n\sigma^*}$	$\varphi(^1B_2)_{\pi\sigma^*}$	$0.800\ \hat{k}\ \frac{e\hbar}{2imc}$
$\varphi(^1B_2)_{\pi\sigma^*}$	$\varphi(^1B_2)_{\sigma\pi^*}$	0

(16) J. A. Pople and J. W. Sidman, *J. Chem. Phys.*, **27**, 1270 (1957).
(17) M. Karplus and J. Kolker, *ibid.*, **34**, 1493 (1963).
(18) S. H. Lin and H. Eyring, *Proc. Nat. Acad. Sci. U. S.*, **68**, 76 (1971).
(19) J. W. Sidman, *J. Chem. Phys.*, **29**, 644 (1958).

grounds, and we can see that $\langle\psi_G|e\sum_i \vec{r}_i|\psi(^1A_1)\rangle$ and $\langle\psi(^1A_2)_{n\pi^*}|\vec{\mu}_m|\psi_G\rangle$, and $\langle\psi(^1A_2)_{n\pi^*}|e\sum_i \vec{r}_i|\psi_G\rangle$ and $\langle\psi_G|\vec{\mu}_m|\psi(^1A_1)\rangle$ are parallel, and $B(^1A_1 \rightarrow {}^1A_2)$ vanishes. $B(^1A_1 \rightarrow {}^1A_2)$ can be made nonzero only when the vibronic effect is included in $\langle\psi(^1A_1)|e\sum_i \vec{r}_i|\psi(^1A_2)_{n\pi}\rangle$, $\langle\psi_G|e\sum_i \vec{r}_i|\psi(^1A_1)\rangle\langle\psi(^1A_2)_{n\pi^*}|\vec{\mu}_m|\psi_G\rangle$ and $\langle\psi(^1A_2)_{n\pi^*}|e\sum_i \vec{r}_i|\psi_G\rangle \times \langle\psi_G|\vec{\mu}_m|\psi(^1A_1)\rangle$. This may explain the fact that the observed MCD for the $n \rightarrow \pi^*$ transition is so weak and that the MCD for the $n \rightarrow \pi^*$ transition is very sensitive to the type of substituents and to the position of substitution.[21]

In discussing the intensity of the absorption spectra for the symmetry-forbidden $n \rightarrow \pi^*$ transition, Pople and Sidman[16] consider the perturbation due to the vibronic interaction to affect only the excited $^1A_2$ state but not to affect the ground $^1A_1$ state. From eq 13, it is apparent that other excited electronic states involved in eq 13 might also be perturbed by the vibronic coupling, which complicates the calculation of the MCD for the $n \rightarrow \pi^*$ transition.

B. The $^1A_1 \rightarrow {}^1B_1$ Transition. The $^1A_1 \rightarrow {}^1B_1$ transition corresponds to the $n \rightarrow \sigma^*$ transition. To carry out a numerical calculation of the MCD strength $B(A \rightarrow B)$ using eq 13, it is convenient to define the general terms in eq 13 by $B(A \rightarrow B)_G$ and evaluate eq 13 term by term. That is

$$B(A \rightarrow B)_G = I_m\left\{\vec{r}_{AB}\left[\frac{\vec{r}_{GA} \times (\vec{\mu}_m)_{BG}}{\hbar\omega_{GB}^{\circ}} + \frac{\vec{r}_{BG} \times (\vec{\mu}_m)_{GA}}{\hbar\omega_{GA}^{\circ}}\right]\right\} \quad (28)$$

and

$$B(A \rightarrow B)_{AB} = I_m\left\{\frac{\vec{r}_{AB}(\vec{r}_{BB} - \vec{r}_{AA}) \times (\vec{\mu}_m)_{BA}}{\hbar\omega_{BA}^{\circ}}\right\} \quad (29)$$

The latter arises from setting G in the first and second summations of eq 13 equal to A and B, respectively. Substituting the matrix elements of electric and magnetic moments given in Tables I and II into eq 28 and 29, we obtain $B(^1A_1 \rightarrow {}^1B_1)_{n\sigma^*} = -1.11 \times 10^{-45}$; $B(^1A_1 \rightarrow {}^1B_1)_{n\pi^*} = -0.704 \times 10^{-45}$; $B(^1A_1 \rightarrow {}^1B_1)_{\pi\pi^*} = 0$; $B(^1A_1 \rightarrow {}^1B_1)_{\sigma\pi^*} = 0$; $B(^1A_1 \rightarrow {}^1B_1)_{\pi\sigma^*} = -0.327 \times 10^{-45}$. From these results, we can see that although $B(^1A_1 \rightarrow {}^1B_1)_G$ decreases steadily with increasing energy, the series involved in the calculation of $B(^1A_1 \rightarrow {}^1B_1)$ do not converge very rapidly; we can, however, estimate the order of magnitude of $B(^1A_1 \rightarrow {}^1B_1)$, $B(^1A_1 \rightarrow {}^1B_1) = -2.2 \times 10^{-45}$.

C. The $^1A_1 \rightarrow {}^1A_1$ Transition. The MCD strength $B(^1A_1 \rightarrow {}^1A_1)$ for the $\pi \rightarrow \pi^*$ transition can be evaluated similarly. We find $B(^1A_1 \rightarrow {}^1A_1)_{\pi\pi^*} = 0$; $B(^1A_1 \rightarrow {}^1A_1)_{n\pi^*} = 0$; $B(^1A_1 \rightarrow {}^1A_1)_{n\sigma^*} = 0$; $B(^1A_1 \rightarrow {}^1A_1)_{\sigma\pi^*} = -4.44 \times 10^{-45}$; $B(^1A_1 \rightarrow {}^1A_1)_{\pi\sigma^*} = -2.51 \times 10^{-45}$. Again it shows that the infinite series appearing in eq 13 do not converge very rapidly, and we can only make a rough estimation of the MCD strength for $\pi \rightarrow \pi^*$ transition, which gives $B(^1A_1 \rightarrow {}^1A_1) = -7.0 \times 10^{-45}$. It is interesting to notice that while the intensity of the electronic absorption spectra for the $\pi \rightarrow \pi^*$ transition is ten times stronger than that for the $n \rightarrow \sigma^*$ transition,[19] the MCD strengths for the $\pi \rightarrow \pi^*$ and $n \rightarrow \sigma^*$ transitions are comparable, $B(^1A_1 \rightarrow {}^1B_1)$ smaller than $B(^1A_1 \rightarrow {}^1A_1)$. This is because in the intensity of the electronic absorption spectra for a particular electronic transition, the square of the transition moment of that particular electronic transition is involved, while in the MCD only the first power of the transition moment is involved.

Acknowledgment. The authors wish to thank the National Institutes of Health, Grant GM 12862, National Science Foundation, Grant GP 28631, and the Army Research-Durham, Contract DA-ARO-D-31-124-72-G15, for support of this work. The authors also wish to thank the referee for some helpful suggestions.

(20) P. L. Goodfriend, F. W. Birss, and A. B. F. Duncan, *Rev. Mod. Phys.*, **32**, 307 (1960); S. M. Foster and S. F. Boys, *ibid.*, **32**, 303 (1960).

(21) C. Djerassi, E. Bunnenberg, and D. L. Elder, *Pure Appl. Chem.*, **25**, 57 (1971), and the references given therein.

Paramagnetism and Semiconductivity in Doped Charge-Transfer Complexes

by Mufaro J. Hove, Brian M. Hoffman,*[1] and Robert J. Loyd

Department of Chemistry and Materials Research Center, Northwestern University, Evanston, Illinois 60201 *(Received August 23, 1971)*

Publication costs assisted by the Advanced Research Projects Agency of the Department of Defense

We have studied the epr and conductivity of the nonionic charge-transfer (D-A) complexes carbazole-tetracyanoquinodimethane and carbazole-2,3-dichloro-5,6-dicyanobenzoquinone. These complexes are intrinsically nonionic and therefore diamagnetic, but they exhibit weak, temperature-dependent paramagnetism due to the presence of paramagnetic impurities. Interactions among unpaired impurity spins result in a nonmagnetic ground state and paramagnetic excitations. The complexes behave as semiconductors with activation energy for conduction greater than that for the creation of the paramagnetic spins, but doping the complexes with A^-, analogous to n doping in inorganic semiconductors, suggests that both the conductivity and the paramagnetic properties are associated with the unpaired electrons on the A^- anions.

Introduction

The continued interest in the conductivity of organic charge-transfer complexes has involved attempts to establish some relationship between the paramagnetic electrons and the charge carriers responsible for the observed conductivity, but up to now no universal relationship has been found between the epr and electrical parameters.[2] There are two types of organic donor–acceptor (D–A) complexes: paramagnetic ionic (D^+A^-) and diamagnetic nonionic (DA).[3] In this notation D represents an electron donor and A an electron acceptor. The resistivities of these systems are in the range of 10^{14}–10^{-2} ohm cm, and most of the complexes show a temperature-dependent conductivity characteristic of semiconducting materials. In general, the ionic complexes show higher conductivities than the nonionic ones.

Our report deals with the epr and conductivity studies on the charge-transfer complexes of the nonionic type (DA), carbazole–tetracyanoquinodimethane and carbazole–2,3 - dichloro - 5,6 - dicyanobenzoquinone. These complexes are intrinsically nonionic and therefore diamagnetic, but they exhibit weak paramagnetism due to the presence of paramagnetic impurities. Temperature-dependent studies of the epr signal intensity show that interactions among the unpaired impurity spins result in a nonmagnetic ground state and paramagnetic excited state. The complexes behave as semiconductors with activation energy for conduction greater than that for the creation of the paramagnetic spins, but doping the complexes with A^-, analogous to n doping in inorganic semiconductors, suggests that both the conductivity and the paramagnetic properties are associated with the unpaired electrons on the anions.

Experimental Section

(*a*) *Preparation of Complexes.* Carbazole (CARB), tetracyanoquinodimethane (TCNQ), and 2,3-dichloro-5,6-dicyano-1,4-benzoquinone (DDQ) were purified by sublimation. The complexes (CARB–TCNQ and CARB–DDQ) were prepared by mixing equimolar solutions of the donor (CARB) and acceptor (TCNQ, DDQ) in boiling chloroform. The dark solution was allowed to stand at room temperature for several hours. CARB–TCNQ was obtained as a dark blue crystalline powder and CARB–DDQ was obtained as a green crystalline powder. Elemental analysis indicated that both complexes (CARB–TCNQ and CARB–DDQ) are 1:1. Li^+DDQ^- and Li^+TCNQ^- were prepared by mixing hot solutions of Li^+I^- and DDQ and TCNQ in hot acetonitrile. The doped complexes were prepared by adding varying small amounts of Li^+A^- to the hot reaction mixture immediately after the donor and acceptor solutions were mixed.

(*b*) *Measurements. Infrared–Visible Absorption.* Absorption spectra of the complexes in the infrared region were made on the Beckman IR-5 infrared spectrophotometer in KBr pellets. Visible absorption spectra were examined in KBr pellets and dilute acetonitrile solution, using a Cary 14 recording spectrophotometer. The lithium salt of the acceptors (Li^+-TNCQ$^-$ and Li^+DDQ) and the neutral molecules of the donor and acceptors were used as references.

Electron Paramagnetic Resonance (Epr). Epr measurements were carried out with a Varian Model V4500-10A X-band spectrometer at 100-kHz field modulation. The temperature was controlled by passing heated or cooled nitrogen gas about the sample tube and measured with a thermocouple with a precision of $\pm 1°K$.

(1) Alfred P. Sloan Fellow.

(2) (a) A comprehensive review is F. Gutmann and L. E. Lyons, "Organic Semiconductors," Wiley, New York, N. Y., 1967; (b) Y. Okamoto and Walter Brennen, "Organic Semiconductors," Reinhold, New York, N. Y., 1964.

(3) H. M. McConnell, B. M. Hoffman, and R. M. Metzger, *Proc. Nat. Acad. Sci. U. S.*, **53**, 46 (1965).

The epr studies were done on powder systems, since the signal intensity was insufficient for single-crystal work. The g values of the complexes were measured using the dual-cavity technique with a dilute aqueous solution of potassium peroxylamine disulfonate (g = 2.0054, a_N = 13.0 G) as reference. The microwave frequency was measured with a Hewlett-Packard X-532-B frequency meter.

The g values, determined from the appropriate features of the powder spectrum, were checked by computer simulation with a program which assumes random orientation of spins and performs a double numerical integration over an octant of the unit sphere, utilizing a Gauss–Legendre integration in θ and a Gauss–Tschebyschev integration in Φ. The extremal features in the simulation are sensitive to relative changes of the input g values of $\pm 3 \times 10^{-5}$, which is smaller than the real accuracy of the measurement which is estimated to be ± 0.0005. The program could use either Lorentzian or Gaussian line widths, which for simplicity were assumed to be isotropic.

Studies of the temperature dependence of the epr signal intensity were performed over the range 150–373°K. The g-value anistropy was removed by overmodulation and the intensity was taken to be proportional to the square of the width of the resulting line times its height. The absolute number of spins was determined by comparing the integrated absorption intensity of the sample to that of a known amount of DPPH dispersed in KBr.

The effect of oxygen on the paramagnetism of the complexes was determined by observing the change in the epr signal intensity before and after introducing oxygen into the sample tube.

Conductivity Studies. The resistance of compressed pellets was measured as a function of temperature. The pellets were made on a 0.5-in. diameter die, using an applied force of 10 tons. A suspension of colloidal graphite in methanol was applied to the surface of the pellets to ensure good contact between the electrode plates and the pellet.

The apparatus consists of a Victoreen Model 5010 operational amplifier, wired as a current-to-voltage transducer with a voltage gain of two. The feedback resistors were housed in a Keithley shielded switch, Model 3011, with all co-ax fittings removed, bolted directly to the amplifier. The feedback resistors were Victoreen glass units, ranging from 10^{13} to 10^{6} ohms. Each resistor had a capacitor in parallel to give a time constant of 10 sec. The (−) input was connected to the high-impedance electrode with a rigid rod, and the low-impedance electrode voltage was determined by a potentiometer between ground and the regulated 15-V power supply of the operational amplifier.

The resistance of the compressed pellet was found by subjecting the pellet to a 15-V potential and measuring the current from the potential drop across the known feedback resistance.

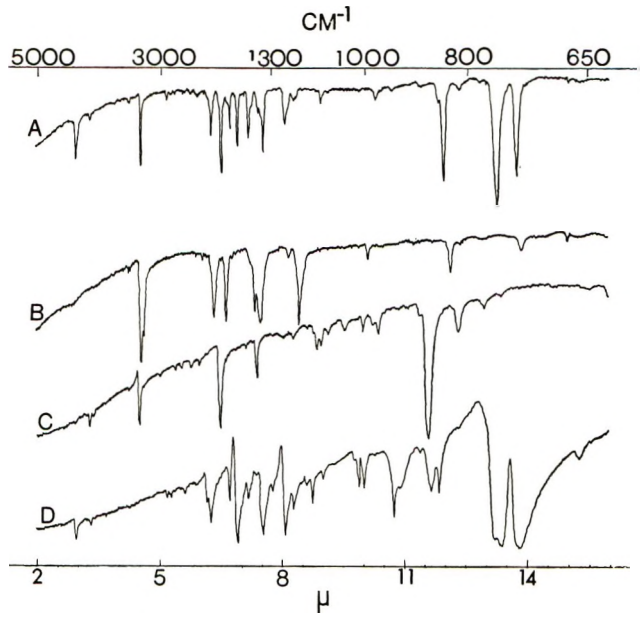

Figure 1. Infrared spectra of (A) CARB–TCNQ, (B) Li^+TCNQ^-, (C) TNCQ, and (D) CARB in KBr pellets.

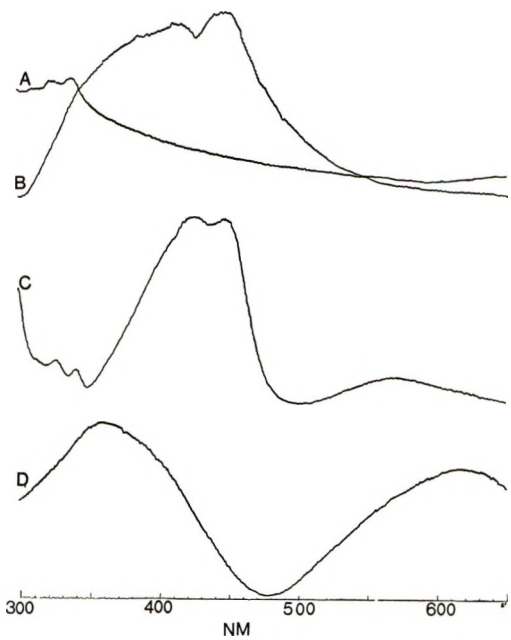

Figure 2. Visible spectra of (A) CARB, (B) TCNQ, (C) CARB–TCNQ, and (D) Li^+TCNQ^- in KBr pellets.

Temperature-dependent measurements were carried out by placing the electrodes in a copper chamber which was then immersed in a slush bath. The copper chamber was continuously swept with dry nitrogen gas to avoid condensation of water vapor on the sample and electrodes.

Results

The infrared and visible spectra of CARB, TCNQ, CARB–TCNQ, and Li^+TCNQ are shown in Figures

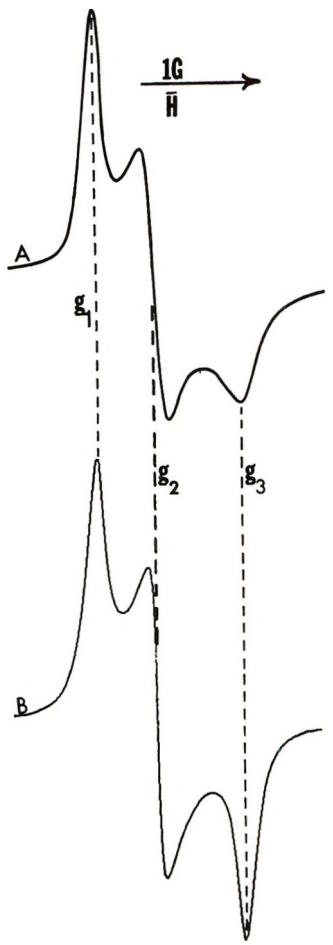

Figure 3. Room temperature electron paramagnetic resonance spectrum of CARB-TCNA: (A) experimental, (B) computer simulation; g values from Table I, Lorentzian component line width 0.11 G.

1 and 2. The infrared bands of CARB–TCNQ and CARB–DDQ in the 2–12-μ region (stretching modes) are a superposition of the spectra of the neutral donor and acceptor molecules and not of the ions, indicating that these complexes are nonionic. Because of the usual face-to-face stacking of the aromatic molecules in charge-transfer systems, the bending modes of the complexes are not expected to be the same as those of the neutral donor and acceptor molecules. The visible spectroscopic measurements also indicate that the bands appearing in the spectra of CARB–TCNQ are a superposition of the spectra of the individual donor and acceptor neutral molecules (Figure 2). The one new feature, the band appearing at 550 μ in Figure 2, is the charge-transfer band,[4] representing an electronic excitation from a nonionic (DA) to an ionic (D^+A^-) state.

These complexes, though nonionic, are weakly paramagnetic. Figure 3A gives a representative spectrum from a CARB–TCNQ sample, and Figure 3B gives the computer simulation using the g values listed in Table I and using a Lorentzian component line width of 0.11 G. Although an anisotropic line width could

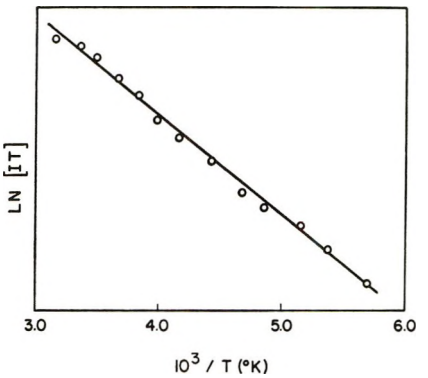

Figure 4. Plot of ln $[IT]$ *vs.* T^{-1} for CARB–TCNQ, I in arbitrary units.

have improved the fit to the intensity of the signal at g_3, the calculated field positions for the maxima agree. Simulation further shows that use of a Gaussian component line is inappropriate.

For isolated spins of concentration n, the signal intensity would follow Curie's law, $I \propto n/T$. Organic crystals in which antiferromagnetic interactions between spins are important often exhibit a nonmagnetic ground state and magnetic excited states with creation energy E_a and an excitation density $\rho(T)$.[5] In such a case

$$I \propto \rho(T)/T \tag{1}$$

with

$$\rho(T) = \rho(\infty) \exp[-E_a/kT] \tag{2}$$

when $E_a > kT$. The validity of this equation for the system studied here is shown by linear plots of ln $[IT]$ *vs.* T^{-1}, such as in Figure 4 for undoped CARB–TCNQ. Observed values of E_a are listed in Table I.

The temperature-dependent studies thus show that the interactions of the unpaired electrons in these

Table I: Epr and Electrical Parameters

	CARB–TCNQ	CARB–DDQ
E_a, eV	0.05 ± 0.01	0.040 ± 0.01
ϵ, eV	0.45 ± 0.20	0.45 ± 0.02
$\rho(\infty)$/mol	0.93–3.5 × 10^{20}	1.8–7.8 × 10^{20}
σ,[a] (ohm cm)$^{-1}$	1.9–7.1 × 10^{-10}	1.5–6.5 × 10^{-11}
g_1	2.0029	2.0074
g_2	2.0026	2.0050
g_3	2.0021	2.0019
g_{av}	2.0025	2.0049
g_{soln}[b]	2.0025	2.0050

[a] Dependent on doping; values are for room temperature. [b] Li^+A^- in acetonitrile solution.

(4) J. Rose, "Molecular Complexes," Pergamon Press, Elmsford, N. Y., 1967.

(5) Z. G. Soos, *J. Chem. Phys.*, **46**, 4284 (1967).

complexes lead to a nonmagnetic ground state, with thermally accessible paramagnetic excited states. The spin concentrations per mole were measured at room temperature for both complexes (Table I) and, together with the value of E_a, allow us to calculate $\rho(\infty)$ using eq 2. The small values of $\rho(\infty)$ prove again that these complexes are basically nonionic and nonmagnetic, since for a completely ionic system $\rho(\infty)$ should be equal to two times Avogadro's number. The impurity spins are not due to adsorbed oxygen, since introducing oxygen into a degassed sample resulted in an irreversible decrease of the epr signal intensity. Doping the complexes increased $\rho(\infty)$ without changing E_a, the line shape, or line widths of the spectral lines. This suggests that A^- impurity centers are responsible for the observed paramagnetism. This view is supported by the fact that the average g value of each complex is equal to the solution g values of the corresponding LiA^- (Table I).

The temperature-dependent studies of the conductivity of compressed pellets show that these complexes are semiconductors

$$\sigma = \sigma(\infty) \exp(-\epsilon/k_B T) \quad (3)$$

$\sigma(\infty)$ is the conductivity at infinite temperature and ϵ is the activation energy for conduction (Figure 5). An ϵ value of 0.45 ± 0.02 eV was obtained for complexes with both acceptors. The temperature-dependent studies were performed in the temperature range 178–298°K. Doping the complexes increased the conductivity without changing the activation energy for conduction, as is shown in Figure 6.

As a means of relating the increases of both $\rho(\infty)$ and $\sigma(\infty)$ upon doping, Figure 6 gives a plot of log $\sigma(\infty)$ *vs.* log $\rho(\infty)$ for CARB–TCNQ. The result is a straight line of slope 1.08, with standard deviation 0.07 (Figure 6, which suggests that the charge carriers and the magnetic spins have the same origin.

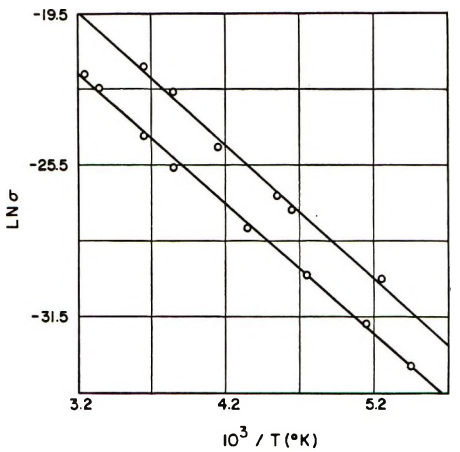

Figure 5. Plot of ln σ *vs.* T^{-1} for CARB–TCNQ (upper) doped, (lower) undoped.

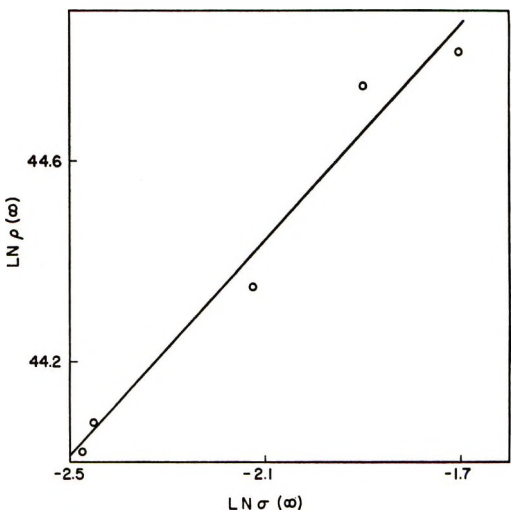

Figure 6: A plot of ln $\rho(\infty)$ *vs.* ln $\sigma(\infty)$ on doped samples of CARB–TCNQ.

Discussion

The Epr Results show that the impurity A^- ions are the source of the observed paramagnetism. The proportionate increase in the epr signal intensity and conductivity on doping with Li^+A^- indicates that the A^- ions are involved in both processes. Two possible models for the nature of the impurity centers are the distributive model and the cluster model. In the cluster model the impurity centers would occur in relatively large domains. However, proportionality of $\sigma(\infty)$ and $\rho(\infty)$ makes this model unattractive, since a linear increase of both quantities is not expected in this case.

The distributive model views the interacting impurity spins as essentially randomly distributed throughout the solid. Spin exchange among the excited magnetic spins is small, since the system is dilute, and is therefore not expected to dominate the line width. The observed narrow line widths would primarily be due to the delocalization of the spins along a chain. The estimated line width $\delta\omega$ for an electron delocalized over N molecules is[6]

$$\delta\omega \sim A/N^{1/2} \quad (4)$$

where A is the line width for a localized spin. Calculations for CARB–TCNQ with $A \sim 10$ G, roughly the total width of the $TCNQ^-$ hyperfine pattern, give an N of the order of 10^3 molecules.

It is not possible from the powder epr results to build a convincing model for the interactions which cause the pairing of the impurity spins. Nevertheless, these results do show that it is possible to "n dope" an organic semiconductor in a manner analogous to that of inorganic semiconductors. Since "p doping" has been observed in organic charge-transfer com-

(6) D. D. Thomas, A. W. Merkl, A. F. Hildebrandt, and H. M. McConnell, *J. Chem. Phys.*, **40**, 2588 (1964).

pounds,[7,8] it appears that the electrical properties of organic compounds are amenable to chemical alteration.

Acknowledgment. We wish to thank Dr. D. F. Shriver for helpful discussions. This work was supported by the Advanced Research Projects Agency of the Department of Defense through the Northwestern University Materials Research Center.

(7) A. Rembaum, A. M. Hermann, F. E. Stewart, and F. Gutmann, *J. Phys. Chem.*, **73**, 513 (1969).

(8) J. H. Lupinski, K. D. Kopple, and I. J. Hertz, *J. Polym. Sci.*, 1561 (1967).

Mutual-Diffusion Coefficients at 25° in the System Silver Nitrate–Water[1]

by John G. Albright and Donald G. Miller*

Chemistry Department, Lawrence Livermore Laboratory, Livermore, California 94550 *(Received June 7, 1971)*

Publication costs assisted by Lawrence Livermore Laboratory, U. S. Atomic Energy Commission

Volume-fixed mutual diffusion coefficients D_v have been determined by the Rayleigh method for aqueous $AgNO_3$ at 25° from 0.05 to 8 mol/l. A laser light source was successfully used to provide sharp fringes at all concentrations even with bath water in the reference path of the Tiselius cell. Our results are in good agreement with previously reported optical data in the region of overlap (0.1 to 1.5 M) but differ significantly from two discrepant series of diaphragm cell measurements for higher concentrations.

I. Introduction

Application[2,3] of irreversible thermodynamics to electrolyte solutions has stimulated interest in obtaining activity, conductance, transference number, and diffusion data for electrolyte solutions from which ionic transport coefficients may be calculated. This paper is concerned with diffusion data for the system $AgNO_3$–H_2O for which t_+ has recently become available.[4] Harned and Hildreth[5] obtained good experimental data for this system in the dilute concentration range (0.003–0.06 M) by the restricted-diffusion conductance method, where M is the concentration in moles per liter. Longsworth[6,7] obtained data in the moderate concentration range (0.1–1.5 M) by the free-diffusion method with Rayleigh interferometric optics. Data extending to higher concentrations, 4 and 9 M, have been obtained with the diaphragm-cell method by Firth and Tyrrell[8] and by Janz, *et al.*,[9] respectively. Because of inherent uncertainties in the diaphragm-cell method and substantial inconsistencies found in the comparison of the two sets of data, it was decided to measure diffusion coefficients to near saturation by the free-diffusion method with Rayleigh interferometric optics.

II. Experimental Section

Preparation of Solutions. All solutions were prepared gravimetrically. Triply distilled water was used throughout. Baker Analytical reagent grade $AgNO_3$ rated at better than 99.9% purity was used without further purification. Sucrose and KCl were used for calibration. Sucrose was obtained from the National Bureau of Standards and rated at better than 99.99% pure. The KCl was from a sample that had been purified by the method of Pinching and Bates.[10] Densities for preparation of solutions were taken from the literature.[11–16]

(1) This work was performed under the auspices of the U. S. Atomic Energy Commission.

(2) D. G. Miller, *J. Phys. Chem.*, **70**, 2639 (1966).

(3) D. G. Miller, *ibid.*, **71**, 616 (1967).

(4) M. J. Pikal and D. G. Miller, *ibid.*, **74**, 1337 (1970).

(5) H. S. Harned and C. L. Hildreth, Jr., *J. Amer. Chem. Soc.*, **73**, 3292 (1951).

(6) L. G. Longsworth in "Structure of Electrolyte Solutions," W. S. Hamer, Ed., Wiley, New York, N. Y., 1959, Chapter 12.

(7) Data for the concentration range 0.1–1.0 M are given in ref 6 as part of the results of thermal-diffusion experiments. Further unpublished data for 0.1–1.5 M obtained by Rayleigh free-diffusion method were graciously sent to us in a private communication and are given in the text with Professor Longsworth's permission.

(8) J. G. Firth and H. J. V. Tyrrell, *J. Chem. Soc.*, 2042 (1962).

(9) G. J. Janz, G. R. Lakshminarayanan, M. P. Klotzkin, and G. E. Mayer, *J. Phys. Chem.*, **70**, 536 (1966).

(10) G. D. Pinching and R. G. Bates, *J. Res. Nat. Bur. Stand.*, **37**, 311 (1946).

(11) G. Jones and J. H. Colvin, *J. Amer. Chem. Soc.*, **62**, 338 (1940).

(12) A. N. Campbell and R. J. Friesen, *Can. J. Chem.*, **37**, 1288 (1959).

(13) A. N. Campbell and K. P. Singh, *ibid.*, **37**, 1959 (1959).

(14) L. J. Gosting and M. S. Morris, *J. Amer. Chem. Soc.*, **71**, 1998 (1949).

(15) L. J. Gosting, *ibid.*, **72**, 4418 (1950).

(16) The densities of the solid reagents used for buoyancy corrections were from the "Handbook of Chemistry and Physics," 47th ed, Chemical Rubber Publishing Co., Cleveland, Ohio, 1968.

Apparatus. A Beckman-Spinco Model-H electrophoresis–diffusion apparatus was used. The instrument was set in the diffusion configuration suggested by the operating manual although the modifications suggested by Creeth, *et al.*,[17] would have been beneficial; other needs of the laboratory restricted modification. A Pyrocell Tiselius electrophoresis cell with bath solution reference path was used. Free-diffusion initial boundaries were formed with a stainless-steel capillary which was plated with gold to prevent reaction with silver nitrate. The bath temperature was measured with a calibrated[18] mercury in glass calorimeter thermometer. All experiments were performed at 25.00° ± 0.01°.

For the first three $AgNO_3$ and first sucrose experiments the standard light source of the instrument, mercury-vapor lamp with filters (λ 5461 Å), was used. Because of the line width of this source, the fringe patterns became blurred and unreadable for $\bar{c}$ greater than 0.5 *M* with water in the reference channel, where $\bar{c}$ denotes the average concentration in moles per liter. In the third $AgNO_3$ experiment at 1.3 *M*, ethylene glycol was added to the bath water to give fringes of reasonable quality.

For the remainder of the experiments the instrument was adapted with a Spectra-Physics Model 115 Neon laser, λ 6328 Å. The mercury-vapor lamp and condensing lenses were removed, and the laser was placed on the cabinet floor with the beam reflected up and then over to the source slit. To smooth the effect of speckle, the beam was oscillated by passing it through a rotating optical flat.[19] A reasonable intensity distribution in the fringe pattern was obtained by placing a large cylindrical lens[20] just behind the source slit to diverge the light passing through the slit. A cylinder lens was placed between the laser and the source slit to narrow the beam and increase the intensity of light at the slit. Although the alignment of the assembly was sensitive to small variations in positions of components, once aligned, it was stable for several days. With this light source, sharp fringes were obtained in all experiments regardless of concentration. The fringe patterns were recorded on Kodak IIaF photographic glass plates. They were read on a Grant microcomparator with card punch output. Fringes obtained with the laser source, however, were more grainy and more difficult to read on the comparator than those from the regular light source.

Experimental Procedure. Theories for the study of diffusion processes by the Rayleigh interferometric method are well established.[21-24] In principle the method is absolute where a magnification factor is obtained from a photograph of a ruled scale placed at the position of the diffusion cell. However, because of problems experienced by Creeth, *et al.*,[17] it was decided to calibrate the instrument with systems for which accurately measured diffusion coefficients are available. It was assumed that problems with the optical system for the experiments with silver nitrate in water would be the same for the calibration experiments, and the effect of these problems on the analysis of data would mostly cancel.

All experiments were allowed to equilibrate for 30 min before initiation of the experiment and at least 40 ml of solution was removed during boundary formulation. At the start of each experiment from three to six photographs were taken to obtain the fractional part of a fringe (fpf). After the fringe pattern became resolved, pictures were taken at regular intervals of $1/t'$ until the boundary had broadened to at least one-third of the length of the fringe pattern, where t' is the time starting at cessation of siphoning.

Analysis of Fringe Patterns. The fringe patterns were slightly bowed, a condition that became more pronounced at higher values of $\bar{c}$. The early pictures, used for the fpf determination, were aligned on the comparator so that the straight portions of the fringe pattern adjacent to each side of the boundary were parallel to the y axis of the comparator. The fpf was then determined by observing the fractional fringe shift across the boundary.

Later pictures, used to determine fringe separations, were placed so that the straight portions of the pattern were parallel to the x axis. The alignment procedure for reading all fringe patterns was such that by starting on a fringe adjacent to the boundary on one side, by shifting the pattern a fpf on the y axis and by proceeding to a position on the x axis symmetrically located on the other side of the boundary, the pattern was again aligned on a fringe. With this alignment procedure, displacements in the y direction due to bowing of fringes within the boundary region were nearly the same at equal distances on either side of the starting boundary position.

By following the symmetrical pairing procedure outlined by Creeth,[24] the positions of symmetrical pairs of fringes, X_j and X_{J-j}, were measured where J is the total number of fringes and j is an integral fringe number. The value of the quotient of the apparent diffusion co-

(17) J. M. Creeth, L. W. Nichol, and P. J. Winzor, *J. Phys. Chem.*, **62**, 1546 (1958).

(18) This thermometer was calibrated against an NBS calibrated platinum resistance thermometer. Two similarly calibrated mercury thermometers were used to check the bath temperature, and good agreement was observed.

(19) The significant problem with speckle in the interference pattern is apparently related to the spatial and temporal coherence of the laser source and the narrow aperture of the source slit. Speckle effects are discussed, for example, by B. J. Thompson in "Progress in Optics," Vol. VII, E. Wolf, Ed., North-Holland Publishing Co., Amsterdam, 1969, Chapter IV.

(20) A 2-cm round sample bottle filled with water was used.

(21) J. St. L. Philpot and G. H. Cook, *Research*, **1**, 234 (1948).

(22) H. Svensson, *Acta Chem. Scand.*, **3**, 1170 (1949).

(23) L. G. Longsworth, *Rev. Sci. Instrum.*, **21**, 524 (1950).

(24) J. M. Creeth, *J. Amer. Chem. Soc.*, **77**, 6428 (1955).

efficient and the calibration constant β was calculated from the expression[24]

$$\left[\frac{1}{n}\sum_j\left(\frac{X_{J-j} - X_j}{z_{J-j} - z_j}\right)\right]^2 = \left(\frac{D'}{\beta}\right)t \qquad (1)$$

where

$$\frac{2j - J}{J} = \text{erf } z_j \qquad (2)$$

Here n is the number of fringe pairs in the summation. Every second or every fifth fringe pair was measured and included in the summation subject to the constraints $2z_j < 2.0$ and $X_{J-j} - X_j > 2.0$ mm.[25] The values of the terms in the summation were generally within $\pm 0.2\%$ of the mean. Except for an early fringe pattern in a few experiments, five or more fringe pairs were included in each summation.

The measured time t', the true time t, and the initial time correction Δt are related by

$$t = t' + \Delta t \qquad (3)$$

With eq 3, eq 1 can be written as

$$\frac{D'}{\beta} + \frac{D'\Delta t}{\beta t'} = \left(\frac{1}{t'}\right)\left[\frac{1}{n}\sum_j\frac{X_{J-j} - X_j}{z_{J-j} - z_j}\right]^2 \qquad (4)$$

By fitting the right-hand side of eq 4 linearly to $1/t'$ by least squares, one obtains D'/β and Δt from the intercept and slope, respectively. At least five and usually six or more values of $D'(\bar{c})/\beta$ were included in this evaluation. The initial time corrections were from 10 to 50 sec.

To find the value of β, two experiments with sucrose and one experiment with KCl were performed. In addition, six of the experiments with $AgNO_3$ lie within the concentration range where they could be compared with the data of Longsworth. The value for the sucrose diffusion coefficient was taken from ref 14 where a minor temperature adjustment from 24.95 to 25.00° was made by multiplying by the viscosity ratio of water at these two temperatures. The reference value for the diffusion coefficient of KCl was an average of values from ref 26 and 27. The average of KCl and the two sucrose solutions gave a value of β of 4.175×10^{-5} with a standard deviation σ of 0.006. The average β based on the data of Longsworth alone was 4.186×10^{-5} with $\sigma = 0.012$. An overall average value of $\beta = 4.180 \times 10^{-5}$ with $\sigma = 0.012$ was used for the calculation of the diffusion coefficients for all the $AgNO_3$–H_2O experiments. No significant difference was observed between the β's from the two different light sources. A calibration table is available in UCRL-73183 describing this work.[28]

Results. In Table I are listed the concentrations and calculated values of the diffusion coefficients for all the experiments on the system $AgNO_3$–H_2O. Since the volume change on mixing may be considered negligible, these diffusion coefficients are relative to the volume fixed frame of reference.

Data[4] for the activity of $AgNO_3$ were numerically differentiated to give $1 + m(\text{d ln } \gamma/\text{d}m)$, and a smooth curve was drawn through the derivatives. Here m is the number of moles per kilogram of solvent. Values at experimental concentrations were obtained from a least-squares fit of points taken from this smooth curve as a function of c. Values of $D_v/(1 + m(\text{d ln } \gamma/\text{d}m))$ have been tabulated in Table I. The previously unpublished data communicated to us by Longsworth[7] are given in Table II with his kind permission.

III. Discussion

The consistency of the calibrations indicates an experimental precision of $\pm 0.25\%$. In spite of the bowing of the fringe pattern only small deviations of the values of $\Delta X/\Delta z$ within each fringe pattern were found experimentally. This is due in part to the alignment procedure. The equal displacement in the y direction at distances along the x axis equally distant from the initial boundary position increased X_J and X_{J-j} so that the difference stayed nearly the same.

The calibration data did not reveal a dependence of β on index of refraction and suggest that changes in β at higher concentrations would be small, if even significant.

Effects that are first order in Δc will cancel in the analysis procedure used here.[24] Consideration of eq 37 and tabulated values of $W(z)$, $U(z)$, and $V(z)$ in ref 24 show that error in calculation owing to the second-order dependence of Δc of the diffusion coefficients will be negligible. Some plots of $\Delta z - \Delta z^*$ *vs.* R of the type considered by Creeth[24] were made. This type of plot is sensitive to bowing of the fringe pattern since fringes near the center of the pattern are matched with fringes near the outside. The slopes of the curves were small but opposite in sign from that expected in terms of first-order dependence of diffusion coefficients on Δc. A similar problem was found and discussed by Creeth, *et al.*[17]

Values of $J/\Delta c$ from experiments with the laser source appeared to lie on a smooth curve with the exception of 5.98 M. The quality of data from that experiment suggested a small error in determination of concentration (<0.06 M) rather than a significant error in the determination of J. The pattern for data for $J/\Delta c$ from the experiments with the mercury-vapor lamp were more scattered which suggests that less reliance be placed on experiments 1–3.

(25) The first of these constraints eliminates fringe pairs at the ends of the fringe pattern where minor optical distortions can cause significant errors. The second constraint eliminates fringe pairs so close together that uncertainties in the measurement of position lead to significant error.

(26) L. J. Gosting, *J. Amer. Chem. Soc.*, 72, 4418 (1950).

(27) L. G. Longsworth, *J. Phys. Chem.*, 61, 1557 (1957).

(28) J. G. Albright and D. G. Miller, UCRL-73183, Lawrence Livermore Laboratory, Livermore, Calif., May 11, 1971.

Table I: $AgNO_3$ Experimental Results at 25°[a]

$\bar{m}$, mol kg^{-1}	$\bar{c}$, mol l.$^{-1}$	Δc, mol l.$^{-1}$	J	Δt, sec	$D_v \times 10^5$, cm^2 sec^{-1}	$D_v/(1 + m(\mathrm{d} \ln \gamma/\mathrm{d}m)) \times 10^5$, cm^2 sec^{-1}
0.0503[a]	0.0501	0.0353	49.32	18	1.625	1.808
0.0978	0.0972	0.0316	51.72	46	1.590	1.833
0.496	0.488	0.0500	79.33	11	1.425	1.951
1.034[a]	1.000	0.0644	86.18	22	1.266	2.045
1.409[a]	1.346	0.0683	89.90	11	1.176	2.098
1.414	1.351	0.0636	98.81	24	1.166	2.083
2.148[a]	2.005	0.0616	79.90	32	1.007	2.135
4.632[a]	4.004	0.0579	71.59	17	0.7113	2.250
7.552[a]	5.982	0.0606	84.15	51	0.5624	2.076
7.588[a]	6.004	0.0709	86.03	29	0.5640	2.082
9.263[a]	6.985	0.0704	84.71	48	0.5186	1.935
11.160[a]	7.986	0.0777	94.68	18	0.4869	1.791

[a] Experiments performed with laser light source.

Table II: $AgNO_3$ Experimental Results Obtained by Longsworth[a]

1°		13°		25°		37°	
$\bar{m}$	$10^5 D_v$	$\bar{m}$	$10^5 D_v$	$\bar{m}$	$10^5 D_v$	$\bar{m}$	$10^5 D_v$
0.2511	0.7677	0.2510	1.1121	0.2510	1.5183	0.2511	1.9783
0.2510	0.7670	0.2512	1.1122	0.2512	1.5183	0.2508	1.9782
0.5016	0.7112	0.5016	1.0404	0.5015	1.4260	0.5018	1.8722
0.5015	0.7112	0.5022	1.0400	0.5018	1.4256	0.5018	1.8725
0.7526	0.6644	0.7525	0.9733	0.7527	1.3493	0.7531	1.7788
		0.7532	0.9760				
1.0037	0.6185	1.0035	0.9136	1.0038	1.2754	1.0040	1.6989
1.0036	0.6196	1.0026	0.9202	1.0034	1.2742	1.0030	1.6933
1.2544	0.5814	1.2548	0.8632	1.2536	1.2106	1.2544	1.6081
		1.2532	0.8753	1.2542	1.2167		
1.5044	0.5473	1.5058	0.8182	1.5052	1.1543	1.5049	1.5497
		1.5040	0.8258	1.5044	1.1512		

[a] Each entry is the result of a separate experiment and the concentration difference in all cases was 0.1 m; the number of fringes varied from 70 to 80. Concentrations, m, are in moles per kilogram of solvent.

The experimental results are plotted in Figure 1 along with optical and conductance data from previous workers. Our optical results are in excellent agreement with Harned and Hildreth's conductance data[5] and Longsworth's optical data[6,7] in the region of overlap (0.05–1.5 M). The two sets of diaphragm cell data[8,9] are discrepant among themselves and deviate substantially from our optical data at higher concentrations, as much as 20–30% from 6 to 8 M.

Janz, *et al.*,[9] used small concentration differences in an attempt to get "differential" coefficients. However, small errors in analysis, even with a good method, can yield large errors in D.

An analysis of the data of Firth and Tyrell[8] suggests that significant error arose in the conversion of their integral diffusion coefficients. Since all of their experiments were performed with pure water as the initial top solution, the conversion error may be expected to be pronounced at higher concentrations. A reasonable comparison with their data was obtained by a recalculation of their integral values, $D_{cm''}{}^{\circ}$ from integrations of the data presented here. It was found that the average per cent-of-value difference between their values of $D_{cm''}{}^{\circ}$ and the recalculated values was only 0.12% with a standard deviation of 0.43%. The difference was slightly greater at the low concentrations, consistent with the general observation that electrolytes in dilute solution diffuse anomalously fast in diaphragm cells.

As a further comparison with the diaphragm cell method, an experiment was performed at one of the author's laboratories[29] with a diaphragm cell which had been calibrated by diffusing 0.8 m urea into water

(29) This experiment was performed at Texas Christian University (J. G. A.) by Mr. Keichi Aoyagi.

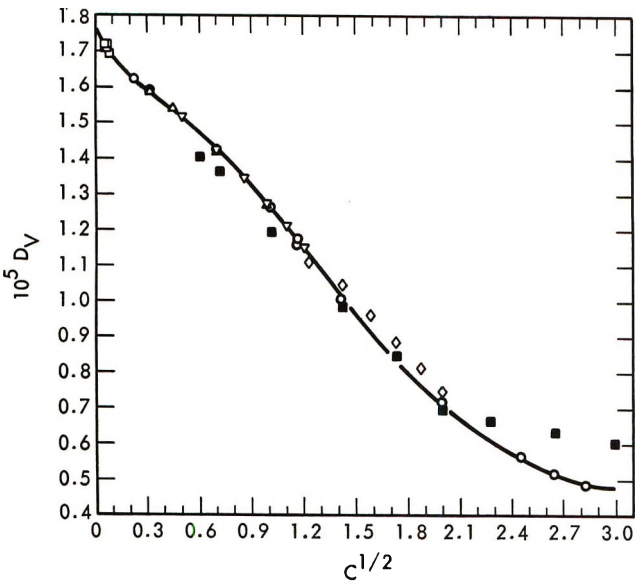

Figure 1. $D_v \times 10^5$ (cm²/sec) *vs.* $c^{1/2}$ (mol$^{1/2}$/l.$^{1/2}$) for the system $AgNO_3$–H_2O at 25°: □, Harned and Hildreth;[5] △, Longsworth;[6] ▽, Longsworth;[7] ○, this research; ■, Janz, *et al.*;[9] ◇, Firth and Tyrell.[8]

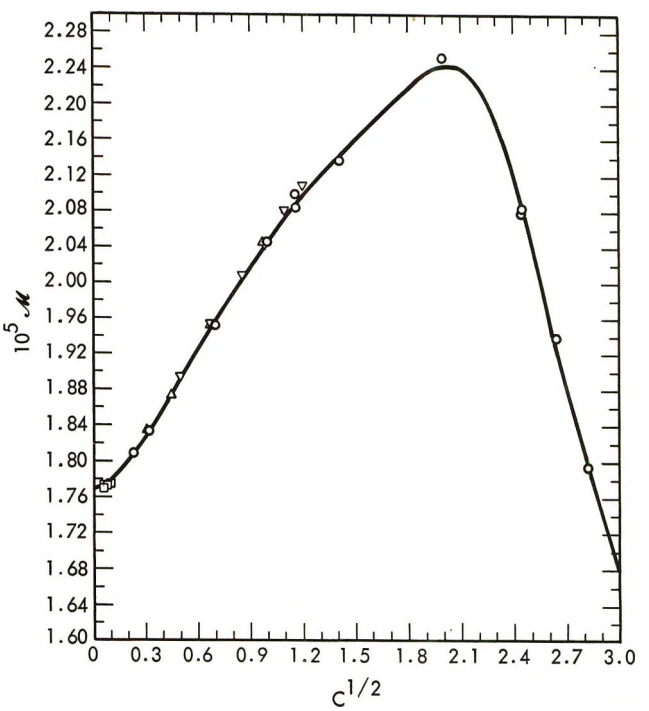

Figure 2. Diffusion coefficients for $AgNO_3$ corrected for thermodynamic driving force; $\mathfrak{M} \times 10^5$ (cm²/sec) *vs.* $c^{1/2}$ (mol$^{1/2}$/l.$^{1/2}$), $\mathfrak{M} = D_v/(1 + m(\mathrm{d} \ln \gamma/\mathrm{d}m))$: □, Harned and Hildreth;[5] △, Longsworth;[6] ▽, Longsworth;[7] ○, this research.

and 1-C^{14} labeled benzene into pure benzene. This $AgNO_3$ experiment was performed at 25° with $\bar{c} = 8.3469\ M$ and $\Delta\bar{c}^\circ = 0.8887\ M$. Final concentrations were accurately determined from density measurements. The measured integral diffusion coefficient was 0.474×10^{-5} cm² sec^{-1} which was in good agreement with the value of 0.475×10^{-5} cm² sec^{-1} calculated from a polynomial which was fit to the data in Table I for $\bar{c} > 2.0\ M$.

Figure 2 is a plot of $\mathfrak{M} = D_v/(1 + m(\mathrm{d} \ln \gamma/\mathrm{d}m))$.

Conclusions. A discussion of the effect of ion-pair formation on diffusion in the $AgNO_3$–H_2O system has been given by Janz, *et al.*[9] Diffusion data, limiting conductance data,[30] and spectral data[31] support the existence of ion-pair formation in this system. In this regard, the continued decrease of diffusion coefficients with increased concentration found for $AgNO_3$–H_2O in this experimental work contrasts sharply with the concentration dependence of diffusion coefficients for KCl and other halides in water. The latter first decrease and then increase with concentration.

Other nitrates also exhibit continually decreasing diffusion coefficients with concentration,[9] but to a lesser extent than $AgNO_3$. This phenomenon qualitatively suggests ion-pair formation for nitrates, and especially so for $AgNO_3$. Moreover, the transference number of Ag^+ increases from 0.464 at infinite dilution to 0.622 at 9 *m*.[4] This may suggest the existence at higher concentrations of ion triplets of the form $Ag(NO_3)_2^-$, which would move more slowly than Ag^+.

One conclusion from the data presented here, in contrast to that previously reported,[9] is that the diffusion coefficients as a function of concentration do not exhibit sharp changes in slope, and thus special mechanisms to account for such changes are unnecessary.

Acknowledgments. The authors wish to express their gratitude to Dr. Longsworth for providing the data listed in Table II. The authors are indebted to Dr. Bernard Shore of the Bio Medical Division of the Lawrence Livermore Laboratory for permitting use of the instrument and facilities. This work was partially supported at Texas Christian University by the Welch Foundation, Grant No. P-225, and J. G. A. wishes to acknowledge his gratitude for this support. Finally, the authors wish to thank Sharon Rudd Albright for her assistance in writing computer programs for data analysis.

(30) A. N. Campbell and E. M. Kartzmark, *Can. J. Chem.*, **33**, 887 (1955).

(31) H. Lee and J. K. Wilmshurst, *Aust. J. Chem.*, **17**, 943 (1964).

Estimating Slow-Motional Rotational Correlation Times for Nitroxides by Electron Spin Resonance[1]

by S. A. Goldman, G. V. Bruno, and J. H. Freed*

Department of Chemistry, Cornell University, Ithaca, New York 14850 *(Received January 3, 1972)*

Publication costs assisted by the National Science Foundation

A simple method of estimating slow-motional rotational correlation times τ_R for nitroxides by esr, which is based on the rigorous theory of Freed, Bruno, and Polnaszek, is discussed. The results can be fit to the expression $\tau_R = a(1 - S)^b$, where S is the ratio of the separation of the outer hyperfine extrema to that for the rigid limit value. The parameters a and b depend upon intrinsic line width, rotational model, and hyperfine parameters, and appropriate results are given.

Recently, there has been considerable interest in the slow-motional esr spectra of nitroxide free radicals.[2] In this motional region, which corresponds to rotational correlation times 10^{-9} sec $\lesssim \tau_R \lesssim 10^{-6}$ sec, the line shape can no longer be described by the earlier relaxation theories.[3] Slow-motional nitroxide spectra have been observed in viscous liquids, solids, and in the hindered rotation of spin-labeled molecules.[2,4]

Using the methods developed by Freed, *et al.*,[5] it is possible to interpret these line shapes in terms of the relevant spin parameters to learn about the dynamics of the molecular reorientational process. This was demonstrated for peroxylamine disulfonate (PADS), $(SO_3)_2NO^{2-}$, where the detailed line shapes were analyzed in terms of their dependence on **A**, **g**, an intrinsic line width, and the rotational correlation time, τ_R.[4] It was also shown that the proper analysis of the observed spectra depends on whether the molecule is undergoing anisotropic rotational reorientation and whether there are significant deviations from a Brownian diffusion model.

The ability to interpret these esr line shapes in terms of molecular dynamics would be particularly useful in the spin-label technique where changes in line shape resulting from variations in molecular size, structure, location of paramagnetic site, etc., could yield information on the nature of the local molecular environment. In principle this can be done for any slow-motional nitroxide spectrum. However, in practice, many of the expected line shape changes are obscured by inhomogeneous line broadening resulting from intramolecular or intermolecular (solvent) hyperfine and dipolar interactions. These interactions decrease the spectral resolution and consequently increase the difficulty in obtaining useful information from the observed line shapes.

From single crystal studies on a variety of nitroxides, it is known that their **A** and **g** tensors are only slightly dependent on the detailed molecular structure and that $A_z \gg A_x \approx A_y$, where the z axis is along the 2p-π orbital of nitrogen, the x axis is along the N–O bond, with the y axis perpendicular to these.[6] Thus a typical nitroxide slow-motional spectrum has two well separated outer hyperfine extrema with an overlapped central region. A useful parameter for describing these spectra is $S = A_z'/A_z$, where A_z' is one-half the separation of the outer hyperfine extrema and A_z is the rigid limit value for the same quantity.[7] The very detailed experimental results for PADS[4] demonstrated that S is a sensitive, monotonically increasing, function of τ_R and this general type of behavior is also characteristic of other nitroxides as studied in this laboratory as well as in others.[2,6,7] Thus, if we know how S is affected by changes in the (1) spin parameters, (2) line width, and (3) rotational diffusion model, then the variation of S with τ_R could generally be applied to nitroxides, and it would be possible to estimate τ_R without the necessity of making detailed line shape calculations and comparisons.

Slow-motional line shapes were calculated for completely asymmetric **A** and **g** tensors as well as for axially symmetric models where the z axis was chosen as the symmetry axis.[8] Spectra simulated under these

(1) Supported in part by the Advanced Research Projects Agency and by a Grant from the National Science Foundation (Grant No. GP-13780).

(2) (a) W. L. Hubbell and H. M. McConnell, *J. Amer. Chem. Soc.*, **93**, 314 (1971); (b) O. H. Griffith and A. S. Waggoner, *Accounts Chem. Res.*, **2**, 17 (1969).

(3) (a) J. H. Freed and G. K. Fraenkel, *J. Chem. Phys.*, **39**, 326 (1963); (b) D. Kivelson, *ibid.*, **33**, 1094 (1960).

(4) S. A. Goldman, G. V. Bruno, C. Polnaszek, and J. H. Freed, *ibid.*, **56**, 716 (1972).

(5) J. H. Freed, G. V. Bruno, and C. Polnaszek, *J. Phys. Chem.*, **75**, 3385 (1971).

(6) O. H. Griffith, D. W. Cornell, and H. M. McConnell, *J. Chem. Phys.*, **43**, 2909 (1965).

(7) R. C. McCalley, E. J. Shimshick, and H. M. McConnell (to be published) discuss parameters closely related to S (*i.e.*, the deviations of high-field and low-field line positions from their respective rigid limit values) in work on spin-labeled oxyhemoglobin.

latter simplifying assumptions showed qualitative agreement with those calculated with the asymmetric parameters with the major differences occurring in the central region of the spectra. For isotropic diffusion, the separation between the outer hyperfine extrema was unaffected (within the accuracy of our computer calculations) by the approximation of axially symmetric A and g. Thus, for simplicity, axial symmetry was assumed in many of the calculations. The value of S was also found to be insensitive to variations in $A_\perp$, $g_{||}$, and $g_\perp$, typical of nitroxide, as long as A_z is kept constant. Changes in the magnitude of A_z, however, do affect the value of S, and this dependence can be approximately expressed in the functional form $S = S(\tau_R A_z)$, *i.e.*, S is simply dependent on the product $\tau_R A_z$. This functional dependence permits scaling our results given below over the range of values of A_z typical for nitroxides (27–40 G) with an error of less than 3%.

The experimental spectra for PADS have been compared to simulated spectra calculated for models of (1) Brownian diffusion, (2) strong jump diffusion, and (3) an approximation to a free-diffusion model (which gives essentially the same results as a moderate jump model). It was shown that the calculated line shapes were very sensitive to the choice of rotational model, and that the spectra simulated with the approximate free-diffusion model came closest to the observed spectra. Slow-motional spectra observed for nitroxides attached to larger molecules in solution exhibit line shapes which, as expected, are more characteristic of Brownian diffusion.[7] In Figure 1, the variation of S with τ_R is shown for Brownian, approximate free, and strong jump-diffusion models,[4] isotropic diffusion, A_z = 32 G and peak-to-peak derivative Lorentzian line widths of 0.3 and 3.0 G. It can be seen that S is model sensitive and for an equivalent value of τ_R,[9] S increases from Brownian to free to a jump reorientational model. We have found that these curves can be fit to the expression

$$\tau_R = a(1 - S)^b$$

to within 2, 3, or 5% in the value of τ_R for a given S, for jump, Brownian, or free diffusion, respectively, with the values of a and b given in the figure caption. It should be noted that for $\tau_R \lesssim 7 \times 10^{-9}$ sec, S is undefinable since the outer lines begin to converge to the motionally narrowed spectrum. For longer τ_R's than shown in Figure 1, the spectrum approaches the rigid limit, and the value of $1 - S$ become comparable to experimental uncertainties.

As previously noted, the detailed esr slow-motional line shape can be greatly affected by the presence of a large intrinsic line width resulting from unresolved inhomogeneous line broadening. It is often difficult to estimate the size of this intrinsic width directly from the slow-motional spectra without detailed spectral

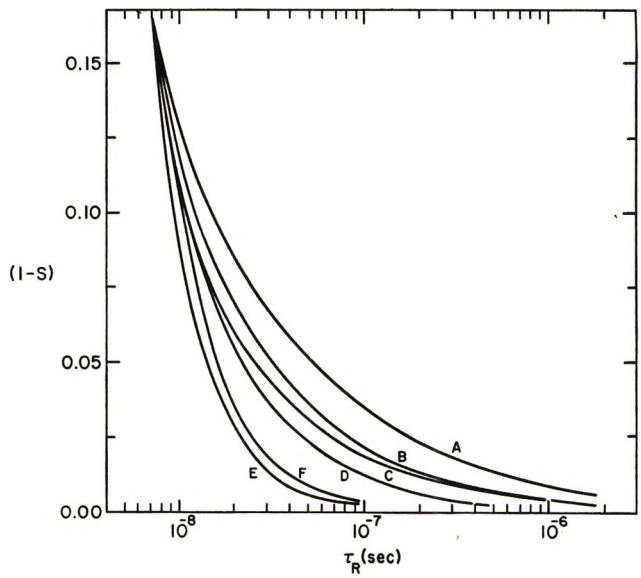

Figure 1. Graph of $(1 - S)$ *vs.* τ_R for nitroxides for different models of isotropic rotational reorientation (from computer simulation). Curves A and B are for Brownian diffusion and derivative widths δ = 0.3 and 3.0 G, respectively, curves C and D are for a moderate jump diffusion and δ = 0.3 and 3.0 G, respectively, and curves E and F are for strong jump diffusion and δ = 0.3 and 3.0 G, respectively. Curves may be approximated by $\tau_R = a(1 - S)^b$ with (A) $a = 2.57 \times 10^{-10}$ sec, $b = -1.78$; (B) $a = 5.4 \times 10^{-10}$, $b = -1.36$; (C) $a = 6.99 \times 10^{-10}$, $b = -1.20$; (D) $a = 1.10 \times 10^{-9}$, $b = -1.01$; (E) $a = 2.46 \times 10^{-9}$, $b = -0.589$; (F) $a = 2.55 \times 10^{-9}$, $b = -0.615$.

simulations. Moreover, in many experimental situations, the magnitude of the inhomogeneous line broadening may increase as the rotation slows. Some estimate of the intrinsic line width and its variation with τ_R can be obtained from line width measurements in both the motional-narrowing and rigid limits. In the studies on PADS, the intrinsic line width, for $\tau_R \lesssim 7 \times 10^{-8}$ sec, was only slightly larger than for the motional-narrowing region, and only for longer τ_R the line width increases to the rigid limit value. The effect of line width on the value of S is shown in Figure 1. For Brownian and free diffusion models, S increases with increasing line width, while for jump diffusion a decrease in S is observed. The uncertainty in estimating τ_R, due to an uncertainty in intrinsic line width, for a given value of S, increases for longer τ_R. Thus for a Brownian diffusion model, and a 1.5 G uncertainty in the intrinsic width, the uncertainty in calculating τ_R for a given value of S increases from about 5% for $\tau_R \approx 1 \times 10^{-8}$ sec, to about 50% for $\tau_R \approx 1 \times 10^{-7}$ sec to

(8) *Cf.* ref 4 and 5 for the method. Typical axial-symmetry simulation times for Brownian diffusion on an IBM 360/65 computer are $\lesssim$6 sec for $\tau_R \lesssim 3 \times 10^{-8}$ sec to 40 sec for $\tau_R \sim 3 \times 10^{-7}$ sec when a rapid diagonalization subroutine developed by Messenger and Gordon (to be published) is utilized. Asymmetric simulations are longer, *e.g.*, $\lesssim$70 sec for $\tau_R \lesssim 3 \times 10^{-8}$ sec including nonisotropic diffusion. Our nitroxide programs are available upon request.

(9) τ_R is normalized so that in the motional narrowing region, all models give the same line widths for the same value of τ_R; *cf.* ref 4.

an order of magnitude for $\tau_R \gtrsim 1 \times 10^{-6}$ sec. We find that linear interpolations along the vertical line between the curves A and B (or C and D, or E and F) give the correct results for intermediate line width values.

The curves in Figure 1 were calculated for isotropic rotational reorientation. For anisotropic diffusion, the approximation of axial symmetry for the spin parameters may no longer be valid and the anisotropic parameters must be used. For simplicity, the rotational diffusion tensor can often be assumed to be axially symmetric with its symmetry axis $z' = x$, y, or z of the molecular fixed axis.[10] Thus $R_{||}$ and $R_\perp$ are the components of the rotational diffusion tensor about the z' and the x' and y' axes, respectively. For $z' = z$ and $R_{||} > R_\perp$, *i.e.*, fast rotation about the molecular z axis, the results are relatively straightforward. This type of rotation preserves the approximate axial symmetry of the spin parameters, and the observed value of S is the value expected for isotropic diffusion and $\tau_R = (6R_\perp)^{-1}$. For relatively more rapid diffusion about the x or y axes, the results are more complicated. For small anisotropies about these axes, *i.e.*, $R_{||} \cong 3R_\perp$, the value of S is very slightly changed from the value calculated for isotropic diffusion and $\tau_{\bar{R}} = (6\bar{R})^{-1} = 1/6(R_\perp R_{||})^{1/2}$, but this corresponds to a decrease of about 8% in the apparent value of τ_R obtained from Figure 1. For larger anisotropies, a decrease in the value of S is observed (*e.g.*, for $\tau_{\bar{R}} = 3.0 \times 10^{-8}$, Brownian diffusion, and a line width = 0.3 G, S decrease from 0.931 for $R_{||}/R_\perp = 1$ to 0.897 for $R_{||}/R_\perp = 20$ or an apparent decrease in τ_R obtained from Figure 1 by a factor of 2). The magnitude of this decrease is independent of whether the x or y axis is the symmetry axis. However, in general, if the axis of rotation is unknown, or does not correspond to a molecular coordinate axis, or if the rotation is completely asymmetric, then estimates of the components of the rotational diffusion tensor can only be obtained from detailed spectral simulations.[8] Further detailed studies of other nitroxides in terms of the general theory[4,5] and the simplified method discussed here are of interest and are being pursued in part in our laboratories.

(10) This is a good approximation for $R_z' \gg R_x'$, R_y' with $R_\perp$ defined as $R_\perp = (R_x' + R_y')/2$.

The Monoisotopic Mass Spectra of Borane Derivatives[1]

by Eileen McLaughlin and R. W. Rozett*

Chemistry Department, Fordham University, New York, New York 10458 *(Received November 2, 1971)*

Publication costs assisted by the Petroleum Research Fund

The monoisotopic mass spectra of borane derivatives are calculated by a least-squares computer technique from polyisotopic information. Alkyl boranes, carboranes, and borane derivatives containing bromine, chlorine, sulfur, nitrogen, oxygen, deuterium, many metals and any monoisotopic element can be handled. Elemental formulas for ions can be established. As examples we investigate the following borane derivatives: $B_{10}H_8N_4$, $C_2B_4H_8$, $CH_3CB_5H_8$, $(CH_3)_2C_2B_6H_6$, $(CH_3)_2C_2B_7H_7$, and $(CH_3)_2C_2B_8H_8$. Finally the sources of error in the procedure are discussed.

Introduction

The mass spectra of borane derivatives which contain elements with a significant fraction of a second or third isotope are even more complex than the polyisotopic mass spectra of the boranes, B_nH_m. For example, in the mass spectrum of decaborane-14, in the mass region of ten boron ions, 165 isotopic variants occur if one takes into account only the boron isotope combinations. If in addition the deuterium variants are counted, 1254 ions could be found. The small natural abundance of deuterium makes the hydrogen case trivial, but the same cannot be said for the presence of ^{13}C in alkyl boranes and carboranes, or for ^{37}Cl and ^{81}Br in haloboranes (see Table IX).

If the mass spectrum is taken to study kinetic or mechanistic details of reactions, the complicated polyisotopic data may be looked upon as a mask hiding monoisotopic information. But from another point of view, the isotopic variation contains additional information which may be used to identify the ions present

(1) This research was supported in part by the Petroleum Research Fund administered by the American Chemical Society (PRF 1233-G2). The instrumentation was supplied in part by the National Science Foundation (GP 8220) and by the New York State Science and Technology Foundation (NYSSF (6)-13).

Table I: Isotopic Variants of $C_2B_2^+$

Mass	$^{12}C_k{}^{13}C_l{}^{10}B_n{}^{11}B_m$ k	l	n	m	$r(k,l)$	$r(n,m)$	$r(k,l;n,m)$	r_{ij}
44	2	0	2	0	1.0000	5.9505×10^{-2}	5.9505×10^{-2}	5.9505×10^{-2}
45	2	0	1	1	1.0000	4.8787×10^{-1}	4.8787×10^{-1}	
45	1	1	2	0	2.2449×10^{-2}	5.9505×10^{-2}	1.3358×10^{-3}	4.8921×10^{-1}
46	2	0	0	2	1.0000	1.0000	1.0000	
46	1	1	1	1	2.2449×10^{-2}	4.8787×10^{-1}	1.0952×10^{-2}	1.0110
46	0	2	2	0	1.2599×10^{-4}	5.9505×10^{-2}	7.4970×10^{-6}	
47	1	1	0	2	2.2449×10^{-2}	1.0000	2.2449×10^{-2}	
47	0	2	1	1	1.2599×10^{-4}	4.8787×10^{-1}	6.1467×10^{-5}	2.2511×10^{-2}
48	0	2	0	2	1.2599×10^{-4}	1.0000	1.2599×10^{-4}	1.2599×10^{-4}

in the spectrum. It is hardly novel to use the characteristic cluster of intensities due to isotopic variants to determine the elemental composition of ions.[2] However, the technique is especially useful in the boranes because of the significant percentage of ^{10}B (20%). Ditter, Gerhart, and Williams showed how the formulas of carboranes could be inferred from their characteristic isotopic patterns.[3] Their technique used successive approximations and was a tribute to their persistence. In this paper we report a computer method which automatically and exactly determines the elemental composition of borane ions and the ions of borane derivatives from their polyisotopic mass spectra. The computer program (Table II) calculates the exact isotopic cluster for boron and another element with a pair of isotopes and provides a least-squares-fitted monoisotopic spectrum. While calculating the monoisotopic spectrum a quantitative measure of the fit of the result is generated. Using this, one may choose between alternate elemental compositions for all the ions in the spectrum. In this respect the procedure represents a substitute for the high-resolution mass spectroscopy of the carboranes.[4]

After discussing the theory of the clusters of intensities due to several elements with isotopic variants, we illustrate the technique with $B_{10}H_8N_4$ and some alkyl boranes and carboranes. Other borane derivatives which may be handled in this fashion are also discussed. Finally, the sources of error in the procedure and its limitations are detailed.

Method

The procedure for calculating the monoisotopic mass spectra of molecules containing several elements, each with a pair of isotopes, can be formulated as follows. The measured intensity at any mass, P_i, is the sum of the abundances, p_{ij}, due to the different formulas which have one or more isotopic variants at that mass. These in turn may be expressed in terms of the intensity of the monoisotopic ion with the same formula, m_j, as in

$$P_i = \sum_j p_{ij} = \sum_j r_{ij} m_j \qquad (1)$$

To calculate a monoisotopic mass spectrum one must first evaluate the coefficients, r_{ij}, from statistical considerations. Then the simultaneous linear equations described by (1), one equation for each experimental intensity, must be solved for the m_j.

The r_{ij} may be calculated from the following eq 2–6.[5] The procedure is illustrated for the formula $C_2B_2^+$ in Table I. We assume that the ion under discussion has n atoms of one isotope of an element and m atoms of the second isotope. The fractional abundance of the ion, $a(n,m)$, is a function of the gross abundance of the first isotope, f_1, and of the second isotope, f_2

$$a(n,m) = w(n,m) f_1^n f_2^m \qquad (2)$$

The statistical weight factor, $w(n,m)$, is a binomial coefficient. It expresses the number of ways of arranging n things of one kind and m things of another kind without regard to order

$$w(n,m) = (n + m)!/n!m! \qquad (3)$$

The relative abundance of the ion, $r(n,m)$, is the ratio of the fractional abundance of the ion to the abundance of the pure isotopic variant of the same formula

$$r(n,m) = a(n,m)/a(0,n + m) \qquad (4)$$

For example, in Table I the abundance of $^{10}B_2^+$ relative to $^{11}B_2^+$ is listed under $r(n,m)$ as 5.9505×10^{-2}. This number was calculated by inserting n, *i.e.*, 2, the number of atoms of the lighter isotope, m, *i.e.*, 0, the number of atoms of the heavier isotope, and the natural abundance of the boron isotopes into eq 2, 3, and 4.

Let us now suppose that the ion in question contains two elements, each with a pair of isotopes and that there are n and m atoms of the isotopes of the first element, and k and l atoms of the two isotopes of the second element, respectively. The abundance of the

(2) J. H. Beynon, "Mass Spectrometry and Its Applications to Organic Chemistry," Elsevier, Amsterdam, 1960, p 305.

(3) J. F. Ditter, F. J. Gerhart, and R. E. Williams, *Advan. Chem. Ser.*, **No. 72**, 191 (1968).

(4) R. L. Middaugh, M. T. Brady, and W. L. Budde, Midwest Regional Meeting of the American Chemical Society, St. Louis, Mo., Oct 1971.

(5) B. Parl, "Basic Statistics," Part III, Doubleday, New York, N. Y., 1967.

Table II

```
C      MONOISOTOPIC BORANE MASS SPECTRA                                    MICS   1
C      BORON-CARBON-HYDROGEN MASS SPECTRA                                  MICS   2
C                                                                          MICS   3
C      R W ROZETT              CHEMISTRY DEPARTMENT      5/71              MICS   4
C      FORDHAM UNIVERSITY      BRONX,N.Y. 10458                            MICS   5
C                                                                          MICS   6
       DIMENSION  A (1000),PK(250),POLMAS(125),PKSUM(125),NAME(10),        MICS   7
      1 AUX(200),IPIV(100),IB(100),IH(100),IC(100),IX(100),ONEMAS(100),    MICS   8
      2PKONE(100)                                                          MICS   9
       DATA IDNO/0/              ,EPS/1.0E-07/,FRCTB1/.8039/,FRCTB0/.1961/MICS  10
       DATA MAX1/1000/,MAX2/250/,MAX3/125/ ,MAX4/100/                      MICS  11
C                                                                          MICS  12
C      ALTERNATE ISOTOPES OF B10/B11 DERIVATIVES                           MICS  13
C         H          H/D        C12/C13    BR79/81    CL35/37    N14/N15   MICS  14
C         O16/O18    S32/S34                                              MICS  15
C                                                                          MICS  16
C      FRACTIONAL ABUNDANCE AND MASSES OF OTHER ELEMENTS                   MICS  17
C      DATA FRCTC2/0.0000/,FRCTC3/1.0000/,MASC13/00/,IDIF/1/               MICS  18
C      DATA FRCTC2/.99985/,FRCTC3/.00015/,MASC13/02/,IDIF/1/               MICS  19
       DATA FRCTC2/0.9889/,FRCTC3/0.0111/,MASC13/13/,IDIF/1/               MICS  20
C      DATA FRCTC2/0.5054/,FRCTC3/0.4946/,MASC13/81/,IDIF/2/               MICS  21
C      DATA FRCTC2/0.7553/,FRCTC3/0.2447/,MASC13/37/,IDIF/2/               MICS  22
C      DATA FRCTC2/0.9963/,FRCTC3/0.0037/,MASC13/15/,IDIF/1/               MICS  23
C      DATA FRCTC2/.99759/,FRCTC3/.00204/,MASC13/18/,IDIF/2/               MICS  24
C      DATA FRCTC2/0.9500/,FRCTC3/0.0422/,MASC13/34/,IDIF/2/               MICS  25
C                                                                          MICS  26
C      TITLE CARD MIN/MAX MASS IN POLY SPECTRA,MIN/MAX NO OF BORONS,       MICS  27
C      HYDROGENS AND OTHER ELEMENTS                                        MICS  28
  114 READ(1,4,END=99)ICODE,MASSMN,MASSMX,NAME,NUMBMX,NUMHMX,NUMCMX,NUMBMICS  29
     1MN,NUMHMN,NUMCMN                                                     MICS  30
    4 FORMAT(3I5,10A4,6I2,5X,4I2)                                          MICS  31
   95 NUMPOL=MASSMX-MASSMN+1                                               MICS  32
   20 ADD=0.0                                                              MICS  33
       ICOL=0                                                              MICS  34
       MAXROW=NUMPOL                                                       MICS  35
   11 DO 79 I=1,MAX1                                                       MICS  36
       A(I)=0.0                                                            MICS  37
   79 CONTINUE                                                             MICS  38
       DO 33 I=1,MAX4                                                      MICS  39
       ONEMAS(I)= 0.                                                       MICS  40
       PKONE(I)=0.                                                         MICS  41
       PKSUM(I)=0.                                                         MICS  42
   33 CONTINUE                                                             MICS  43
       DO 32 I=1,MAX2                                                      MICS  44
       PK(I)=0.0                                                           MICS  45
   32 CONTINUE                                                             MICS  46
C                                                                          MICS  47
C      DATA INPUT                                                          MICS  48
C      INTRODUCE THE INTENSITIES FROM LOW MASS TO HIGH                     MICS  49
   98 READ(1,3)(PKSUM(I),I=1,NUMPOL)                                       MICS  50

    2 FORMAT(16I5)                                                         MICS  51
    3 FORMAT (12F6.2)                                                      MICS  52
C                                                                          MICS  53
C      INTRODUCE THE FORMULAS FROM LOW MASS TO HIGH MASS.                  MICS  54
C      BLANK CARD AFTER LAST FORMULA                                       MICS  55
C      NUMX IS THE MASS APART FROM C,H,B                                   MICS  56
  651 READ(1,2,END=99)NUMB,NUMH,NUMC,NUMX                                  MICS  57
       IF(NUMB+NUMH+NUMC+NUMX.EQ.0) GO TO 655                              MICS  58
  652 MASS2=NUMB*11+ NUMH+NUMC*MASC13+NUMX                                 MICS  59
       IF(MASS2.LT.MASSMN) GO TO 651                                       MICS  60
       MASS1=MASS2-NUMB-NUMC*IDIF                                          MICS  61
```

Table II (*Continued*)

```
      ICOL=ICOL+1                                                          MICS  62
      ONEMAS(ICOL)=MASS2-NUMC*IDIF                                         MICS  63
      IB(ICOL)=NUMB                                                        MICS  64
      IH(ICOL)=NUMH                                                        MICS  65
      IC(ICOL)=NUMC                                                        MICS  66
      IX(ICOL)=NUMX                                                        MICS  67
      NUMBX=NUMB+1                                                         MICS  68
      NU =MASS1-MASSMN+(ICOL-1)*MAXROW                                     MICS  69
      NUMCX=NUMC+1                                                         MICS  70
      IF(MASS1.GE.MASSMN)GO TO 660                                         MICS  71
      IB(ICOL)=999                                                         MICS  72
C                                                                          MICS  73
C     COEFFICIENT MATRIX OF SIMULTANEOUS EQNS                              MICS  74
  660 DO 654 NUMB11=1,NUMBX                                                MICS  75
      NUM=NU+NUMB11                                                        MICS  76
      BABUN=RLABUN(NUMB,NUMB11,FRCTB1,FRCTB0)                              MICS  77
      DO 659 NUMC13=1,NUMCX                                                MICS  78
      NUMC12=NUMC-NUMC13+2                                                 MICS  79
      IF(IB(ICOL).NE.999)GO TO 657                                         MICS  80
      MAS=MASS1+NUMC13*IDIF+NUMB11-IDIF-1                                  MICS  81
      IF(MAS.LT.MASSMN) GO TO 658                                          MICS  82
  657 A(NUM)=A(NUM)+RLABUN(NUMC,NUMC12,FRCTC2,FRCTC3)*BABUN                MICS  83
  658 NUM=NUM+IDIF                                                         MICS  84
  659 CONTINUE                                                             MICS  85
  654 CONTINUE                                                             MICS  86
      GO TO 651                                                            MICS  87
  655 MAXCOL=ICOL                                                          MICS  88
C                                                                          MICS  89
      DO 78  I= 1, NUMPOL                                                  MICS  90
      POLMAS(I)=MASSMN+ADD                                                 MICS  91
      ADD=ADD+1.                                                           MICS  92
   78 CONTINUE                                                             MICS  93
      N=NUMPOL+1                                                           MICS  94
      DO 200 I=N,MAX3                                                      MICS  95
      POLMAS(I)=0.                                                         MICS  96
  200 CONTINUE                                                             MICS  97
C                                                                          MICS  98
C     DATA PRINTOUT                                                        MICS  99
      WRITE(3,34)NUMBMX,NUMHMX,NUMCMX,FRCTB1,NUMBMN,NUMHMN,      NUMCMNMICS 100

     1,FRCTC2,NAME                                                         MICS 101
   34 FORMAT('1',T20,'MONOISOTOPIC MASS SPECTRA OF BORANES & DERIVATIVESMICS 102
     1'///'     FROM BORANE      B',I2,'H',I2,'C',I2,10X,'FRACTION B11= MICS 103
     2',F6.4/'      TO BORANE        B',I2,'H',I2,'C',I2,10X,'FRACTION C1MICS 104
     32= ',F6.4,15X,10A4//)                                              MICS 105
      WRITE (3, 780)   MAXROW, MAXCOL                                    MICS 106
  780 FORMAT ('0',T20,' MAXROW=',I5,          MAXCOL=',I5)               MICS 107
      WRITE(3,981)                                                       MICS 108
      WRITE(3,980)(POLMAS(I),PKSUM(I),I=1,MAXROW)                        MICS 109
  980 FORMAT(4(5X,F10.1,F10.4))                                          MICS 110
  981 FORMAT('0   EXPERIMENTAL INTENSITIES AND MASSES      '//)         MICS 111
C                                                                        MICS 112
C     LEAST SQ SOLUTION OF SIMULTANEOUS EQNS  (IBM SSP)                  MICS 113
      CALL  LLSQ(A  , PKSUM, MAXROW, MAXCOL, 1,PKONE,   IPIV, EPS, IER, MICS 114
     1 AUX)                                                              MICS 115
C                                                                        MICS 116
C     FRACTION OF SUM OF PEAKS AND BASE RELATIVE INTENSITY               MICS 117
      SUMONE= 0.                                                         MICS 118
      ONEMAX= PKONE(1)                                                   MICS 119
      DO 39 I=1,MAXCOL                                                   MICS 120
      IF(PKONE(I))39,39,40                                               MICS 121
   40 SUMONE= SUMONE + PKONE(I)                                          MICS 122
      IF (PKONE(I)  - ONEMAX)  39, 39, 38                                MICS 123
```

Table II (*Continued*)

```
     38 ONEMAX=  PKONE(I)                                                    MICS 124
     39 CONTINUE                                                             MICS 125
        ONEMAX= 100./ONEMAX                                                  MICS 126
        SUMONE= 100./SUMONE                                                  MICS 127
C                                                                            MICS 128
C       SOLUTION PRINTOUT                                                    MICS 129
        WRITE(3,35)                                                          MICS 130
        SUMNEG=0.0                                                           MICS 131
        DO 37 I=1,MAXCOL                                                     MICS 132
        CLAST=  PKONE(I)*SUMONE                                              MICS 133
        IF( CLAST   )115,116,116                                             MICS 134
    115 SUMNEG=SUMNEG+CLAST                                                  MICS 135
    116 CONTINUE                                                             MICS 136
        REL=  PKONE(I)*ONEMAX                                                MICS 137
        J=ONEMAS(I)                                                          MICS 138
        PK(J)=REL                                                            MICS 139
        IF(REL.LE.0.0) PK(J)=0.0                                             MICS 140
        WRITE(3,36) I,ONEMAS(I),PKONE(I),REL,CLAST,IB(I),IH(I),IC(I),IX(I)MICS 141
     36 FORMAT(I10,2F15.3,10X,2F15.3,10X,4I5)                                MICS 142
     37 CONTINUE                                                             MICS 143
     35 FORMAT('0  PEAK NO.        B11 MASS          B11 INTENSITY          MICS 144
       2  REL              FRCT                B     H     C     X     '//)  MICS 145
        B=MAXROW                                                             MICS 146
        AUX(1)= SQRT(AUX(1)/B)                                               MICS 147
        WRITE(3,117)IER,AUX(1),SUMNEG                                        MICS 148
    117 FORMAT('0     IER=  ',I5, '  LST SQ RMS =   '.E15.7,'      NEGATIVMICS 149
       1ES=   ',F16.5)                                                       MICS 150


        IF(IDNO.EQ.0) GO TO 114                                              MICS 151
        L=ONEMAS(1)                                                          MICS 152
        LL=ONEMAS(MAXCOL)                                                    MICS 153
        WRITE(2,3) (PK(I),I=L,LL)                                            MICS 154
        GO TO 114                                                            MICS 155
     99 CALL EXIT                                                            MICS 156
        END                                                                  MICS 157
C                                                                            MICS 158
        FUNCTION RLABUN(N,K,FRCTK1,FRCTK2)                                   MICS 159
        REAL*8 FRCTK,FRCTL,UNUM,DNOM1,DNOM2,W                                MICS 160
C       CALCULATES RELATIVE ABUNDANCES OF MIXED ISOTOPE MOLECULES            MICS 161
        IF(N.NE.0)GO TO 68                                                   MICS 162
        RLABUN=1.0                                                           MICS 163
        RETURN                                                               MICS 164
     68 FRCTK=FRCTK1                                                         MICS 165
        FRCTL=FRCTK2                                                         MICS 166
        UNUM=1.0D 00                                                         MICS 167
        DNOM1=1.0D 00                                                        MICS 168
        DNOM2=1.0D 00                                                        MICS 169
        KK=K-1                                                               MICS 170
        IF (KK)60,60,61                                                      MICS 171
     61 DO 62 I=1,KK                                                         MICS 172
     62 DNOM1=DNOM1*DFLOAT(I)                                                MICS 173
     60 KKK=N-K+1                                                            MICS 174
        IF (KKK)63,63,64                                                     MICS 175
     64 DO 65 I=1,KKK                                                        MICS 176
     65 DNOM2=DNOM2*DFLOAT(I)                                                MICS 177
     63 DO 66 I=1,N                                                          MICS 178
     66 UNUM=UNUM*DFLOAT(I)                                                  MICS 179
     67 W=UNUM/(DNOM1*DNOM2)                                                 MICS 180
        RLABUN=W*FRCTL**(N-K+2)/FRCTL*FRCTK**K/(FRCTK**(N+1))                MICS 181
        IF(RLABUN.LT.1.0D-12)RLABUN=1.0D-12                                  MICS 182
        RETURN                                                               MICS 183
        END                                                                  MICS 184
```

ion relative to that of the pure isotopic ion is the product of the separate relative abundances for each element. The probability of the occurrence of the isotopic variation in element 1 is independent of the isotopic arrangement in element 2

$$r(n,m;k,l) = r(n,m)r(k,l) \quad (5)$$

For example, in Table I the relative abundance of $^{12}C^{13}C^{10}B_2^+$, $r(1,1;2,0)$, is listed as 1.3358×10^{-3}. It is the product of the abundance of $^{12}C^{13}C$ relative to $^{12}C_2$, 2.2449×10^{-2}, and the abundance of $^{10}B_2$ relative to $^{11}B_2$, 5.9505×10^{-2}.

If two or more ions with the same formula but with different numbers of each isotope (n',m',k',l') occur at the same mass, the abundance of the ions in question relative to the pure isotopic ion is the sum of the separate relative abundances. The two probabilities are mutually exclusive

$$r(n,m;k,l;n',m';k',l') = r(n,m;k,l) + r(n',m';k',l') \quad (6)$$

In Table I for instance two isotopic variants of the formula $C_2B_2^+$ occur at mass 45, $^{12}C_2{}^{10}B^{11}B^+$, and $^{12}C^{13}C^{10}B_2^+$. Their relative abundances are 4.8787×10^{-1} and 1.3358×10^{-3}, respectively. The relative abundance of all isotopic variants of formula $C_2B_2^+$ which occur at mass 45 is the sum of these abundances, or 4.8921×10^{-1}. With these formulas all the coefficients r_{ij} may be calculated. The i index specifies the mass of the isotopic variant; the j indicates a specific elemental formula.

Finally one must solve the simultaneous equations (one for each experimental intensity) for the monoisotopic intensities (one for each monoisotopic formula). A least-squares technique which avoids the pitfalls of the usual procedure for calculating monoisotopic mass spectra has been described in recent compilation of the monoisotopic mass spectra of the boranes.[6] The program of Table II, MICS, is a generalization of the program published previously, MIBS, and replaces it.

Examples

Tables III to VIII contain the results for six compounds derived by the MICS program from published polyisotopic mass spectra. In Table III, for example, the formulas and monoisotopic intensities for $B_{10}H_8N_4$ are given.[7] These were derived in the following way. The published polyisotopic mass spectrum, the natural abundance of the boron and nitrogen isotopes, and a chemically reasonable set of formulas were fed into MICS. The program calculates a least-squares-fit set of monoisotopic intensities and provides the root-mean-square deviation of the derived monoisotopic intensities from the original data. Should negative intensities result, the solution is easily restricted to positive monoisotopic intensities by removing the formula of the offensive peak and resolving for the intensities.

Table III: $B_{10}H_8N_4$

Mass	Formula	Intensity
105	$B_9H_6^+$	1.4
106	$B_9H_7^+$	2.9
107	$B_9H_8^+$	2.1
110	B_{10}^+	42.3
111	$B_{10}H^+$	17.4
112	$B_{10}H_2^+$	48.1
113	$B_{10}H_3^+$	7.0
114	$B_{10}H_4^+$	40.6
115	$B_{10}H_5^+$	15.5
116	$B_{10}H_6^+$	100.0
117	$B_{10}H_7^+$	9.1
118	$B_{10}H_8^+$	99.4
145	$B_{10}H_7N_2^+$	6.2
146	$B_{10}H_8N_2^+$	80.9
173	$B_{10}H_7N_4^+$	4.5
174	$B_{10}H_8N_4^+$	69.5
	RMD	0.21

Table IV: $C_2B_4H_8$

Mass	Formula	Intensity
69	$C_2B_4H^+$	20.5
70	$C_2B_4H_2^+$	9.4
71	$C_2B_4H_3^+$	20.3
72	$C_2B_4H_4^+$	8.8
73	$C_2B_4H_5^+$	100.0
74	$C_2B_4H_6^+$	70.4
75	$C_2B_4H_7^+$	2.2
76	$C_2B_4H_8^+$	57.7
	RMD	0.49

Table V: $CH_3CB_5H_8$

Mass	Formula	Intensity
79	$C_2B_5^+$	5.9
80	$C_2B_5H^+$	1.0
81	$C_2B_5H_2^+$	14.1
83	$C_2B_5H_4^+$	9.3
84	$C_2B_5H_5^+$	26.0
85	$C_2B_5H_6^+$	15.9
86	$C_2B_5H_7^+$	65.4
87	$C_2B_5H_8^+$	61.9
88	$C_2B_5H_9^+$	87.4
89	$C_2B_5H_{10}^+$	8.4
90	$C_2B_5H_{11}^+$	100.0
	RMD	0.30

Other reasonable sets of formulas were then run, and the set with the lowest root-mean-square deviation is reported in Table III. A natural abundance of 19.61% was used for ^{10}B and 0.37% for ^{15}N. Either of these figures could cede to new evidence. For boron es-

(6) E. McLaughlin, T. E. Ong, and R. W. Rozett, *J. Phys. Chem.*, 75, 3106 (1971).

(7) R. L. Middaugh, *Inorg. Chem.*, 7, 1011 (1968).

Table VI: $(CH_3)_2C_2B_6H_6$

Mass	Formula	Intensity
117	$C_4B_6H_3^+$	10.0
118	$C_4B_6H_4^+$	6.4
119	$C_4B_6H_5^+$	9.6
120	$C_4B_6H_6^+$	8.4
121	$C_4B_6H_7^+$	8.0
122	$C_4B_6H_8^+$	8.3
123	$C_4B_6H_9^+$	13.7
124	$C_4B_6H_{10}^+$	25.3
125	$C_4B_6H_{11}^+$	8.7
126	$C_4B_6H_{12}^+$	100.0
	RMD	0.78

Table VII: $(CH_3)_2C_2B_7H_7$

Mass	Formula	Intensity
128	$C_4B_7H_3^+$	0.0
129	$C_4B_7H_4^+$	2.3
130	$C_4B_7H_5^+$	1.8
131	$C_4B_7H_6^+$	7.8
132	$C_4B_7H_7^+$	0.0
133	$C_4B_7H_8^+$	15.7
134	$C_4B_7H_9^+$	13.9
135	$C_4B_7H_{10}^+$	19.0
136	$C_4B_7H_{11}^+$	18.8
137	$C_4B_7H_{12}^+$	1.7
138	$C_4B_7H_{13}^+$	100.0
	RMD	0.85

Table VIII: $(CH_3)_2C_2B_8H_8$

Mass	Formula	Intensity
140	$C_4B_8H_4^+$	1.9
142	$C_4B_8H_6^+$	6.7
143	$C_4B_8H_7^+$	3.8
144	$C_4B_8H_8^+$	2.9
145	$C_4B_8H_9^+$	13.8
147	$C_4B_8H_{11}^+$	26.5
148	$C_4B_8H_{12}^+$	43.7
149	$C_4B_8H_{13}^+$	15.2
150	$C_4B_8H_{14}^+$	100.0
	RMD	0.94

pecially, variable natural abundances have been observed and isotope enrichment may occur during chemical processing.[7]

The other carboranes and alkyl carboranes studied were processed in the same fashion.[3] They include $C_2B_4H_8$ (Table IV), $CH_3CB_5H_8$ (Table V), $(CH_3)_2C_2B_6H_6$ (Table VI), $(CH_3)_2C_2B_7H_7$ (Table VII), and $(CH_3)_2C_2B_8H_8$ (Table VIII). The results must be used with the caution that the polyisotopic spectra were published as line drawings. More accurate monoisotopic spectra could be derived from digital data.

Other Derivatives of the Boranes

Table IX lists the more common polyisotopic elements which can be handled by the MICS program in addition to boron. As we note, only two isotopes of the elements are permitted, so sulfur and oxygen derivatives of the boranes are handled by neglecting ^{17}O, ^{33}S, and ^{36}S. These isotopes are present in such small abundance that the approximation is excellent. Any one of the following metals may replace any one of the elements in Table VIII: Cu, Ga, Rb, Ag, Sb, Eu, Lu, Re, or Ir. The common factor is the presence of a pair of isotopes (or a close approximation), with the lower isotope in sufficient abundance. The program solves for the monoisotopic abundance of the lighter isotope.

Table IX: Fractional Abundances in Borane Derivatives

^{79}Br	0.5054	^{81}Br	0.4946
^{35}Cl	0.7553	^{37}Cl	0.2447
^{32}S	0.950	^{34}S	0.0422[a]
^{12}C	0.9889	^{13}C	0.0111
^{14}N	0.9963	^{15}N	0.0037
^{16}O	0.99759	^{18}O	0.00204[b]
^{1}H	0.99985	^{2}H	0.00015

[a] We must neglect ^{33}S (0.0076) and ^{36}S (0.00014). [b] Omitting ^{17}O (0.00037).

If $B_xP_yM_z$ represents the formulas of compounds which can be handled, then P stands for any one of the polyisotopic elements previously mentioned, while M stands for any combination of the following (at least approximately) monoisotopic elements: H, F, I, P, Be, Al, As, He, Na, Cs, Co, Au, Bi, Sc, Y, Nb, Rh, La, Tb, Ho, Tm, and Ta. In addition ions such as $C_nH_m^+$ in carboranes and HCl^+, or Br^+ in haloboranes, are permitted. Any combination of x, y, or z may be zero in the formula above. This feature is especially helpful for removing background peaks such as H_2O^+ or N_2^+.

Some special note should be taken of the deuterium derivatives of the boranes. The naturally occurring deuterium content of the boranes may be taken into account explicitly and exactly. The effect is usually undetectable, but it becomes more important as the number of hydrogen atoms in the ion increases. In $B_{20}H_{26}$, for example, the first isotopic peak has a relative size of 0.00015×26 or 0.0039.[8] Since the largest possible peak is 100, the largest contribution possible is 0.39. Hydrogen, consequently, can be treated as a monoisotopic element. Deliberately deuterated boranes can be treated exactly if the deuteration is random and not site-selective. The statistics used to calculate the coefficients of eq 1 assume random occupation of the combinations. Even here the deuterated

(8) F. W. McLafferty, "Interpretation of Mass Spectra," W. A. Benjamin, New York, N. Y., 1967, p 210.

borane could be accommodated by treating the site-selective deuterium as a monoisotopic element in the ions in which it occurs.

Error Analysis

Several limitations on the use of the technique have been noted above or previously published. It was said, for example, that the mass spectrum of $B_{20}H_{26}$ could not be resolved into a monoisotopic spectrum.[6] This was rather hastily attributed to the presence of impurities, though the spectra of other boranes could be resolved despite the presence of nonboron peaks. To study the problem we calculated an arbitrary but exact polyisotopic spectrum for $B_{20}H_{26}$ and proceeded to find the cause of our previous failure. The neglect of the natural abundance of deuterium was found to be unimportant. The presence of perturbed intensities was no more troublesome than in other molecules. It was noted, however, that the contribution of any one formula to a measured intensity is quite small since each ion containing 20 boron atoms will be spread over 21 separate masses. In fact, rounding errors are of the same order of magnitude as the contribution of the monoisotopic formula to the measured intensity. With the idea that it would be more sensitive to solve for the most abundant ion rather than for the pure isotope, we wrote a program which solved for intensity of the 17 times more abundant $^{11}B_{16}{}^{10}B_4$ rather than for $^{11}B_{20}$. This proved to be no improvement. The procedure merely multiplies the coefficients in (1) by a constant, with no effect on the results. Finally, it was discovered that the number of significant figures in the polyisotopic data was the controlling factor. If four significant figures after the decimal are used, good intensities and no negatives are generated. With three places, tolerably accurate intensities are produced. With two places about 1% of the sum of the intensities are negative. One place produces 12% negatives and completely meaningless intensities in the monoisotopic spectrum. Since our previous data had been read from a graph to the nearest integer, the failure to produce an acceptible monoisotopic spectrum from the experimental information is not surprising.[9] The conclusion we must draw is that the monoisotopic mass spectra from boranes with higher molecular weights can only be generated from increasingly more precise polyisotopic intensities.

Finally one might mention some limitations. First of all, not all polyisotopic mass spectra can be resolved into monoisotopic intensities by any method. Whenever there are more monoisotopic peaks to be established than there are polyisotopic measurements to determine them, the problem is mathematically insoluble. For example if BD_3^+, CD_2^+, and ND^+ are present simultaneously, all isotopic variants will occur at masses 16 and 17. Measurements at these two masses are insufficient to determine the three monoisotopic intensities. For the sake of argument we have assumed that the mass spectrum is a low resolution measurement, and no ^1H is present. Secondly, some polyisotopic mass spectra cannot be resolved into monoisotopic spectra even though in theory they fulfill the mathematical criterion mentioned above. If a sufficient number of polyisotopic peaks do not extend above the detection threshold of the mass spectrometer in question, then the experimenter as a matter of fact is unable to resolve the spectrum with the data available. A third limitation occurs when we attempt to resolve the mass spectrum of two similar complex ions. Each ion determines a column of coefficients in the set of simultaneous equations described by (1). If these columns are quite similar, the two columns of the matrix of coefficients are not mathematically independent, and the least-squares matrix method cannot be carried out. This is particularly true if both monoisotopic formulas occur at the same mass. If $B_5H_{11}^+$ and B_6^+, both at mass 66, are part of a spectrum, their similar coefficients prevent simultaneous solution; one or the other must be chosen. For simpler ions this limitation is not important.

(9) L. H. Hall and W. S. Koski, *J. Amer. Chem. Soc.*, **84**, 4205 (1962).

Efficiency of the Electrochemiluminescent Process

by P. M. Schwartz, R. A. Blakeley, and B. B. Robinson*

RCA Laboratories, Princeton, New Jersey 08540 *(Received November 11, 1971)*

Publication costs assisted by RCA Laboratories

A steady-state analysis is presented for electrochemiluminescence produced by a periodic driving voltage. The light emission efficiency is calculated and the results are compared with measurements made on a system of rubrene–tetra-*n*-butylammonium perchlorate–benzonitrile. The theory indicates that the losses inherent in cyclic operation should only limit the quantum efficiency to 82.8% if singlet excited states are created directly and 41.4% if they are created by triplet annihilation. The measured differential quantum efficiency is 8.7%. The observation that the average rubrene molecule emits many photons before it is destroyed indicates that the spurious reactions which limit cell life should not limit cell efficiency. Since the singlet fluorescence of rubrene is very efficient and the triplet states are highly vulnerable to quenching reactions, it is concluded that triplet reactions play a dominant role in the cell process. The observed efficiency is quite competitive with those observed in electroluminescent diodes and indicates that ecl systems would make useful devices if cell lifetimes can be extended.

Introduction

The phenomenon of electrochemiluminescence (ecl) has been studied experimentally and theoretically by a number of workers.[1] Only a small part of this work has been devoted to the efficiency of the ecl process. In addition, all the theoretical analysis has been pertinent to the controlled-double-potential-step experiment. The quantum efficiency of the ecl cell provides a valuable clue to the basic processes involved and is a parameter of central interest to any consideration of the display device potential of ecl. In this paper we present a theoretical analysis of the ecl process for the case of cyclic boundary conditions assuming rapid recombination. These boundary conditions are not only easier to achieve experimentally but also the conditions of greatest interest for continuous operation device applications. We also present the results of efficiency measurements on the rubrene–tetra-*n*-butylammonium perchlorate (TBAP)–benzonitrile (BN) system. The measured efficiencies, 8.7%, compare favorably with those of electroluminescent diodes for device applications, indicating that ecl systems have excellent device potential if cell lifetimes can be extended. Comparison of the measurements with the theory indicates that the results are consistent with the conclusion, based on other evidence, of Chang, Hercules, and Roe[2] that most of the excited molecules which take part in the recombination are in triplet states which are quite susceptible to quenching processes.

Theory

The ecl process has often been described by the following condensed set of reactions.[2]

$$A + e^- \longrightarrow A^- \quad (1)$$

$$A \longrightarrow A^+ + e^- \quad (2)$$

$$A^- \longrightarrow A^+ + 2e^- \quad (3)$$

$$A^+ + 2e^- \longrightarrow A^- \quad (4)$$

$$A^+ + A^- \longrightarrow A^* + A \quad (5)$$

$$nA^* \longrightarrow nA + h\nu \quad (6)$$

$$A^* + Q \longrightarrow A + Q' \quad (7)$$

Here, A represents a molecule of the active species, A* represents an excited state of that species, $h\nu$ represents a photon, and Q represents some excited state quencher.

We consider a one-dimensional system (see Figure 1) governed by the above reactions and bounded at the origin by an electrode. If we let A, A^+, and A^- stand for the concentrations of those species, then the behavior of the system is described by the equations

$$\frac{\partial A}{\partial t} + \frac{\partial}{\partial x}(Av_A) = 2RA^+A^- \quad (8)$$

$$\frac{\partial A^{+,-}}{\partial t} + \frac{\partial}{\partial x}(A^{+,-}v_{A^{+,-}}) = -RA^+A^- \quad (9)$$

where v_A, v_{A^+}, and v_{A^-} are the respective average velocities and R is the anion–cation recombination coefficient; the equations of momentum transfer

$$\frac{\partial va}{\partial t} + va\frac{va}{\partial x} - \frac{qa}{m}E + \frac{va}{\tau} + \frac{kT}{am}\frac{\partial a}{\partial x} = 0 \quad (10)$$

where $a = A$, A^+, or A^-; and Poisson's equation. The first term of the momentum equation is negligible at the low frequencies of interest. The electric fields in the ecl solution are sufficiently small to make the third term smaller than the last (diffusion-dominated flow). The second term is of order v_a^2/l, where l is the scaling length

(1) A comprehensive list of references is available in A. Zweig, *Advan. Photochem.*, **6**, 425 (1968).

(2) J. Chang, D. M. Hercules, and D. K. Roe, *Electrochim. Acta*, **13**, 1197 (1968).

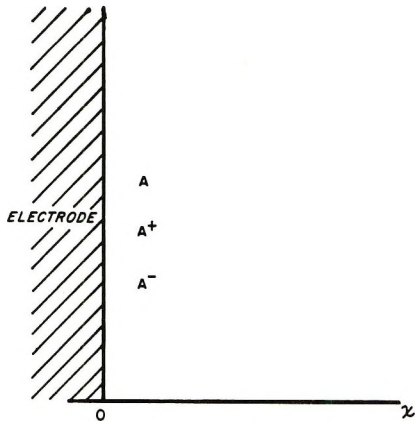

Figure 1. One-dimensional model of an ecl cell with neutral, anion, and cation of fluorescent molecule A in solution.

for the gradients in the system. This is negligible compared to the last term, which is of order v_{thermal}^2/l. We can, therefore, rewrite the momentum transfer equation as

$$va = -(D/a)(\partial a/\partial x) \tag{11}$$

$$a = A,\ A^+,\ \text{or}\ A^-$$

$$D = (kT/m)\tau$$

where D is the diffusion coefficient of molecule A, k is Boltzmann's constant, T is the temperature, m is the molecular mass, and τ is the collision time of the molecule in solution. Equation 11 can be used to convert the equations of particle conservation to

$$\frac{\partial A}{\partial t} - D\frac{\partial^2 A}{\partial x^2} = 2RA^+A^- \tag{12}$$

and

$$\frac{\partial A^{\pm}}{\partial t} - D\frac{\partial^2 A^{\pm}}{\partial x^2} = -RA^+A^- \tag{13}$$

Equations 11, 12, and 13 describe the ecl system when they are solved consistent with suitable electrode boundary conditions at the origin. The right-hand sides of eq 12 and 13 make this a difficult nonlinear system of equations which has been solved with the aid of a computer by Feldberg[3,4] for the case of two-pulse operation and by Cruser and Bard[5] for continuous operation. In the limit of large R there is negligible coexistence of A^+ and A^- ions at any position in the cell. In this limit the only quantities needed to discuss the cell operation are $A + A^+ + A^-$ and $A^- - A^+$, both of which obey the simple heat equation

$$(\partial n/\partial t) - D(\partial^2 n/\partial x^2) = 0 \tag{14}$$

which can be solved analytically by well-known methods.[6] Now, recombination ceases to be a bulk phenomenon and occurs only at planes separating regions where only A^+ or A^- have nonzero values. In the basic ecl process there is the assumption that no molecules are destroyed. This provides us with a boundary condition at the electrode.

$$\frac{\partial}{\partial x}(A + A^+ + A^-)|_{x=0} = 0 \tag{15}$$

If we solve the problem by Fourier analysis we find $n_1 = A_0 - A - A^+ - A^- = 0$, where A_0 is the original molecular concentration. We solve the problem for a harmonic boundary condition for n_2 at the electrode.

$$n_2(0, t) = A^- - A^+ = A_0 e^{-j\omega t} \tag{16}$$

Then because the heat conduction equation is linear the solution for any arbitrary boundary condition on n_2 can then be found by the proper Fourier construction. Taking

$$n_2 = N(x)e^{-j\omega t} \tag{17}$$

we find

$$n_2 = A^- - A^+ = A_0 \exp\left\{-\sqrt{\frac{\omega}{2D}}\,x\right\} \sin\left\{\omega t - \sqrt{\frac{\omega}{2D}}\,x\right\} \tag{18}$$

where the phase has been arbitrarily adjusted.

The light is emitted at recombination planes where $n_2(x_c) = 0$ (see Figure 2). There are infinite numbers of these located at

$$x_c^n = \sqrt{\frac{2D}{\omega}}\,(\omega t \pm n\pi);\quad n = 0, 1, 2, \ldots \tag{19}$$

The rate of production of photons at each plane is given by

$$P^n(x_c^n, t) = \eta\frac{J(x_c^n, t)}{e} = \eta\sqrt{\frac{D\omega}{2}}A_0 \exp\left\{-\sqrt{\frac{\omega}{2D}}\,x_c^n\right\} \tag{20}$$

where η is the fraction of recombinations that produce a photon. A simple integration yields the total number of photons produced from the entire cell during one cycle

$$\frac{\text{no. of photons}}{\text{cycle}} = \sqrt{\frac{2D}{\omega}}\eta A_0 \tag{21}$$

The current at the electrode is given by

$$J(0, t) = eD\frac{\partial}{\partial x}(A^- - A^+)|_{x=0} = -e\sqrt{D\omega}A_0 \sin\left(\omega t + \frac{\pi}{4}\right) \tag{22}$$

(3) S. W. Feldberg, *J. Amer. Chem. Soc.*, **88**, 390 (1966).
(4) S. W. Feldberg, *J. Phys. Chem.*, **70**, 3928 (1966).
(5) S. A. Cruser and A. J. Bard, *J. Amer. Chem. Soc.*, **91**, 267 (1969).
(6) H. S. Carslaw and J. C. Jaeger, "Conduction of Heat in Solids," Oxford University Press, London, 1959.

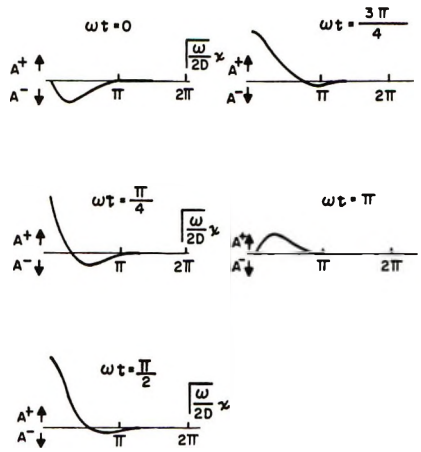

Figure 2. Density profiles for the cyclic mode of operation as a function of distance from the electrode for several times during the cycle.

One can integrate eq 22 to obtain the total number of ions leaving the electrode during a cycle

$$\frac{\text{no. of ions}}{\text{cycle}} = 3.414\sqrt{\frac{D}{\omega}}\,A_0 \qquad (23)$$

The quantum efficiency is obtained by dividing the total number of photons emitted by the cell (eq 21 gives the number at one electrode) by the number of ions entering the system from one electrode (23); one obtains

$$\text{quantum efficiency} = 0.828\eta \qquad (24)$$

The efficiency found in eq 24 is independent of frequency. Therefore, eq 24 also gives the efficiency for any arbitrary periodic solution.

We see from eq 24 that the inherent losses of the periodic mode of operation only limit its potential to an efficiency of 83%. This loss is due to the annihilation of ions which are created and swept back to the electrode during the cycle without experiencing recombination.

Measurements

A series of measurements was made on electrochemical cells which contained a solution of 2×10^{-3} *M* rubrene and 10^{-1} *M* tetra-*n*-butylammonium perchlorate (TBAP) in benzonitrile. The benzonitrile used was MCB Spectroquality that was stored in a desiccator over phosphorus pentoxide. The TBAP was Polarographic Grade obtained from Southwestern Analytical Chemical. It was dried *in vacuo* at ~80° and stored in a vacuum desiccator. The rubrene purchased from Aldrich Chemical was purified by liquid chromography on a column of activated alumina using trichloroethylene as the solvent. The rubrene was recovered by evaporating the solvent and then baking *in vacuo* at 200–250° for several hours. Because of its sensitivity to photoinduced reactions, the processing and storage of the rubrene was done at reduced light levels. However, once the working solution for the cells was degassed it was stable at normal light levels.

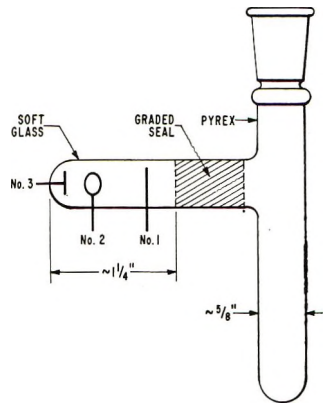

Figure 3. Typical ecl cell.

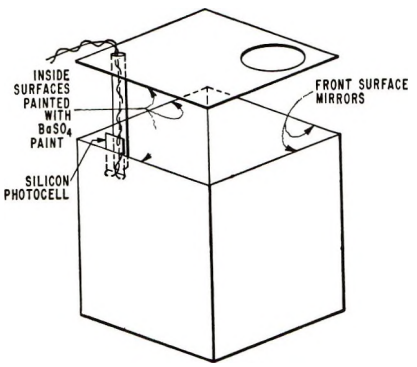

Figure 4. Integrating box for light output measurements.

A typical cell is shown in Figure 3. The electrodes are platinum, and a stopcock can be fitted to the ground-glass joint so that the cell may be sealed under vacuum. In order to prepare a cell for the light output measurements, the solids were weighed out and placed in the cell along with the appropriate volume of benzonitrile. The cell was then evacuated, and the solution was degassed by several freeze–thaw cycles.

The measurements were performed by placing the part of the cell containing the electrodes in an integrating box like that shown in Figure 4. The diffuse reflecting surfaces were formed with Eastman Kodak No. 6080 white reflectance paint. The photocell in the box was standardized against one that had been calibrated by the National Bureau of Standards. A voltage square wave was applied between electrodes no. 1 and 2. The output of the photocell was measured with an operational amplifier in a current follower circuit, and the average current through the cell during each half of the period was measured by connecting electrode no. 2 to the input of the circuit in Figure 5. The voltage outputs of the amplifier circuits were measured with a digital voltmeter.

The light output as a function of the current through the cell was measured for several different square wave

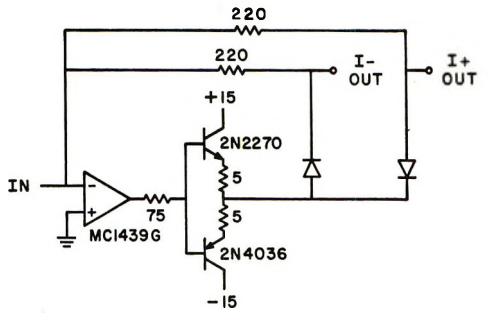

Figure 5. Current follower circuit for measuring current during each half-cycle.

periods. Typical results for a cell are shown in Figure 6. The slope of the lines in Figure 6 is the differential quantum efficiency (DQE) of the ecl cell. This is the experimental quantity that corresponds to the quantum efficiency calculated in eq 24. The lines in Figure 6 are offset along the abscissa because of the current needed to charge the double-layer capacitors at the electrodes to the oxidation and reduction potentials.

The slope of the lines for the larger periods in Figure 6 corresponds to a DQE of 8.7%. For each frequency the excitation of the cell was increased until the light output saturated or decreased. At the higher frequencies the measured DQE appeared to decrease; however, this could have been caused by uneven charging of the electrodes so that parts of the electrodes had achieved the reaction potentials while other parts had not. This value for the DQE implies that η, the ecl efficiency, is only $\sim$0.1.

Discussion

Since normal rubrene fluorescence is 83% efficient, we expect $\eta \simeq 0.83$ in eq 24 and the efficiency to be $\sim$70% if singlet excited states dominate the recombination reaction. On the other hand, it takes four ions to create one photon if triplet states dominate. This would indicate a maximum efficiency for this process of $\sim$40%, which could be seriously degraded further by the well-established tendency for triplets to experience

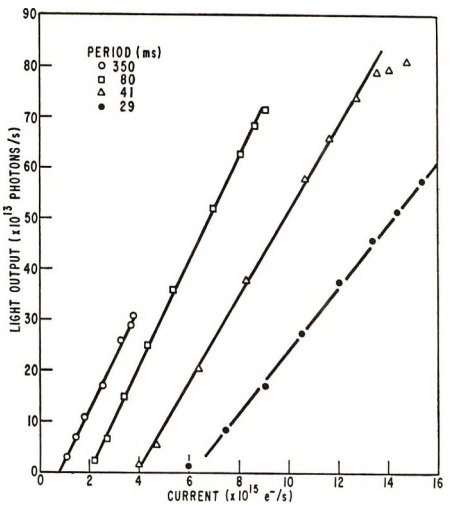

Figure 6. Output characteristics of a rubrene ecl cell.

quenching reactions. We conclude that high quantum efficiency is indicative of singlet reactions and low quantum efficiency is indicative of triplet reactions. These theoretical expectations assume that the molecules are not destroyed by some spurious reaction at a rate which is comparable to the rate at which they emit photons. This assumption has been confirmed experimentally by measuring the operating lifetime of a cell. In this way we have found that the average number of molecules destroyed in the ecl chain is smaller than the number that emit a photon. The measured efficiencies, $\sim$9%, are, therefore, consistent with the conclusion of Chang, Hercules, and Roe[2] based on other evidence that most of the excited states participating in the recombination process are triplet states. The measured efficiencies compare favorably with those observed in electroluminescent diodes and indicate that ecl systems would make useful devices if cell lifetimes can be significantly extended.

Acknowledgments. We wish to thank Professor J. Turkevich for his advice on some of the experimental work and to acknowledge the advice and encouragement of Dr. M. C. Steele and Dr. R. D. Larrabee.

The Influence of Hydrophobic Interactions on the Electrochemical Selectivity Ratios of Liquid Membranes Responsive to Organic Ions

by George Baum

Research and Development Laboratories, Corning Glass Works, Corning, New York 14830 *(Received January 17, 1972)*

Publication costs assisted by Corning Glass Works

The principles of hydrophobic interactions and of a model homogeneous, permselective liquid membrane described by Sandblom, Eisenman, and Walker, are integrated in a simple treatment of the electrochemical selectivity characteristics of membranes responsive to organic ions. The selectivity characteristics of liquid membranes permselective toward amino acids and toward choline derivatives are shown to obey the relationship $\log K_{ij} = (\Delta f_{t,ji}{}^{w\to e} - \Delta F_{t,i}{}^{e\to s})/23.05S$, where $\Delta f_{t,ji}{}^{w\to e}$ is an additive, constitutive free energy of transfer term available from the distribution coefficients of amino acids, $\Delta F_{t,i}{}^{e\to s}$ is a solvent-adjusted term, and S is the Nernst slope factor.

In a theoretical examination of a model homogeneous, permselective, liquid ion-exchange membrane, Sandblom, Eisenman, and Walker[1] related the electrode selectivity to a combination of a solvent-dependent, site-independent term and a term dependent on both solvent and site properties. The solvent-dependent term was shown to be related to the ratio of the distribution coefficients of the ion of interest and the counterion between the aqueous solution and the hydrophobic liquid membrane phase. For liquid-membrane electrodes, which are tailored for selectivity towards organic ionic species, it may be anticipated that the ionic distribution between the aqueous and organic phases would play a major role in establishing the selectivity between organic counterions. Higuchi and coworkers[2] have recently prepared a plasticized polymer membrane electrode (the membrane does not contain an ion-exchange agent) which exhibits a very favorable response to several tetraalkylammonium salts. They observed that the potential difference between the tetraalkylammonium salts qualitatively corresponded to the free energy of transfer of each additional methylene group from an aqueous to a hydrophobic environment. We will show that the selectivity characteristics of permselective liquid membranes toward organic ions can be described by a simple analysis based on the concepts of hydrophobic interactions.

Experimental Section

Potential measurements were conducted as previously described[3] using the electrochemical cell

$$\text{Ag/AgCl}|\text{satd KCL}|\text{liquid membrane}|\text{sce}$$

All measurements were made in unstirred solutions at 25° ± 1°. The liquid membrane consists of a 5% solution of acetylcholine tetra(*p*-chlorophenyl)borate in either 3-*o*-nitroxylene, dibutyl phthalate, or tri-(2-ethylhexyl)phosphate.

The isobutyrylcholine was prepared by the condensation of isobutyric anhydride with 2-(dimethylamino)-ethanol and subsequent quaternization with iodomethane.

Results and Discussion

The large, positive free-energy change accompanying the solution of hydrocarbons in water has its origin in a large negative entropy change associated with localized structuring of water.[4] From the distribution coefficients of a series of amino acids in water and ethanol, Cohn and Edsall observed that the free energy of transfer of amino acids is an additive and constitutive molecular property.[5]

Matsui and Freiser[6] constructed several electrodes where the permselective liquid membrane consisted of a quaternary amine surfactant dissolved in a water immiscible organic solvent. The electrode was then equilibrated against an aqueous acidified amino acid solution and selectivity factors toward a series of amino acids were obtained. Using the data reported by Matsui and Freiser, we can test the premise that the potential response of the liquid membrane ion-exchange electrodes towards organic ions is related to the free energy of transfer of the organic ion from an aqueous to a hydrophobic environment.

(1) J. P. Sandblom, G. Eisenman, and J. L. Walker, *J. Phys. Chem.*, **71**, 3862 (1967).

(2) T. Higuchi, C. R. Illian, and J. L. Tossounian, *Anal. Chem.*, **42**, 1674 (1970).

(3) G. Baum, *Anal. Lett.*, **3**, 105 (1970).

(4) H. S. Frank and M. W. Evans, *J. Chem. Phys.*, **13**, 507 (1945).

(5) E. J. Cohn and J. T. Edsall, "Proteins, Amino Acids and Peptides," Reinhold, New York, N. Y., 1943.

(6) M. Matsui and H. Freiser, *Anal. Lett.*, **3**, 161 (1970).

The potential response of an ion-selective electrode towards a solution of primary (i) and secondary (j) ions can be described by the empirical equation

$$E_{ij} = E' + \frac{2.3RT}{F} \log (a_i + K_{ij}a_j) \qquad (1)$$

where E' is a constant and K_{ij} is the selectivity ratio. A simple procedure to evaluate K_{ij} is to determine the potential response in single electrolyte solutions where $a_i = a_j$; then, if the slope factors are equal, K_{ij} is given by

$$\log K_{ij} = \frac{E_j - E_i}{S} \qquad (2)$$

where S is the term $2.3RT/F$ of eq 1.

The conversion between ΔF and ΔE is given by

$$\Delta F \text{ (cal)} = 23.05\Delta E \text{ (mV)}$$

We now set i as the primary amino acid and j as the secondary amino acids. Combining eq 1 and 2 gives

$$\log K_{ij} = \frac{[\Delta F_{t,j} - \Delta F_{t,i}]}{23.05S} \qquad (3)$$

$$= \frac{\Delta f_t}{23.05S}$$

Equation 3 is applied to the data of Matsui and Freiser for an electrode equilibrated against leucine and an electrode equilibrated against phenylalanine. The log of the corresponding observed selectivity ratio is shown to be related to the difference in the free energy of transfer between the primary and secondary amino acid (Figures 1 and 2). Although there is considerable scatter in the data points, the general trend of the data follows the calculated slope given in eq 3.

We recently published the selectivity ratios of a liquid membrane acetylcholine selective electrode toward a series of choline esters.[7,8] In general, as the alkyl length of the ester increased, the selectivity of the

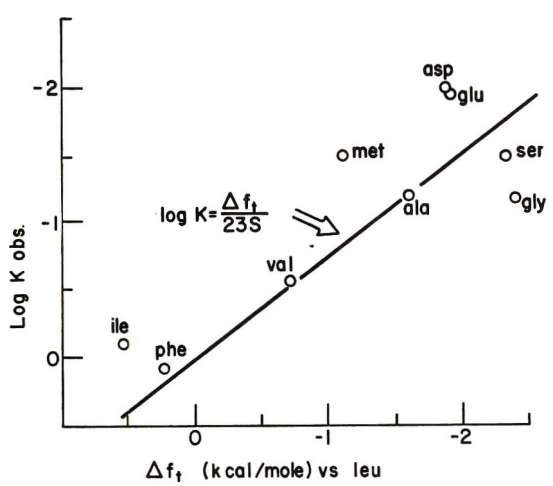

Figure 1. Correlation of observed selectivity ratio with Δf_t for a leucine equilibrated membrane.

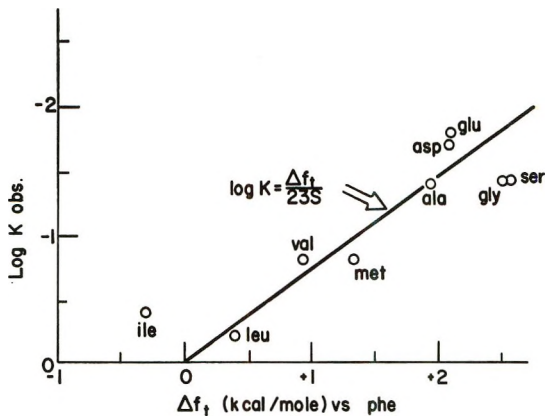

Figure 2. Correlation of observed selectivity ratio with Δf_t for a phenylalanine equilibrated membrane.

electrode toward the ester increased. The liquid membrane utilized in that study consisted of acetylcholine tetra(*p*-chlorophenyl)borate dissolved in 3-*o*-nitroxylene. The solvent has a strong effect on the selectivity of the electrode. Selectivity factors for two additional solvents are now reported. When dibutyl phthalate is used as the solvent for the choline salt, the magnitude of the selectivity factors is diminished. Tri(2-ethylhexyl) phosphate as a solvent yields even lower selectivity ratio values. These results are summarized in Table I. All values given are calculated from the potential response at 10^{-1} M single electrolyte solutions.

Table I: Selectivity Ratio toward Choline Esters

	Tri(2-ethylhexyl) phosphate	Dibutyl phthalate	3-*o*-Nitroxylene
Choline	1	1	1[a]
Acetylcholine	1.08	6.85	37.6[a]
Acetyl-β-methylcholine			121[a]
Isobutyrylcholine			118
Propionylcholine	3.36	18.2	121[a]
Butyrylcholine	10.2	57.6	407[a]
Valerylcholine			1550[a]

[a] Values reported in ref 9.

The free energy of transfer (ΔF_t) of a solute i in going from water to a solvent(s) is given by

$$\Delta F_t^{w\to s} = RT \ln \frac{a_{i,w}}{a_{i,s}}$$

$$= RT \ln D_i^{w\to s} + RT \ln \frac{\gamma_{i,w}}{\gamma_{i,s}}$$

where $D_i^{w\to s}$ is the distribution coefficient obtained

(7) G. Baum and F. B. Ward, *Anal. Biochem.*, **42**, 487 (1971).

(8) G. Némethy and H. A. Scheraga, *J. Phys. Chem.*, **66**, 1773 (1962).

from solubility data and γ is the appropriate activity coefficient. Since we will ultimately be concerned with the ratio of activity coefficients of structurally related species at a single concentration, the term involving activity coefficients is considered negligible in the present treatment. The ΔF_t terms for amino acids going from water to ethanol have been compiled.[5] The relationship between $\Delta F_t^{w\to e}$ and $\Delta F_t^{w\to s}$ is

$$\Delta F_t^{w\to s} = \Delta F_t^{w\to e} + \Delta F_t^{e\to s} \quad (4)$$

The difference in ΔF_t between solutes i and j is

$$[\Delta F_{t,j}^{w\to s} - \Delta F_{t,i}^{w\to s}] = [\Delta F_{t,j}^{w\to e} - \Delta F_{t,i}^{w\to e}] - [\Delta F_{t,i}^{e\to s} - \Delta F_{t,j}^{e\to s}] \quad (5)$$

To evaluate eq 5, the following considerations are made. (1) Choline is taken as solute i and the choline ester is solute j. Since ΔF_t is an additive and constitutive property, we employ the side-chain contributions ($\Delta f_t^{w\to e}$) derived for amino acids to evaluate $[\Delta F_{t,j}^{w\to e} - \Delta F_{t,i}^{w\to e}]$. (2) Insufficient data are available in the literature to estimate the $\Delta F_t^{w\to e}$ term for -OH of choline or for —O—C(=O)— of the choline ester. If we assume that the polar components are roughly equal, the difference in $\Delta F_t^{w\to e}$ for these two substituents can be estimated by a steric argument. Since the magnitude of the entropy change associated with the hydrophobic interaction is related to the molecular volume of the group involved,[8] and —C(=O)— is about the same size as $-CH_2-$, the same Δf_t contribution can be used. (3) Tanford has observed that ΔF_t is not significantly affected by the nature of the solvent for amino acids with nonpolar side chains. However, considerable solute–solvent interaction is encountered when polar substituents such as hydroxyl are present.[9] Thus

$$\Delta F_{t,i}^{e\to s} \gg \Delta F_{t,j}^{e\to s}$$

and eq 5 becomes

$$[\Delta F_{t,j}^{w\to s} - \Delta F_{t,i}^{w\to s}] = \Delta f_{t,ji}^{w\to e} - \Delta F_{t,i}^{e\to s} \quad (6)$$

Combining eq 3 and 6 gives

$$\log K_{ij} = \frac{(\Delta f_{t,ji}^{w\to e} - \Delta F_{t,i}^{e\to s}}{23.05S} \quad (7)$$

The values used for $\Delta f_{t,ji}^{w\to e}$ are given in Table II; the term $\Delta F_{t,i}^{e\to s}$ is a constant dependent only on the nature of the solvent.

The selectivity data obtained for choline and choline esters were treated graphically by eq 7 (Figure 3). The data points for all six choline esters obtained with the nitroxylene liquid membrane closely followed eq 7. It is particularly significant that isobutyrylcholine lies close to the position predicted for a branched side chain rather than at a position near the linear butyryl ester. Only three esters were examined with the dibutyl phthalate membrane and the trioctyl phosphate membrane. Both sets of data are consistent with eq 7. From intercept values, the magnitude of $\Delta F_{t,i}^{e\to s}$ for each solvent can be evaluated. The slopes and transfer terms obtained for each solvent membrane are summarized in Table III. The solvent-adjusted free energy of transfer term is related to the ability of the solvent to stabilize the polar hy-

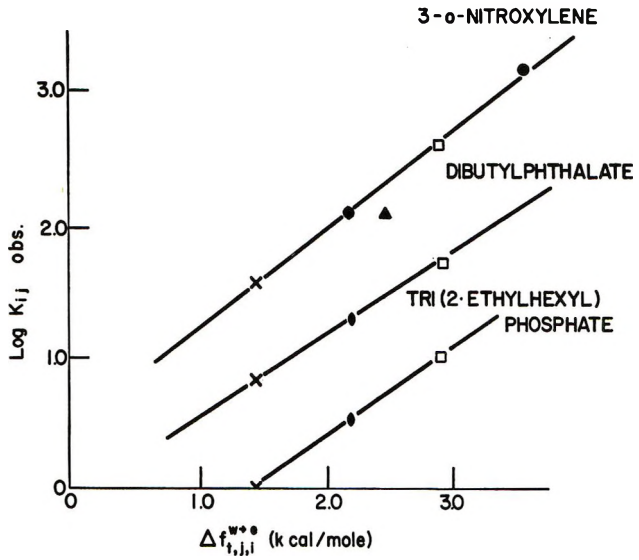

Figure 3. Relationship between observed selectivity ratio and free energy of transfer function: ●, propionylcholine; ○, acetyl-β-methylcholine; □, butyrylcholine; ●, valerylcholine; ▲, isobutyrylcholine.

Table II: Estimated Difference of Free Energy of Transfer between Choline and Choline Esters[a]

Choline ester	$\Delta f_t^{w\to e}$, cal/mol
Acetylcholine	1460
Propionylcholine	2190
Butyrylcholine	2920
Valerylcholine	3550
Isobutyrylcholine	2420
Acetyl-β-methylcholine	2190

[a] The following substituent factors were used: CH_3-, $-CH_2-$, —C(=O)— = +730 cal/mol; isobutyl = +2420 cal/mol.

Table III

Solvent	Observed slope × 10^3 (eq 7)[a]	$\Delta F_{t,i}^{e\to s}$, kcal/mol
3-o-Nitroxylene	0.63	+0.328
Dibutyl phthalate	0.61	−0.07
Tri(2-ethylhexyl) phosphate	0.65	−1.0

[a] Calculated values for $1/2.305S = 0.75 \times 10^{-3}$.

(9) Y. Nozaki and C. Tanford, *J. Biol. Chem.*, **246**, 2211 (1971).

droxyl substituent of choline. The ordering of the $\Delta F_{t,i}^{e \rightarrow s}$ values is the same as the corresponding macrodielectric constants for the solvents, although no direct relationship is established.

These results are consistent with the relationships developed by Sandblom, Eisenman, and Walker. The selectivity characteristics of the liquid membranes described above are shown to depend on the sum of a term related to the ion–counterion distribution coefficients and a solvent-site dependent term.

Equilibrium and Kinetic Properties of 9,10-Phenanthrenequinone-3-sulfonate in Aqueous Solutions

by M. W. Cheung and J. H. Swinehart*

Department of Chemistry, University of California, Davis, Davis, California 95616 *(Received August 9, 1971)*

Publication costs borne completely by The Journal of Physical Chemistry

The equilibrium and kinetic properties of partially reduced aqueous solutions of the potassium salt of 9,10-phenanthrenequinone-3-sulfonate (PQS) at pH 11.0 and 4.9 have been investigated and the results are reported. At pH 11.0 the enthalpies and entropies for the equilibria

$$R^{2-} + T \underset{k_{-1}}{\overset{k_1}{\rightleftharpoons}} D^{2-} \qquad K_1 \tag{1}$$

$$D^{2-} \underset{k_{-2}}{\overset{k_2}{\rightleftharpoons}} 2S^{-} \qquad K_2 \tag{2}$$

$$R^{2-} + T \underset{k_{-3}}{\overset{k_3}{\rightleftharpoons}} 2S^{-} \qquad K_3 \tag{3}$$

where R^{2-}, T, D^{2-}, and S^{-} represent the reduced, oxidized, dimeric, and free radical (semiquinone) forms of PQS at pH 11.0 are (1) -3 ± 3 kcal/mol, 10 ± 10 eu; (2) 7 ± 2, 6 ± 7; and (3) 4 ± 1, 16 ± 3, respectively. At 25° values of K_1, K_2, and K_3 are $(7.2 \pm 2.2) \times 10^3\ M^{-1}$, $(5.5 \pm 1.0) \times 10^{-4}\ M$, and 3.7 ± 0.7. At pH 11.0 assuming mechanisms in which $R^{2-} + T \rightleftarrows D^{2-} \rightleftarrows 2S^{-}$ or $R^{2-} + T \rightleftarrows 2S^{-} \rightleftarrows D^{2-}$, and using temperature-jump relaxation techniques, the activation parameters $\Delta H^{\pm}$ and $\Delta S^{\pm}$ for k_2 are 10.5 ± 0.9 kcal/mol and -9 ± 3 eu, respectively, and for k_{-2} are 2.5 ± 0.7 kcal/mol and -21 ± 3 eu, respectively. At 25° values of k_2 and k_{-2} are $(1.35 \pm 0.25) \times 10^3\ sec^{-1}$ and $(2.41 \pm 0.18) \times 10^6\ M^{-1}\ sec^{-1}$. At pH 4.9 the equilibrium present is $RH_2 + T \underset{k_{-4}}{\overset{k_4}{\rightleftharpoons}} DH_2$, where RH_2, T, and DH_2 represent the reduced, oxidized, and dimeric forms of PQS at this pH. Values of k_4 and k_{-4} at pH 4.9 and 9° have been determined in H_2O and D_2O. The role of hydrogen bond formation in the dimerization process is discussed.

Introduction

Quinones have a two-electron change between the oxidized and reduced forms. They are biologically important[1] because numerous naturally occurring quinones are extracted from living organisms.[2] Michaelis[3] has characterized a number of quinonelike and flavin systems. The equilibrium properties of several quinone systems[4,5] and the kinetic and equilibrium properties of the riboflavin system[6,7] have been studied. The equilibria present at 25° in partially reduced aqueous solutions of 9,10-phenanthenequinone-3-sulfonate (PQS) were first characterized by Michaelis and coworkers[8-10] using potentiometric titration techniques. This work reports a complete study of the thermodynamic and kinetic properties of the PQS system at pH 11.0. Some data are also reported at pH 4.9.

(1) H. Beinert and R. H. Sands in "Free Radicals in Biological Systems," M. S. Blois, Jr., *et al.*, Ed., Academic Press, New York, N. Y., 1961, Chapter 2.

(2) M. Barbier and E. Lederer, *Biochimie*, **22**, 236 (1957).

(3) L. Michaelis, *J. Phys. Chem.*, **54**, 1 (1950).

(4) H. Diebler, M. Eigen, and P. Matthies, *Z. Naturforsch. B*, **16**, 629 (1961).

(5) N. K. Bridge and G. Porter, *Proc. Roy. Soc.*, **244**, 259, 276 (1958).

(6) J. H. Swinehart, *J. Amer. Chem. Soc.*, **87**, 904 (1965).

(7) J. H. Swinehart, *ibid.*, **88**, 1056 (1966).

Experimental Section

Chemicals. Phenanthrene-3-sulfonic acid was prepared from phenanthrene by sulfonation with concentrated sulfuric acid. Phenanthrene-3-sulfonic acid was analyzed by converting it into its *p*-toluidine salt. The melting point of the salt was determined to be 216–217°, which is in good agreement with the reported value of 217°.[11] PQS was prepared from phenanthrene-3-sulfonic acid by oxidation with chromic oxide in glacial acetic acid.[12]

Anal. Calcd for $C_{14}H_7O_5SK$: C, 51.5; H, 2.2; S, 9.8. Found: C, 50.3; H, 2.7; S, 9.4.

Figure 1 shows the spectra of PQS at various states of reduction at pH 11.0. The oxidized form, T, has the following absorption maxima and the corresponding log ϵ_{max}: 225 nm (4.5), 265 nm (4.5), 325 nm (3.6), and 415 nm (3.1). Partially reduced solutions of PQS (R^{2-} + T) have a broad peak centered around 660 nm (dimer≡D^{2-}) and an absorption maximum at 485 nm (log ϵ_{max} = 3.7, semiquinone≡S^{-}) with a shoulder at 525 nm, in good agreement with the reported values.[9] The hydroquinone form of PQS, R^{2-}, does not have absorption maxima in the visible region but has a sharp peak at 355 nm. At pH 4.9, the absorption spectrum of T in the visible region has an absorption maximum at 420 nm (log ϵ_{max} = 3.15) while the reduced form, RH_2, practically does not absorb in the visible region. The partially reduced PQS solutions do not have additional absorption maxima but have an excess absorbance in the 550–700-nm region. The structures of the species present at pH 4.9 and their p*K*'s are summarized in Table I. The dimer in each pH region is assumed to be a combination of two semiquinone molecules or an oxidized and reduced molecule.

Potassium ferricyanide (Baker and Adamson); potassium hydrogen phosphate, potassium acetate, potassium chloride (J. T. Baker); sodium hydroxide (0.1 *N*) (Bio Rad Laboratories); deuterium oxide (99.81%) (International Chemical and Nuclear Corp. Chemical and Radiation Division); palladium-on-charcoal (Matheson Coleman and Bell), and glacial acetic acid (Allied Chemical) were used without further purification.

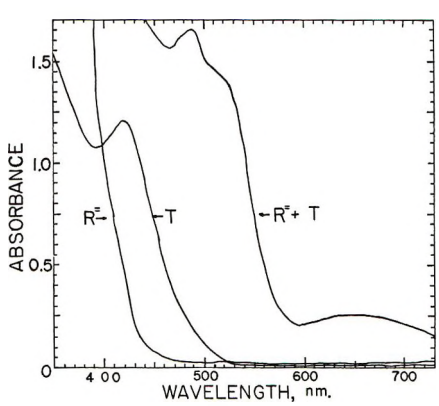

Figure 1. Spectral properties of solutions of PQS at pH 11.0. Concentrations: T, 9.0×10^{-4} *M*; (R^{2-} + T), 50% reduced T solution; R^{2-}, 1.0×10^{-3} *M*. *t* = 22°, path length 1.00 cm.

Table I: Species Present at pH 4.9 and Their p*K*'s

Structure at pH 4.9	p*K*	Name	Abbreviated symbol pH 4.9	Abbreviated symbol pH 11.0
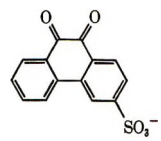	≥11.5	Oxidized form of PQS	T	T
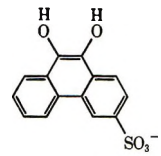	8	Reduced form of PQS	RH_2	R^{2-}
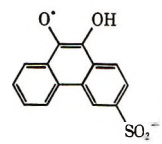	7.5	Semiquinone form of PQS	SH	S^{-}

Preparation of Solutions. All solutions were prepared with deionized distilled water. Solutions of PQS were prepared shortly before each experiment to avoid possible decomposition of the compound,[8] especially at pH 11.0. Solutions in D_2O at pD 4.9 were prepared by weighing the desired amount of PQS, potassium chloride, and potassium acetate into 0.065 ml of 17.5 *M* glacial acetic acid. Sufficient D_2O was added to bring the volume to 50 ml. Thus the quinone solutions contain a minimum of 99.77% D_2O. All solutions were prepared and run into the spectral cells in an all-glass system which was constantly flushed with oxygen-free nitrogen gas, such that the solutions never came in contact with oxygen. Sodium hydroxide and potassium hydrogen phosphate were used to maintain solutions at pH 11.0, and potassium acetate and glacial acetic acid at pH 4.9. The ionic strength of all the solutions was maintained at 0.06 with KCl.

Apparatus and Methods. (*a*) *Equilibrium Studies by Spectral and Potentiometric Methods at pH 11.0.* Partially reduced PQS solutions were transferred to a Beckman 1-cm quartz cell. Spectral measurements were performed on a Cary Model 14 recording spectrophotometer, with a temperature control good to ±0.5° in the cell compartment.

In the potentiometric titrations, potassium ferri-

(8) L. Michaelis and E. S. Fetcher, *J. Amer. Chem. Soc.*, **59**, 2460 (1937).

(9) L. Michaelis and S. Granick, *ibid.*, **70**, 624 (1948).

(10) L. Michaelis, G. F. Boeker, and R. K. Reber, *ibid.*, **60**, 202 (1938).

(11) L. F. Fieser, *ibid.*, **51**, 2460 (1929).

(12) A. Werner, *Ann. Chem.*, **321**, 341 (1902).

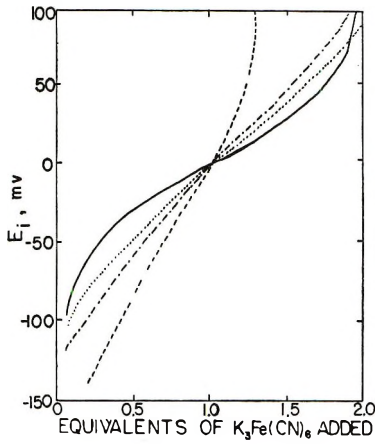

Figure 2. Potentiometric titration curves for PQS at pH 11.0 and t = 30°. Concentrations of PQS: ——, 3 × 10^{-4} M; · · · ·, 5 × 10^{-3} M; —·—·—, 1.0 × 10^{-2} M; — — —, 2.0 × 10^{-2} M.

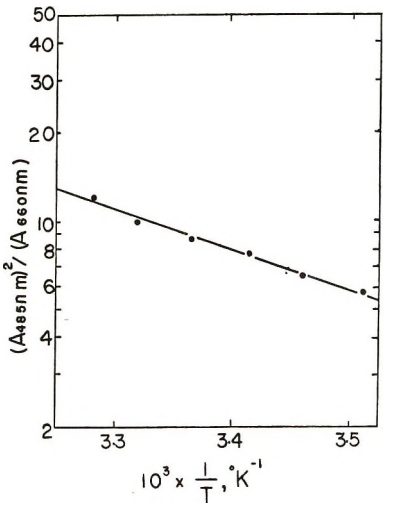

Figure 3. Plot of ln $(A_{485nm})^2/A_{660nm}$ *vs.* $10^3/T$.

cyanide solution was used to titrate against the reduced form of PQS. The voltage of the cell Pt|R^{2-}, T, S^-, and D^{2-}||calomel electrode at various stages of oxidation was measured on a Beckman Expandomatic pH meter. Figure 2 is a typical titration curve with potentials plotted against equivalents of $K_3Fe(CN)_6$ added. The normal potential, when 1 equiv of $K_3Fe(CN)_6$ was added, was taken as the zero point. The temperatures of the titration solutions were thermostated to ±0.5°. The pH's of the solutions were measured on a pH meter which was standardized against commercially available pH buffers.

The equilibrium constants K_1, K_2, and K_3 associated with the equilibrium processes represented by eq 1–3 were calculated according to the methods developed by Michaelis and his coworkers[8,13] and Elema[14]

$$R^{2-} + T \underset{k_{-1}}{\overset{k_1}{\rightleftharpoons}} D^{2-} \qquad K_1 \qquad (1)$$

$$D^{2-} \underset{k_{-2}}{\overset{k_2}{\rightleftharpoons}} 2S^- \qquad K_2 \qquad (2)$$

$$R^{2-} + T \underset{k_{-3}}{\overset{k_3}{\rightleftharpoons}} 2S^- \qquad K_3 \qquad (3)$$

(*b*) *Kinetic Studies.* Kinetic studies were carried out on a temperature-jump relaxation instrument manufactured by the Messanlagen Studiengeschellschaft, GmbH, Goettingen, Germany. Relaxation techniques were devised to study the kinetics of rapid reactions. A small temperature perturbation is applied to the system, and the resulting "relaxation" to equilibrium occurs with a characteristic relaxation time, τ. The relaxation time is related to the rate constants and equilibrium concentrations of the species at the new temperature in a unique way, which is dependent on the mechanism of the reaction. For a detailed account of the theory and application of relaxation technique, one may refer to the article by Eigen and DeMaeyer[15] and the book by Caldin.[16]

The kinetics were also studied by the stopped-flow technique. A Gibson–Durrum stopped-flow apparatus was used.

Results

Equilibrium Studies at pH 11.0. Equilibria 1, 2, and 3 were considered. The equilibrium represented by eq 2 was studied spectrophotometrically. The absorption peak at 485 nm was assigned to S^-, and that at 660 nm to D^{2-}.[9] Table II contains the data of this spectral study at μ = 0.06 (KCl), and Figure 3 is a plot of ln $(A_{485\text{ nm}})^2/A_{660\text{ nm}})$ *vs.* $1/T$. The calculated value of $\Delta H_2°$ is 6.4 ± 0.4 kcal/mol.

The equilibria were studied by potentiometric titration methods described under Experimental Section.

Table II: Data for Determination of $\Delta H_2°$ for the Equilibrium $D^{2-} \rightleftarrows 2S^-$ [a]

t, °C	$A_{485\text{ nm}}$	$A_{660\text{ nm}}$	$(A_{485\text{ nm}})^2/A_{660\text{ nm}}$
32.0	1.360	0.159	11.63
28.5	1.338	0.180	9.94
24.0	1.300	0.197	8.57
20.0	1.270	0.215	7.51
16.0	1.228	0.236	6.38
12.0	1.189	0.253	5.59

[a] Conditions: [T] > [R^{2-}], total initial concentration = 9 × 10^{-4} M; μ = 0.06; pH 11.0; path length = 1 cm.

(13) L. Michaelis, *Chem. Rev.*, 16, 243 (1935).

(14) B. Elema, *J. Biol. Chem.*, 100, 149 (1933).

(15) M. Eigen and L. DeMaeyer in "Techniques of Organic Chemistry," Vol. VIII, Part II, A. Weissberger, Ed., Interscience, New York, N. Y., 1963.

(16) E. F. Caldin, "Fast Reactions in Solutions," Blackwell Scientific Publications, Oxford, U. K., 1964.

Figure 2 is a typical potentiometric titration curve. Table III presents average values of K_1, K_2, and K_3 at various temperatures obtained by titration of reduced PQS solutions in the concentration range 3×10^{-4} to 2×10^{-2} M. Plots of these data gave the following values of ΔH° and ΔS° for the various equilibrium concentration quotients: K_1, -3 ± 3 kcal/mol, 10 ± 10 eu; K_2, 7 ± 2, 6 ± 7; K_3, 4 ± 1, 16 ± 3. Experiments carried out at 40° showed deviations from the plots used to give the thermodynamic parameters. This deviation will be discussed under Discussion.

Table III: Summary of Equilibrium Concentration Quotients Determined by Potentiometric Titration Methods[a]

Temp, °C	$10^{-3}K_1$, M^{-1}	10^4K_2, M	K_2
12.0	8.2 ± 1.6	2.7 ± 0.7	2.7 ± 0.2
22.0	7.8 ± 3.4	5.1 ± 1.4	3.4 ± 0.7
30.0	6.6 ± 3.4	7.0 ± 1.2	4.3 ± 1.1

[a] pH = 11.0, μ = 0.06.

Kinetic Studies. (*a*) *pH 11.0.* Figure 4 is a plot of the reciprocal of the relaxation time, $1/\tau$, *vs.* four times the absorbance at 485 nm ($4A_{485\text{ nm}}$) at 12, 22, 30, and 40° and at pH 11.0. The value of $4A_{485\text{ nm}}$ is proportional to $4[S^-]$. No linear relationship was obtained when $1/\tau$ was plotted against ($[R^{2-}] + [T]$) or the absorbance at 660 nm, which is proportional to $[D^{2-}]$. Relaxation expressions for mechanisms in which reaction 1 equilibrates rapidly compared to (2) (mechanism A) or reaction 3 equilibrates rapidly compared to (2) (mechanism B) are

$$\frac{1}{\tau_A} = \frac{k_2K_1([R^{2-}] + [T])}{1 + K_1([R^{2-}] + [T])} + 4k_{-2}[S^-] \qquad \text{(mechanism A)}$$

$$\frac{1}{\tau_B} = \frac{4k_{-2}K_3([R^{2-}] + [T])[S^-]}{4[S^-] + K_3([R^{2-}] + [T])} + k_2 \qquad \text{(mechanism B)}$$

if $K_1([R^{2-}] + [T]) > 1$ or $K_3([R^{2-}] + [T]) > 4[S^-]$, which are conditions fulfilled in the experiments, each expression reduces to

$$\frac{1}{\tau} = k_2 + 4k_{-2}[S^-]$$

Therefore on the basis of the relaxation expressions, combined with the scatter in the data, mechanisms A and B cannot be distinguished. The slope and intercept of the plot of $1/\tau$ *vs.* $4A_{485\text{ nm}}$ gives $k_{-2}/\epsilon_{485\text{ nm}}$ and k_2, respectively. Table IV contains a summary of the rate constants. The value of k_{-2} is calculated using $\epsilon_{485\text{ nm}} = 5000\ M^{-1}\ \text{cm}^{-1}$. Figure 5 contains plots of $10^{-3}k_{-2}/T$ and k_2/T *vs.* $1/T$. The values of the rate

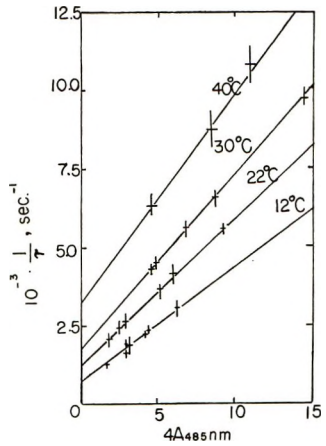

Figure 4. Plots of $1/\tau$ *vs.* $4A_{485\text{ nm}}$ at 12, 22, 30, and 40°.

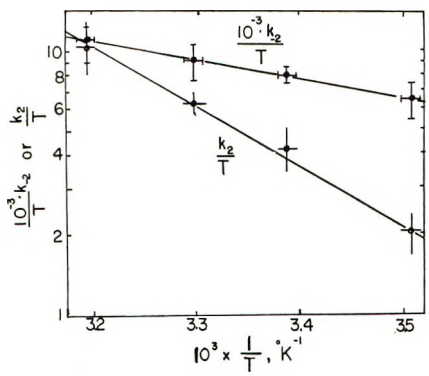

Figure 5. Plots of ln k_{-2}/T and ln k_2/T *vs.* $1/T$.

constants at 25° and the activation parameters $\Delta H^\pm$ and $\Delta S^\pm$ are $k_2 = (1.35 \pm 0.25) \times 10^3\ \text{sec}^{-1}$, 10.5 ± 0.9 kcal/mol, -9 ± 3 eu, and $k_{-2} = (2.41 \pm 0.18) \times 10^6\ M^{-1}\ \text{sec}^{-1}$, 2.5 ± 0.7, -21 ± 3.

Table IV: Summary of the Kinetic Data for PQS System[a]

Temp, °C	$10^{-3}k_2$, sec^{-1}	$10^{-3}k_{-2}/\epsilon_{485\text{ nm}}$, sec^{-1} cm	$10^{-6}k_{-2}$,[b] M^{-1} sec^{-1}	$10^{-6}k_{-2}$,[c] M^{-1} sec^{-1}
12	0.60 ± 0.14	0.38 ± 0.06	1.75 ± 0.71	1.87 ± 0.28
22	1.28 ± 0.26	0.47 ± 0.03	2.53 ± 0.95	2.35 ± 0.14
30	1.90 ± 0.22	0.56 ± 0.08	2.72 ± 0.77	2.78 ± 0.40
40	3.23 ± 0.75	0.67 ± 0.10	*d*	3.36 ± 0.51

[a] pH 11.0 and μ = 0.06 (KCl). [b] Calculated from equilibrium and kinetic data. [c] Calculated from kinetic data and $\epsilon_{485\text{ nm}} = 5000\ M^{-1}\ \text{cm}^{-1}$. [d] Not calculated because equilibrium concentration quotient at this temperature was not determined.

Other mechanisms such as reaction 1 equilibrates rapidly compared to reaction 3 (mechanism C) or reaction 3 equilibrates rapidly compared to reaction 1 (mechanism D) are less favorable as will be described under Discussion.

In an attempt to distinguish between mechanisms A and B, stopped-flow experiments were performed.

If mechanism A was operative, while the pre-equilibrium ($R^{2-} + T \rightleftarrows D^{2-}$) would be too fast for detection by the stopped-flow apparatus, it was hoped that a rapid decrease in optical density would be observed in the spectral region around 660 nm and a rapid optical density increase between 485 and 550 nm. If mechanism B was operative, a rapid decrease of optical density between 485 and 550 nm and a rapid increase in optical density at the spectral region around 660 nm should be observed. Results from the rapid mixing of T and its reduced form, R^{2-}, by stopped-flow techniques at pH 11.0 and 12° were not conclusive because the expected half-lives for the kinetic processes were of the order of the time required for mixing and could not be distinguished from the mixing process.

(*b*) *pH 4.9.* At pH 4.9, the only equilibrium present in the solutions is[17]

$$RH_2 + T \underset{k_{-4}}{\overset{k_4}{\rightleftharpoons}} DH_2 \qquad K_4 \qquad (4)$$

and RH_2 and T are the species designated in Table I. A partially reduced PQS solution, prepared by mixing PQS in excess over the reduced form of PQS, has an absorption maximum at 420 nm whose absorbance could be predicted by calculation considering only PQS being diluted by the hydroquinone. Even at relatively high concentrations (10^{-2} *M*), there was no absorption maxima in the spectral region between 550 and 700 nm for the partially reduced PQS solution at pH 4.9. However, the overall absorbance of the partially reduced PQS solutions in the 550–700-nm region is higher than that expected from only T and RH_2. This spectral observation indicates that only a very small amount of a third species is present in the partially reduced PQS solution at pH 4.9, and it absorbs in the 550–700-nm region, which suggests that the intermediate is a dimer. These observations are in agreement with those reported by Michaelis and Schubert.[17] Thus, if only equilibrium 4 is important, $1/\tau$, the reciprocal of the relaxation time, equals k_4 ($[RH_2] + [T]$) + k_{-4} and a plot of $1/\tau$ *vs.* ($[RH_2] + [T]$) should be linear. Experiments were done in both H_2O and D_2O to determine what role hydrogen plays in the process represented by equilibrium 4. The slope of the plot gives k_4, and the intercept gives k_{-4}. Figure 6 is a plot of $1/\tau$ *vs.* ($[RH_2] + (T)$] in H_2O and D_2O. Values of $10^{-6}k_4$ (M^{-1} sec^{-1}) and $10^{-4}k_{-4}$ (sec^{-1}) in H_2O and D_2O at pH 4.9, μ = 0.06, and 9° are 1.3 ± 0.1 and 3.4 ± 0.2, and 5.4 ± 0.1 and 2.6 ± 0.2.

Discussion

Equilibrium Studies at pH 11.0. From spectral studies, the value of $\Delta H_2°$ for the equilibrium $D^{2-} \rightleftarrows 2S^-$ is calculated to be 6.4 ± 0.4 kcal/mol. From potentiometric titrations data, $\Delta H_2°$ calculated from a plot of ln K_2 *vs.* $1/T$ is 7 ± 2 kcal/mol.

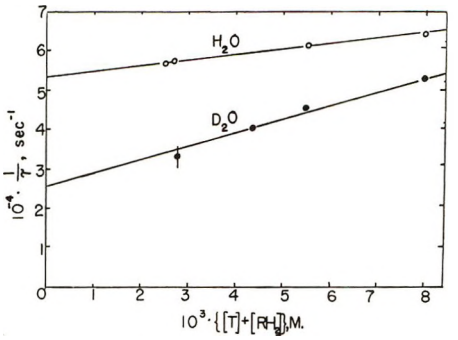

Figure 6. Plots of $1/\tau$ *vs.* $\{[RH_2] + [T]\}$ in H_2O and D_2O at pH 4.9 and t = 9°.

The potentiometric titration data obtained at 40°, however, deviate from plots of ln K *vs.* $1/T$. Michaelis and Fetcher[8] noted that part of PQS in an alkaline solution was lost due to decomposition which increased with temperature. The loss of PQS and the presence of the decomposed species which were probably in equilibrium with the other species present is a probable explanation for the titration data obtained at 40°.

The value of $\Delta H_2°$ calculated from temperature-jump relaxation data is comparable to that obtained from equilibrium studies (see Discussion, Kinetic Studies). The value of $\Delta S_2°$ for this equilibrium was calculated to be 6 ± 7 eu. These thermodynamic data are reasonable for reactions of this type.[7] The value of $\Delta S_2°$ indicates the presence of some interaction between the solvent molecules and the species involved. Both the dimer and the free radical are negatively charged. The freeing of the free radicals from the dimer would increase the interaction with the solvent molecules ($\Delta S°$ positive). On the other hand, the orientation of the solvent molecules around the free radicals is more effective with an attendant loss of freedom of motion ($\Delta S°$ negative).[18] The value of $\Delta S_2°$ evaluated for such a process is therefore reasonable.

Kinetic Studies. (*a*) *pH 11.0.* A linear plot was obtained when $1/\tau$ was plotted against $4A_{485\text{ nm}}$. However this behavior alone would not be able to distinguish the four possible mechanisms from one another. Activation parameters could be used to help distinguish between the possibilities.

Assuming either mechanism A or mechanism B the following activation parameters were calculated: $\Delta H_2^{\pm}$ = 10.5 ± 0.9 kcal/mol, $\Delta S_2^{\pm}$ = −9 ± 3 eu, $\Delta H_{-2}^{\pm}$ = 2.5 ± 0.7 kcal/mol and $\Delta S_{-2}^{\pm}$ = −21 ± 3 eu. These results are reasonable for either mechanism. For a solution reaction in which dimerization of ions of like charge occurs, $\Delta S_{-2}^{\pm}$ = −21 ± 3 eu is reasonable. Comparable $\Delta S^{\pm}$ values of similar reactions are com-

(17) L. Michaelis and M. P. Schubert, *J. Biol. Chem.*, 119, 133 (1937).

(18) A. A. Frost and R. G. Pearson, "Kinetics and Mechanism," 2nd ed, Wiley, New York, N. Y., 1963.

mon in the literature.[19,20] The classical electrostatic model will predict a less negative value.[18] This indicates that other contributions to entropy change may occur. More effective interaction of the activated complex with the solvent molecules and a different orientation of the latter with the former may account for some of the contributions. The value of $\Delta S_{-2}^{\ddagger}$ indicates that the activated complex is similar in structure to the dimeric product, D^{2-}. This is further illustrated by comparing the values of $\Delta S_2^{\ddagger}$ with ΔS_2°. The significant difference indicates that the freeing of the free radicals from the dimer is only partial in the activated complex.

Assuming mechanism A or B, k_{-2} was obtained as $k_{-2}/\epsilon_{485\text{ nm}}$ (see Table IV) from the kinetic studies. Values of rate constant k_{-2} could be evaluated either from the results of k_2 and K_2 or from the reported values of $\epsilon_{485\text{ nm}} = 5000\ M^{-1}\ \text{cm}^{-1}$ for the free radical. Using the values of k_{-2} calculated from k_2 and K_2, the molar absorptivity of S^-, $\epsilon_{485\text{ nm}}$, could be calculated. $\epsilon_{485\text{ nm}}$ is calculated to be $(5.1 \pm 0.4) \times 10^3\ M^{-1}\ \text{cm}^{-1}$, which is in good agreement with the value reported by Michaelis and Granick of $(5 \pm 1) \times 10^3\ M^{-1}\ \text{cm}^{-1}$.[9] Table IV contains results of k_{-2} by both methods of calculation. If ΔH_2° is calculated from enthalpies of activation for k_2 and k_{-2}

$$\Delta H_2^{\circ} = \Delta H_2^{\ddagger} - \Delta H_{-2}^{\ddagger} = 8 \pm 2\ \text{kcal/mol}$$

This value is in good agreement with the values calculated from potentiometric titrations data (7 ± 2 kcal/mol) and absorbance data (6.4 kcal/mol) under Equilibrium Studies.

Assuming mechanism C, a plot of $1/\tau$ *vs.* $4A_{485\text{ nm}}$ gives $k_{-3}/\epsilon_{485\text{ nm}}$ as slope and k_3/K_1 as intercept. Using values of K_1 calculated from equilibrium data and $\epsilon_{485\text{ nm}} = 5000\ M^{-1}\ \text{cm}^{-1}$,[9] k_3 and k_{-3} and thus K_3 are calculated. Although it is possible to obtain an enthalpy change comparable to that from equilibrium studies, the data scattering from the straight line makes this mechanism less likely. Further, $\Delta S_{-3}^{\ddagger} = -21 \pm 3$ eu associated with reaction represented by k_{-3} is inconsistent with this mechanism.

Assuming mechanism D, a similar plot will give slope as $k_1/K_3\epsilon_{485\text{ nm}}$ and intercept as k_{-1}. Again using equilibrium data K_3 and $\epsilon_{485\text{nm}}$, k_1 and k_{-1} and thus K_1 are calculated. A similar argument as mentioned above makes this mechanism less favorable. Further, $\Delta S_1^{\ddagger}$, which is associated with the dimerization reaction represented by rate constant k_1, can be calculated to be 6 ± 4 eu. The value is not reasonable for the dimerization process.

(*b*) *pH 4.9.* The rate constant ratios $k_4(H_2O)/k_4(D_2O) = 0.39$ and $k_{-4}(H_2O)/k_{-4}(D_2O) = 2.1$ for the rate constants in equilibrium 4 at pH 4.9 and 9° provide some information about the mechanism. The ratio of equilibrium concentration quotients

$$\frac{K_4(D_2O)}{K_4(H_2O)} = \frac{k_4(D_2O)/k_{-4}(D_2O)}{k_4(H_2O)/k_{-4}(H_2O)} = 5.4$$

suggests that hydrogen bond formation is important in stabilizing the dimer. The actual rate constant ratios indicate that in the activated complex for k_4 and k_{-4}, one hydrogen bond is forming and breaking, respectively. The data do not distinguish as to whether electron transfer takes place prior to, simultaneously with, or after hydrogen bond formation. Activation parameters were not obtained. Work is continuing on this aspect of the problem.

Acknowledgment. This investigation was supported by the Public Health Service Research Grant GM 11767 from the National Institutes of Health.

(19) F. Foerster and P. Dolch, *Z. Elektrochem.*, **23**, 137 (1917).
(20) F. Giardani, *Gazz. Chim. Ital.*, **54**, 844 (1929).

The Osmotic Properties of Polystyrenesulfonates. II. The Donnan Equilibrium[1]

by P. Chu, A. Sarkar, and J. A. Marinsky*

Department of Chemistry, State University of New York at Buffalo, Buffalo, New York 14214
(Received April 5, 1971)

Publication costs borne completely by The Journal of Physical Chemistry

The Donnan equilibrium of nine univalent and two divalent cationic forms of polystyrenesulfonate and simple salts (chlorides) of the same counterions have been studied by means of uncharged membranes impermeable to the polyelectrolyte. The data have been used to facilitate examination of the magnitude of the molal activity coefficient of the polyelectrolyte counterion in these mixtures.

Introduction

A number of investigations of the colligative properties of mixtures of ionized polyelectrolytes and simple uni-univalent salts have shown that each component in such mixtures behaves essentially as if it is unaffected by the presence of the other. This behavior[2-7] has been expressed in the form of the following additivity rule (AR) for the osmotic pressures

$$\pi = \pi_2 + \pi_3 \tag{1}$$

where π is the osmotic pressure of the ternary system and π_2 and π_3 are the respective osmotic pressures of polyelectrolyte and salt in the absence of the other and at their concentration values in the mixture.

In a mixed solution which consists of m_2 moles of z-valent polymer and m_3 moles of uni-univalent salt per 1000 g of water, the osmotic pressure, π, the water activity, a_w, and the practical osmotic coefficient, ϕ, bear the following well known relationship

$$\begin{aligned} \pi/kT = -m_w \ln a_w &= \phi(m_2 + m_+ + m_-) \\ &= \phi(m_2 + zm_2 + 2m_3) \\ &= \phi[m_2(z+1) + 2m_3] \end{aligned} \tag{2}$$

Since $z >>> 1$

$$\pi/kT \cong \phi(m_2 z + 2m_3) \tag{3}$$

From the empirical additivity rule[2-7]

$$\pi/kT = (\pi_2 + \pi_3)/kT = m_2 z\phi_2 + 2m_3\phi_3 \tag{4}$$

where ϕ_2 and ϕ_3 correspond to the osmotic coefficient of the pure component at the observed concentration value.

Our analysis[8] of data from a recent investigation of the ternary system, sodium polyacrylate, sodium chloride, and water (NaPAA–NaCl–H_2O) by Okubo, Ise, and Matsui[9] suggest that the above equation is more correctly expressed when the osmotic pressure of components of the mixture (and their osmotic coefficients) corresponds to their values at the equilibrating water activity rather than to their values at the observed concentrations.

This demonstrated additivity of the colligative properties of the individual components of polyelectrolyte–simple salt mixtures may provide insight with respect to the interpretation of Donnan distribution data. In such equilibria the chemical potential of simple salt in the presence of polyelectrolyte is equal to the chemical potential of the membrane-separated pure salt and

$$a_{3(m_2 z + m_3)} = A_{3(M_3)} \tag{5}$$

Since there is apparently little interaction between polyelectrolyte and simple salt their physical chemical behavior may be deduced from independent consideration of the pure components. The effective concentration of the polyelectrolyte can be denoted as $m_2 z\gamma_{\pm 2}$ where its mean molal activity coefficient, $\gamma_{\pm 2}$, is expressed by

$$\gamma_{\pm 2} = (\gamma_2{}^+)^{z/z+1}(\gamma_2{}^-)^{1/z+1} \tag{6}$$

Since $z >>> 1$, $\gamma_2{}^-$ approaches a limiting value of 1 and

$$\gamma_2{}^{\pm} \simeq \gamma_2{}^+ \tag{7}$$

The activity of the salt in the mixture is then given by

$$(m_2 z\gamma_2{}^+ + m_3)(m_3)(\gamma_3{}^{\pm})^2 = a_{3(m_2 z + m_3)} \tag{8}$$

the $\gamma_3{}^{\pm}$ correcting for long range Debyean-like interaction between mobile cations and anions. To a first approximation, in moderately dilute systems, the value of $\gamma_3{}^{\pm}$ should be equal or nearly equal to the mean

(1) This paper is based in part on a dissertation submitted by P. Chu in partial fulfillment of the requirements of the degree of Doctor of Philosophy, Feb 1967.

(2) (a) M. Nagasawa, M. Izumi, and I. Kagawa, *J. Polym. Sci.*, **37**, 375 (1959); (b) M. Nagasawa, A. Takahashi, M. Izumi, and I. Kagawa, *ibid.*, **38**, 213 (1959).

(3) Z. Alexandrowicz, *ibid.*, **56**, 115 (1962).

(4) Z. Alexandrowicz, *ibid.*, **43**, 337 (1960).

(5) R. A. Mock and C. A. Marshall, *ibid.*, **13**, 263 (1954).

(6) A. Katchalsky, R. Cooper, J. Upadhyoy, and A. Wasserman, *J. Chem. Soc.*, 5198 (1961).

(7) F. T. Wall and M. I. Ertel, *J. Amer. Chem. Soc.*, **79**, 1556 (1957).

(8) J. A. Marinsky, *J. Phys. Chem.*, **75**, 3890 (1971).

(9) T. Okubo, N. Ise, and F. Matsui, *J. Amer. Chem. Soc.*, **89**, 3697 (1967).

molal activity coefficient of the polyelectrolyte–free salt solution in the Donnan equilibrium system.

The following relationship derives from the above reasoning

$$(m_2 z \gamma_2^+ + m_3)(m_3) = M_3^2 \quad (9)$$

and

$$\gamma_2^+ = \frac{M_3^2 - m_3^2}{z m_2 m_3} \quad (10)$$

For di-univalent salts

$$\gamma_2^{2+} = \frac{M_3^3 - m_3^3}{z m_2 m_3^2} \quad (11)$$

It was the objective of this research program to examine the γ_2^+ property of the polyelectrolyte counterion in polyelectrolyte–salt mixtures with the above expression. Donnan equilibrium studies of nine univalent and two divalent cation salts of polystyrenesulfonate containing varying amounts of the simple chloride salt with a common cation were made for this purpose.

In a typical experiment, polyelectrolyte and simple salt, initially at atmospheric pressure, p, were separated with an uncharged membrane impermeable only to the macromolecule. Solvent and salt were transported across the membrane until equilibrium of all transferable ion species was achieved. There was restraint of solvent transfer and at salt equilibrium the additional pressure, P, that developed above the polyelectrolyte–salt phase in these experiments raised the activity of the solvent so that it approached the solvent activity of the pure salt solution. The chemical potential, μ, of water and salt in the separate phases, however, was not demonstrated to be equal in these experiments.

Experimental Section

All chemicals were reagent grade and were used without further purification except tetrabutylammonium chloride, which was prepared by passing the commercially available bromide solution through a Dowex-1 chloride form ion-exchange resin. The preparation of univalent salts of polystyrenesulfonate has been given elsewhere.[10] The calcium ion form of PSS (mol wt ≈ 500,000) was prepared by neutralization of HPSS with standard $Ca(OH)_2$ until a pH of 5–6 was obtained for the product mixture. The magnesium ion (and in a few instances the calcium ion) form of PSS was prepared by passing HPSS through a deep cation-exchange resin bed of the appropriate divalent ion form. Care was taken to ensure the absence of acid in the column effluent by monitoring its pH. The product solutions (pH ~6) were dialyzed to remove low molecular weight impurities. The dilute solution, after dialysis, was concentrated by evaporation during exposure of the dialysis bag to a current of air at the ambient room temperature. The β-emitting, high specific activity radioactive nuclide 3×10^5-year chlorine-36 was purchased from the Nuclear Science and Engineering Corp. of Pittsburgh, Pa.

The Donnan equilibrium of polyelectrolyte and simple salt was studied in a cell which consisted of three compartments made of Lucite. The compartments, each with a capacity of approximately 2.5 ml, were separated by a visking membrane with an exposed area of 15 cm². Entry holes through the top of each circular compartment were used to fill the compartments with the desired solutions. The middle compartment contained the polyelectrolyte solution. The two outside compartments were filled with salt solutions of different concentrations. The inlet holes were sealed with a chemically inert tape to restrain solvent transport and the whole apparatus was agitated until equilibrium was reached. Usually 4 to 12 hr, depending on the relative concentrations of the solutions, was required to achieve equilibrium as evinced by the equivalence of salt concentration in the two outside compartments.

The analysis of solutions at equilibrium was performed as follows. The concentration of the salt solution which contained radioactive chlorine-36 as a tracer was determined by chlorine activity measurement. The salt concentration in the polyelectrolyte–salt mixture solution was determined by the same method. Employment of the radioactive nuclide, chlorine-36, for the measurement of the chloride concentration is believed to have many advantages over other methods, such as micropotentiometric titration with standardized $AgNO_3$ solution. The tracer method has higher sensitivity and eliminates the interference which is caused by the presence of polyelectrolyte in our case. The total cation concentration of the mixture was obtained by converting the mixture *via* ion exchange into polystyrenesulfonic acid and hydrochloric acid and by titrating the column effluent with standard base. The polymer concentration is the difference between total cation concentration and the amount of salt contained in the mixture. Owing to the high viscosity of the polymer solution, the amount of sample was always measured on a weight basis. The density of polymer was measured and molality and molarity were made available in this way.

A radiation Instrument Development Laboratories Model 49-50 scaler was used with a Model 2-6, 2π flow counter for proportional counting. The decay of chlorine-36 is characterized by β radiation of 0.71 MeV maximum energy. Inherent difficulties were encountered when solid samples were employed in the measurement. Careful attention needed to be given to the attainment of a suitable and reproducible geometrical arrangement and to the proper consideration of scattering and absorption of radiation by the sample

(10) P. Chu and J. A. Marinsky, *J. Phys. Chem.*, 71, 4352 (1967).

and its mount. The following approach proved to be satisfactory. (i) A weighed portion of the solution was transferred to a 2.5-cm diameter aluminum counting planchet on which a glass fiber filter paper was placed. The solution was absorbed by the paper uniformly. (ii) The sample was evaporated to dryness under an infrared lamp. In the case of HCl, the solution was exactly neutralized with NaOH before evaporation.

The dimension and weight of planchets and the glass fiber paper were kept as constant as possible: diameter, 2.4 cm; weight of planchets, 0.72–0.75 g; weight of filter paper, 0.30–0.032 g. A constant and reproducible geometry was assured by this procedure. With the low Z material of the planchets, the back scattering problem was minimized as well.

Because our samples had finite thickness, self absorption needed to be considered. Nervik and Stevenson[11] have carefully measured the self-scattering and self-absorption effects in various materials for β^- emitters of various maximum energies. Fortunately, in the concentration range studied, the thickness of our samples varied less than a maximum of 6 mg/cm^2. In this thickness range, a maximum correction factor of 4% was required. The correction factor varies very little from material to material in this energy region and thickness range (β_{max} = 0.71 MeV, total thickness = 10 mg/cm^2). Nevertheless, an experimental correction curve for different sample thickness was prepared and this correction was applied to each sample whenever necessary.

Results

The equilibrium data have been tabulated in Table I. The equilibrium concentrations of polyelectrolyte, m_2, and salt, m_3, in the central compartment are presented in columns 1 and 2 of each table. The concentration of salt in the two end compartments (M_3) is listed in column 3. The computed value of γ_2^+ is given in column 4. The precision of the analysis of M_3, zm_2, and ($zm_2 + m_3$) was found to be ±1% with standard samples employed to examine this aspect and is the basis for the error limits designated in the table for γ_2^+.

Discussion

If the basic assumptions that are made in the development of eq 10 and 11 are essentially correct, it should be possible to predict the trend in the value of γ_2^+ for comparison with the values of γ_2^+ obtained experimentally. It has been suggested here, on the basis of earlier examination of the additivity rule,[2-8] that in polyelectrolyte–salt mixtures the physical–chemical behavior of the polyelectrolyte should be unaffected by the presence of salt, its osmotic properties being identifiable with those of the pure polyelectrolyte at the water activity of the mixture.[8] If this is indeed

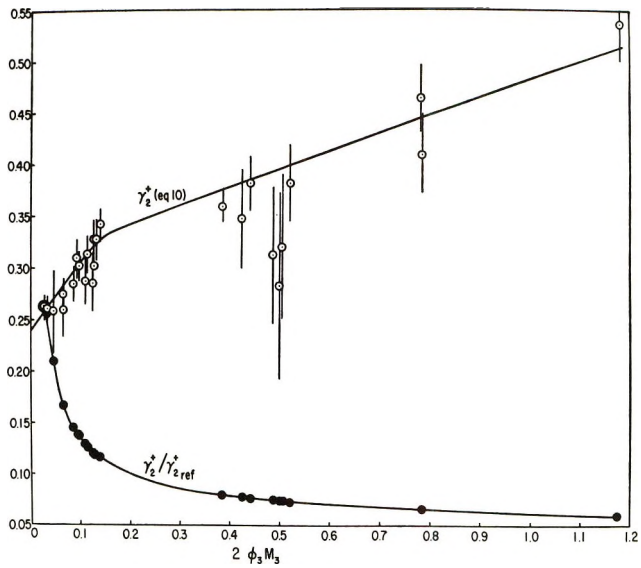

Figure 1. Comparison of $\gamma_2^+/\gamma_{2ref}^+$ with γ_2^+ (eq 10); NaPSS–NaCl–H_2O system.

the case, the value of γ_2^+, relative to a reference state concentration, should be calculable for each experimental situation with the integrated form of the Gibbs–Duhem equation to facilitate such a comparison. Such an approach has been used successfully to calculate the activity coefficient ratio of two exchanging ions in cross-linked polystyrenesulfonate ion-exchange resins.[12]

Even though, in the experiments that have been described, equilibrium of the water component in the separated phases may not have been reached, there is a sufficiently good estimate of the water activity from its upper limit value (deduced from the concentration of the polyelectrolyte-free salt) to assign reasonably accurate ϕ_2 and m_2z values[13] to test the correlative potential of this kind of analysis.

With decreasing water activity (increasing polyelectrolyte concentration) the computed value of $\gamma_2^+/\gamma_{2ref}^+$ decreases predicting γ_2^+ behavior contrary to that observed. This result is shown in Figure 1 for the NaPSS–NaCl–H_2O system where the values of $\gamma_2^+/\gamma_{2ref}^+$ have been normalized to coincide with the γ_2^+ value obtained from eq 10 at the highest water activity (lowest external salt concentration).

The results of earlier research have indicated that the osmotic coefficient of a polyelectrolyte is identifiable with its counterion activity coefficient. A theoretical examination of this relationship by Katchalsky and coworkers[14] appears to substantiate this empirical

(11) W. E. Nervik and P. C. Stevenson, *Nucleonics*, **10**, No. 3, 18 (1952).

(12) M. M. Reddy and J. A. Marinsky, *J. Macromol. Sci-Phys.*, **B5** (1), 135 (1971).

(13) M. Reddy and J. A. Marinsky, *J. Phys. Chem.*, **74**, 3884 (1970).

(14) A. Katchalsky, Z. Alexandrowicz, and O. Keden in "Chemical Physics of Ionic Solutions," B. E. Conway and R. G. Barradas, Ed., Wiley, New York, N. Y., 1966, p 295.

Table I: Donnan Distribution Studies

m_2	m_3	M_3	γ_2^+
	HPSS, HCl, H_2O		
0.0277	0.00732	0.0104	0.269 ± 0.018
0.0302	0.00960	0.0132	0.283 ± 0.018
0.0328	0.0495	0.0547	0.334 ± 0.068
0.0396	0.0267	0.0327	0.337 ± 0.038
0.0457	0.0457	0.0518	0.285 ± 0.050
0.0830	0.0189	0.0284	0.286 ± 0.018
0.0850	0.0286	0.0391	0.292 ± 0.041
0.103	0.0227	0.0353	0.313 ± 0.017
0.1035	0.0260	0.0386	0.302 ± 0.022
0.141	0.0509	0.0708	0.337 ± 0.023
0.142	0.0248	0.0425	0.339 ± 0.016
0.160	0.0508	0.0730	0.338 ± 0.018
0.184	0.0617	0.0888	0.359 ± 0.025
0.194	0.0354	0.0616	0.370 ± 0.019
0.218	0.0293	0.0565	0.365 ± 0.017
0.220	0.0355	0.0627	0.342 ± 0.017
0.228	0.0200	0.0446	0.349 ± 0.014
0.250	0.0485	0.0837	0.384 ± 0.019
0.267	0.297	0.353	0.459 ± 0.059
0.341	0.538	0.613	0.471 ± 0.078
	NaPSS, NaCl, H_2O		
0.0250	0.0204	0.0234	0.258 ± 0.040
0.0610	0.0272	0.0342	0.259 ± 0.025
0.0820	0.0094	0.0170	0.260 ± 0.013
0.0923	0.0061	0.0136	0.262 ± 0.011
0.1084	0.0528	0.0665	0.286 ± 0.028
0.1238	0.0312	0.0455	0.284 ± 0.017
0.1246	0.254	0.271	0.282 ± 0.090
0.1275	0.0213	0.0346	0.274 ± 0.015
0.1345	0.0419	0.0581	0.287 ± 0.022
0.1452	0.0345	0.0520	0.302 ± 0.014
0.1472	0.0322	0.0500	0.309 ± 0.018
0.1486	0.0490	0.0678	0.302 ± 0.022
0.1640	0.249	0.274	0.320 ± 0.071
0.1688	0.239	0.264	0.312 ± 0.066
0.193	0.0448	0.0696	0.328 ± 0.020
0.193	0.0374	0.0605	0.313 ± 0.018
0.200	0.0420	0.0672	0.328 ± 0.018
0.219	0.195	0.230	0.348 ± 0.048
0.2496	0.169	0.209	0.359 ± 0.038
0.284	0.0399	0.074	0.343 ± 0.016
0.317	0.186	0.239	0.382 ± 0.026
0.343	0.224	0.282	0.382 ± 0.038
0.529	0.331	0.426	0.411 ± 0.038
0.656	0.298	0.424	0.465 ± 0.033
0.938	0.432	0.636	0.537 ± 0.035
	LiPSS, LiCl, H_2O		
0.0210	0.0279	0.0303	0.238
0.0476	0.0317	0.0380	0.291
0.0609	0.0469	0.0559	0.324
0.0673	0.0540	0.0638	0.318
0.115	0.0608	0.0772	0.324
0.119	0.0412	0.0573	0.324
0.143	0.0367	0.0544	0.307
0.157	0.0566	0.0804	0.367
0.162	0.0562	0.0784	0.328
0.183	0.0511	0.0744	0.313
0.188	0.0588	0.0873	0.377
0.204	0.0627	0.0932	0.372
	NH_4PSS, NH_4Cl, H_2O		
0.0955	0.0509	0.0622	0.263
0.1176	0.0395	0.0532	0.273
0.1318	0.0423	0.0583	0.289
0.144	0.0461	0.0639	0.295
0.195	0.0389	0.0625	0.316
0.2145	0.0343	0.0591	0.315
0.3121	0.0692	0.112	0.359
0.332	0.0652	0.110	0.363
0.4525	0.2570	0.3427	0.442
0.4816	0.2825	0.3755	0.450
	KPSS, KCl, H_2O		
0.0390	0.0086	0.0126	0.253
0.0445	0.0299	0.0352	0.259
0.0650	0.0102	0.0164	0.249
0.0813	0.0810	0.0903	0.242
0.0917	0.0923	0.1044	0.281
0.0960	0.0255	0.0362	0.270
0.0960	0.0289	0.0400	0.276
0.145	0.0196	0.0349	0.294
0.145	0.0217	0.0368	0.281
0.148	0.0182	0.0340	0.306
0.165	0.0999	0.121	0.281
0.166	0.0848	0.1066	0.297
0.246	0.0325	0.0584	0.295
0.253	0.0378	0.0642	0.282
0.302	0.0368	0.0669	0.280
	CsPSS, CsCl, H_2O		
0.0337	0.0412	0.0446	0.210
0.0445	0.0216	0.0259	0.213
0.0650	0.0319	0.0388	0.235
0.0680	0.0569	0.0644	0.235
0.0885	0.0327	0.0419	0.237
0.0981	0.0393	0.0503	0.256
0.1020	0.0287	0.0392	0.237
0.1034	0.0368	0.0482	0.255
0.1247	0.0626	0.0773	0.264
0.1271	0.0440	0.0576	0.247
0.1490	0.0522	0.0690	0.262
0.156	0.0396	0.0567	0.267
0.159	0.0599	0.0776	0.254
0.2619	0.0633	0.0937	0.288
0.280	0.0481	0.0798	0.301
	TMAPSS, TMACl, H_2O		
0.0574	0.0180	0.0242	0.254
0.0657	0.0203	0.0274	0.254
0.0946	0.0168	0.0270	0.281
0.143	0.0542	0.0714	0.279
0.1432	0.0388	0.0557	0.288
0.1500	0.0224	0.0383	0.287
0.270	0.187	0.237	0.434
0.447	0.194	0.275	0.438
0.617	0.267	0.395	0.514

Table I (*Continued*)

m_2	m_3	M_3	γ_2^+
	TEAPSS, TEACl, H_2O		
0.0393	0.0272	0.0311	0.213
0.0699	0.0340	0.0420	0.256
0.0750	0.0237	0.0312	0.232
0.0835	0.0478	0.0565	0.228
0.0966	0.0506	0.0610	0.238
0.1111	0.0197	0.0303	0.242
0.1112	0.0222	0.0330	0.241
0.1150	0.0278	0.0398	0.254
0.1240	0.0660	0.0811	0.272
0.1985	0.0558	0.0799	0.297
0.2460	0.0424	0.0722	0.329
0.3040	0.0548	0.0905	0.311
	TBAPSS, TBACl, H_2O		
0.0349	0.0395	0.0436	0.247
0.0459	0.0166	0.0215	0.245
0.0719	0.0426	0.0516	0.277
0.0841	0.0564	0.0634	0.177
0.0885	0.0581	0.0674	0.227
0.0944	0.0642	0.0738	0.190
0.112	0.0312	0.0430	0.251
0.118	0.0610	0.0742	0.248
0.1302	0.0695	0.0841	0.248
0.1429	0.0586	0.0725	0.218
0.162	0.0680	0.0856	0.246
0.1919	0.0613	0.0830	0.266
0.2184	0.0760	0.1023	0.283
0.3227	0.0981	0.1399	0.315

m_2	m_3	M_3	γ_2^+
	$Ca(PSS)_2$, $CaCl_2$, H_2O		
0.0457	0.01113	0.0124	0.093 ± 0.019
0.049	0.0078	0.00865	0.058 ± 0.013
0.0542	0.02233	0.0240	0.0992 ± 0.030
0.0678	0.00674	0.00838	0.0917 ± 0.0072
0.078	0.0100	0.0120	0.0985 ± 0.0075
0.087	0.0129	0.0150	0.0890 ± 0.0093
0.1015	0.01224	0.0150	0.101 ± 0.013
0.108	0.0189	0.0219	0.0972 ± 0.016
0.114	0.00890	0.0112	0.0776 ± 0.0086
0.114	0.00752	0.01035	0.106 ± 0.008
0.129	0.0126	0.0166	0.126 ± 0.012
0.246	0.0247	0.0346	0.176 ± 0.015
	$Mg(PSS)_2$, $MgCl_2$, H_2O		
0.0336	0.00936	0.0107	0.138 ± 0.023
0.1047	0.01778	0.02185	0.145 ± 0.018
0.106	0.01658	0.02035	0.133 ± 0.008
0.110	0.0290	0.03535	0.214 ± 0.027
0.1116	0.02044	0.0252	0.160 ± 0.019
0.1618	0.0320	0.0414	0.231 ± 0.014
0.194	0.0612	0.0756	0.279 ± 0.034
0.217	0.03066	0.0418	0.217 ± 0.020
0.252	0.0287	0.0418	0.238 ± 0.019
0.265	0.04057	0.0584	0.304 ± 0.024
0.317	0.0392	0.0604	0.329 ± 0.024
0.350	0.0423	0.0668	0.381 ± 0.027

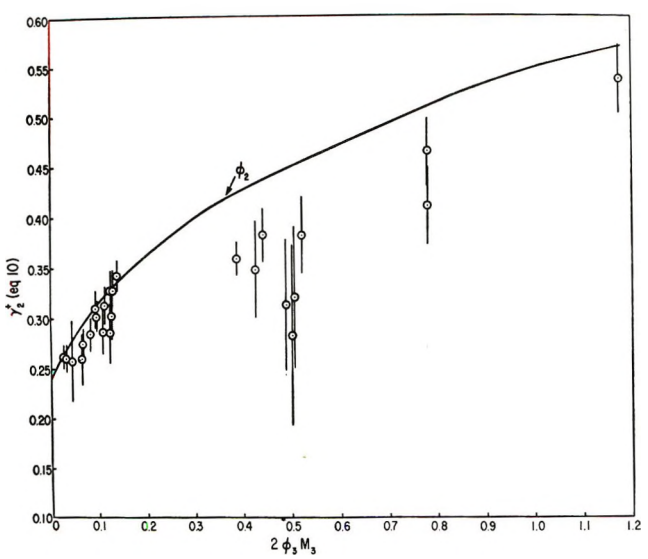

Figure 2. Comparison of ϕ_2 with γ_2^+ (eq 10); NaPSS–NaCl–H_2O system.

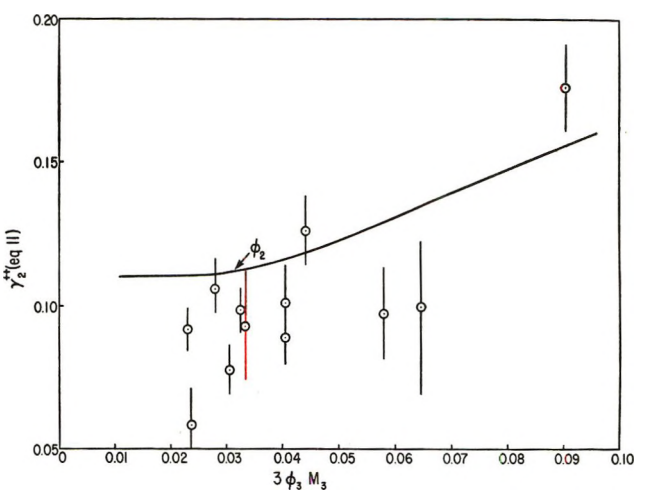

Figure 3. Comparison of ϕ_2 with γ_2^{2+} (eq 11); $Ca(PSS)_2$–$CaCl_2$–H_2O system.

observation. Indeed, when ϕ_2 is compared with γ_2^+ in these experiments there is fair agreement between them as well. This result is seen in Figures 2 and 3 where ϕ_2[13,15] and γ_2^+ are compared for the NaPSS–NaCl–H_2O and $Ca(PSS)_2$–$CaCl_2$–H_2O systems.

Until recently this correlation of ϕ_2 with γ_2^+ would have been accepted without further discussion. Indeed, the earlier use of this concept by one of us (J. A. M.) has facilitated correlation of Donnan distribution data obtained with cross-linked gels.[16,17] In addition, it has provided the basis for fairly accurate predictions of

(15) M. Reddy, J. A. Marinsky, and A. Sarkar, *J. Phys. Chem.*, **74**, 3891 (1970).

ion-exchange selectivity.[16,18] In fact, this research project, conceived initially to test further the additivity behavior of polyelectrolyte and simple salt, was expected to be facilitated by employing this relationship between ϕ_2 and γ_2^+.

In the most recent work by J. A. M., however, it has been shown conclusively that the use of the integrated form of the Gibbs–Duhem equation to compute activity coefficient ratios of counterions in ion-exchange gels for the interpretation of ion-exchange selectivity is more useful than the earlier approach that identifies ϕ_2 with γ_2^+.[16,18] A more satisfying correlation of prediction with experiment was obtained. In the earlier examination of this problem[16,18] additional parameters needed to be invented to achieve the same predictive quality in the computations.

The integrated form of the Gibbs–Duhem equation has also been employed recently to compute relative molal activity coefficient values for salt-free polymethacrylic acid at different degrees of dissociation and concentration.[19] The correlation obtained between these values and estimates of deviations from ideality that were derived from parallel potentiometric studies of the pure polyelectrolyte further demonstrate the validity of this approach to γ_2^+.

It is believed on the basis of the above arguments that if the additivity rule is valid and polyelectrolyte behaves as if no simple salt is present in the MPSS, MCl, H_2O systems, use of the integrated form of the Gibbs–Duhem equation should have resolved relative counterion activity coefficient values that describe the physical–chemical properties of the polyelectrolyte most accurately.

The fact that γ_2^+ and ϕ_2 resemble each other closely while there is no such relationship predicted between them when the Gibbs–Duhem equation is employed may indicate that the observed additivity behavior of polyelectrolyte and simple salt[2-8] is a fortuitous result and that a complicated interaction between polyelectrolyte and simple salt is instead operative. If this is the case the assumption that the Gibbs–Duhem equation may be used to analyze the three-component systems as hypothetical two-component systems is false and responsible for the complete lack of agreement between ϕ_2 and γ_2^+ computed by this approach.

Acknowledgment. The authors wish to express their appreciation to T. A. Brodof of the Dow Chemical Co. for supplying sodium polystyrenesulfonate and to the U. S. Atomic Energy Commission for financial support through Contract No. AT(30-1)-2269.

(16) J. A. Marinsky, "Interpretation of Ion-Exchange Phenomena" in "Ion Exchange," Vol. 1, Marcel Dekker, New York, N. Y., 1966, p 353.

(17) J. A. Marinsky, *J. Phys. Chem.*, **71**, 4349 (1967).

(18) J. A. Marinsky, *ibid.*, **71**, 1572 (1967).

(19) G. Torrence, S. Amdur, and J. A. Marinsky, *ibid.*, **75**, 2144 (1971).

Thermodynamics of the Association of Aqueous Europium(III) and Sulfate Ions

by Clarence F. Hale and F. H. Spedding*

Ames Laboratory, U. S. Atomic Energy Commission and Department of Chemistry, Iowa State University, Ames, Iowa 50010 *(Received February 25, 1972)*

Publication costs assisted by Ames Laboratory, U. S. Atomic Energy Commission

Differential uv absorption spectrophotometry was employed to investigate the formation of aqueous $EuSO_4^+$ from Eu^{3+} and SO_4^{2-} as a function of europium(III) and sulfate concentrations, wavelength, temperature, and constant (0.045 *m*) and variable ionic strengths below 0.046 *M*. The equations used to determine the association constant of $EuSO_4^+$ were modified to correct for any interference due to the presence of $Eu(SO_4)_2^-$ and $NaSO_4^-$ ions. The association constants at infinite dilution were found to be 4.69×10^3, 7.09×10^3, 10.96×10^3, and 16.78×10^3 at 25.0, 38.5, 51.6 and 65.1°, respectively, yielding $\Delta H_1^\circ = 6.2$ kcal/mol and $\Delta S_1^\circ = 37.4$ cal/(mol deg) after assuming $\Delta Cp_1^\circ = 0$. When these association constants were interpreted in terms of a finite ΔCp_1° term, the resulting ΔH_1° and ΔS_1° values at 25° agree very well with those obtained from calorimetry. The association constant at 25° is in excellent agreement with those obtained from conductance studies, but not with those from investigations employing different methods. The discrepancy has been noted before and evidence is now given to show that it was probably due to significant formation of the $Eu(SO_4)_2^-$ complex in those previous investigations other than conductance. The sign and magnitude of the ΔH_1° and ΔS_1° terms strongly suggest that in dilute aqueous solutions the monosulfato complex is primarily inner-sphere. A limited study was also made on the disulfato system at the same constant ionic strength, temperatures, and wavelengths as for the monosulfato complex.

Introduction

Previous investigations on the formation of aqueous monosulfato rare earth(III) ions as illustrated in eq 1a show little, if any, agreement in their equilibrium constants reported for zero ionic strength.[1-5]

$$RE^{3+} + SO_4^{2-} = RESO_4^+ \qquad (1a)$$

Comparisons are difficult to make for those studies at high ionic strengths, particularly in various media, due to differences in the activity coefficient term or to undefined medium effects.[6,7] Of particular interest are those formation constants determined at low ionic strengths by spectrophotometry[2,3,8] and conductance.[4] The results obtained from conductance studies should be highly reliable since the work was carried out in very dilute stoichiometric solutions without the addition of added "inert" electrolytes. However, the equilibrium values from spectrophotometry have been criticized, since they are significantly lower than those from conductance studies. The reasons given for this descrepancy have been vague and inconclusive.[2] In fact, the usefulness itself of spectrophotometry for this type of investigation has been severely questioned.[9,10]

It has been postulated that the aqueous rare earth(III) monosulfate ions are primarily outer-sphere; *i.e.*, at least one water molecule separates the rare earth and sulfate ions. This belief probably stems from their similarity to the first row transition metal bivalent sulfates which generally have been considered as outer-sphere: *e.g.*, fairly consistent equilibrium constant values within each series and failure of sulfate ion to affect[11] the visible absorption spectra of the aquated cations for both series in dilute solutions. However, these observations for the rare earth ions could be explained as due to the high degree of shielding of their 4f bonding electrons by the filled 5s and 5p orbitals. Manning has analyzed the K_1/K_2 ratios for many of the aqueous rare earth chlorides and some sulfates in terms of hydration numbers and a theorem proposed by Bjerrum. He concluded that the rare earth sulfates are clearly of the outer-sphere type.[7]

On the contrary, the recent solvent extraction and calorimetric studies of aqueous rare earth sulfate formation in 2 *M* $NaClO_4$ by DeCarvalho aud Choppin[12] strongly support the inner-sphere model. Ultrasonic absorption studies of aqueous monosulfate formation on a number of rare earths have led Fay, Litchinsky,

(1) L. G. Sillin and A. E. Martell, "Stability Constants," 2nd ed, Metcalfe and Cooper Ltd., London, 1964, p 237.

(2) J. C. Barnes, *J. Chem. Soc.*, 3880 (1964).

(3) J. C. Barnes and C. B. Monk, *Trans. Faraday Soc.*, **59**, 578 (1963).

(4) F. H. Spedding and S. Jaffe, *J. Amer. Chem. Soc.*, **76**, 882 (1954).

(5) R. M. Izatt, D. Eatough, J. J. Christensen, and C. H. Bartholomew, *J. Chem. Soc. A*, 47 (1969).

(6) T. Sekine, *J. Inorg. Nucl. Chem.*, **26**, 1463 (1964).

(7) P. G. Manning, *Can. J. Chem.*, **43**, 2911 (1965).

(8) T. W. Newton and G. M. Arcand, *J. Amer. Chem. Soc.*, **75**, 2449 (1953).

(9) C. B. Monk, "Chemical Physics of Ionic Solutions," 1st ed, B. E. Conway and R. G. Barradas, Ed., Wiley, New York, N. Y., 1966, p 185.

(10) C. B. Monk, "Electrolytic Dissociation," 1st ed, Academic Press, London, 1961, p 191.

(11) J. Smithson and R. J. P. Williams, *J. Chem. Soc.*, 457 (1958).

(12) R. G. DeCarvalho and G. R. Choppin, *J. Inorg. Nucl. Chem.*, **29**, 737 (1967).

and Purdie to the conclusion that the complexes formed are predominately inner-sphere.[13] In addition, there is some belief that the first row transition metal sulfates may actually be inner-sphere.[14]

Owing to these conflicting opinions, an investigation was initiated to determine (1) why the formation constants for the monosulfate complex obtained from spectrophotometry have been significantly lower than those from conductance and (2) whether the complex formed between rare earth(III) ion and sulfate ion is primarily of the inner- or outer-sphere type.

It was decided to use europium perchlorate, since it was the only rare earth(III) ion that was found to exhibit a new absorption peak (240 mμ at 25°) when small amounts of sulfate ion were added to a dilute solution of the salt. Although some other rare earth perchlorates do show a general broadening and increase in their uv absorption peaks upon the addition of sodium sulfate, this is not considered as conclusive evidence for a new species.[15] Interference due to $Eu(SO_4)_2^-$ ion could not be reduced to acceptable levels. Therefore, a limited study was also made on this system, since the necessary data required to correct for its presence under the same experimental conditions as employed in the mono- investigation were not available. However, suitable thermo-dynamic data were available for $NaSO_4^-$.[16,17]

Experimental Section

Reagents. The stock and test solutions were prepared volumetrically using doubly distilled water. All glassware employed was made of Pyrex and except for the beakers possessed class "A" tolerances.

The europium perchlorate stock solutions were made up by dissolving the oxide (99.97% pure) with reagent grade perchloric acid so that the resulting solution had a very slight excess of acid. The concentrations of these stock solutions were determined by EDTA titration.

The stock sodium sulfate solutions were prepared directly from Baker Analyzed reagent grade salt, after drying at 140°. The purity of the salt was verified gravimetrically by precipitation of the sulfate as the barium salt.

The sodium perchlorate stock solutions were made up from the reagent grade salt manufactured by the G. Frederick Smith Chemical Co. without further purification. It was analyzed by weighing as the anhydrous salt, after drying at 600°. The concentrations of all the stock solutions were known to an accuracy of ±0.2%.

The test solutions were prepared directly in 200-ml flasks by the use of burets and pipets at 25.0°. Those used in the constant ionic strength studies were made up to possess the same 0.045 ± 0.001 *m* ionic strength at all experimental temperatures at equilibrium. They were prepared in pairs, each having identical stoichiometric concentrations of each salt, except the reference solutions which contained no sodium sulfate. The differential absorbancies of 12 to 14 and 8 to 10 of these pairs were measured at each temperature and wavelength for those investigations at constant and variable ionic strengths, respectively. Sodium perchlorate was used only in those test solutions made up to a constant ionic strength. The test solutions were found to possess pH's of 5.0 ± 0.1. To calculate the changes in molar concentration with temperature, the densities of the test solutions were assumed to be those of pure water. The errors thus introduced were calculated to be insignificant at the low ionic strengths used.

Analysis of the Test Solutions. A Cary Model 14 recording spectrophotometer was utilized for the measurement of the experimental absorbancies. It was equipped with a thermostatable cell compartment and cell holders. An external water bath, held to at least ±0.1° at all the temperatures employed, was used to supply the constant temperature liquid for the Cary and to prewarm those test solutions studied above 25°. The experimental temperatures were determined to have an accuracy of ±0.1° at 25.0, 38.5, and 51.6° and ±0.2° at 65.1°.

The optical cells employed were cylindrical and made by Aminco from fused quartz. To correct for mismatching and base-line drift, the sample and reference cells were filled with distilled water and compared at all the wavelengths employed. This was done at the experimental temperature before and after the initial and final test solutions were examined. The absorbancies of the two cells with distilled water were never found to differ by more than 0.004 absorbancy unit. During this investigation, the path lengths were varied from 2 to 10 cm, so that the majority of experimental absorbancies would fall between 0.2 and 1.0.

The optical cells were filled by the use of a special pipet so designed that it could be quickly loaded and drained. The cells were emptied by a needle-nosed Pyrex tube attached to an aspirator. Three to four rinsings were generally found necessary before the differential absorbancies became constant. Readings were then taken every 10 min until no change was noted for at least 20 min. For maximum accuracy, all readings were taken manually and not from a recording of the spectra.

Equations and Definitions of Terms. The molar thermodynamic equilibrium constant $K_1°$ for the as-

(13) D. P. Fay, D. Litchinsky, and N. Purdie, *J. Phys. Chem.*, **73**, 544 (1969).

(14) Discussion of paper on Section II in "Chemical Physics of Ionic Solutions," 1st ed, B. E. Conway and R. G. Barradas, Ed., Wiley, New York, N. Y., 1966, pp 281–290.

(15) T. W. Newton and F. B. Baker, *J. Phys. Chem.*, **61**, 934 (1957).

(16) I. L. Jenkins and C. B. Monk, *J. Amer. Chem. Soc.*, **72**, 2695 (1950).

(17) G. Atkinson and C. J. Hallada, *ibid.*, **84**, 721 (1962).

sociation of europium(III) and sulfate ions as expressed by eq 1b is the product of its formation constant K_1 and its activity coefficient factor ($y_\pm$).

$$Eu^{3+} + SO_4^{2-} \rightleftharpoons EuSO_4^+ \quad (1b)$$

$$K_1 = \frac{[EuSO_4^+]}{[Eu^{3+}][SO_4^{2-}]} \quad (2a)$$

$$K_1^\circ = K_1\left\{\frac{y_{EuSO_4^+}}{(y_{Eu^{3+}})(y_{SO_4^{2-}})}\right\} \quad (2b)$$

Similarly for disulfato formation

$$EuSO_4^+ + SO_4^{2-} \rightleftharpoons Eu(SO_4)_2^- \quad (3)$$

$$K_2 = \frac{[Eu(SO_4)_2^-]}{[EuSO_4^+][SO_4^{2-}]} \quad (4a)$$

$$K_2^\circ = K_2\left\{\frac{y_{Eu(SO_4)_2^-}}{(y_{EuSO_4^+})(y_{SO_4^{2-}})}\right\} \quad (4b)$$

In this investigation the activity coefficient factor, although unknown, was assumed to have been invariant at each temperature for those studies made at constant ionic strength. To keep the equations as simple as possible, the hydration spheres of the ions have not been shown.

The derivations of eq 5a, 7, and 9 used to evaluate K_1, K_2, $(\epsilon_1 - \epsilon^\circ)$ and $(\epsilon_2 - \epsilon^\circ)$ from the differential absorbancy data assumed that the Beer–Lambert law[18] and the law of mass action were applicable over the experimental conditions employed. Their derivations have been given elsewhere (see ref 10 and 19, pp 186 and 274–277, respectively). Equation 7 shows a slight modification to correct for the concentration of $NaSO_4^-$ ion pairs. At the concentrations and wavelengths employed, the absorptions by sodium sulfate were found to be unimportant. Also, the formation of bisulfate ion was calculated to be insignificant.

$$\frac{[SO_4^{2-}]}{\bar{a}} = \frac{1}{K_1(\epsilon_1 - \epsilon^\circ)} + \frac{[SO_4^{2-}]}{(\epsilon_1 - \epsilon^\circ)} \quad (5a)$$

$$[SO_4^{2-}] = S - [EuSO_4^+] - [NaSO_4^-] \quad (5b)$$

$$[EuSO_4^+] = \frac{A_s - A_r}{(\epsilon_1 - \epsilon^\circ)L} \quad (5c)$$

$$[NaSO_4^-] = \frac{Q(N + 2S)[SO_4^{2-}]}{1 + Q[SO_4^{2-}]} \quad (6)$$

$$\{\bar{a} + K_2[SO_4^{2-}]\{\bar{a} - (\epsilon_2 - \epsilon^\circ)\}\} = (\epsilon_1 - \epsilon^\circ) - \frac{1}{K_1}\left\{\frac{\bar{a}}{[Eu^{3+}]}\left(1 + \frac{[NaSO_4^-]}{[SO_4^{2-}]}\right)\right\} \quad (7)$$

$$[Eu^{3+}] = \frac{E}{1 + K_1[SO_4^{2-}] + K_1K_2[SO_4^{2-}]^2} \quad (8)$$

$$\bar{a} = (\epsilon_2 - \epsilon^\circ) + \left\{\left[(\epsilon_1 - \epsilon^\circ) - \bar{a}\left(1 + \frac{1}{K_1[SO_4^{2-}]}\right)\right]\frac{1}{[SO_4^{2-}]}\right\}\frac{1}{K_2} \quad (9)$$

$$[SO_4^{2-}] = S - \frac{A_s - A_r}{L} \times \left\{\frac{1 + 2K_2[SO_4^{2-}]}{(\epsilon_1 - \epsilon^\circ) + (\epsilon_2 - \epsilon^\circ)K_2[SO_4^{2-}]}\right\} - [NaSO_4^-] \quad (10)$$

$$K_1 = \frac{\bar{a}}{[SO_4^{2-}]\{(\epsilon_1 - \epsilon^\circ) + (\epsilon_2 - \epsilon^\circ)K_2[SO_4^{2-}] - \bar{a}(1 + K_2[SO_4^{2-}])\}} \quad (11)$$

where $\bar{a} = (A_s - A_r)/EL$, $\bar{a} = (A_s - A_r)/SL$, $Q = [NaSO_4^-]/\{[Na^+][SO_4^{2-}]\}$, E = molar concentration of $Eu(ClO_4)_3$, S = molar concentration of Na_2SO_4, N = molar concentration of $NaClO_4$, L = path length in centimeters (same for both sample and reference cells), A_s = absorbancy of the sample solution, A_r = absorbancy of the reference solution, ϵ° = molar extinction coefficient of Eu^{3+}, ϵ_1 = molar extinction coefficient of $EuSO_4^+$, ϵ_2 = molar extinction coefficient of $Eu(SO_4)_2^-$, [X] = molar concentration of X at equilibrium

$$\left\{\log K_1 - \frac{\Delta Z^2 A I^{1/2}}{1 + I^{1/2}}\right\} = \log K_1^\circ - (\Delta Z^2 A D)I \quad (12)$$

$\Delta Z^2 = \Sigma Z^2(\text{products}) - \Sigma Z^2(\text{reactants})$, Z = charge on the ion, D is an empirical constant whose value is a function of the temperature, pressure, electrolytes, and medium employed, A is the Debye–Hückel constant (temperature and pressure dependent), and I = equilibrium ionic strength

$$I = 6E + 3S + N - 6[EuSO_4^+] - 8[Eu(SO_4)_2^-] - 2[NaSO_4^-] \quad (13)$$

Determination of K_1, K_1°, and K_2. Equation 5a was used for the single study at constant ionic strength in which the stoichiometric europium perchlorate concentrations were held constant, while those of sodium sulfate were allowed to vary. The presence of $Eu(SO_4)_2^-$ was ignored. First a plot of $S/\bar{a}$ *vs.* S was made by allowing $[SO_4^{2-}] = S$. The resulting slope, $1/(\epsilon_1 - \epsilon^\circ)$, was used to calculate the initial $[EuSO_4^+]$ concentrations from eq 5c. The $[NaSO_4^-]$ concentrations were then obtained from eq 6, assuming $[SO_4^{2-}] = S$. The first values for $[SO_4^{2-}]$ were then calculated from eq 5b and the procedure was repeated, using progressively more accurate $[SO_4^{2-}]$ values each time, until the change in K_1 as determined from the intercept was less than 0.1%.

A value of 5.0 was used for the formation constant of the $NaSO_4^-$ ion pair, Q, at 25° and infinite dilution.[16] Equation 11 was used with $D = 0.3$ to calculate its

(18) F. Daniels, J. H. Mathews, J. W. Williams, P. Bender, and R. A. Alberty, "Experimental Physical Chemistry," 5th ed, McGraw-Hill, New York, N. Y., 1956, p 20.

(19) J. C. Rossotti and H. Rossotti, "The Determination of Stability Constants," 1st ed, Maple Press Co., York, Pa., 1961, p 277.

ionic strength dependence. It was felt that this value for D, as recommended by Davies,[20] could be safely used because of the fairly low ΔZ^2 term of -4 for $NaSO_4^-$ formation and the dilute ionic strengths employed. The temperature dependence of Q was calculated from the van't Hoff equation (assuming $\Delta Cp^\circ = 0$) using the ΔH° value of 1.1 kcal/mol determined calorimetrically at 25° by Atkinson and Hallada.[17]

Accurate K_1 values were obtained at a constant ionic strength of 0.045 m from studies where the stoichiometric sulfate concentrations were held constant while those of europium were allowed to vary. The basic procedure was very similar to the one just discussed for eq 5a. First K_1 and $(\epsilon_1 - \epsilon^\circ)$ were obtained from an experimental set of differential absorbancies by using eq 7 in conjunction with eq 6, 8, and 10, which initially set K_2 and $(\epsilon_2 - \epsilon^\circ) = 0$, $[Eu^{3+}] = E$, and $[SO_4^{2-}] = S$. An iterative process was then employed using refined values for $[SO_4^{2-}]$, $[NaSO_4^-]$, and $[Eu^{3+}]$, until the change in K_1 was less than 0.1%, generally after six to eight cycles.

These initial K_1 and $(\epsilon_1 - \epsilon^\circ)$ values were then employed in eq 9 in conjunction with eq 6 and 10 to obtain K_2 and $(\epsilon_2 - \epsilon^\circ)$ at a constant ionic strength of 0.045 m. Here the stoichiometric europium concentrations were held constant while those of sulfate were allowed to vary. Again, an iterative process was used which set $[SO_4^{2-}] = S$ for the first cycle. The procedure was repeated using progressively more accurate $[SO_4^{2-}]$ and $[NaSO_4^-]$ concentrations each time, until the change in K_2 was less than 0.1%; four cycles were required.

These initial K_2 and $(\epsilon_2 - \epsilon^\circ)$ values were then used to obtain better K_1 and $(\epsilon_1 - \epsilon^\circ)$ values from eq 7 as described above. These in turn were employed to obtain better K_2 and $(\epsilon_2 - \epsilon^\circ)$ values from eq 9 by repeating the above iterative process. This procedure was repeated until the change in both K_1 and K_2 was less than 0.1%; three cycles were required.

The final $(\epsilon_1 - \epsilon^\circ)$, $(\epsilon_2 - \epsilon^\circ)$, and K_2 values from the constant ionic strength studies, in which corrections were made for the presence of both $Eu(SO_4)_2^-$ and $NaSO_4^-$ ion pairing, were then employed in the investigation made to determine K_1 at various ionic strengths. It was assumed that the differential extinction coefficients at any one wavelength and temperature remained invariant over the entire ionic strength range of 0.046 to 0.006 M. Since K_2 was determined only at 0.045 m, Davies' equation[20] was used to calculate its value at the other ionic strengths employed. Due to the short extrapolation, low $|\Delta Z^2|$ value, and the small correction which K_2 makes to K_1, this use of Davies' equation provided the desired accuracy. Since K_2 was measured at each of the temperatures employed, no previous knowledge of ΔH_2 was required.

First $[EuSO_4^+]$ was calculated directly from eq 5c. Then an approximate ionic strength for a single test solution was determined from eq 13 by ignoring the presence of $Eu(SO_4)_2^-$ and $NaSO_4^-$. Using this approximate ionic strength, K_2 and Q were obtained from Davies' equation. Then, setting $[SO_4^{2-}] = S$, the initial $[NaSO_4^-]$ and $[SO_4^{2-}]$ concentrations were calculated using eq 6 and 10. Next, K_1 was calculated directly from eq 11, $[Eu^{3+}]$ from eq 8, $[Eu(SO_4)_2^-]$ from eq 2a and 4a and $[EuSO_4^+]$ from eq 2a. After this process was completed for the desired number of test solutions having different ionic strengths, but whose differential absorbancies were measured at the same wavelength and temperature, the resulting K_1 values were extrapolated to infinite dilution using eq 12 in the usual manner. The intercept yielded the desired molar thermodynamic formation constant K_1°. This process was repeated, but without eq 5c, using progressively more accurate $[SO_4^{2-}]$ concentrations, until the change in K_1° was less than 0.1%. Generally, only two iterations were required to reach convergence.

The method of least squares was used exclusively throughout this investigation. All of the data were weighted in the manner described by Wolberg.[21] In the calculations leading to K_1, K_1°, and K_2, the Pierce–Chauvenet rejection criterion was invoked to reject any experimental points falling outside the 95% confidence level.[22] Each time a point was rejected, that particular set of iterations was repeated from the beginning. After converting the equations into FORTRAN IV computer language, an IBM Model 360 digital computer performed the calculations.

Results

The absorbancies of dilute aqueous europium perchlorate solutions (1×10^{-3} to 10×10^{-3} M) were studied at 25° by recording the spectra of the pure solutions *vs.* distilled water from 300 to 200 mμ. Only five peaks were observed and they possessed very low extinction coefficients; *i.e.*, $\epsilon^\circ < 1$. A strong absorption started around 240 mμ and continued beyond 200 mμ, the limit of the spectrophotometer. Jorgensen reports that a peak exists for europium(III) ion at 188 mμ.[23] The extinction coefficients, based on decadic logarithms, were calculated to be 2.2×10^2, 1.3×10^2, 5×10^1, 9, and 1.4 l./(mol cm) at 200, 210, 220, 230, and 240 mμ, respectively. The peak reported at 210 mμ by Stewart and Kato[24] was not found.

The addition of sodium sulfate to 5×10^{-3} M solutions of europium perchlorate, so that the final solutions were 1×10^{-3} to 20×10^{-3} M in sulfate ion, produced

(20) C. W. Davies, "Ion Association," 1st ed, Butterworths, London, 1962, p 41.

(21) J. R. Wolberg, "Prediction Analysis," 1st ed, Van Nostrand, New York, N. Y., 1967, p 36.

(22) W. Chauvenet, "Spherical and Practical Astronomy," Vol. V, Lippincott, Philadelphia, Pa., 1868, p 558.

(23) C. K. Jorgensen and J. S. Brinen, *Mol. Phys.*, 6, 629 (1963).

(24) D. C. Stewart and D. Kato, *Anal. Chem.*, 30, 164 (1958).

Table I: Formation Constants and Differential Extinction Coefficients[a] for the Monosulfato System at a Constant Ionic Strength of 0.045 *m* as a Function of Wavelength and Temperature

	Temp, °C							
	25.0		38.5		51.6		65.1	
λ, mμ	K_1	$(\epsilon_1 - \epsilon^\circ)$	K_1	$(\epsilon_1 - \epsilon^\circ)$	K_1	$(\epsilon_1 - \epsilon^\circ)$	K_1	$(\epsilon_1 - \epsilon^\circ)$
230	568	70.4	789	70.9	1131	69.7	1670	67.9
236	564	80.9	798	84.6	1132	87.5	1637	88.3
240	576	81.0	791	87.6	1131	93.0	1691	95.8
245	565	75.0	795	83.7	1129	92.4	1689	97.9
250	578	63.3	789	73.7	1136	83.8	1716	92.1
255	575	49.6	805	59.6	1120	71.0	1704	80.5

[a] Units: l./(mol cm).

a new peak at 240 mμ, which was proportional to the sulfate concentration. This observation confirmed that reported by Barnes.[2]

The initial study to determine K_1 was made at 25° by measuring the changes in the differential absorbancies from 230 to 250 mμ for a series of solutions in which the europium concentration was held constant at 5×10^{-3} *M*, while that of the sulfate ion was varied from 3×10^{-3} to 13×10^{-3} *M*. The ionic strength was held constant at 0.049 *m*.

The experimental data were found to fit eq 5a very well. However, K_1 was a distinct function of wavelength, *i.e.*, 275, 289, and 337 at 230, 240, and 250 mμ, respectively. This drift was much greater than that expected from the experimental error. The simplest explanation was that the disulfate complex was also being formed in appreciable amounts and, since the $(\epsilon_1 - \epsilon^\circ)/(\epsilon_2 - \epsilon^\circ)$ ratio would not be expected to remain constant with wavelength, K_1 would also become a function of wavelength.[25]

A check on this hypothesis of di-ligand interference was made by studing the association at approximately the same ionic strength and temperature, but now at significantly lower sulfate:europium ratios; *i.e.*, <1. The stoichiometric sulfate concentrations were held constant while those of europium(III) were allowed to vary.

The resulting differential absorbancies were found to fit eq 7 very well, yielding linear curves at each experimental wavelength from 225 to 255 mμ, even though K_2 and $(\epsilon_2 - \epsilon^\circ)$ were set equal to zero. The K_1 values were now invariant with wavelength and much larger than before, *i.e.*, 600 as compared to about 300. Results from this study were used to select the best constant ionic strength and range of salt concentrations to reduce the formation of $Eu(SO_4)_2^-$ as much as possible, yet providing accurate formation constants and extinction coefficients for the monosulfate complex. These were calculated to be 1.1×10^{-3} *M* for sulfate and 1.4 to 8×10^{-3} *M* for europium at a constant ionic strength of 0.045 *m* over the wavelength range of 230 to 255 mμ.

The final formation constants and extinction coefficients for the monosulfate complex at the ionic strength of 0.045 ± 0.001 *m* for all the temperatures and wavelengths studied are shown in Table I.[26] The formation constants at each temperature were found to be independent of wavelength. The averages of the standard deviations for K_1 were found to be 1.1, 1.0, 0.6, and 1.1% at 25.0, 38.5, 51.6, and 65.1°, respectively. The Pierce–Chauvenet rejection criterion generally discarded one point and never more than four.

The final formation constants and extinction coefficients for the disulfate complex as a function of wavelength and temperature are shown in Table II. The K_2 values at all temperatures displayed no real trend with wavelength; however, there was considerably more scatter and higher standard deviations than those found in the K_1 investigation. The averages of the standard deviations in K_2 were found to be 10, 4, 7, and 12% at 25.0, 38.5, 51.6, and 65.1°, respectively. This loss of accuracy was expected, since at the ionic strengths employed the $[Eu(SO_4)_2^-]/[EuSO_4^+]$ ratios could not even be raised above unity. The best values for K_2 were determined to be 18, 25, 50, and 54 at 25.0, 38.5, 51.6, and 65.1°, respectively. A value of 6.2 ± 0.5 kcal/mol for ΔH_2 at the experimental ionic strength of 0.045 *m* was obtained using the van't Hoff equation, after setting $\Delta Cp_2 = 0$. This lead to a ΔS_2 value of 26 ± 2 cal/(mol deg). The uncertainties given for ΔH_2 and ΔS_2 were the experimental standard deviations. No attempt was made to interpret the data in terms of a finite ΔCp_2 term because of the large uncertainties in K_2.

The variable ionic strength investigations were car-

(25) Since $[Eu(SO_4)_2^-]/[EuSO_4^+] = K_2[SO_4^{2-}]$, keeping the concentration of sulfate ion as low as possible is the most important single factor in reducing $Eu(SO_4)_2^-$ formation.

(26) The raw differential absorbancy data for the test solutions at all the ionic strengths, wavelengths and temperatures employed will appear immediately following this article in the microfilm edition of this volume of the journal. Single copies may be obtained from the Business Operations Office, Books and Journals Division, American Chemical Society, 1155 Sixteenth St., N.W., Washington, D. C. 20036, by referring to code number JPC-72-1887. Remit check or money order for $4.00 for photocopy or $2.00 for microfiche.

Table II: Formation Constants and Differential Extinction Coefficients[a] for the Disulfato System at a Constant Ionic Strength of 0.045 *m* at a Function of Wavelength and Temperature

	Temp, °C							
	25.0		38.5		51.6		65.1	
λ, mμ	K_2	$(\epsilon_2 - \epsilon^\circ)$	K_2	$(\epsilon_2 - \epsilon^\circ)$	K_2	$(\epsilon_2 - \epsilon^\circ)$	K_2	$(\epsilon_2 - \epsilon^\circ)$
230	19	155	27	161	53	139	61	145
236	19	169	28	169	46	170	56	177
240	17	170	29	163	51	165	54	184
245	19	143	22	160	49	158	53	177
250	12	143	23	129	51	137	48	160
255	19	87	23	100	49	113	50	130

[a] Units: l./(mol cm).

ried out from 0.006 to 0.046 *M* over the same wavelength and temperature range covered in the constant ionic strength studies. It was found impossible to go any lower than 0.006 *M* and still retain the desired accuracy in the absorbancies.

The thermodynamic formation constants, K_1°, obtained from the extrapolations of the K_1 values to infinite dilution are given in Table III. As in the study at constant ionic strength, K_1° showed no definite trend with wavelength. The averages of the standard deviations were found to be 1.5, 2.1, 2.8, and 3.9% at 25.0, 38.5, 51.6, and 65.1°, respectively. The final values for K_1 and K_1° given in Table IV were obtained by averaging those from 230 to 255 mμ.

Table III: Thermodynamic Formation Constants ($K_1^\circ \times 10^{-3}$) for the Monosulfato System at Infinite Dilution as a Function of Wavelength and Temperature

λ,	Temp, °C			
mμ	25.0	38.5	51.6	65.1
230	4.67	6.90	10.85	16.36
236	4.64	6.93	10.85	16.65
240	4.74	6.99	10.96	16.82
245	4.67	7.25	11.13	17.04
250	4.70	7.10	11.07	16.77
255	4.68	7.34	10.91	17.02

Table IV: Final Formation Constants for Aqueous Monosulfato Europium(III) Ion

	Ionic strength			
	0.045 *m*		→ 0	
Temp, °C	$K_1 \times 10^{-2}$	$\kappa_1 \times 10^{-2}$	$K_1^\circ \times 10^{-3}$	$\kappa_1^\circ \times 10^{-3}$
25.0	5.71 ± 0.06	5.69	4.69 ± 0.07	4.68
38.5	7.95 ± 0.08	7.89	7.09 ± 0.15	7.04
51.6	11.30 ± 0.07	11.16	10.96 ± 0.31	10.82
65.1	16.85 ± 0.18	16.52	16.78 ± 0.65	16.45

Since the molar concentration scale is a function of temperature, the K_1 and K_1° values were converted first to the molal scale before the changes in enthalpy and entropy were calculated. To distinguish between the two concentration scales, the ones on the molal scale have been written as κ_1 and κ_1°. These conversions were accomplished simply by multiplying K_1 and K_1° by the density of pure water (see Table IV). For the K_1° conversions no error was introduced, but this was not true for those at constant ionic strength. However, in the ΔH_1 calculations it was the change in density with temperature that was important and not its absolute value. Even in the subsequent ΔS_1 calculations, the error introduced by the above assumption, although slightly larger, was calculated to be well within the experimental error.

The logarithms of the κ_1 and κ_1° data from Table IV were found to exhibit quadratic behavior when plotted *vs.* T. The resulting equations are shown below with their uncertainties (experimental standard deviations).

$$\log \kappa_1 = 3.2595 - 1.3358 \times 10^{-2}T + 3.9127 \times 10^{-5}T^2 \pm 0.00009$$

$$\log \kappa_1^\circ = 0.77315 + 6.1729 \times 10^{-3}T + 1.1868 \times 10^{-5}T^2 \pm 0.0030$$

These two equations were used to calculate ΔH_1 and ΔH_1° at each experimental temperature from the relationship $\Delta H_1^\circ = RT^2(\partial \ln \kappa_1^\circ/\partial T)$. An average ΔH_1 and ΔH_1° applicable to a temperature of 45° were also obtained from linear plots of $\log \kappa_1$ and $\log \kappa_1^\circ$ *vs.* $1/T$; *i.e.*, ΔCp_1 and ΔCp_1° were set equal to zero. These thermodynamic values in addition to the entropy and heat capacities, calculated from $\Delta S_1^\circ = \Delta H^\circ/T + R \ln \kappa_1^\circ$ and $\Delta Cp_1^\circ = (\partial \Delta H_1/\partial T)_p$, are given in Table V.

Discussion

As previously mentioned, the literature values reported for K_1 and K_1° at 25° from earlier investigations show little, if any, agreement; *e.g.*, K_1° values range from 2300 to 5300. Two of these studies warrant discussion, because of their importance to this investigation.

Barnes[2] has studied the association of europium(III) ion with sulfate at a constant ionic strength of 0.049 *M*

Table V: Thermodynamic Functions for the Formation of Aqueous Monosulfato Europium(III) Ion from This Investigation[a]

A. Ionic Strength = 0.045 *m*

Temp, °C	$\Delta Cp_1 = 0$ ΔH_1	$\Delta Cp_1 = 0$ ΔS_1	ΔH_1	ΔS_1	ΔCp_1
25.0	5.1 ± 0.3	29.6 ± 1.2	4.1	26	59
38.5			4.9	29	66
51.6			5.8	32	74
65.1			6.9	35	82

B. Ionic Strength → 0

Temp, °C	$\Delta Cp_1^\circ = 0$ ΔH_1°	$\Delta Cp_1^\circ = 0$ ΔS_1°	ΔH_1°	ΔS_1°	ΔCp_1°
25 0	6.2 ± 0.3	37.4 ± 1.0	5.4	35	46
38.5			6.0	37	49
51.6			6.7	39	53
65.1			7.4	41	62

[a] ΔH_1 in kcal/mol and ΔS_1 and ΔCp_1 in cal/(mol deg), respectively.

and a temperature of 25° by employing differential absorption spectrophotometry. He did this work at only one wavelength (240 mμ) and ignored the formation of $NaSO_4^-$ ion pairing. To obtain the thermodynamic formation constant for $EuSO_4^+$ at infinite dilution he used Davies' equation[20] instead of measuring the formation constant as a function of ionic strength. His value of 2.3×10^3 (correction for $NaSO_4^-$ ion pairing would raise it about 10%) is significantly lower than 4.7×10^3 found in this study. He reported no interference from the formation of the disulfate species although his salt concentrations and ionic strength were almost identical with those used initially in this study, in which K_1 was found to be a function of wavelength due to the formation of significant amounts of $Eu(SO_4)_2^-$. Barnes' conclusion that the linear fit he obtained using eq 5a proved that $EuSO_4^+$ was the only sulfato complex present was incorrect, since as pointed out quite convincingly by Kruh,[27] such a linear fit does not exclude the presence of higher order complexes, even in appreciable amounts.

The conductance study made at 25° by Spedding and Jaffe[4] on a series of aqueous rare earth sulfates has provided very accurate values for K_1°. Their work was carried out at ionic strengths as low as 2.5×10^{-4} *M*. Since pure salts were employed without the addition of added "inert" electrolytes, interference due to $NaSO_4^-$ was completely eliminated while that due to $Eu(SO_4)_2^-$ was made insignificant. The large deviations from the Onsager equation were interpreted as due to monosulfato complex formation. Although europium sulfate was not studied, the rare earths lying on either side of it were. Using $\mathring{a}$ values obtained from emf studies and the Debye–Hückel limiting law, a value of 4.6×10^3 at infinite dilution was calculated for both $SmSO_4^+$ and $GdSO_4^+$ formation. This value for K_1° is in excellent agreement with that of 4.7×10^3 from this investigation.

The recent calorimetric studies by Izatt, Eatough, Christensen, and Bartholomew[5] and Fay and Purdie[28] on the formation of aqueous $EuSO_4^+$ ion make possible a direct comparison of our enthalpy and entropy data for the infinitely dilute solution at 25°. Their ΔH_1° and ΔS_1° values ranged from 3.64 to 4.13 kcal/mol and 28.4 to 30.6 cal/(mol deg), respectively, and are in fair agreement with those of 5.4 kcal/mol and 35 cal/(mol deg) from this investigation. The differences can probably be attributed to the dissimilar analytical and extrapolation methods employed. Our average ΔCp_1° value of 52 cal/(mol deg) also compares favorably with that of 70 cal/(mol deg) calculated for $Cr(OH_2)_5NCS^{2+}$ formation in aqueous solution from 14 to 95° by Postmus and King.[29]

At different finite ionic strengths, direct comparisons of our thermodynamic data with those of others becomes much more difficult, particularly when the "inert" media are not identical. However, for an association reaction where there is a decrease in total charge, as in eq 1b and 3, theory predicts that in dilute solutions both the ΔH_1 and ΔS_1 terms should decrease as the ionic strength increases. This expected trend is well illustrated when the results from this study at infinite dilution and 0.045 *m* (see Table V) are compared with those in 2 *M* $NaClO_4$ by DeCarvalho and Choppin.[12] They employed a direct calorimetric method which yielded 3.88 kcal/mol and 19.3 cal/(mol deg) at 25° for ΔH_1 and ΔS_1, respectively.

Due to the ability to separate and study the complex species of inert cations, definite thermodynamic information can be obtained concerning inner- and outer-sphere formation. Most of this work has been done using cobalt(III) and chromium(III) ions (see pp 238 and 241 of ref 1). The thermodynamic values for the formation of the monosulfate complex of these cations are shown in Table VI.

The enthalpy term arises from the difference in bond energies of the products and reactants, whereas the

Table VI: Thermodynamics of Inner- and Outer-Sphere Monosulfato Formation of Co(III) and Cr(III) Ions[a]

Cation	ΔH_1^{out}	ΔH_1^{in}	ΔS_1^{out}	ΔS_1^{in}	*I*, *M*
$Co(NH_3)_6^{3+}$	0.4	...	16.6	...	→ 0
$Cr(OH_2)_6^{3+}$	0	7.2	4.9	29	1 ($NaClO_4$)
$Co(NH_3)_5OH_2^{3+}$	−0.3	...	3.8	...	1 ($NaClO_4$)

[a] ΔH_1 and ΔS_1 in kcal/mol and cal/(mol deg), respectively.

(27) R. Kruh, *J. Amer. Chem. Soc.*, **76**, 4865 (1954).
(28) D. P. Fay and N. Purdie, *J. Phys. Chem.*, **73**, 3462 (1969).
(29) C. Postmus and E. L. King, *ibid.*, **59**, 1208 (1955).

entropy measures the overall change in the order of the system which accompanies the reaction. For outer-sphere formation, ΔH_1 or ΔS_1 values near zero would be expected, since the primary hydration spheres are largely unaffected. However, for inner-sphere formation, the opposite would be true, particularly where the ΔZ^2 term is large as in the present and analogous studies with Co(III) and Cr(III) ions.

Comparing the $\Delta H_1°$ and $\Delta S_1°$ values from this investigation with those from Table VI for inert systems strongly indicates that $EuSO_4^+$ is primarily an inner-sphere complex. This conclusion was also drawn by DeCarvalho and Choppin from their studies made in 2 *M* sodium perchlorate at 25°.[12]

It should be noted that the K_1 values obtained from this study actually represent the sum of the formation constants for the inner- and outer-sphere species. Merely making the spectroscopic studies at various wavelengths cannot by itself enable one to separate K_1 into its component parts. Also, since the activity of water was essentially constant during these experiments, nothing was learned regarding whether sulfate ion was acting as a mono- or bidentate ligand.

Davies[20] has recommended that at 25° 0.3 be employed instead of his older value of 0.2 for *D* in eq 12. He gives much evidence to show that this value described fairly well the activity coefficients for a number of 1–1, 1–2, and 2–1 electrolytes up to stoichiometric concentrations of 0.010 *M* and a few 3–1 electrolytes to 0.035 *M*. In this investigation (where the ΔZ^2 term equals −12), the much larger value of 0.6 was obtained for *D* at 25°. The difference in these two values for *D* becomes very apparent when an extrapolation from an ionic strength of 0.10 *M* to infinite dilution is considered. Here, the $K°$ obtained by using Davies' recommended value of 0.3 for *D* would be more than 50% larger than that calculated by employing 0.6. Therefore, for reactions possessing large ΔZ^2 terms, it is strongly recommended that the low ionic strength dependence of *K* be measured, if accurate $K°$ values are desired. Many investigators[2,20-32] have employed Davies' equation to directly calculate $K_1°$ values for eq 1a using data obtained at ionic strengths around 0.1 *M*. Therefore, their equilibrium constants for the infinite dilute solution should be considered as only qualitative.

In many studies similar to that reported in this paper, interferences due to disulfate and $NaSO_4^-$ formation were partially or even completely ignored. Therefore, it seemed worthwhile to use our data to calculate what the effect would have been to κ_1, ΔH_1, and ΔS_1 if these additional complex species had not been taken into consideration. For these calculations ΔCp_1 and $\Delta Cp_1°$ were set equal to zero. Ignoring $Eu(SO_4)_2^-$ but not $NaSO_4^-$ would have increased κ_1 by 2% at 25° and 14% at 65°, while increasing ΔH_1 and ΔS_1 by 12 and 17%, respectively. Ignoring only $NaSO_4^-$ formation would have lowered κ_1 by 13% at both 25 and 65°, while essentially leaving ΔH_1 and ΔS_1 unaffected. If both $Eu(SO_4)_2^-$ and $NaSO_4^-$ formation had been ignored, a decrease in κ_1 of 11% at 25° and 1% at 65° and an increase in ΔH_1 and ΔS_1 of 12 and 6%, respectively, would have resulted.

This investigation has shown that the spectrophotometric method, when suitable absorption bands are available, is capable of accurate studies on the formation of complex ions. This is particularly true if full advantage of the technique is made, by carrying out each investigation at more than a single wavelength. Also, it has shown that many of the discrepancies reported for the association constants of $RESO_4^+$ at infinite dilution can be attributed to the use of Davies' equation for extrapolation to infinite dilution and failure to correct for the presence of undesirable sulfate complexes.

Acknowledgment. Special thanks are due to Gary Manns for writing some of the initial computer programs and to Rudy Jungst, who very carefully prepared and analyzed many of the test solutions used in this investigation.

(30) P. G. Manning and C. B. Monk, *Trans. Faraday Soc.*, **58**, 938 (1962).

(31) S. H. Laurie and C. B. Monk, *J. Chem. Soc.*, 3343 (1963).

(32) D. W. Archer and C. B. Monk, *Trans. Faraday Soc.*, **62**, 1583 (1966).

A Study of the Thermodynamic and Spectral Properties of Molecular Complexes of Iodine with Several Aminopyridines

by Joan M. Daisey and Anthony J. Sonnessa*

Department of Chemistry, Seton Hall University, South Orange, New Jersey 07079 *(Received February 7, 1972)*

Publication costs assisted by Seton Hall University

Thermodynamic properties K_f, ΔH_f, and ΔS_f were obtained spectrophotometrically for the complexes of several aminopyridines with iodine in cyclohexane solution. The large values of K_f and ΔH_f make these complexes one of the strongest of the pyridine–iodine complexes studied to date. Arguments are presented which indicate that the donors used in this study form 1:1 complexes with iodine which are of the n–aσ type. Visible and ultraviolet spectral properties of the charge-transfer (CT) complexes are also presented. Two distinct CT bands were observed for the 4-aminopyridine and 4-*N*,*N*-dimethylaminopyridine complexes. In general, the CT bands are found to be broader on the low-frequency side of the maximum, similar to the parent pyridine complex with iodine.

Molecular complexes of the charge-transfer (CT) type of N-heterocyclic compounds have been subject to several studies. Reid and Mulliken[1] studied the complex formed with pyridine as donor and iodine as acceptor. A number of authors[2] have studied methyl and halogen substituted pyridines CT interactions with I_2 in different solvents. However, aminopyridines as donors have not been looked at to any great extent. Bhaskar and Singh[2c] have reported results of the CT interaction between 2- and 4-aminopyridines with I_2, using chloroform as the solvent. It would be desirable to obtain results for these systems in the more inert hydrocarbon solvents. The low solubility of the donors in these solvents requires the use of longer path length cells in the spectrophotometric studies in the visible region. However, there are a number of advantages to working at low concentration. Dimerization of both donor[3] and acceptor[4] are minimized at low concentrations. The greater transparency of the hydrocarbon solvent in the uv region makes possible an examination of the charge-transfer band, which usually occurs in this region. The equilibrium constants obtained in dilute solutions are closer to the thermodynamic constants, and also the minimal interaction between solvent and donor and acceptor molecules facilitates comparison of experimental results with theoretical predictions.

In general, the N-heterocyclics studied to date form 1:1 complexes with I_2 which are of n–aσ type, with relatively high equilibrium constants.[5] Moreover, the stronger complexes appear to follow many of the predictions derived from Mulliken's theory of CT complexes,[6] apparently exhibiting few of the anomalies found for the weaker complexes.[7] The larger values of the equilibrium constants would result in less uncertainty in the measured values of these constants, as well as the measured values of the extinction coefficients.

The aminopyridines are particularly interesting for a study of their donor properties because of the presence of two nitrogens each having a lone pair of electrons to donate. Hence, it is of interest to determine whether or not 2:1, as well as 1:1 complexes are formed, and if only 1:1 complexes are formed, is complexation occuring through the lone pair on the ring nitrogen or the lone pair on the amino group. This paper will report the results for the equilibrium constants K_f and the thermodynamic functions ΔH_f, ΔS_f, and ΔG_f obtained from the visible spectra of these complexes. In addition, the spectral properties of the blue-shifted visible iodine bands and the ultraviolet charge-transfer bands for these complexes will be discussed. An attempt will be made to correlate these properties with the theory proposed by Mulliken.[6]

Experimental Section

Reagents. Iodine from Allied Chemical Co. was sublimed twice under vacuum and stored in a desiccator

(1) C. Reid and R. S. Mulliken, *J. Amer. Chem. Soc.*, **76**, 3869 (1954).

(2) (a) V. G. Krishna and B. B. Bhowmik, *ibid.*, **90**, 1700 (1968); (b) W. J. McKinney, M. K. Wong, and A. I. Popov, *Inorg. Chem.*, **7**, 1001 (1968); (c) K. R. Bhaskar and S. Singh, *Spectrochim. Acta*, **23A**, 1155 (1967); (d) G. Aliosi, G. Cauzzo, and U. Mazzucato, *Trans. Faraday Soc.*, **61**, 1406 (1965); (e) G. Aliosi, G. Gauzzo, and U. Mazzucato, *ibid.*, **63**, 1858 (1967); (f) R. D. Srivastava and G. P. Prasad, *Spectrochim. Acta*, **22**, 825 (1966).

(3) K. V. Ramiah and P. G. Puranik, *J. Mol. Spectrosc.*, **7**, 89 (1961).

(4) R. M. Keefer and T. L. Allen, *J. Chem. Phys.*, **25**, 1059 (1957).

(5) R. S. Mulliken and W. F. Person, *Ann. Rev. Phys. Chem.*, **13**, 107 (1962).

(6) R. S. Mulliken and W. F. Person, "Molecular Complexes, a Lecture and Reprint Volume," Wiley, New York, N. Y., 1969.

(7) G. Kortum and W. M. Vogel, *Z. Elektrochem.*, **59**, 16 (1955).

over P_2O_5; the desiccator was flushed with argon before closing. All pyridine derivatives used in this study were supplied by the Aldrich Chemical Co. and were sublimed under vacuum at 50–60°. Infrared spectra and melting points were obtained and these agreed with published results. The following donors (with their symbols) were studied: 2-, 3-, and 4-aminopyridines (2AP, 3AP, and 4AP), 2-amino-4-methylpyridine (2A4MP), 2-amino-6-methylpyridine (2A6MP), 2-*N*,*N*-dimethylaminopyridine (2NN), and 4-*N*,*N*-dimethylaminopyridine (4NN). Matheson Coleman and Bell Spectroquality cyclohexane was used with no further purification.

Stock solutions of iodine and the various aminopyridines were prepared no more than 1 day before an experiment and were stored under nitrogen if they were not used within 2–3 hr after preparation. Stock solutions were made up by weight. Aliquots of the donor stock solutions were pipetted into preweighed 50.0-ml volumetric flasks and then weighed to determine the exact amount of stock solution. Iodine concentration in most cases was approximately 10^{-4} M. The exact concentration was determined by averaging the absorbance measured at 522 nm of two or three samples of iodine in cyclohexane and using the previously determined extinction coefficient of 960 M^{-1} cm^{-1} at 25°. Concentrations so obtained agreed to within 1%.

Spectral Measurements. Spectra were recorded on a Cary Model 15 spectrophotometer using quartz cells of 5.0 and 10.0 cm path lengths in the visible region and 0.1-, 0.5-, and 1.0-cm cells in the ultraviolet region. Both sample compartment and solutions were kept at constant temperature, the temperature maintained constant to ±0.1°. The solutions used in the spectral studies were made up immediately before each spectrum was measured by adding a constant aliquot of iodine stock solution to each of the donor solutions, each kept at constant temperature. All spectra were recorded within 5 min after the addition of iodine.

Equilibrium Constant Determination. For the determination of apparent equilibrium constants using the visible absorption spectra, the concentration of iodine was kept constant and the donor concentrations were varied. In each case curves of the type shown in Figure 1 resulted. All exhibited a clearly defined isosbestic point indicating a single equilibrium. The absorption in the visible region of all systems remained quite constant over a 2-hr period at most donor concentrations, except for 3-aminopyridine. In this case the spectrum of the 3-aminopyridine–iodine system changed quite rapidly when the donor–acceptor ratio reached about 18 to 1, due probably to a reaction occurring in the system. Donor concentrations used in obtaining the visible spectra ranged from 1×10^{-4} to 2×10^{-3} M, except in the case of 2-*N*,*N*-dimethylaminopyridine. Due to the low equilibrium constant for the complex of this donor, the concentrations used for this donor ranged from 1×10^{-2} to 5×10^{-2} M. The iodine concentration was about 1×10^{-4} M for all donors.

Several methods are available for determining equilibrium constants K_f for molecular complexes from spectral data. A recent review is contained in the book by Foster.[8] For the complexes under consideration here the equilibrium assumed is

$$D + I_2 \longrightarrow D \cdot I_2 \qquad (1)$$

from which K_f is defined as

$$K_f = \frac{(D \cdot I_2)}{(D)(I_2)} \qquad (2)$$

where $(D \cdot I_2)$, (D), and (I_2) are the equilibrium concentrations of the complex, aminopyridine donor, and iodine, respectively. As is usually done, it is assumed that the activity coefficients of all species are equal to unity in the dilute solutions used. Rose and Drago[9] have presented a graphical method which can be applied to the spectral data obtained from the blue-shifted and unperturbed visible iodine bands, and the CT bands of the complex. As has been pointed out by other workers,[2a,d] it is also possible to calculate K_f directly from the change in absorbance of the visible iodine band (see Figure 1). This method, used in this study, is more rapid and convenient than the Rose–Drago method and also readily lends itself to statistical analysis. The results obtained from the two methods were in good agreement for the complexes in this study. In this method the decrease in absorbance of the visible iodine band, due to the addition of donor, is taken as a measure of complex concentration. The final absorbance of this band is taken as a measure of uncomplexed iodine. Measurements are made on the low-frequency side of the band where interferences with overlapping bands are minimal. As a check calculations were made at three different wavelengths at intervals of 10 nm. Knowing the initial concentration of donor and iodine, tbe equilibrium concentrations in eq 2 can be calculated and the value of K_f obtained. The values of K_f obtained at the three wavelengths were averaged and the statistical uncertainty at the 99% confidence level was obtained. The uncertainties in the values of K_f for the complexes in this study are ±5–10%.

A 1:1 stoichiometry is observed for all the aminopyridine–iodine complexes in cyclohexane. However, tests were made for the possibility that some 2:1 or 1:2 donor–acceptor complexes may be forming. The work of Thompson,[10] in which computer simulated absorbance data were used to determine the effect of the presence of a 1:2 complex, *i.e.*, one donor to two iodine

(8) R. Foster, "Organic Charge-Transfer Complexes," Academic Press, New York, N. Y., 1969.

(9) N. J. Rose and R. S. Drago, *J. Amer. Chem. Soc.*, **81**, 6138 (1959).

(10) C. C. Thompson, Jr., *Can. J. Chem.*, **47**, 2605 (1969).

molecules, on the equilibrium constants calculated on the basis of an assumed 1:1 interaction, was used in this study. Using eq 9 from Thompson's work,[10] it was estimated that the amount of 1:2 complex is 10^6 times smaller than the amount of 1:1 complex even if there is a difference of only two orders of magnitude in the equilibrium constants. Thompson also reports that the presence of 2:1 donor–iodine complex would result in an increase in K_f with increasing donor concentration. This was not observed in the systems in this study. It is quite certain that only 1:1 complexes are present in the compounds studied, under the experimental conditions described above.

Calculation of the Thermodynamic Quantities. Enthalpies of complexation ΔH_f for the aminopyridine–iodine complexes in cyclohexane in the temperature range from 284.5 to 308.4°K were determined from the slope of the plot of log K_f *vs.* $1/T$. Linear regression analysis was used to obtain the best straight line and the value of ΔH_f. The uncertainty for each ΔH_f was calculated from the uncertainty in the slope of the line. The Gibbs free energy and the entropy of complexation, ΔG_f and ΔS_f, and their uncertainties were calculated at 25° from K_f in the usual way.

Measurement of the Ultraviolet Charge-Transfer Band. Accurate measurements of the positions and intensities of the uv charge-transfer (CT) bands in these complexes present a problem because of donor absorption in this region. In order to obtain the CT bands the usual difference technique was employed. In this method a solution of donor plus iodine in cyclohexane solvent contained in the sample cell was run *vs.* the same concentration of donor in solvent contained in the reference cell. CT spectra were usually determined using the same concentration ranges of donor and iodine as used for the determination of the equilibrium constants. The absorbance values obtained in this way were corrected for the known iodine absorption. For the donors 2A4MP, 4NN, and 4AP, in which more than 3–4% of the donor is complexed, a correction for overcompensation of donor in the reference cell was applied to the iodine-corrected absorbances. The molar absorptivities $\epsilon_{CT}(\nu)$ were calculated at 25-Å intervals through the CT band using the relation

$$\epsilon_{CT}(\nu) = \frac{A}{l(D \cdot I_2)} \tag{3}$$

where A is the corrected absorbance at each wavelength, l is the path length, and $(D \cdot I_2)$ is the molar concentration of the complex. The latter was calculated from the equilibrium constants. Plots of $\epsilon_{CT}(\nu)$ *vs.* the frequency ν were made and the areas under the curves were measured with a planimeter. Each curve was traced twice in each direction, and the areas could be reproduced to within 1–2%. Oscillator strengths f_{CT} were then calculated using

$$f_{CT} = 4.319 \times 10^{-9} \int_{\nu} \epsilon_{CT}(\nu)\, d\nu \tag{4}$$

Values reported for $\epsilon_{CT}(\max)$, the molar absorptivity at maximum absorption, and f_{CT} are the averages of measurements of from 3 to 12 spectra. Uncertainties are reported at the 95% confidence level. The transition dipole moment, μ_{CT} was calculated from f_{CT} using

$$\mu_{CT} = \left[\frac{3he^2 f_{CT}}{8\pi^2 mc\nu_{CT}(\max)}\right]^{1/2} \tag{5}$$

$$\mu_{CT} = \left[\frac{2.125 \times 10^{-30} f_{CT}}{\nu_{CT}(\max)}\right]^{1/2}$$

where $\nu_{CT}(\max)$ is the frequency at the maximum of the CT band and the symbols have their usual meaning.

Results and Discussion

Thermodynamic Functions. The values of K_f, ΔH_f, ΔG_f, and ΔS_f obtained for the 1:1 complexes of the various aminopyridines with iodine are presented in Table I. The values of K_f range from a low value of 8.65 M^{-1} for 2-*N*,*N*-dimethylaminopyridine to a high value of 5230 M^{-1} for 4-*N*,*N*-dimethylaminopyridine. The values of K_f, in general, are higher than those found for most complexes in which bonding occurs through the π-electron system of the ring;[11] in fact, they are much more in line with n–aσ complexation found for other pyridine derivatives.[2] In the previous work[2] a linear correlation between pK_a and log K_f has been used as evidence for n–aσ complexation. The pK_a values for the aminopyridines have been shown to correspond to the protonation of the ring nitrogen.[12–14]

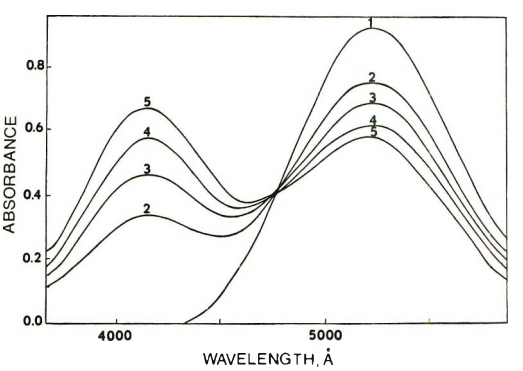

Figure 1. Visible spectra of solutions of iodine and 2-amino-4-methylpyridine in cyclohexane at 25°; $[I_2] = 0.97 \times 10^{-4}$ M; [2A4MP], $M \times 10^4$: (1) 0.0, (2) 4.47, (3) 6.96, (4) 9.94 (5) 11.93; cell length, 10.0 cm.

(11) G. Briegleb, "Elektronen-Donator-Acceptor-Komplexe," Springer-Verlag, 1961.

(12) A. Albert in "Physical Methods in Heterocyclic Chemistry," Vol. 1, A. R. Katritzky, Ed., Academic Press, New York, N. Y., 1963.

(13) D. D. Perrin, Ed., "Dissociation Constants of Organic Bases in Aqueous Solution," International Union of Pure and Applied Chemistry, Butterworth, London, 1965.

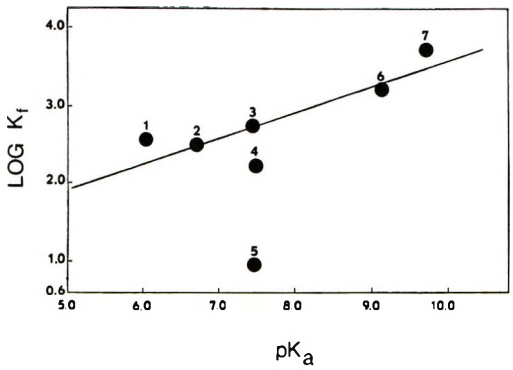

Figure 2. The relationship between log K_f and the pK_a of the donor: (1) 3AP, (2) 2AP, (3) 2A4MP, (4) 2A6MP, (5) 2NN, (6) 4AP, (7) 4NN; values of pK_a taken from ref 13 and 14.

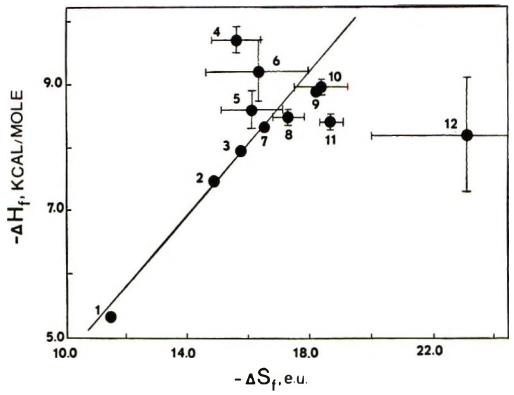

Figure 3. The relationship between $-\Delta H_f$ and $-\Delta S_f$ for some pyridine–iodine complexes; (1) 3-chloropyridine, (2) Py; (3) 2-picoline, (4) 4NN, (5) 2A4MP, (6) 4AP, (7) 3-picoline, (8) 2AP, (9) 4-picoline, (10) 3AP, (11) 2A6MP, (12) 2NN. Data for points 1, 2, 3, 7, and 9 from ref 2a.

Figure 2 shows that, except for 2-amino-6-methylpyridine and 2-*N*,*N*-dimethylaminopyridine, the correlation is quite good. This is what would be expected if complexation is occurring at the ring nitrogen. In the cases of the 2-*N*,*N*-dimethyl and 6-methyl derivatives with their bulkier methyl substituents, a deviation from this correlation would be expected when comparing the larger iodine acceptor with the smaller proton.

If complexation is occurring at the ring nitrogen, it would be reasonable to expect the values of log K_f for the 2-, 3-, and 4-aminopyridines (2AP, 3AP, and 4AP, respectively) to follow the same relative order as the pK_a values of the donor, *i.e.*, 4AP > 2AP > 3AP, since the basicity of the donor should be a key factor in determining the strength of the complex. The order which is actually found is 4AP > 3AP > 2AP, which suggests that, while complexation is occurring at the ring nitrogen, the amino group in the 2 position is hindering the approach of the iodine atom. In order to further pursue this idea, equilibrium constants for the 2-amino-6-methylpyridine (2A6MP) and 2-amino-4-methylpyridine (2A4MP) donors were determined. As can be seen from Table I, increasing steric hindrance by the addition of a methyl group in the 6 position in 2AP reduces the equilibrium constant by approximately one-half. On the other hand, when the additional methyl group is in the 4 position, the equilibrium constant is doubled. Neither of these results would be expected on the basis of complexation occurring at either the amino nitrogen or through the π-electron system of the ring. In the latter case, electronic effects should be dominant and the equilibrium constants for both methyl-substituted compounds should be somewhat larger than that observed for 2AP. If the amino group were the site of complexation, substitution of a methyl group meta to the amino group should produce only small inductive effects resulting in very little difference in the equilibrium constants for the 4- and 6-methyl derivatives. The extremely large difference between K_f values for the 2-*N*,*N*- and 4-*N*,*N*-dimethylaminopyridines, more than three orders of magnitude, further substantiates complexation at the ring nitrogen with large steric hindrance in the 2NN case. Similar steric effects have been reported for lutidine–iodine complexes.[2f,15] It is interesting to note that an infrared study[16] of hydrogen bonding between methanol and alkyl-substituted pyridines indicates that steric hindrance to hydrogen bonding also exists when bulky substituents are present in the 2 or 2,6 positions.

There have been a number of reports of linear correlations between the enthalpy and entropy of complex formation.[6,8,11] A plot of $-\Delta H_f$ *vs.* $-\Delta S_f$ for the aminopyridine–iodine complexes is shown in Figure 3. The experimental uncertainties in these values are also shown in the figure. Because of the small number of complexes in this investigation and the relatively small range in the enthalpies of these complexes, the thermodynamic data obtained in heptane solution by Krishna and Bhowmik[2a] for some other pyridine–iodine complexes are included in Figure 3. Experimental uncertainties were not reported but are probably of the same order of magnitude as obtained in this work. It is apparent that there is a fairly good overall correlation, considering the experimental uncertainties, between $-\Delta H_f$ and $-\Delta S_f$ for this class of donors. This is to be expected, for the donors are all structurally similar and interaction with the iodine in all cases undoubtedly is occurring through the lone pair on the ring nitrogen. The larger negative value for the 2NN case is in line with the conclusion that there is a large steric effect in this complex.

Visible Spectra. As shown in Figure 1, the addition of donor causes the I_2 band at 523 nm to decrease in intensity and at the same time a new band appears at a

(14) A. Weisstuch and A. C. Testa, *J. Phys. Chem.*, **74**, 2299 (1970).
(15) A. I. Popov and R. H. Rygg, *J. Amer. Chem. Soc.*, **79**, 4622 (1957).
(16) T. Kitao and C. H. Jarboe, *J. Org. Chem.*, **32**, 407 (1967).

Table I: Thermodynamic Data for the Aminopyridine–Iodine Complexes in Cyclohexane, 25.0°

Donor[b]	K_f, l./mol	Log K_f	pK_a[a]	$-\Delta G_f$, kcal/mol	$-\Delta H_f$, kcal/mol	$-\Delta S_f$, eu
2NN	8.7 ± 1.0	0.94	7.50	1.30 ± 0.20	8.2 ± 0.9	23.0 ± 4.0
2A6MP	130 ± 10	2.10	7.41	2.90 ± 0.10	8.4 ± 0.1	18.5 ± 0.5
2AP	280 ± 30	2.45	6.71	3.40 ± 0.20	8.5 ± 0.1	17.0 ± 1.0
3AP	380 ± 10	2.58	6.03	3.50 ± 0.05	9.0 ± 0.2	18.0 ± 1.0
2A4MP	580 ± 40	2.76	7.48	3.80 ± 0.10	8.6 ± 0.3	16.0 ± 1.5
4AP	1580 ± 80	3.20	9.11	4.40 ± 0.10	9.2 ± 0.5	16.0 ± 2.0
4NN	5230 ± 250	3.72	9.71	5.08 ± 0.10	9.7 ± 0.2	15.5 ± 0.5

[a] From ref 13 and 14. [b] 2AP, 2-aminopyridine; 3AP, 3-aminopyridine; 4AP, 4-aminopyridine; 2A6MP, 2-amino-6-methylpyridine; 2A4MP, 2-amino-4-methylpyridine; 4NN, 4-*N*,*N*-dimethylaminopyridine; 2NN, 2-*N*,*N*-dimethylaminopyridine.

Table II: Visible and Ultraviolet Spectral Data for the Aminopyridine–Iodine Complexes in Cyclohexane, 25°

Donor[a]	$\nu_{BS} \times 10^{-4}$, cm^{-1}	$\Delta\nu_{BS}$,[b] cm^{-1}	ϵ_{BS}, m^{-1} cm^{-1}	f_{BS}	λ_{Donor}, nm	$\nu_{CT}(max) \times 10^{-4}$, cm^{-1}	$\epsilon_{CT}(max) \times 10^{-4}$, M^{-1} cm^{-1}
2A6MP	2.381	4690	1630 ± 60	0.030 ± 0.002	233.0	4.170	3.9 ± 0.8
					290.5		
2AP	2.404	4920	1770 ± 20	0.035 ± 0.002	231.0	4.210	3.6 ± 0.4
					290.0		
3AP	2.410	4980	1810 ± 30	0.036 ± 0.001	232.0	4.125	6.0 ± 0.5
					292.0		
2A4MP	2.425	5150	1900 ± 60	0.036 ± 0.001	233.0	4.210	5.2 ± 0.4
					287.0		
4AP	2.440	5270	1950 ± 90	0.036 ± 0.001	232.5	4.445	1.6 ± 0.5
					262.5 (sh)	3.945	6.9 ± 0.8
4NN	2.47	5570	2280 ± 40	0.045 ± 0.002	252.5	4.370	2.3 ± 0.1
					285.0 (sh)	3.740	4.9 ± 0.1

	f_{CT}	μ_{CT}, D	$\Delta\nu_H$, cm^{-1}	$\Delta\nu_L$, cm^{-1}	$\Delta\nu_{1/2}$, cm^{-1}	I_D,[c] eV
(2A6MP)	1.2 ± 0.2	8.0 ± 1.0	2600	4400	7000	9.1
(2AP)	0.9 ± 0.1	7.0 ± 1.0	2600	3300	5900	9.3
(3AP)	1.6 ± 0.2	9.0 ± 1.0	2600	2400	5000	9.0
(3A4MP)	1.4 ± 0.1	8.5 ± 0.5	2800	3000	5800	9.3
(4AP)	0.2 ± 0.1	3.0 ± 1.5	2000	1500	3500	10.2
	1.4 ± 0.3	9.0 ± 2.0	2000	2500	4500	8.4
(4NN)	0.43 ± 0.03	4.6 ± 0.3	2300	2100	4400	9.8
	1.08 ± 0.03	7.8 ± 0.2	1900	3100	5000	7.7

[a] See Table I for abbreviations. [b] Relative to the visible iodine band at 19,120 cm^{-1}. [c] See text for calculation of I_D.

lower wavelength. The intensity and position of this blue-shifted iodine band depend on the particular donor used, as can be seen from the values presented in Table II. The blue-shifted iodine band has been observed for many donors possessing nonbonded electrons, such as amines and sulfides.[6,11]

A comparison of the position and intensity of the blue-shifted iodine bands in Table II with these properties for the unperturbed iodine band is of interest. One can see that the extent of shift, $\Delta\nu_{BS}$, the difference in the wave number of the blue-shifted iodine band and the wave number of the unperturbed band, varies significantly from donor to donor. If one accepts the interpretation of Mulliken and others[2a,6] that the extent of blue-shift is a measure of the extent of interaction between donor and I_2, and therefore, of the extent and strength of complexation, one would expect a correlation between $\Delta\nu_{BS}$ and some thermodynamic property of the complex. Thus, the plot in Figure 4 of log K_f *vs.* $\Delta\nu_{BS}$ indicates an excellent correlation between these quantities for the complexes in this study.

The intensification of the blue-shifted iodine bands relative to the unperturbed I_2 band, seen in Table II, has been generally observed for these bands in complexes. Mulliken[6] explains this effect as due to increased mixing of the excited state of iodine with either the charge-transfer state of the complex or with the ground state of I_2, which results from the shift in position of the iodine excited state to higher energy on complexation. It would follow from this explanation that

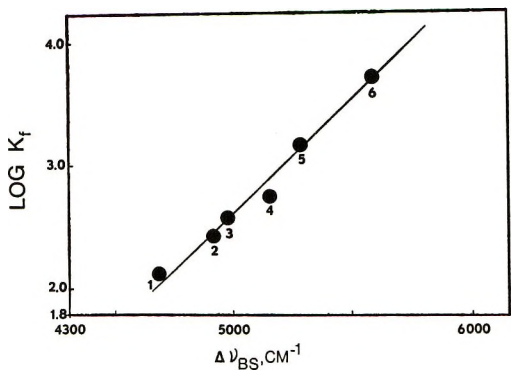

Figure 4. The relationship between log K_f and $\Delta\nu_{BS}$ for the aminopyridine–iodine complexes in cyclohexane at 25.0°: (1) 2A6MP, (2) 2AP, (3) 3AP, (4) 2A4MP, (5) 4AP, (6) 4NN.

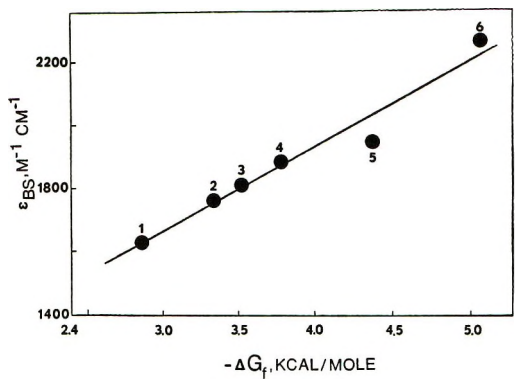

Figure 5. The relationships between ϵ_{BS} and $-\Delta G_f$ for the aminopyridine–iodine complexes in cyclohexane at 25°: (1) 2A6MP, (2) 2AP, (3) 3AP, (4) 2A4MP, (5) 4AP, (6) 4NN.

the extinction coefficient of the blue-shifted band, ϵ_{BS}, for the different donors should correlate with $-\Delta G_f$, used as a measure of the extent or strength of complexation. Figure 5 shows a plot of ϵ_{BS} *vs.* ΔG_f and the excellent correlation is apparent.

Charge Transfer Spectra. Table II presents the spectral properties of the ultraviolet CT bands for the I_2 complexes studied. As can be seen from Table II the iodine complexes of 4AP and 4NN show two distinct bands in the ultraviolet. The existence of more than one CT band has been reported previously for the aromatic hydrocarbon donors and for the n-type donors anisole and the styrylpyridines. More will be said about this later.

A number of general trends can be seen from the data in Table II. First, it is apparent that the wave number of the CT band decreases as the strength of the complex, as measured by $-\Delta H_f$, increases. Secondly, the intensity of the CT band as measured by ϵ_{CT}(max), f_{CT} or μ_{CT}, increases as the strength of interaction, measured by $-\Delta G_f$ or $-\Delta H_f$, increases. As pointed out by Mulliken and Person,[6] n-donors show fairly good correlation between μ_{CT} and the strength of interaction. To test this hypothesis further, $-\Delta H_f$ is plotted *vs.* μ_{CT} in Figure 6 for the aminopyridine–iodine complexes from this study, along with other substituted pyridine–iodine complexes reported by Krishna and Bhowmik.[2a] This plot shows at least a general trend toward increasing μ_{CT} with increasing $-\Delta H_f$, as predicted by the theory. In both of the above correlations the low-frequency bands for 4-*N*,*N*-dimethylaminopyridine and 4-aminopyridine are used, since they give the best correlation with the thermodynamic functions (see below). It is found experimentally that there is a good linear correlation between the ionization potential of the donor and the position of the CT band for a series of related donors with the same acceptor.[6,11] Except for 4AP,[17] ionization potentials for the aminopyridines are not yet available. However, Mulliken and Person[6] have given an empirical relation for the energy of the

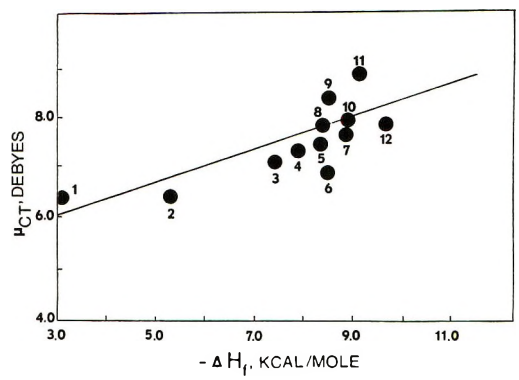

Figure 6. The relationships betweeen μ_{CT} and $-\Delta H_f$ for some pyridine–iodine complexes at 25°: (1) 2-chloropyridine, (2) 3-chloropyridine, (3) pyridine, (4) 2-picoline, (5) 3-picoline, (6) 2AP, (7) 4-picoline, (8) 2A6MP, (9) 2A4MP, (10) 3AP, (11) 4AP, (12) 4NN; data for points 1, 2, 3, 4, 5, and 7 from ref 2a.

CT band in terms of the ionization potentials I_D of aliphatic amine donors in iodine complexes

$$h\nu_{CT}(\text{max}) = 0.38I_D + 1.70 \quad (6)$$

where I_D is expressed in electron volts. It is found that the pyridine–iodine complex also fits this relation quite well. Since the aliphatic amine and pyridine complexes with iodine are apparently n–aσ type complexes, as we believe the aminopyridine–iodine complexes are also, we have used the above relation to estimate the ionization potentials for the donors used in this study. The results of these calculations are given in Table II. For the case of 4AP and 4NN, in which two bands are observed upon complexation, two ionization potentials are calculated. Basila and Clancy[17] report a value of 8.97 eV for 4AP which they believe to be a π-ionization potential. The low-frequency band for 4AP has a value of 8.4 eV from our calculations, which is in quite good agreement with the above. However, it is this low-frequency band which correlates

(17) M. R. Basila and D. J. Clancy, *J. Phys. Chem.*, **67**, 1551 (1963).

best with the theoretical expectations, as discussed above. Since the complexation most likely involves the n-electrons of the ring nitrogen, it would seem that the ionization potential reported by Basila and Clancy may be the n-ionization potential rather than the π-ionization potential, assuming that eq 6 adequately expresses the ionization potentials for the donors in this study.

Band Shapes. Another important spectral property of CT bands is the band shapes. Table II summarizes the band shape parameters given in terms of $\Delta\nu_H$, $\Delta\nu_L$, and $\Delta\nu_{1/2}$. The quantities $\Delta\nu_H$ and $\Delta\nu_L$ are the differences between $\nu_{CT}(max)$ and the high and low frequencies, respectively, at which the extinction coefficient is half the maximum value, and $\Delta\nu_{1/2}$ is the width of the CT band at half maximum intensity. For symmetrical bands $\Delta\nu_H = \Delta\nu_L = 0.5\ \Delta\nu_{1/2}$. Charge-transfer bands, in general, are unsymmetrical, usually being broader on the high-frequency side of the maximum. Briegleb[11] has shown that the relation $\Delta\nu_{1/2} = 2.4\Delta\nu_L$ is frequently followed by many complexes. However, the pyridine–iodine complex CT band has been found to be broader on the low-frequency side of the maximum,[18] and the aminopyridine–iodine complexes resemble the parent pyridine complex in this respect, as can be seen from Table II. The aminopyridine complexes with iodine appear to follow the relation $\Delta\nu_{1/2} \simeq 1.8\Delta\nu_L$.

As can be seen from Table II, the half band widths for the aminopyridine–iodine complexes decrease with increasing complex strength. This is the reverse of the case found for the aliphatic amine–iodine complexes.[6] The direct relationship between $\Delta\nu_{1/2}$ and the strength of complexation is attributed to large resonance interaction in these stronger amine complexes which results in an increase in the equilibrium N–I distance in the CT state as compared to the ground state N–I distance. On the basis of this interpretation, it would seem that the decrease in $\Delta\nu_{1/2}$ with increasing complex strength observed for the complexes in this study might be due to a relatively larger N–I distance in the ground state as compared to the CT state. This could be caused by a repulsion term in the ground state arising when donor and acceptor are brought together in the complex. The repulsion would cause the minimum in the potential energy curve for the ground state to be moved to the right relative to the CT state. The CT transition would then intersect the upper CT curve on the less steep side of the curve, *i.e.*, to the right of the minimum, resulting in a smaller spread in the allowed transitions and a smaller value of $\Delta\nu_{1/2}$.

One of the more interesting results of this study in the ultraviolet region is the discovery of two distinct bands in the CT spectra of the 4AP and 4NN complexes with iodine (see Table II). The bands in both cases are of the order of 100 Å removed from the donor bands. Spectra of several of the other complexes, particularly the 2A6MP complex, appear to be composed of two unresolved overlapping bands. Many reports of multiple charge transfer bands occur in the literature.[2d,11,19-23] The large majority of these complexes have been of the $b\pi$–$a\pi$ type, with donors such as substituted benzenes and acceptors such as TCNE and chloranil. Only two cases of double CT bands with I_2 as an acceptor have been reported. In one case,[2d] styrylpyridine was the donor and in the second,[23] anisole was the donor. Let us consider the possibility that the two bands are associated with transitions from two different donor orbitals, the n orbital of the ring nitrogen and the π orbitals of the ring. The pyridine molecule belongs to C_{2v} and the highest filled π orbitals of the pyridine ring possess b_2 and a_2 symmetry. However, only the b_2 orbital has proper symmetry to overlap with the σ_u orbitals of the iodine, assuming the same C_{2v} symmetry for the complex, so that a transition would be allowed from the b_2 orbital only. Thus, the two CT bands could arise, one from a transition from the n orbital, the other from a transition from the b_2 π orbital. If, as is true in many cases, the n and π orbitals are close in energy, then the two CT bands will overlap, resulting in a single asymmetric band.[14] However, substitution in the 4 position by a strongly electron donating amino or *N*,*N*-dimethylamino group should cause a wider separation in the energies of the n and π orbitals resulting in two distinct bands, as is indeed observed. In the case of the two complexes with 4AP and 4NN which exhibit two distinct CT bands, it was shown above that the spectral properties of the low-frequency bands correlate with the thermodynamic functions and that these correlations indicated a complexation at the n-electrons of the ring nitrogen. Hence, it would appear that the low-frequency bands are to be correlated with the transitions from the n orbital, while the high-frequency bands in these complexes are due to transitions from the π system of the donor.

Acknowledgment. J. M. D. wishes to thank the National Science Foundation for a Graduate Traineeship award during part of this work.

(18) R. S. Mulliken, *J. Amer. Chem. Soc.*, **91**, 1237 (1969).
(19) R. E. Merrifield and W. D. Philips, *ibid.*, **80**, 2778 (1958).
(20) E. M. Voigt, *ibid.*, **86**, 3611 (1964).
(21) A. Zweig, *J. Phys. Chem.*, **67**, 506 (1963).
(22) L. E. Orgel, *J. Chem. Phys.*, **23**, 1352 (1955).
(23) P. A. D. DeMaine, *ibid.*, **26**, 1189 (1957).

On the Viscosity of Concentrated Aqueous Solutions of Tetraalkylammonium Bromides

by D. Eagland* and G. Pilling

School of Chemistry, University of Bradford, Bradford 7, England *(Received March 15, 1971)*

Publication costs borne completely by The Journal of Physical Chemistry

Viscosity and density data are presented on solutions of $(CH_3)_4NBr$, $(C_2H_5)_4NBr$, $(C_3H_7)_4NBr$, and $(C_4H_9)_4NBr$ in the concentration range 0–4 *m* and over the temperature range 15–35°. Use is made of the Vand equation, $\ln \eta/\eta_0 = 2.5\phi/(1 - k\phi)$, developed for concentrated suspensions, by substitution of the transformation $\phi = cV_e^\circ$, where η/η_0 is the relative viscosity, ϕ is the volume fraction of the dispersion, c is the molal salt concentration, and V_e° is the "effective flowing volume" of the electrolyte at infinite dilution. The values of V_e° obtained for the four salts are shown to correlate with the B coefficient of the Jones–Dole equation for dilute solutions of the salts by the substitution in the Einstein equation for viscosity of $B = 2.5V_e^\circ$. Values of V_e, the "effective flowing volume," as a function of concentration and temperature are also obtained from the recent equation of Breslau and Miller, $V_e = [-2.5c + \{2.5c^2 - 4(10.05c^2)(1 - \eta/\eta_0)\}^{1/2}]/2(10.05)c^2$, and shown to correlate well with the limiting value of V_e° obtained from the Mooney equation. The behavior pattern obtained of V_e as a function of temperature gives indications of the hydration behavior of concentrated solutions of the four salts.

Introduction

Recent viscosity measurements by Kay and coworkers[1] on a series of tetraalkylammonium halides in aqueous solution at concentrations up to 0.2 *M* utilized the Jones–Dole treatment of flow of dilute electrolyte solutions[2] to determine the constant B of the equation

$$\eta/\eta_0 = 1 + A\sqrt{C} + BC \qquad (1)$$

The square root term of eq 1 has been shown to be dependent on long-range interionic forces by Falkenhagen and coworkers[3-5] and hence the coefficient A may be calculated from the Debye–Hückel theory. The coefficient B has not, to date, yielded to a fundamental theoretical treatment, but many workers have related it in a qualitative manner to ion–solvent interactions. Kay, *et al.*, interpreted the values of B obtained from their data in terms of the structuring properties of the tetraalkylammonium salts with regard to water. The Jones–Dole equation is limited in its applicability to concentrations up to 0.1–0.2 *M*, and no comparable treatment has been attempted for concentrated solutions of electrolytes. However, Nightingale[6] and Miller and Doran[7] have utilized the Eyring treatment of viscosity,[8] based on the theory of rate processes, to investigate the viscosities of electrolyte solutions up to concentrations of the order of 10 *M*. Recently Breslau and Miller[9] noted the similarity in concentration between concentrated electrolyte solutions and high volume fraction dispersions and utilized the equation obtained by Thomas[10] for volume fractions ≤ 0.25

$$\eta/\eta_0 = 1 + 2.5\phi + 10.05\phi^2 \qquad (2)$$

where η and η_0 are the viscosities of the dispersion and dispersion medium, respectively, and ϕ is the measured volume fraction. Using the substitution $\phi = cV_e$ where c is the molar concentration of electrolyte and V_e is the "effective volume of the flowing unit," an expression for V_e was obtained.

$$V_e = \frac{-2.5c + [(2.5c)^2 - 4(10.05c^2)(1 - \eta/\eta_0)]^{1/2}}{2(10.05)c^2} \qquad (3)$$

An alternative treatment to the power series in ϕ due to Thomas, which successfully correlates viscosity data in the field of concentrated dispersions, is that due to Vand[11] of the form

$$\ln \eta/\eta_0 = \frac{2.5\phi}{1 - k\phi} \qquad (4)$$

where k is termed a particle interaction constant. Substitution as in the Breslau and Miller model of $\phi = cV_e$ yields the equation

(1) R. L. Kay, T. Vituccio, C. Zawoyski, and D. F. Evans, *J. Phys. Chem.*, **70**, 2336 (1966).
(2) G. Jones and H. Dole, *J. Amer. Chem. Soc.*, **51**, 2950 (1929).
(3) H. Falkenhagen and H. Dole, *Phys. Z.*, **30**, 611 (1929).
(4) H. Falkenhagen, *ibid.*, **32**, 745 (1931).
(5) H. Falkenhagen and E. L. Vernon, *Phil. Mag.*, **14**, 537 (1932).
(6) E. R. Nightingale, Jr., *J. Phys. Chem.*, **66**, 894 (1962).
(7) M. L. Miller and M. Doran, *ibid.*, **60**, 186 (1956).
(8) S. Gladstone, K. J. Laidler, and H. Eyring, "The Theory of Rate Processes," McGraw-Hill, New York, N. Y., 1941.
(9) B. R. Breslau and I. F. Miller, *J. Phys. Chem.*, **74**, 1056 (1970).
(10) D. G. Thomas, *J. Colloid Sci.*, **20**, 267 (1965).
(11) J. Vand, *J. Phys. Chem.*, **52**, 277 (1948).

$$\ln \eta/\eta_0 = \frac{2.5cV_e}{1 - kcV_e} \quad (5)$$

Rearranging and taking logs to base 10 gives

$$\frac{c}{\log \eta/\eta_0} = \frac{2.303}{2.5V_e} - \frac{2.303kc}{2.5} \quad (6)$$

Thus a plot of $c/\log \eta/\eta_0$ against c should be linear with a slope of $2.303k/2.5$ and an intercept of $2.303/2.5V_e$ when $c \rightarrow 0$. This effective flow volume as $c \rightarrow 0$ can be termed "the limiting value V_e^0 of the effective flow volume," as distinct from the values of V_e obtained from the Breslau and Miller treatment which may be utilized to obtain V_e as a function of the molal concentration.

We report here upon viscosity and density data obtained for $(CH_3)_4NBr$, $(C_2H_5)_4NBr$, $(C_3H_7)_4NBr$, and $(C_4H_9)_4NBr$ in the concentration range 0–4 m over a temperature range of 15–40°, the effective flow volumes of the salts, and the B coefficients of the particular salts.

Experimental Section

Purification of Material. B. D. H. laboratory grade $(CH_3)_4NBr$ was reprecipitated twice from hot aqueous methanol (15 vol. % of water) by the addition of diethyl ether. The solution was filtered prior to the addition of ether. The white crystalline product was dried at 110° for 12 hr.

$(C_2H_5)_4NBr$ (B. D. H. laboratory grade), $(C_3H_7)_4NBr$ (Eastman Kodak White Label), and $(C_4H_9)_4NBr$ (Eastman Kodak White Label) were reprecipitated twice from chloroform after filtration by the addition of diethyl ether. $(C_2H_5)_4NBr$ and $(C_3H_7)_4NBr$ were dried at 110° for 12 hr before use, but such treatment produced decomposition of $(C_4H_9)_4NBr$. This also proved difficult to store due to its hygroscopic nature; final preparation of $(C_4H_9)_4NBr$ therefore consisted of a short drying period of 6 hr at 80° prior to dissolution in chloroform and a further short drying period of the precipitate at 80° followed by immediate preparation of the solution.

The purity of the salts was determined by potentiometric titration with $AgNO_3$ which had itself been standardized with P.V.S. reagent grade NaCl of 99.99% purity. All salts had a purity greater than 99.8%.

Preparation of Solutions. All solutions were prepared on a molal basis using redistilled conductivity water of $< 10^{-6}$ ohm^{-1} conductivity prepared by the method of Franks.[12]

Measurement of Density and Viscosity. The densities of the solutions were measured at 15, 20, 25, 30, and 35° using a capped 10-ml pycnometer and were vacuum and buoyancy corrected. They are precise to ±0.0001 g cm^{-3}.

Viscosity measurements at the specified temperatures were obtained using a series of British Standard suspended level viscometers with flow times for water ranging from approximately 100 sec to in excess of 1200 sec.

The viscometers were calibrated with high-purity conductivity water using eq 7

$$\eta/\rho = Ct - B/t \quad (7)$$

where η is the absolute viscosity, ρ is the density, and t the flow time in seconds. The values of viscosity and density of water at the specified temperatures were taken from Hardy, *et al.*,[13] and Swindells, *et al.*[14]

For flow times less than 1000 sec the reproducibility is ±0.25 sec, and for flow times in excess of 100 sec the reproducibility is better than ±1 sec, the time measurements being carried out using stopwatches which had negligible errors in absolute time measurement over the times involved and which were of ±0.01 sec accuracy. All the viscosity and density measurements were carried out in a constant temperature bath controlled to within ±0.02° of the specified temperature.

Results and Discussion

The absolute viscosities of the tetraalkylammonium bromide solutions were computed by means of eq 7. The data are presented in ref 15 together with the solution densities, which were obtained by direct measurement in all cases, and the visometer constants associated with eq 7.

The data utilized in the paper have been obtained on a molal concentration basis because of the problems which arise from the bulky nature of the R_4N^+ ion. As pointed out by Nightingale[6] the molar scale of concentration is satisfactory for most common inorganic salts because the density of a 1 M solution is such that 1 l. contains very close to 54 mol of water. For $(CH_3)_4NBr$, $(C_2H_5)_4NBr$, $(C_3H_7)_4NBr$, and $(C_4H_9)_4NBr$, however, 1 l. of a M solution contains 49, 46, 43, and 39 mol of water, respectively. Thus data expressed on a molar concentration scale are subject to exaggeration at concentrations in excess of 1 M.

The viscosity and density data listed in ref 15 were utilized to calculate V_e of the Breslau–Miller model according to eq 3 for $(CH_3)_4NBr$, $(C_2H_5)_4NBr$, $(C_3H_7)_4NBr$, and $(C_4H_9)_4NBr$ as a function of concentration and temperature, the values obtained being illustrated in Figures 1–4. Several points of interest arise from the data on the basis of the Breslau–Miller model;

(12) F. Franks, *Chem. Ind. (London)*, 204 (1961).

(13) R. C. Hardy and R. L. Cottingham, *J. Res. Nat. Bur. Stand.*, **42**, 573 (1949).

(14) J. F. Swindells, J. R. Cow, and T. B. Godfrey, *ibid.*, **48**, 1 (1952).

(15) Listings of absolute viscosities and solution densities will appear immediately following this article in the microfilm edition of this volume of the journal. Single copies may be obtained from the Business Operations Office, Books and Journals Division, American Chemical Society, 1155 Sixteenth Street, N.W., Washington, D. C. 20036, by referring to code number JPC-72-1902. Remit check or money order for $3.00 for photocopy or $2.00 for microfiche.

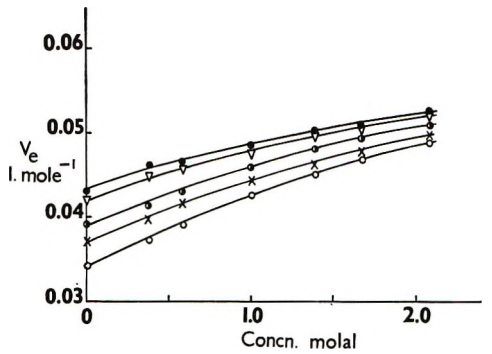

Figure 1. The "effective flowing volume" V_e of $(CH_3)_4NBr$ as a function of concentration and temperature: ○, 15°; ×, 20°; ◑, 25°; ▽, 30°; ●, 35°.

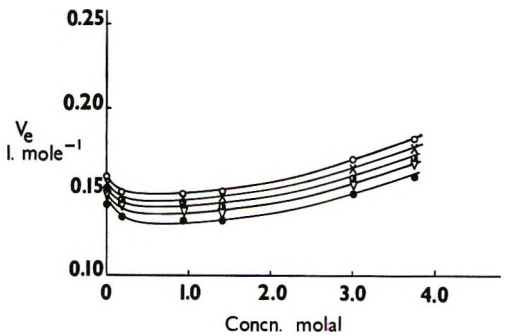

Figure 2. The "effective flowing volume" V_e of $(C_2H_5)_4NBr$ as a function of concentration and temperature: ○, 15°; ×, 20°; ◑, 25°; ▽, 30°; ●, 35°.

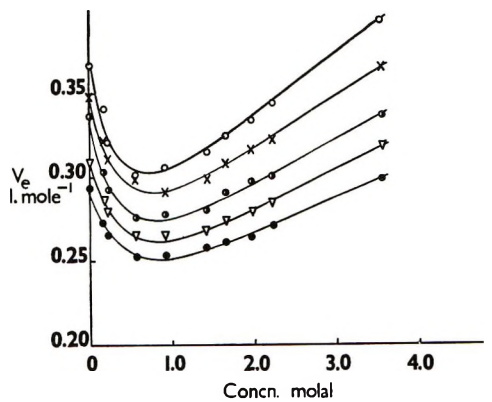

Figure 3. The "effective flowing volume" V_e of $(C_3H_7)_4NBr$ as a function of concentration and temperature: ○, 15°; ×, 20°; ◑, 25°; ▽, 30°; ●, 35°.

all the salts show a systematic dependence on concentration which Breslau and Miller were not able to observe with normal electrolytes; $(C_2H_5)_4NBr$, $(C_3H_7)_4NBr$, and $(C_4H_9)_4NBr$ show a consistent pattern of V_e decreasing with increasing concentration to a minimum, which appears at a similar concentration for all three salts, followed by an increase in V_e with a further increase in concentration. $(CH_3)_4NBr$, however, shows completely different behavior, V_e as a function of concentration reveals no indication of a minimum, and the

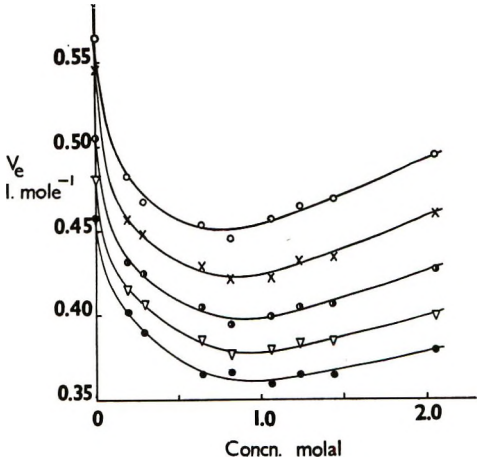

Figure 4. The "effective flowing volume" V_e of $(C_4H_9)_4NBr$ as a function of concentration and temperature; ○, 15°; ×, 20°; ◑, 25°; ▽, 30°; ●, 35°.

magnitude obtained (0.04–~0.05 l. mol^{-1}) is of the same order as the values of V_e obtained by Breslau and Miller for normal electrolytes. In addition, it is interesting to note the temperature dependence of V_e for $(CH_3)_4NBr$ is the reverse of that of $(C_2H_5)_4NBr$, $(C_3H_7)_4NBr$, and $(C_4H_9)_4NBr$, the magnitude of V_e increasing with increasing temperature. [A similar inversion of temperature dependence between $(CH_3)_4NBr$ and the other salts was noticed by Bunzl[16] in a study of the 0.97-μ near-infrared band of the salts in water but was not commented upon.]

Figures 5–7 illustrate the plot of $c/\log \eta/\eta_0$ against c for $(CH_3)_4NBr$, $(C_2H_5)_4NBr$, $(C_3H_7)_4NBr$, and $(C_4H_9)_4NBr$, respectively, derived from the Vand model of dispersion viscosity according to eq 6. Table I lists the limiting values of the effective flowing unit V_e°, obtained from the appropriate intercept, for the four salts. V_e° shows a similar temperature dependence to V_e for the Breslau–Miller model, decreasing with decreasing temperature for $(CH_3)_4NBr$ and increasing with decreasing temperature for the other three salts. The Vand model therefore suggests that large roughly spherical ions such as $(C_2H_5)_4N^+$, $(C_3H_7)_4N^+$, and $(C_4H_9)_4N^+$ give rise to a meaningful unique limiting value of effective flowing volume for the cor-

Table I: The "Limiting Value of the Effective Flowing Unit," V_e°, of the Vand Model (l. mol^{-1})

Salt	15°	20°	25°	30°	35°
$(CH_3)_4NBr$	0.034	0.037	0.039	0.042	0.043
$(C_2H_5)_4NBr$	0.159	0.154	0.152	0.147	0.142
$(C_3H_7)_4NBr$	0.366	0.348	0.328	0.309	0.293
$(C_4H_9)_4NBr$	0.565	0.543	0.505	0.480	0.457

(16) K. W. Bunzl, *J. Phys. Chem.*, **71**, 1398 (1967).

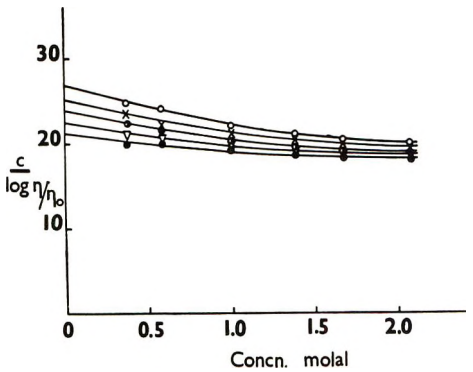

Figure 5. $c/\log \eta/\eta_0$ *vs.* c for $(CH_3)_4NBr$ at 15°, ○; 20°, ×; 25°, ◑; 30°, ▽; 35°, ●.

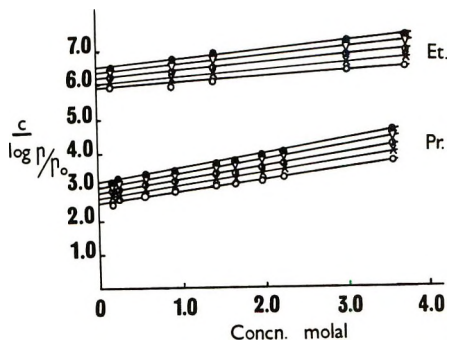

Figure 6. $c/\log \eta/\eta_0$ *vs.* c for $(C_2H_5)_4NBr$ (Et) and $(C_3H_7)_4NBr$ (Pr) at 15°, ○; 20°, ×; 25°, ◑; 30°, ▽; 35°, ●.

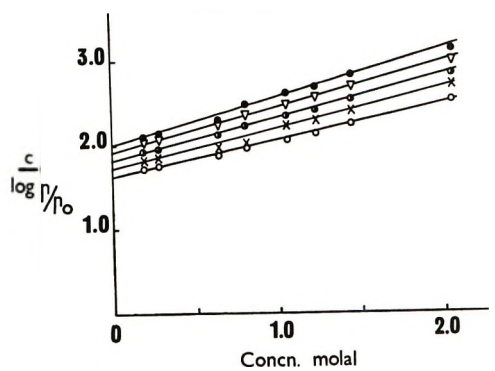

Figure 7. $c/\log \eta/\eta_0$ *vs.* c for $(C_4H_9)_4NBr$ at 15°, ○; 20°, ×; 25°, ◑; 30°, ▽; 35°, ●.

responding salt; a more doubtful value is obtained in the case of $(CH_3)_4NBr$.

Several workers have attempted to relate the Einstein equation for viscosity of a dispersion[17]

$$\eta/\eta_0 = 1 + 2.5\phi$$

with the Jones–Dole equation by performing the transformation

$$\phi = cV$$

where V is an estimate of the molar volume of the solute molecules in solution. The B coefficient can then be related to V by the relationship

$$B = 2.5V$$

Having now obtained unique values for the "limiting effective volume flow unit," $V_e°$, for the series of tetraalkylammonium salts at relatively high concentrations, it is important to seek a correlation with the Jones–Dole B coefficient obtained from low concentration viscosity data. Thus utilizing the relationship

$$B = 2.5V_e°$$

values of the B coefficient have been obtained as a function of temperature for the four salts and are summarized in Table II together with the corresponding values of the B coefficient obtained by Kay and coworkers on dilute (<0.2 M) solutions of the tetraalkylammonium bromides. The good agreement between the values obtained in this work and those of Kay, *et al.*, points to the validity of treating concentrated solutions of the tretraalkylammonium salts on the basis of the Vand model, assuming that complete dissociation of the salt takes place in solution, giving rise to the large spherical entity of the tetraalkylammonium ion.

Table II: The Jones–Dole B Coefficient as a Function of Temperature

Salt	15°	20°	25°	30°	35°
$(CH_3)_4NBr$	0.085	0.093	0.098	0.105	0.108
a	(0.075)	(0.090)	0.083	(0.095)	(0.100)
$(C_2H_5)_4NBr$	0.398	0.386	0.381	0.368	0.355
a	(0.39)	(0.36)	0.34	0.33	(0.32)
$(C_3H_7)_4NBr$	0.915	0.870	0.820	0.773	0.733
a	(0.93)	(0.87)	0.82	(0.77)	(0.73)
$(C_4H_9)_4NBr$	1.41	1.36	1.26	1.20	1.14
a	(1.41)	(1.32)	1.24	(1.18)	(1.12)

[a] Data of Kay and coworkers; the data at 25° are experimental points, the data in parentheses are obtained from the temperature dependencies published by Kay.

Interpretation of the B coefficients for the tetraalkylammonium bromides in terms of the structuring effects of the electrolyte upon water has been fully reported by Kay and does not require detailed repetition. It is sufficient to say that the conclusions deduced point to $(CH_3)_4NBr$ being a slight structure breaker with respect to water and the other salts being increasingly stronger promotors of water structure as the size of the R_4N^+ ion increases.

The behavior of the effective flowing volume V_e as a function of concentration and temperature obtained from the model of Breslau and Miller is consistent with the limiting value at zero concentration $V_e°$ obtained for the Vand model, as the extrapolations in Figures 2–5 show. The behavior pattern of V_e must therefore

(17) A. Einstein, *Ann. Phys.*, **19**, 289 (1906).

be examined for a possible model of hydration structure interaction at the higher salt concentrations. The slight increase of V_e of $(CH_3)_4NBr$ with increasing concentration from 0.04 to 0.05 l. mol^{-1} suggests ion–dipole interactions between the $(CH_3)_4N^+$ ion and water molecules and gives rise to electrostrictive hydration of the $(CH_3)_4N^+$; increasing the salt concentration causes further disruption of the water equilibrium, releasing more "free" water, which results in the continuous increase in V_e. The temperature dependence of V_e is consistent with this interpretation; V_e increases with increasing temperature, as expected when disruption of the normal water structure equilibrium by increased temperature provides more "free" water molecules for subsequent interaction.

$(C_2H_5)_4NBr$, $(C_3H_7)_4NBr$, and $(C_4H_9)_4NBr$ have a completely different dependence of V_e on both concentration and temperature. The behavior pattern is similar for all three salts, in that all show a minimum in V_e with respect to concentration at the same concentration but the magnitude of V_e increases rapidly with increasing size of the R_4N^+ ion. The calculated B coefficients indicate that the increasing magnitude of V_e may be associated with an enhancement effect upon the structure of water. Evidence to support this view is suggested by a comparison of $V_e°$, the limiting value of V_e, with Stokes law volumes of the salts, calculated from the molecular model and mobility measurements at infinite dilution;[18] the data are listed in Table III. $V_e°$ at 25° of $(CH_3)_4NBr$ is in good agreement with the Stokes law volume calculated from mobility measurements but very much less than the molecular model volume; increasing size of the R_4N^+ ion results in $V_e°$ becoming progressively greater than the "mobility" and the "molecular model" Stoke law volumes. Such behavior might be expected from the increasing sensitivity of $V_e°$ to hydration interactions with increasing size of the R_4N^+ ion.

Table III: "Stokes Law" Volumes of the Tetraalkylammonium Bromides at 25°

Salt	"Stokes law" volumes, l. mol^{-1}	
	a	b
$(CH_3)_4NBr$	0.124	0.040
$(C_2H_5)_4NBr$	0.180	0.065
$(C_3H_7)_4NBr$	0.252	0.171
$(C_4H_9)_4NBr$	0.323	0.282

[a] Calculated on the basis of molecular model dimensions. [b] Calculated from mobility measurements at infinite dilution.

In a discussion of partial molar volume data of tetraalkylammonium bromides Wen and Saito[19] and Frank[20] suggest that increasing salt concentrations give rise to interactions between water clusters surrounding neighboring cations, resulting in negative deviations from the expected partial molar volumes of the salts. The deviation becomes more marked the longer the alkyl group; V_e might therefore be expected to show a similar behavior pattern as a function of salt concentration. The cosphere concept of Gurney[21] supports this view, the effect of overlap of hydration spheres being shown to lead to greater stability of the hydration structure but with less structure formation in total. Evidence for the concentration dependence of V_e may be inferred from the partial molar volume data of Wen and Saito. The plot of partial molar volume against $\sqrt{c}$ in the case of $(C_2H_5)_4NBr$ and $(C_3H_7)_4NBr$ does not show a linear dependence; both salts show a further downward bend at a concentration of approximately 0.7 M. This kink is not evident in the case of $(C_4H_9)_4NBr$, probably because the minimum value of the partial molar volume occurs close to this concentration, effectively masking any kink. Such behavior implies a constant factor in the series of salts which, since all are bomides, provides a possibility of a hydration interaction involving the bromide ion. The cosphere concept of Gurney indicates that hydration interaction between cation and anion results in a negative contribution to the partial molar volume; hence the kink in the data of Wen and Saito could be produced by interaction between the hydration sphere of the bromide ion and the combined cation–cation hydration sphere. The minimum value observed of V_e appears to coincide in concentration with the downward kink in partial molar volume, suggesting that this value may be associated with interaction of the cation–cation and anion hydration spheres. The continuous and steady increase of V_e observed for $(C_2H_5)_4NBr$, $(C_3H_7)_4NBr$, and $(C_4H_9)_4NBr$ at higher concentrations still exhibits the same temperature and alkyl group size dependence as V_e at low salt concentrations, suggesting the continuing predominance of hydration interactions which may as proposed by Frank[20] produce incipient clathrate formation in solution, of the form suspected to remain from the melting and dilution of the clathrates known to be formed by the larger tetraalkylammonium salts.[22]

(18) R. A. Robinson and R. H. Stokes, "Electrolyte Solutions," Butterworths, London, 1965.

(19) W. Y. Wen and S. Saito, *J. Phys. Chem.*, **68**, 2639 (1964).

(20) H. S. Frank, *Z. Phys. Chem. (Leipzig)*, **B228**, 364 (1964).

(21) R. W. Gurney, "Ionic Processes in Solution," McGraw-Hill, New York, N. Y., 1954.

(22) G. A. Jeffrey and R. K. McMullen, *Progr. Inorg. Chem.*, **8**, 43 (1967).

Catalytic Activity of Cold-Worked and Quenched Gold for the Decomposition of Hydrogen Peroxide

by Shozo Kishimoto* and Migaki Nishioka

Chemistry Department, Faculty of Science, Kobe University, Rokkodai, Nada-ku, Kobe, Japan *(Received January 28, 1972)*

Publication costs borne completely by The Journal of Physical Chemistry

Changes in hardness and thermoelectric force were observed for cold-worked gold in the range of annealing temperature 100–200° (T_d), where dislocations disappear. A sudden decrease in the catalytic activity for the decomposition of hydrogen peroxide was found to take place in the same range (T_d). Consequently, it is concluded that the surface terminations of dislocations of cold-worked gold play the part of active sites for the reaction. An increase in the vacancy concentration was observed after quenching from 800–1000° to 0°. On the other hand, the quenched catalysts were inactive for the reaction. It is suggested that the presence of surface emergent point defects of gold has no effect on the catalytic activity.

Much effort has been paid to study the relationship between surface emergent defects in solids and their catalytic activity. Uhara and coworkers[1-3] have shown that lattice defects (point defects and dislocations) play an important role for various catalytic reactions in the case of cold-worked metals, in view of the fact that the thermal deactivation temperature was approximately the same as the disappearance temperature of defects during annealing. Eley and MacMahon,[4] studying the effect of annealing on the catalytic activity of copper for the decomposition of hydrogen peroxide, showed that the dependence of activity on annealing temperature is similar to the result obtained by Uhara and coworkers.[1] However, they pointed out that the concentration of surface emergent defects has no effect on their activity and that each crystallographic plane has its own activity. Keating, Rozner, and Youngblood[5] showed that the increase in the activity of platinum plate for the decomposition of hydrogen peroxide is apparently due to deformation by the detailed metallurgical characterization since the possible effects of preferred orientation and increased surface area of cold-worked metals proved to be negligible. On the other hand, little has been known about the catalytic behavior of quenched metals. It is well known that vacancies are generated during quenching. In the study of the catalytic decomposition of formic acid on gold powder, Bhakta and Taylor[6] found the generation of high activity after quenching and attributed it to surface defects. Duell and Robertson[7] showed a similar effect on flashing metals at temperature near the melting point. The purpose of this study was to establish the role of defect structure of cold-worked and quenched gold on the decomposition of hydrogen peroxide and on some physical properties. The type of defects and the recovery temperature ranges are markedly affected by the presence of impurities as well as by the nature and degree of working. Consequently, it is desirable to employ the same specimens for the measurements of both catalytic activities and physical properties. The measurement of thermoelectric force and hardness are most convenient to this purpose.

Experimental Section

The pure hydrogen peroxide used was obtained by vacuum distillation of 30% commercial hydrogen peroxide at 30 mm pressure after removing the contained stabilizers by means of adsorption on stannic acid. The rate of the decomposition of 3% solution was determined volumetrically with a modified Warburg apparatus at 30 ± 0.1°. Well-annealed gold (99.9% or higher purity) was rolled to a constant degree (84% compression) at room temperature. These rolled specimens (50 × 0.17 × 0.005 cm) were used as the catalyst (surface area approximately 17.5 cm²). The annealing of specimens was carried out in an electric furnace for 1 hr at various temperatures. The quenched samples were obtained in the following manner. The specimens were suspended in a vertical furnace for 1 hr at different temperatures, then allowed to fall into water at 0°. The micro-hardness (H) was determined with a micro-Vickers hardness tester. The thermoelectric

(1) I. Uhara, S. Yanagimoto, K. Tani, G. Adachi, and S. Teratani, *J. Phys. Chem.*, 66, 2691 (1962).

(2) I. Uhara, S. Kishimoto, T. Hikino, Y. Kageyama, H. Hamada, and Y. Numata, *ibid.*, 67, 996 (1963).

(3) I. Uhara, S. Kishimoto, Y. Yoshida, and T. Hikino, *ibid.*, 69, 880 (1965).

(4) D. D. Eley and D. M. MacMahon, *J. Catal.*, 14, 193 (1969).

(5) K. B. Keating, A. G. Rozner, and J. L. Youngblood, *ibid.*, 4, 608 (1965).

(6) M. A. Bhakta and H. A. Taylor, *J. Chem. Phys.*, 44, 1264 (1966).

(7) M. J. Duell and A. J. B. Robertson, *Trans. Faraday Soc.*, 57, 1416 (1961).

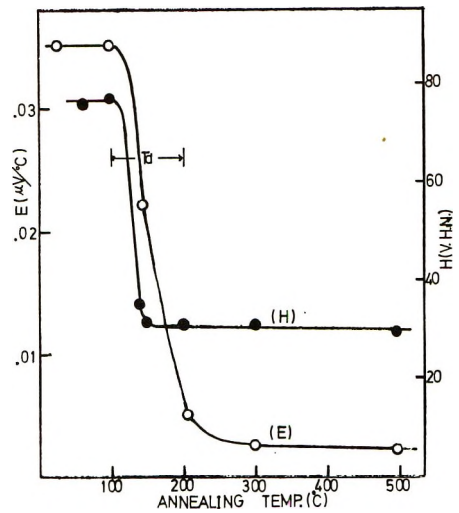

Figure 1. Thermoelectric force (E) and hardness (H) of cold-worked gold as functions of annealing temperature.

force (E) was measured by means of the method previously described.[8]

Results and Discussion

As Figure 1 shows, the changes in E and H of cold-worked gold are considerable in the range of about 100–200° (T_d). In comparison with Clarebrough and coworkers' results,[9,10] these changes are attributed to the disappearance of dislocations. The dependence of the catalytic activity on annealing temperature is shown in Figure 2. The sudden change observed in the range 100–200° corresponds to T_d in Figure 1. This result is similar to the case of cold-worked silver catalysts obtained by Uhara and coworkers for the decomposition of hydrogen peroxide.[3] We may conclude analogously that the active sites of gold catalyst for the reaction are the surface terminations of dislocations. It can be pointed out that the other possible factors affecting the catalytic activity are decrease in surface area and change in preferred orientation due to annealing. Kabe, Mizuno, and Yasumori[11] found that the roughness factors of palladium foil were only 2.0–1.0 in the range of annealing, 150–800°. As a clue to elucidate this problem, it certainly seems desirable to obtain information about the catalytic behavior of single crystals and to study the influence of defects. On quenching, the whole or part of the vacancies can be trapped in the lattice, and the presence of these nonequilibrium vacancies gives rise to the increase in E, as expressed by $\Delta E = A \exp(-E_f/T_q)$, where A is a constant, E_f the formation energy of a vacancy, and T_q the quenching temperature. E_f is obtained from Figure 3A; E_f = 1.0 eV for the range T_q = 1100–1300°K. As Figure 3B shows, the values of H after quenching were the same as that of well-annealed specimens. It is concluded that the generation of dislocations does not occur during quenching. Making a comparison between the present results and other investigations,[12,13] these

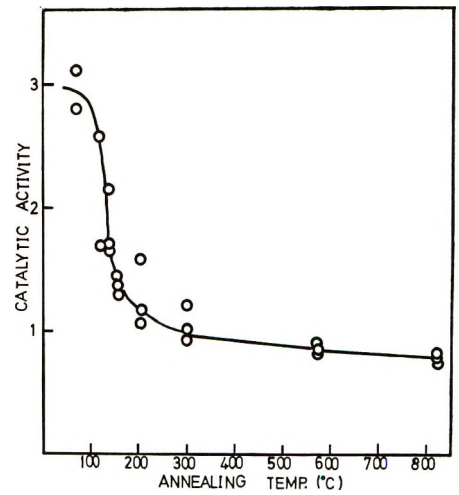

Figure 2. Catalytic activity of cold-worked gold as a function of annealing temperature.

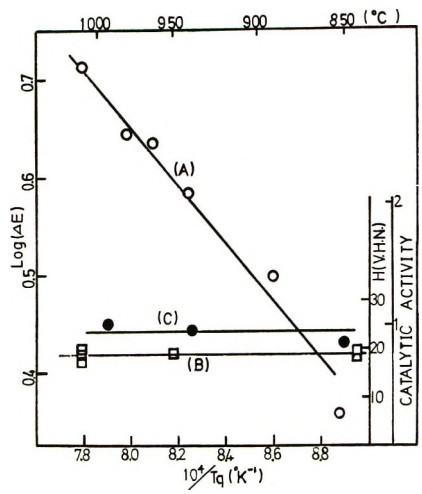

Figure 3. Logarithmic plot of thermoelectric increment (A), hardness (B), and catalytic activity (C) of quenched gold as functions of the reciprocal of quenching temperature (T_q).

phenomena can be attributed to the formation of vacancies. On the other hand, the quenched catalysts are inactive for the reaction as shown in Figure 3C; that is, the catalytic activity does not depend on T_q. It is suggested that surface emergent point defects of quenched gold have no effect on the catalytic activity, contrary to dislocations produced by cold-working.

Acknowledgment. The authors wish to thank professor I. Uhara for reading the manuscript and for helpful discussions.

(8) S. Kishimoto, *J. Phys. Chem.*, **66**, 2694 (1962).

(9) L. M. Clarebrough, M. E. Hargreaves, and M. H. Loretto, *Phil. Mag.*, **6**, 115 (1962).

(10) "Recovery and Recrystallization of Metals," Commonwealth Scientific and Industrial Research Organization, Australia, 1963.

(11) T. Kabe, T. Mizuno, and I. Yasumori, *Bull. Chem. Soc. Jap.*, **40**, 2047 (1967).

(12) J. E. Bauerle and J. S. Koehler, *Phys. Rev.*, **6**, 107 (1957).

(13) T. Broom and R. K. Ham, "Vacancies and Other Point Defects in Metals and Alloys," The Institute of Metals, London, 1958.

Thermodynamics of Acid–Base Equilibria. II. Ionization of *m*- and *p*-Hydroxybenzotrifluoride and the Concept of Fluorine Double Bond–No Bond Resonance

by Charles L. Liotta,*[1a] D. F. Smith, Jr.,[1a] Harry P. Hopkins, Jr.,[1b] and K. A. Rhodes[1b]

School of Chemistry, Georgia Institute of Technology, Atlanta, Georgia 30332, and Department of Chemistry, Georgia State University, Atlanta, Georgia 30332 *(Received January 12, 1971)*

Publication costs assisted by the National Science Foundation and the Department of the Interior, Office of Water Resources Research

The free energy, enthalpy, and entropy of ionization of *p*- and *m*-hydroxybenzotrifluoride in water at 25° have been determined from pK_a measurements as a function of temperature. The enthalpy of ionization was also determined by high-precision solution calorimetry. The thermodynamic data for the para and meta isomers are pK_a 8.675, 8.950; $\Delta H°$ 4.99, 5.24 kcal/mol; and $\Delta S°$ −23.0, −23.3 cal/(deg mole), respectively. The results suggest that double bond–no bond resonance is unimportant in the ionization of *p*-hydroxybenzotrifluoride.

Recently, several workers have criticized the concept of fluorine double bond–no bond resonance as a significant influence in rate and equilibrium processes. Streitwieser and his coworkers[2] have concluded from their studies on the base-catalyzed exchange rates for replacement of hydrogen for tritium in 1*H*-undecafluorobicyclo[2.2.1]heptane and on the base-catalyzed protodetritiation kinetics on 9-substituted 9-tritiated fluorines that fluorine hyperconjugation is not significant in stabilizing fluoroalkyl anions. From electron paramagnetic resonance studies on 2-trifluoromethylsemiquinone, Stock and Suzuki[3] have concluded that carbon–fluorine hyperconjugation is much less significant than carbon–hydrogen hyperconjugation. Sheppard[4] has reported that the original work by Roberts, *et al.*,[5] concerning the pK_a of *p*-trifluoromethylanilinium ion in 50% aqueous ethanol is in error and that the σ_p value needed to place the *p*-CF_3 substituent on a linear free energy plot with other meta- and para-substituted anilinium ions is +0.65 rather than +0.74. Stock and his coworkers[6] have pointed out that a σ_p/σ_m ratio of 1.26 ± 0.01 is obtained for the trifluoromethyl derivatives of benzoic acid, aniline, and dimethylaniline, and have concluded that there is nothing unusual about the polar contribution of the trifluoromethyl substituent.[7,8]

It has been reported by Jones[9] that *p*-hydroxybenzotrifluoride, when dissolved in aqueous base at room temperature, is readily hydrolyzed with the loss of fluoride ion.[10] Roberts[5] has used this observation as evidence for charge delocalization in the anion *via* double bond–no bond resonance interaction (I). In order to gain further insight into the extent of charge delocalization in this system, the thermodynamic quantities, $\Delta\bar{F}°$, $\Delta\bar{H}°$, and $\Delta\bar{S}°$, for the ionization

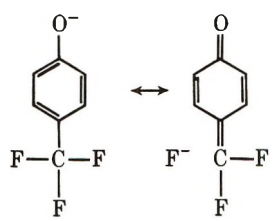

I

process have been determined in water at 25°. These quantities have been shown to be valuable in assessing the nature and degree of interaction of a substituent with the reaction center and the nature of the solute–solvent interaction. The enthalpies of ionization of

(1) (a) Georgia Institute of Technology; (b) Georgia State University.

(2) A. Streitwieser, Jr., and D. Holtz, *J. Amer. Chem. Soc.*, **89**, 692 (1967); A. Streitwieser, Jr., A. P. Marchand, and A. H. Pudjaatmaka, *ibid.*, **89**, 693 (1967).

(3) L. M. Stock and J. Suzuki, *ibid.*, **87**, 3909 (1965).

(4) W. A. Sheppard, *ibid.*, **87**, 2410 (1965).

(5) J. D. Roberts, R. L. Webb, and E. A. McElhill, *ibid.*, **72**, 408 (1950).

(6) F. W. Baker, R. C. Parish, and L. M. Stock, *ibid.*, **89**, 5677 (1967).

(7) Stock, *et al.*,[6] however, used the incorrect ρ_p for the aniline system; σ_p/σ_m is actually 1.33, showing that there is a small enhancement of polar effect over that predicted from the corresponding benzoic acids. Stock has commented (private communication) that 1.33 is still rather close to 1.26 and that the difference does not represent a sizable enough effect to invoke the concept of fluorine double bond–no bond resonance.

(8) Dewar has indicated that, in general, substituent effects are more efficiently propagated from the para position than from the meta position; σ_p/σ_m = 1.2: M. J. S. Dewar, "Hyperconjugation," Ronald Press, New York, N. Y., 1962, pp 159–172; M. J. S. Dewar and A. P. Marchand, *J. Amer. Chem. Soc.*, **88**, 354 (1966).

(9) R. G. Jones, *ibid.*, **69**, 2346 (1947).

(10) Sheppard[4] has indicated that *p*-trifluoromethylaniline also appears to decompose in aqueous solution upon standing.

m- and *p*-hydroxybenzotrifluoride were determined by two methods: (a) measurement of the pK_a's as a function of temperature, and (b) high-precision solution calorimetry.

Experimental Section

(*a*) *pK_a Measurements.* The pK_a of *m*-hydroxybenzotrifluoride in aqueous solution has been determined from 14.90 to 55.96° by a method described previously.[11] Since the para isomer is known to react at room temperature with aqueous base,[9,12] measurements of pH of 50% neutralized solutions were determined with respect to time using a Beckman Model 1019 pH meter and 50% neutralized *p*-nitrophenol as the calibration standard. In all cases linear plots were obtained which, when extrapolated to $t = 0$, gave the pK_a of the acid. The pK_a of *p*-hydroxybenzotrifluoride was determined in this manner from 8.75 to 32.80°. The ionic strength of the solutions was kept low (0.0017 *M*) and it was assumed that the use of 50% neutralized *p*-nitrophenol as the calibration standard (a compound of very similar structure to *p*-trifluoromethylphenol), also at the same low ionic strength (0.0017 *M*), would result in a cancellation of activity coefficients.[11-13]

(*b*) *Calorimeter Measurements.* The heats of ionization for the meta isomer were determined from the heat released when 5 ml of 4.83 *N* NaOH is introduced into the calorimeter containing a solution (980 ml) with a known weight of the phenol. The meta isomer was vacuum distilled on a spinning band column and stored in a sealed vial until immediately before the measurements. The observed heats for seven determinations, which have been corrected for the heat of dilution of the NaOH (q for 5 ml of 4.83 *N* NaOH diluted to 980 ml was calculated from "Selected Values of Chemical Thermodynamic Properties," National Bureau of Standards, U. S. Government Printing Office, Washington, D. C., Table 92-2, as $q = 0.39$ cal), are shown in Table I. The ΔH of neutralization values were plotted against the square of the concentration of dissolved phenol and extrapolated to infinite dilution to obtain $\Delta\bar{H}_N°$.

The neutralization reaction carried out in the calorimeter for the para isomer involved the same type procedure except that smaller samples were used because of the appreciable heat effect accompanying the hydrolysis of the anion. The size of the sample chosen produced a heat effect well within the capabilities of the calorimeter, but did not change the drifts after the reaction by more than 35%. Within several minutes after the introduction of the sample, the thermal drifts had reached a value that was only slowly decreasing (the drifts immediately after the reaction were within 10% of those after the second calibration some 5–8 min later). The first set of drifts that could be obtained after the reaction was used to extrapolate back to the midpoint of the reaction which was determined from the temperature–time curve during the reaction. With this procedure, the small heat effect (increase of ~0.02 cal/sec in the drifts) due to the hydrolysis was compensated for in the calculations.

Table I: Heat of Neutralization Data for *m*-Hydroxybenzotrifluoride with 5 ml of 4.83 *N* NaOH

Mol × 10³	q(cor) cal	$-\Delta H_N$, kcal/mol
15.542	129.8	8.39
10.210	85.1	8.33
9.5006	78.4	8.25
4.543	37.3	8.20
4.5125	37.1	8.23
4.2189	34.9	8.26
4.376	35.9	8.22
		$\Delta\bar{H}_N°$(extrapolated) = 8.10 ± 0.05 kcal/mol

The corrected heats and calculated ΔH of neutralization value are tabulated in Table II. The samples used in the calorimetry studies were vacuum sublimed and sealed into individual glass bulbs which were broken to introduce the sample into the solution. All of the runs were at concentrations below the lowest concentration used for the meta isomer, and the average ΔH_N is taken to be $\Delta\bar{H}_N°$, the infinite dilution value.

Table II: Heat of Neutralization Data for *p*-Hydroxybenzotrifluoride with 5 ml of 4.83 *N* NaOH

Mol × 10³	q(cor), cal	$-\Delta H_N$, kcal/mol
3.132	26.89	8.58
3.774	30.42	8.06
4.125	33.88	8.21
3.606	29.99	8.31
2.962	25.26	8.53
2.479	20.48	8.26
2.607	21.30	8.17
1.897	16.47	8.68
		Av = 8.35 ± 0.06

The calorimetry values for $\Delta\bar{H}_N°$ have been combined with the $\Delta\bar{H}° = 13.34$ kcal/mol for the ionization process of H_2O[14,15] to yield $\Delta\bar{H}°$ for the ionization process in water of the meta and para isomers. The

(11) C. L. Liotta, K. H. Leavell, and D. F. Smith, Jr., *J. Phys. Chem.*, 71, 3091 (1967).

(12) C. L. Liotta and D. F. Smith, Jr., *Chem. Commun.*, 416 (1968).

(13) W. F. O'Hara, T. Hu, and L. G. Hepler, *J. Phys. Chem.*, 67, 1933 (1963).

(14) J. Hale, R. M. Izatt, and J. J. Christensen, *ibid.*, 67, 2605 (1963).

(15) C. E. Vanderzee and J. A. Swanson, *ibid.*, 67, 2608 (1963).

$\Delta\bar{S}°$ values were obtained from combination of $\Delta\bar{G}°$ and $\Delta\bar{H}°$.

The calorimeter design follows very closely that described previously.[16] A few modifications have improved the reliability and overall operation of the calorimeter. Temperature changes are followed with a set of 100-ohm thermistors placed in parallel and a high-sensitivity Mueller bridge. For a temperature increase of 1°, the effective resistance of the thermistors decreases by approximately 1 ohm. In principle, this arrangement can measure a temperature increment directly to the nearest 0.0001°. However, the heat leaks into the system were adjusted to effect a temperature change of 0.001° in a 20–30-sec time interval, making it more practical to follow the temperature to the nearest 0.001° and interpolate to the nearest 0.0001°. Time intervals between successive temperatures were automatically recorded with a Sodeco printing counter activated by a switch. The calorimeter was calibrated electrically before and after the neutralization reaction. The initial temperatures were such that the reaction midpoint was at 25 ± 0.1°.

The most significant modification involves a unique sample introduction mechanism which eliminates the appreciable uncertainty usually associated with the determination of the heat of sample injection. In previous calorimeters of this type, this quantity was 1–2 ± 0.5 calories. The new mechanism involves a thin polyethylene bag sealed with paraffin and attached to the stirrer. The sample is introduced by turning two stainless steel knife blades a precise distance with a timing motor. The heat associated with introducing the sample with this mechanism is below the detection limits of the calorimeter, eliminating a major source of error.

Results

(*a*) *pK_a Measurements.* Tables III and IV summarize the pK_a–temperature data for *p*- and *m*-hydroxybenzotrifluoride, respectively. In addition, Table III contains the change in pH with respect to time—time zero being taken as the pK_a at the particular temperature.

Table III: The Time and Temperature Dependence of the pH of Half-Neutralized Solutions of 0.0017 *M* *p*-Hydroxybenzotrifluoride

Temp, °C	pK_a	Time, sec					
	0	100	200	300	400	600	800
8.90	8.968	8.963	8.958	8.953	8.948	8.937	8.927
10.16	8.929	8.920	8.910	8.901	8.891	8.871	8.852
12.80	8.844	8.836	8.827	8.819	8.810	8.793	8.775
17.20	8.795	8.780	8.764	8.748	8.732	8.701	8.668
20.95	8.728	8.700	8.670	8.635	8.611	8.553	8.494
22.60	8.708	8.673	8.636	8.600	8.565	8.494	8.424
28.05	8.650	8.571	8.495	8.423	8.350	8.205	
29.65	8.648	8.561	8.472	8.384	8.296	8.119	
32.89	8.623	8.494	8.364	8.253	8.107		

Table IV: The Temperature Dependence of the pK_a of *m*-Hydroxybenzotrifluoride

Temp, °C	pK_a	Temp, °C	pK_a	Temp, °C	pK_a
15.12	9.1095	23.51	8.982	34.62	8.833
15.88	9.094	24.35	8.960	36.82	8.804
16.67	9.087	25.13	8.952	39.12	8.784
17.39	9.069	26.60	8.939	41.40	8.757
18.14	9.0615	27.81	8.914	44.50	8.734
18.64	9.049	28.95	8.898	45.63	8.712
19.55	9.0375	30.37	8.885	49.50	8.687
20.35	9.0325	31.52	8.876	51.20	8.669
21.40	9.020	32.00	8.871	51.60	8.667
22.70	8.990	32.20	8.867	53.07	8.654

Equations 1 and 2 express the pK_a values of *p*- and

$$pK_a = 1117.7/T + 4.949 \quad (1)$$

$$pK_a = 1128.1/T + 5.179 \quad (2)$$

m-hydroxybenzotrifluoride, respectively, as a function of absolute temperature.[17] The pK_a, enthalpy, and entropy values at 25° for each of these isomers are listed in Table V.

Table V: The Thermodynamic Data at 25° Derived from the pK_a–Temperature Data

	pK_a	$\Delta\bar{H}°$, kcal/mol	$\Delta\bar{S}°$, cal/(deg mol)
p-CF_3	8.675	5.12 ± 0.3	−22.7 ± 1.0
m-CF_3	8.950	5.16 ± 0.1	−23.7 ± 0.4

(*b*) *Solution Calorimetry.* The inherent time dependence in the pK_a determinations for *p*-hydroxybenzotrifluoride leads to large error in the derived $\Delta\bar{H}°$ and $\Delta\bar{S}°$ values, making it difficult to compare these values profitably to those of the meta isomer. The heats of ionization for the para and meta isomers were therefore investigated by means of high-precision solution calorimetry. A time dependence was also encountered in the calorimetry studies for the para isomer, but the effect on the measurement of the heat of neutralization could be minimized by the extrapolation procedures. In this way, accurate $\Delta\bar{H}°$ values

(16) W. F. O'Hara, T. Wu, and L. G. Hepler, *J. Chem. Educ.*, **38**, 512 (1961).

(17) Three-parameter pK_a–T equations have also been derived from the data in Tables I and II: (a) $pK_{a(p\text{-}CF_3)} = 10{,}511.1/T - 58.7881 + 0.108051T$, (b) $pK_{a(m\text{-}CF_3)} = 3051.4/T - 7.3937 + 0.020516T$. (The constants were calculated by the method of orthogonal polynomial: N. W. Please, *Biochem. J.*, **56**, 196 (1954).) These authors feel, however, that the pK_a–T data on these compounds are insufficiently precise to permit the use of the above nonlinear equations in $1/T$ to compute the thermodynamic functions.

for both isomers were obtained and combined with the $\Delta\bar{G}^\circ$ values obtained from the pK_a measurements, yielding $\Delta\bar{S}^\circ$ values for both isomers to ± 0.2 cal/(deg mol). These values are tabulated in Table VI.

Table VI: The Thermodynamic Data Derived from the Calorimetric Measurements and the pK_a's at 25°

	pK_a	$\Delta\bar{H}^\circ$, kcal/mol	$\Delta\bar{S}^\circ$, cal/(deg mol)
p-CF_3	8.675	4.99 ± 0.08	-23.0 ± 0.2
m-CF_3	8.950	5.24 ± 0.08	-23.3 ± 0.2

Discussion

It has been postulated that the entropy of ionization qualitatively reflects the relative degree of solvent orientation around the un-ionized and ionized solute species involved in the equilibrium.[11,18] For example, let us consider the ionization of p- and m-nitrophenol in water. The entropies of ionization for the para and meta isomers have been found to be -16.9[19a] and -21.1[19b] cal/(mol deg), respectively. To a good approximation, it may be assumed that solvation of the un-ionized forms is the same and that entropy differences reflect the relative orientation of solvent molecules around the ionized (charged) species. While the negative charge on the oxygen of the p-nitrophenoxide ion can be delocalized over the entire molecule by direct resonance interaction with the nitro group (electromeric effect), this type of interaction should be unimportant in describing the meta isomer. As a result, one would expect the negative charge on the m-nitrophenoxide ion to be more localized on the oxygen atom. This would result in a tight solvation of the anion of the meta isomer and a comparatively loose solvation of the anion of the para isomer. This description is qualitatively reflected in the relative entropies of ionization. A comparison of the entropies of ionization of m- and p-cyanophenol[20] (-21.8 and -20.0 cal/(mol deg), respectively) and m- and p-formylphenol[11,21,22] (-23.4 and -20.2 cal/(mol deg), respectively) again reveals that charge delocalization of the para isomer produces a more positive entropy of ionization.

While Table IV reveals that the entropy of ionization of the para isomer is more positive than that of the meta isomer, the difference amounts to only 0.3 cal/(mol deg). This small difference indicates that charge delocalization in the anion is small and that fluorine double bond–no bond resonance does not contribute significantly to this system.

Analysis of the thermodynamic pK_a values (25°) determined in this study with the thermodynamic pK_a's of a wide variety of meta- and para-substituted phenols[23] produces the following substituent parameters: $\sigma_{(p\text{-}CF_3)} = +0.56$ and $\sigma_{(m\text{-}CF_3)} = +0.45$, the ratio $\sigma_{(p\text{-}CF_3)}/\sigma_{(m\text{-}PF_3)}$ being equal to 1.25, which is essentially identical with the ratio of the corresponding benzoic acids (1.26),[12] a reference system in which double bond–no bond resonance should be unimportant. One may conclude, therefore, that the electrical effects of the trifluoromethyl group operating in the benzoic acid system are the same as those operating in the corresponding phenolic system.

In summary, analysis of the relative entropies of ionization and relative pK_a values of p- and m-hydroxybenzotrifluoride suggests that double bond–no bond resonance interaction is unimportant in the ionization of p-hydroxybenzotrifluoride.

Acknowledgment. This work was supported by the Department of the Interior, Office of Water Resources Research, as authorized under the Water Resources Research Act of 1964 and by the National Science Foundation Grant.

(18) Preprints of Papers, Symposium on Linear Free Energy Correlations, Oct 19–21, 1965, pp 94–95.

(19) (a) R. A. Robinson and A. Perperl, *J. Phys. Chem.*, **67**, 2860 (1963). A value of -22.5 cal/(mol deg) has been reported by T. L. Cottrell, *et al.*, *J. Chem. Soc.*, 1016 (1948), but is believed to be less reliable. (b) L. P. Fernandez and L. G. Hepler, *J. Amer. Chem. Soc.*, **81**, 1783 (1959).

(20) H. C. Ko, W. F. O'Hara, T. Hu, and L. G. Hepler, *J. Amer. Chem. Soc.*, **86**, 1003 (1964).

(21) F. J. Millero, J. C. Ahluwalia, and L. G. Hepler, *J. Chem. Eng. Data*, **9**, 319 (1964).

(22) P. D. Bolton, F. M. Hall, and I. H. Reece, *J. Chem. Soc.*, 709 (1967); *Spectrochim. Acta*, **22**, 1825 (1966).

(23) J. E. Leffler and E. Grunwald, "Rates and Equilibria of Organic Reactions," Wiley, New York, N. Y., 1963, p 373.

Mass Spectrometric Determination of the Heat of Formation of Ethynyl Radical, C_2H, and of Some Related Species[1]

by Jeffrey R. Wyatt[2] and Fred E. Stafford*

Department of Chemistry and the Materials Research Center, Northwestern University, Evanston, Illinois 60201
(Received July 15, 1971)

Publication costs assisted by the Northwestern University Materials Research Center

An integral furnace mass spectrometer has been used to measure the equilibrium partial pressure of ethynyl radical, C_2H, present when graphite reacted with H_2, C_2H_2, or CH_4 at 1950–2230°K; $\Delta H_f°_{298}(C_2H) = 130 \pm 5$ kcal mol^{-1} (543 ± 20 kJ mol^{-1}) has been determined. From the examination of a similar system with nitrogen as an inlet gas, new lower limits of 149 and 136 kcal mol^{-1} (624 and 568 kJ mol^{-1}) have been assigned to the heats of formation of CNC and C_3N, respectively. The ionization potential of C_2H was measured, I.P.(C_2H) = 11.6 ± 0.5 eV. Using the above data the following dissociation energies have been assigned [kcal mol^{-1} (kJ mol^{-1})]: D(H–C_2H) = 128 (535); D(H–C_2H^+) = 134 (560); D(H–C_2) = 120 (502); D(H–C_2^+) = 131 (547). The proton affinities of C_2 and C_2H are calculated to be 7.1 and 7.5 eV using I.P.(C_2) = 12.2 eV. The ionization potential of C_3 was measured, I.P.(C_3) = 12.1 ± 0.2 eV.

Introduction

Although the existence of an ethynylium (C_2H) had been reported by several laboratories, its heat of formation remained uncertain.[3-9] After reviewing the literature, Bauer, *et al.*,[10] adopted a value of 116 kcal mol^{-1}; a value of 114 kcal was listed in the JANAF tables.[11] Observing the trend D(H–CH_2CH_3) = 98 kcal[12] and D(H–$CHCH_2$) = 103 kcal,[12] one would expect a lower limit of D(H–C_2H) greater than 103 kcal, and therefore $\Delta H_f(C_2H)$ greater than 105 kcal. An upper limit of 123 kcal has been inferred from photochemical data.[13]

This paper presents the first direct determination of the heat of formation of C_2H from a study of the high-temperature reaction of graphite with various hydrocarbons. In addition, the reaction of graphite with nitrogen was studied.

For both of these systems, species with molecular weights greater than 140 have been reported.[14,15] A hypothesis about the origin of these species is presented.

Experimental Section

Unless specifically noted, the experimental details were the same for both the graphite + hydrocarbon and graphite + nitrogen systems. A general description of the mass spectrometer, the integral furnace assembly, and the vacuum inlet system used in this study has been given previously.[14,16]

Shown in Figure 1 is a cross section of the crucible, which was filled about three-quarters full of 10-mesh graphite. The crucibles were machined from ZTA graphite (density 1.95, National Carbon Co.) or GRAPH-I-TITE A (density 1.91, Carborundum, Inc.). No experimental difference was observed between runs using crucibles made from these graphites. ATJ graphite (density 1.73, National Carbon Co.) used in earlier experiments was found to be more porous to both nitrogen and hydrogen than the more dense graphites. For a given flow rate of inlet gas, the molecular beam intensity of N_2^+ or H^+ was about one-half of that in a crucible made from the higher density graphites.

(1) Supported by the Advanced Research Projects Agency through the Northwestern University Materials Research Center, Grant SD-67.

(2) Recipient of predoctoral fellowship No. 5-FO3-AP41183-03 funded by the Air Pollution Control Office of the Environmental Protection Agency.

(3) W. A. Chupka, J. Berkowitz, D. J. Meschi, and H. A. Tasman, *Advan. Mass Spectrom.*, **2**, 99 (1963).

(4) E. L. Cochran, F. J. Adrian, V. A. Bowers, *J. Chem. Phys.*, **40**, 213 (1964).

(5) D. E. Milligan, M. E. Jacox, and A. Marguin, *ibid.*, **46**, 4562 (1967).

(6) P. Dong, Ph.D. Thesis, University of Paris, 1965.

(7) J. A. Meyer and D. W. Setser, *J. Phys. Chem.*, **74**, 3452 (1970). Corrected value for the upper limit for $\Delta H_f(C_3N)$ is 149 kcal mol^{-1}, D. W. Setser, private communication.

(8) K. H. Homann and H. G. Wagner, *Z. Elektrochem.*, **69**, 20 (1965).

(9) A. Farr, O. Strausz, and H. Gunning, *Trans. Faraday Soc.*, **61**, 1946 (1965).

(10) W. Tsang, S. H. Bauer, and M. Cowperthwaite, *J. Chem. Phys.*, **36**, 1768 (1962).

(11) "JANAF Thermodynamic Tables," D. R. Stull, Ed., Clearinghouse for Federal Scientific and Technical Information, Springfield, Va., 1968, Document No. PB-168,370. Tables as issued to Jan 1971.

(12) T. L. Cottrell, "The Strengths of Chemical Bonds," Academic Press, New York, N. Y., 1958.

(13) R. Cherton, *Bull. Soc. Sci. Liege*, **11**, 203 (1942).

(14) S. J. Steck, G. A. Pressley, Jr., S. S. Lin, and F. E. Stafford, *J. Chem. Phys.*, **50**, 3196 (1969).

(15) J. Berkowitz, *ibid.*, **36**, 2533 (1962).

(16) S. J. Steck, G. A. Pressley, Jr., and F. E. Stafford, *J. Phys. Chem.*, **73**, 1000 (1969).

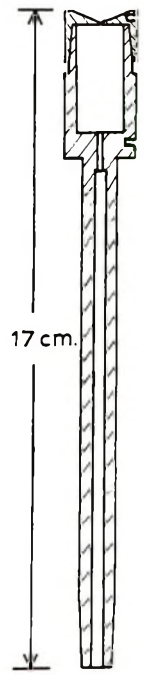

Figure 1. Cross section of the graphite crucible which was covered with 20-mil tantalum. In all of the studies the orifice diameter was 0.5 ± 0.05 mm.

The orifice diameter was 0.5 ± 0.05 mm; intensity and other limitations did not permit it to be varied.

The system was heated by electron bombardment. By adjustment of the height of the filaments (this required disassembling the furnace) it was possible to reduce temperature gradients, as measured by optical pyrometry, to less than 10° for the temperature range 1700–2250°K.

The mass spectrometer was normally operated under the following conditions: emission current, 1.2 mA (which corresponds to a trap current of 10^{-5} A); ionizing electron voltage, 15–19 V; and accelerating voltage, 4 kV. Ions were detected with a 50% transmission grid and 20 stage Cu–Be secondary electron multiplier operated at 4 kV.

A movable beam defining slit, "shutter," located between the furnace assembly and the ion source permitted the differentiations of ions which originated from the crucible, graphite lid, radiation shields, and/or background gases. The relationship of the slit to the various parts of the furnace assembly is depicted in Figure 2.

All of the inlet gases, nitrogen, hydrogen, acetylene, and methane, were obtained from the Matheson Co.; there were no observed impurities and they were used without purification.

Data were gathered and partially reduced by an on-line PDP 8/S computer system.[17] This system was extremely useful in measuring time-averaged ionization efficiency curves for species with low intensities and shutter profiles (ion intensity *vs.* shutter position) for

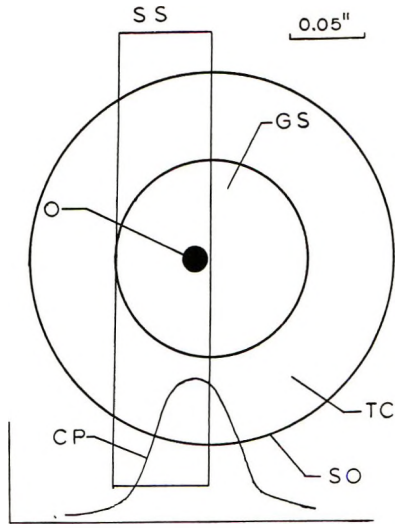

Figure 2. View of the shutter and furnace assembly as seen from the ion source, showing the relationship of the shutter slit (SS) to the furnace assembly consisting of the crucible orifice (O), graphite surface of the lid (GS), tantalum cover (TC), and shield opening (SO). The intensity of C_3^+ (CP) is shown as function of the position of the center of the slit.

permanent gases. Further data reduction was done at the University computing facility.

Data and Experimental Results

A. Carbon + Nitrogen. The reaction of nitrogen with graphite was studied in order to investigate the presence of C_xN_y species including those of molecular weight up to 144 as reported earlier.[15]

In order to test for equilibration, the heat of formation of CN was determined. As shown in Figure 3, a second law analysis of the data yields $\Delta H_{f,298}(CN)$ = 100 ± 3 kcal mol^{-1}; a third-law treatment of the same data yields 102 ± 2 kcal. These are in good agreement with the JANAF[18] value of 104 ± 2.5 kcal which is based on the latest ionization[19,20] and other[21] data.

Table I lists the ion intensities observed for various species at the highest temperature and pressure. The sensitivity factor used to convert ion intensity to pressure was chosen to minimize the difference between the calculated and experimental pressures of both C and C_3. The maximum assigned intensity of C_3N^+, *m/e* 50, was not as low as for CNC^+, *m/e* 38, due to a hydrocarbon, $C_4H_2^+$, background. These data were used to calculate lower limits for the heat formation of CNC and C_3N. At a temperature of 2233°K and a nitrogen pressure of 5 × 10^{-3} Torr, no other C_xN_y species were

(17) J. R. Wyatt, G. A. Pressley, Jr., and F. E. Stafford, *High Temp. Sci.*, 3, 130 (1971).

(18) "JANAF Tables," CN entry dated 6/30/69. See ref 11.

(19) V. H. Dibeler and S. K. Liston, *J. Chem. Phys.*, 48, 4765 (1968).

(20) J. Berkowitz, W. A. Chupka, and T. A. Walter, *ibid.*, 50, 1497 (1969).

(21) D. W. Setser and D. H. Stedman, *ibid.*, 49, 467 (1968).

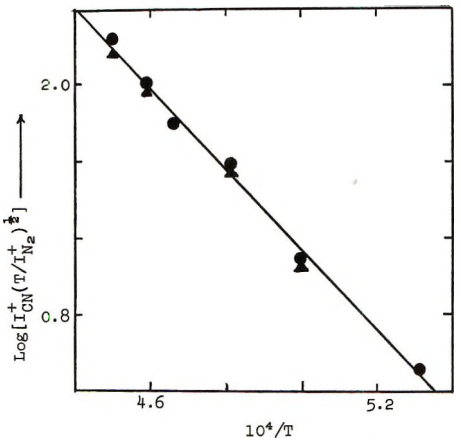

Figure 3. A second-law plot for the reaction: C(s) + $^1/_2N_2$ → CN. Two N_2 pressures were used. Circles represent higher pressure and triangles represent lower pressure.

detected. The instrument detectability limit under these conditions corresponded to an internal crucible pressure of 2×10^{-8} Torr.

Table I: Representative Data from C + N_2 System[a]

Ion	Beam intensity, 10^{-11} A	Sensitivity factor,[b] S_C/S_X	$P_{crucible}$,[c] 10^{-10} atm	P_{JANAF}, 10^{-10} atm
C	0.25	1.00	18	25
C_2	0.11	0.44	4.0	2.5
C_3	3.3	0.29	63	45
CN	2.8	0.64	130	230
$^{15}N^{14}N$	6.3	1.28	6.0×10^4 [d]	...
(C_2N)	0.008	0.29[e]	0.17	15
(C_3N)	0.09	0.29[e]	1.9	...

[a] T = 2233°K, 18-eV electrons, Run 701119. [b] Includes cross section, multiplier gain, and voltage above threshold corrections. [c] $P = I^+(\text{sens factor})T/S$, S = 3 A °K atm^{-1}. [d] Corrected to $^{14}N_2$. [e] Assumed equal to C_3.

The heat of formation of CNC was calculated to be greater than 149 kcal mol^{-1}. Free energy functions were taken from the JANAF tables for the reaction 2C(s) + $^1/_2N_2$ = CNC.

It has been possible to deduce a maximum for the heat of formation of CNC of 172 kcal. This is based upon the fact that CNC has an absorption band from 288–283 mμ which does not show evidence of dissociation;[22] therefore, D(C–NC) greater than 102 kcal mol^{-1} was assumed. The relationship of these quantities is shown in Figure 4. The isomer CNC was chosen over CCN because the minimum heat of formation of CCN must be greater than 194 kcal, using D(C–CN) less than 83 kcal, based upon the dissociation observed for the absorption of 345-mμ radiation by CCN.[23]

It was possible also to calculate a lower limit of 136 kcal mol^{-1} for the heat of formation of C_3N. The free

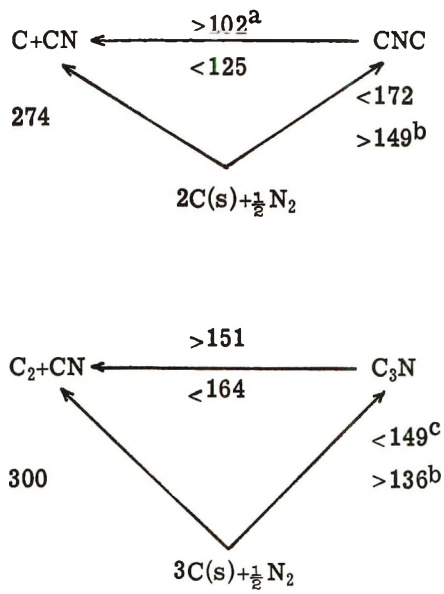

Figure 4. Energetics of the carbon + nitrogen system for CNC and C_3N. [a]Reference 22. [b]Present work. [c]Reference 7.

energy function for C_3N was estimated using the JANAF free energy functions for C_4 and C_2N_2 [$\text{fef}_{C_3N} = {}^1/_2(\text{fef}_{C_4} + \text{fef}_{C_2N_2}) - R \ln 2$]. Setser[7] has reported an upper limit for the heat of formation of C_3N of 149 kcal mol^{-1} based upon $\Delta H_f(C_4N_2)$ = 127 kcal.[11] The relationship of these limits is shown in Figure 4.

B. Carbon + Hydrocarbons. As found previously,[14] there were shutterable peaks corresponding to C_xH_y species to beyond mass 140. Detailed shutter profiles of these species showed that they were not effusing from the crucible orifice, but rather from the volume between the inner radiation shield and the crucible. Examples of the profiles, scanned under computer control, are shown in Figure 5. Only H^+, C^+, C_2^+, C_3^+, C_2H^+, and $C_2H_2^+$ had profiles which implied they were originating directly from inside the crucible. All of the other peaks (see ref 14), including H_2^+, had similar profiles. A profile of this type, m/e 67, is shown also in Figure 5.

Intensities were measured for H^+, C^+, C_2^+, C_3^+, C_2H^+, and $C_2H_2^+$ at various temperatures using hydrogen, acetylene, or methane as inlet gases. A representative sample of observed ion currents is shown in Table II. Since the shutter percentage of m/e 25 was greater than that of any other hydrocarbon species, most of the intensity must be due to the ionization of C_2H. The shutter percentage of C_2H^+ decreased with decreasing temperature until at temperatures less than 1900°K it was the same as that for acetylene. In order to correct for the contribution of fragment C_2H^+ to the (C_2H^+/C_2H) intensity, the following procedure was used: the background intensity at m/e 25 was

(22) A. J. Merer and D. N. Travis, *Can. J. Phys.*, **44**, 353 (1966).
(23) A. J. Merer and D. N. Travis, *ibid.*, **43**, 1795 (1965).

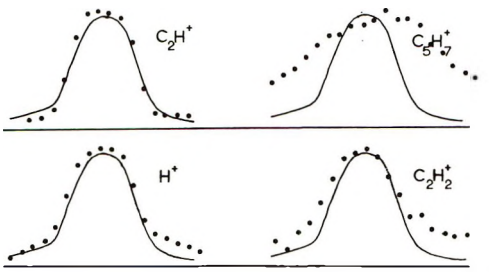

Figure 5. Comparison of the shutter profiles of H^+, C_2H^+, $C_2H_2^+$, and $C_5H_7^+$ to that of C_3^+ (solid curve). From such profiles it is concluded that only H^+, C_2H^+, $C_2H_2^+$, C_3^+, along with C^+ and C_2^+ (not shown) originated directly from the crucible. All of the other ions had profiles which were similar to that of $C_5H_7^+$.

assumed to be entirely due to fragment C_2H^+, this intensity was multiplied by 100%/(100 C_2H_2 shutter %) and subtracted from the total intensity at m/e 25 to obtain the beam intensity of C_2H. This correction is minor at the higher temperatures. Operation at ionization voltages less than 15 V, which would have prevented this problem, was not feasible due to the low ion intensity of C_2H. Instrument sensitivities were calculated from intensities measured for C^+, C_2^+, and C_3^+, using pressures given in the JANAF tables as was done for the C + N_2 system, as shown in Table I.

Table II: Representative Data for the Carbon + Hydrocarbon System[a]

T, °K	Ion	Total intensity, 10^{-11} A	Shutter %	Beam[b] intensity, 10^{-11} A	Pressure,[c] 10^{-8} atm
2233	H	60	72	43	570
	C_2H	1.1	73	0.68[b]	0.12
	C_2H_2	45	33	15	1.9
2111	H	47	69	36	450
	C_2H	0.57	65	0.26[b]	0.044
	C_2H_2	28	34	9.5	1.1
2036	H	33	67	22	270
	C_2H	0.27	60	0.06[b]	0.010
	C_2H_2	19	32	6.1	0.71

[a] 18-eV electrons, Run 710318. [b] C_2H_2 beam intensity corrected for the C_2H^+/C_2H_2 contribution (see text); in this case the C_2H^+/C_2H_2 contributions were 15, 28, and 53% of the observed beam intensity. [c] Using sensitivity = 3.3 A °K atm^{-1} (for m/e 12).

To help confirm equilibrium, the heat of formation of acetylene was calculated from the intensity of H^+ and $C_2H_2^+$. For various runs these values of $\Delta H_{f,298}$·(C_2H_2) were within ±3 kcal of the accepted value[24] of 54 kcal mol^{-1}. The differences are attributed to the uncertainty in extrapolating the ratio of the cross sections of H, C_2H_2, C, C_2, and C_3 and in setting the low ionizing electron voltages (15–19 V) that were used.

Analysis of the data, which yields $\Delta H_{f,298}(C_2H)$ = 130 ± 3 kcal mol^{-1} using the third-law method for various equilibria, is shown in Table III. The error limit is the standard deviation of the data. A second-law treatment had too much scatter to be used.

Table III: Comparison of Third-Law Values of $\Delta H_f°_{298}(C_2H)$ from Various Runs

Run	Inlet gas	T, °K	Reaction	$\Delta H_f°_{298}(C_2H)$, kcal mol^{-1}
710318	H_2	2233	2C(s) + H → C_2H	131
		2153		130
		2036		129
		2233	C_2 + C_2H_2 → 2C_2H	133
710402	C_2H_2	2188	2C(s) + H → C_2H	126
		2188	C_2 + C_2H_2 → 2C_2H	130
		2188	2C(s) + C_2H_2 → 2C_2H	133
		2091		131
		2008		130
710411	CH_4	2168	C_2 + C_2H_2 → 2C_2H	131
		2168	2C(s) + C_2H_2 → 2C_2H	130
		2063		135
		1968		126
				130 ± 3

The ionization potential of C_2H was determined by point by point averaging 100 pairs of shutter open, shutter closed scans taken at 0.1-V increments of the ionizing electron voltage. Figure 6 shows the comparison of the ionization efficiency data for C_2H to those obtained for C and C_2H_2 at the same temperature. A value of 11.6 ± 0.5 eV is obtained for the ionization potential of C_2H; the large uncertainty is due to the low ion intensity. Combining this value with the A.P. of C_2H^+ from C_2H_2 of 17.22 eV,[25] one obtains $\Delta H_{f,298}(C_2H)$ = 131 ± 12 kcal mol^{-1}.

The ionization potential of C_3 also was measured. By decreasing the resolution of the instrument it was possible to acquire simultaneously ionization efficiency curves for C_3 and $H^{35}Cl$ (background species). Analysis of the data showed I.P.(C_3) to be 0.85 eV less than I.P.(HCl). Using a 0.2-eV correction for C_3 being at 2000°, the following result is obtained: I.P.(C_3) = 12.1 eV = 12.74[26] − 0.85 + 0.2 ± 0.2 eV. This is in line with an earlier and probably less exact value of 12.6 ± 0.6 eV.[26] Consequently $D(C^+–C_2)$ = 6.7 eV.

Discussion

A. Carbon + Nitrogen. As is shown in Figure 4, $\Delta H_{f,298}(CNC)$ must be between 149 and 172 kcal mol^{-1}. This value is more limited than the JANAF value of

(24) J. D. Cox and G. Pilcher, "Thermochemistry of Organic and Organometallic Compounds," Academic Press, New York, N. Y., 1970.

(25) R. Botter, V. H. Dibeler, J. A. Walker, and H. M. Rosenstock, *J. Chem. Phys.*, **44**, 1271 (1966).

(26) J. G. Dillard, H. M. Rosenstock, J. T. Herron, K. Draxl, J. L. Franklin, and F. H. Field, NSRDS-NBS 26 (1969).

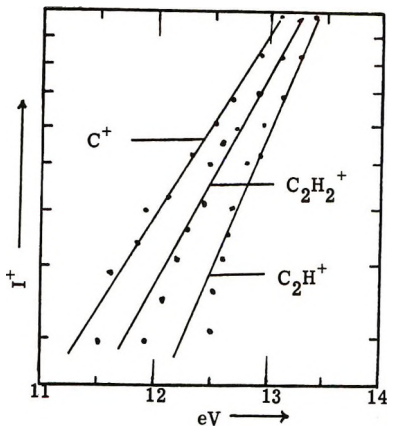

Figure 6. Semilog plot of the ion intensity of C, C_2H, and C_2H_2 *vs.* ionizing electron voltage (uncalibrated). Using I.P.(C) = 11.30 and I.P.(C_2H_2) = 11.40 eV,[26] I.P.(C_2H) = 11.5–11.6 eV is obtained; 11.6 eV was chosen with limits of ±0.3 eV. Since all of the ions were at the same temperature (only beam intensities were used), no temperature correction was made.

133 ± 30 kcal. Safrany and Jaster[27] believe ΔH_f(CNC) must be on the order of 149 kcal to explain the reaction of N_2* with C_2N_2. Limits on the heat of formation of C_3N and CNC should be useful in formulating possible reaction mechanisms for various C + N_2 systems.[28,29]

B. Carbon + Hydrocarbons. The value of 130 kcal mol^{-1} determined for $\Delta H_f(C_2H)$ is greater than the previous upper limit of 123 kcal. If the correct value were indeed 123 kcal mol^{-1} then the observed ion intensity of C_2H should have been tenfold larger, which would have been detected easily. The possibility of extensive fragmentation is not likely because I.P.(C_2H) is 11.6 eV, whereas A.P.(C_2^+/C_2H) or A.P.(H^+, C_2^-/C_2H) must be above 16 or 15.2 eV, respectively; extensive fragmentation is observed to occur when the respective I.P. and A.P. lie close to each other.[30-32]

Another possible cause of systematic error is that equilibrium was not attained in the reactor. This was observed for a similar system by Chupka, *et al.*[3] Owing to physical limitations of the system, it was not possible to vary the orifice area significantly to check for nonequilibrium. In contrast, there are several observations which indicate the system is at equilibrium. There was no dependence of the heat of formation of C_2H upon inlet gas nor reaction chosen as shown in Table III. Acetylene was at equilibrium in the system. Finally, when studied in an identical reactor, the carbon–nitrogen system attained equilibrium. These pieces of evidence notwithstanding, the possibility that equilibrium is not reached is a serious drawback of this and other gas inlet experiments. We feel, however, that the present study on C_2H has been done as well as the best existing technique permits.

The previous upper limit was based on a study by Cherton[13] of the photolysis of acetylene. When 236-mμ (121 kcal mol^{-1}) radiation was used, the formation of diacetylene was observed. The first step was assumed to be $C_2H_2 + h\nu \rightarrow C_2H + H$; however, no direct evidence was given for this step nor for the purity of the exciting radiation. There is no spectroscopic evidence for dissociation. In a careful study of acetylene absorption, Ingold and King[33] concluded that if a continuum exists in the 220–240-mμ region, it must be extremely weak ($\epsilon < 0.01$ cm^{-1}). Since dissociation occurs and the extinction coefficient of acetylene increases rapidly at shorter wavelengths ($\epsilon_{184.9\mu m}$ = 20 cm^{-1}),[34] one must know exactly the spectral content of the exciting radiation in order to interpret correctly the data of a photochemical study.

Setser and Meyer[7] concluded that $\Delta H_f(C_2H)$ is less than 122 kcal mol^{-1} from studying the following reaction: Ar* + $HC_2CN \rightarrow$ Ar + HC_2 + CN*. Their calculation depends directly upon $\Delta H_f(HC_2CN)$ estimated to be 91 kcal mol^{-1} using the Group Additivity method of Benson, *et al.*[35] The "Laidler" tables of Cox and Pilcher[24] give 91.8 kcal. Assuming $\Delta H = 0$ for $C_2H_2 + C_2(CN)_2 = 2HC_2CN$, one obtains 90.5 kcal. Conversely, our $\Delta H_f(C_2H)$ = 130 combined with the Setser and Meyer data gives $\Delta H_{f,298}(HC_2CN)$ = 101 kcal mol^{-1}. We do not know the reason for this descrepancy.

The experimental electron impact ionization potentials of C_2H are 11.6 (present) and 11.25 eV.[6] When combined with A.P.(C_2H^+/C_2H_2) = 17.22 eV,[25] these are in slightly better agreement with the present $\Delta H_f(C_2H)$.

The heat of formation of C_2H is related directly to the CC–H and HCC–H bond dissociation energies. A comparison of various carbon–hydrogen bond energies is presented in Table IV. It is interesting to note how much stronger the carbon–hydrogen bonds are in acetylene than in the other hydrocarbons. Similarly, Chupka, *et al.*,[36] have compared the gas phase behavior of metal dicarbides and oxides. Likewise, one can compare, as shown in Table V, the hydrides of

(27) D. R. Safrany and W. Jaster, *J. Phys. Chem.*, **72**, 3305 (1968).
(28) C. F. Cullis and J. G. Yates, *Acta Crystallogr.*, **17**, 1433 (1964).
(29) M. W. Slack, E. S. Fishburne, and A. K. Johnson, *J. Chem. Phys.*, **54**, 1652 (1971).
(30) R. W. Kiser, J. G. Dillard, and D. L. Dugger, *Advan. Chem. Ser.*, **No. 72**, 153 (1968).
(31) J. W. Hastie and J. L. Margrave, *High Temp. Sci.*, **1**, 481 (1969).
(32) F. E. Stafford, Paper L-4, Proceedings of the Nineteenth Annual Conference on Mass Spectrometry and Allied Topics, Atlanta, Ga., 1971.
(33) C. K. Ingold and G. W. King, *J. Chem. Soc.*, 2725 (1953).
(34) M. Zelikoff and L. M. Aschenbrand, *J. Chem. Phys.*, **24**, 1034 (1956).
(35) S. W. Benson, F. R. Cruickshank, D. M. Golden, G. R. Haugen, H. E. O'Neal, A. S. Rodgers, R. Shaw, and R. Walsh, *Chem. Rev.*, **69**, 279 (1969).
(36) W. A. Chupka, J. Berkowitz, C. F. Giese, and M. G. Inghram, *J. Phys. Chem.*, **62**, 611 (1958).

C_2 and O. The hydrogen bonds show similar trends for both the neutrals and positive ions. Using I.P.(C_2) = 12.2 eV[37] and I.P.(C_2H) = 11.6 eV (present), the proton affinities of C_2 and C_2H are 7.1 and 7.5 eV, respectively.

Table IV: Comparison of D_{298}(C–H) and Average $\bar{D}_{298}$(C–nH) for Various Simple Hydrocarbons

Bond	D, kcal mol^{-1}	Average bond	D, kcal mol^{-1}
C_2H_5–H	98[a]	C_2–6H	98[b]
CH_3–H	105[a]	C–4H	99[b]
C_2H_3–H	103[c]	C_2–4H	98[b]
C_2H–H	128[d]	C_2–2H	123[b]

[a] Benson, *et al.*, ref 35. [b] Cox and Pilcher, ref 24. [c] JANAF tables. [d] Present work.

Table V: Comparison of (H–X–H) Bonds

Bond	D, kcal mol^{-1}	Bond	D, kcal mol^{-1}
C_2H–H	128[a]	HO–H	118[c]
C_2H^+–H	134[a]	HO^+–H	132[d]
C_2–H	120[a]	O–H	101[c]
C_2^+–H	131[b]	O^+–H	120[d]

[a] Present work. [b] Present work and using I.P.(C_2) = 12.2 eV, ref 21. [c] JANAF tables, ref 11. [d] NRSDS-NBS, ref 26.

Several groups of workers[38-41] have debated the importance of the following reaction in the combustion of acetylene: $O + C_2H_2 \rightarrow OH + C_2H$. From the values given in Table V it is clear that this reaction is about 26 kcal endothermic, which would disfavor it.

Although the hydrocarbons that had a molecular weight greater than 26 were not observed originating from the inside of the crucible, they were found to be coming from the region between the crucible and the inner radiation shield. These species were not insignificant in comparison to the intensities of C_2H^+ and $C_2H_2^+$. The relative intensities of the various hydrocarbon ions were comparable to those observed previously in this laboratory.[14] No further hypotheses are made concerning the genesis of these hydrocarbons except to note that they are formed at high temperatures, low pressures, and nonequilibrium conditions. These species may play a role in such nonequilibrium situations as flames or volcanoes in the primordial atmosphere.

Acknowledgment. We thank Dr. Joseph Berkowitz for stimulating discussions and for making available unpublished photoionization results.

(37) V. H. Dibeler and S. K. Liston, *J. Chem. Phys.*, **47**, 4548 (1967).
(38) J. B. Homer and G. B. Kistiakowsky, *ibid.*, **46**, 4213 (1967).
(39) D. Gutman and S. Matsuda, *ibid.*, **52**, 4123 (1970).
(40) C. A. Arrington, W. Brennen, G. P. Glass, J. V. Michael, and H. Niki, *ibid.*, **43**, 525 (1965).
(41) J. N. Bradley and G. B. Kistiakowsky, *ibid.*, **35**, 264 (1961).

what's happening on the frontiers of chemical research?

in short, critical articles that cover all areas *of chemical research.*

Whether you are a practicing chemist, professor or student, you want to keep up with the latest developments. Yet few of you have the time to read thoroughly all the journals of primary publications. ACCOUNTS fills the gap.

Written by investigators active in the fields reviewed, ACCOUNTS' concise, brief articles place recent developments in perspective—and relate them to earlier work and their probable future significance.

Once you start relying on ACCOUNTS to keep you informed, you'll wonder how you got along without its monthly arrival.

Complete and mail back the form below. We'll prove how valuable this publication can be to you.

American Chemical Society / 1155 Sixteenth Street, N.W., Washington, D.C. 20036

Please send me ACCOUNTS OF CHEMICAL RESEARCH at the following subscription rates:

ACS members:	☐ U.S. $ 5.00	☐ Canada, PUAS $ 9.00	☐ Other Nations $10.00
Nonmembers:	☐ U.S. $15.00	☐ Canada, PUAS $19.00	☐ Other Nations $20.00

Name _____ Title _____

Employer _____

Address: ☐ Home ☐ Business _____

City _____ State/Country _____ Zip _____

Nature of employer's business? ☐ Manufacturing or processing ☐ Academic ☐ Government ☐ Other _____ (Please indicate)

Note: Subscriptions at ACS Member Rates are for personal use only.

☐ I am an ACS member ☐ I am not an ACS member

Payment must be made in U.S. currency, by international money order, UNESCO coupons, U.S. bank draft; or order through your book dealer.

323

Inorganic Chemistry is the one...

that publishes both experimental and theoretical fundamental studies in *all phases of inorganic chemistry*.

These studies include synthesis and properties of new compounds, quantitative studies regarding structure, and thermodynamics and kinetics of inorganic reactions. Articles may range from the borders of organic chemistry to the borders of theoretical physics . . . giving you a broad expanse of authoritative information.

Besides the 35 or more papers presented in each monthly issue, you'll also profit from the shorter *Notes* and the *Correspondence* sections, that provide an informal medium of exchange for scientific views and ideas.

Inorganic Chemistry is the one . . . to order right now for your own professional interests. Simply complete and return the form below.

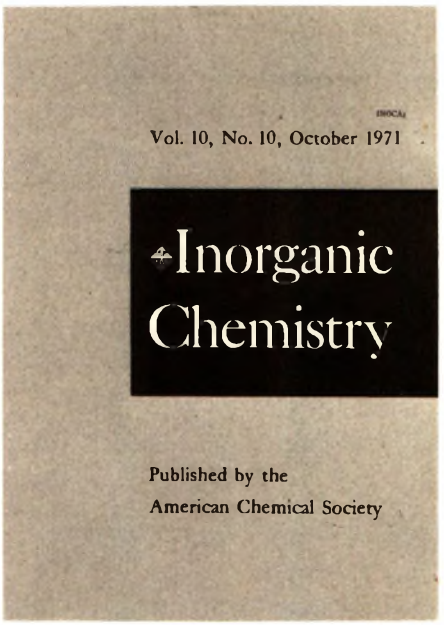

American Chemical Society / 1155 Sixteenth Street, N.W., Washington, D.C. 20036

Please enter my subscription to **Inorganic Chemistry** at the rates checked below:

ACS Members: ☐ U.S. $18.00 ☐ Canada, PUAS $22.00 ☐ Other Nations $23.00

Nonmembers: ☐ U.S. $54.00 ☐ Canada, PUAS $58.00 ☐ Other Nations $59.00

☐ Bill me ☐ Bill employer ☐ Payment enclosed (Payable to American Chemical Society)

Name _____ Title _____

Employer _____

Address: ☐ Home ☐ Business _____

City _____ State/Country _____ Zip _____

Nature of employer's business? ☐ Manufacturing or processing ☐ Academic ☐ Government ☐ Other _____ (Please indicate)

Note: Subscriptions at ACS Member Rates are for personal use only.

☐ I am an ACS member ☐ I am not an ACS member

Payment must be made in U.S. currency, by international money order, UNESCO coupons, U.S. bank draft; or order through your book dealer.

P3A